Study of CuII-complexes for potential diagnostic and therapeutic applications in CuII-related diseases

Enrico Falcone

UNIVERSITÉ DE STRASBOURG

ÉCOLE DOCTORALE DES SCIENCES CHIMIQUES

Institut de Chimie – UMR 7177

THÈSE présentée par :

Enrico Falcone

soutenue le : **27 septembre 2021**

pour obtenir le grade de : **Docteur de l'université de Strasbourg**

Discipline/ Spécialité : Chimie biologique et thérapeutique

Étude de complexes de Cu^{II} à visée diagnostique et thérapeutique dans les maladies liées au cuivre

THÈSE dirigée par :

M. FALLER Peter Professeur, Université de Strasbourg

RAPPORTEURS :

Mme DELANGLE Pascale Chercheur, CEA Grenoble

Mme POLICAR Clotilde Professeur, ENS-PSL Paris

AUTRES MEMBRES DU JURY :

M. ULRICH Gilles Directeur de recherches, CNRS-Université de Strasbourg

M. BAL Wojciech Professeur, IBB-PAS Warsaw

To my beloved granny

Before the Bronze Age,
before history began,
bent to the smith's need.
(Mary Soon Lee, Copper Haiku)

Table of Contents

Acknowledgments/Remerciements/Ringraziamenti i

Declaration of Honour v

List of publications vi

List of abbreviations viii

Résumé xii

Introduction xii

Résultats et discussions xv

Conclusion générale xxi

Références xxii

1. Introduction 1

1.1 Metals in biology 1

1.2 Copper: *"a veteran covered with glory"* 1

1.2.1 Chemistry of Cu in aqueous solution: coordination and reactivity 1

1.2.2 Cu in biological systems 3

1.2.2.1 An evolutionary perspective 3

1.2.2.2 Biological functions of Cu: from redox catalysis to neuromodulation 4

1.2.2.3 Mechanisms of Cu toxicity 5

1.2.3 Cu homeostasis in humans 6

1.2.3.1 Systemic Cu trafficking 6

1.2.3.2 Serum Cu trafficking 6

1.2.3.3 Cellular Cu uptake 8

1.2.3.4 Intracellular Cu trafficking 8

1.2.3.5 Regulation of cellular Cu homeostasis 10

1.2.3.6 Cu speciation in bodily secretions and excretions 11

1.2.4 Cu coordination to proteins and peptides 12

1.2.4.1 Cu^{II} carriers 12

1.2.4.2 Cu^{I} carriers 13

1.2.4.3 Cu-enzymes 14

1.2.5 Cu-related human diseases 16

1.2.5.1 Genetic disorders of Cu metabolism 16

1.2.5.2 Neurodegenerative diseases 18

1.2.5.3 Cancer 19

1.3 Aim of the thesis 20
2. Luminescent probes for exchangeable Cu 21
2.1 Introduction 21
2.1.1 Exchangeable Cu measurement 21
2.1.1.1 Drawbacks of common elemental analysis and imaging methods 21
2.1.1.2 Indirect estimation of NCC – the *Walshe's index* 21
2.1.1.3 Chelation-free methods – *ultrafiltrable Cu* 21
2.1.1.4 Chelation-based methods – *exchangeable* or *chelatable Cu* 22
2.1.2 Requisites for application of a Cu^{II}-probe in Cu_{EXC} measurement 24
2.1.2.1 Affinity 24
2.1.2.2 Reversibility 25
2.1.2.3 Selectivity 26
2.1.2.4 Detectability 27
2.2 Luminescent probes for Cu^{II} – State of the art 28
2.2.1 Turn-off probes 28
2.2.2 Turn-on probes 28
2.2.2.1 Reactivity-based chemodosimeters 29
2.2.2.2 Putative coordination-based turn-on probes 29
2.2.3 Ratiometric probes 33
2.2.4 Applications of Cu^{II}-probes in biological media 37
2.3 Insights into the mechanism of a putative reversible turn-on probe 41
2.3.1 Introduction 41
2.3.2 Results and discussion 41
2.3.3 Conclusions 45
2.3.4 Experimental section 45
2.3.4.1 Materials 45
2.3.4.2 Synthesis of PHP 45
2.3.4.3 Preparation of stock solutions 46
2.3.4.4 Spectroscopic analysis 46
2.3.4.5 HPLC-DAD analysis 46
2.3.4.6 Isolation of the fluorescent product 46
2.4 Development of turn-off ATCUN/Ln^{III} probes for Cu^{II} 47
2.4.1 Introduction 47
2.4.1.1 ATCUN-based Cu^{II}-probes – State of the art 47
2.4.1.2 Lanthanides 48

2.4.1.3 Ln-based Cu^{II}-probes – State of the art 49
2.4.1.4 Design of an ATCUN/Tb^{III}-based probe for Cu^{II} 52
2.4.2 Results and discussion 52
2.4.3 Conclusions 55
2.4.4 Experimental section 56
2.4.4.1 Materials 56
2.4.4.2 Peptide synthesis 56
2.4.4.3 Preparation of stock solutions 58
2.4.4.4 Luminescence measurements 58
2.5 Improvement of the kinetic responsiveness of ATCUN/Tb^{III}-based probes 59
2.5.1 Introduction 59
2.5.1.1 The Ala-His-His motif 59
2.5.1.2 Mechanism of Cu^{II}-exchange/transfer by ATCUN peptides 60
2.5.2 Results and discussion 60
2.5.2.1 Kinetics of Cu^{II} transfer in biological media 61
2.5.2.2 Ternary complexes 62
2.5.2.3 pH-dependence of the luminescence response 64
2.5.3 Conclusions 65
2.5.4 Experimental section 66
2.5.4.1 Materials 66
2.5.4.2 Peptide synthesis 66
2.5.4.3 Preparation of stock solutions 68
2.5.4.4 Luminescence measurements 68
2.5.4.5 UV-vis spectroscopy 68
2.5.4.6 EPR spectroscopy 68
2.6 From intensiometric to ratiometric ATCUN/Ln^{III} probes 71
2.6.1 Assessment of a poly-Proline spacer 71
2.6.1.1 Results and discussion 72
2.6.2 Development of ratiometric probes for Cu^{II} using the Tb^{III}/Eu^{III} couple 74
2.6.2.1 Tb^{III}/Eu^{III}-based ratiometric sensors 74
2.6.2.2 SEA ligation 74
2.6.2.3 Design of an ATCUN/Tb^{III}/Eu^{III}-based ratiometric probe 76
2.6.2.4 Results and discussion 76
2.6.3 Optimization of ATCUN/Tb^{III}/Eu^{III}-based probe for biological applications 79
2.6.3.1 Results and discussion 80

2.6.4 Conclusions 82
2.6.5 Experimental section 82
2.6.5.1 Materials 82
2.6.5.2 Synthesis of $RTH^{W\text{-}NBD}$ 82
2.6.5.3 Synthesis of $AHH^{W/Tb}$-SEA^{off} 84
2.6.5.4 Synthesis of $CP_9^{pic/Eu}$ 86
2.6.5.5 Synthesis of $AHH^{W/Tb\text{-}pic/Eu}$ (SEA ligation) 88
2.6.5.6 Synthesis of $AHH^{Cs124/Tb}$-SEA^{off} 90
2.6.5.7 Synthesis of $CP_6^{Cs124/Eu}$ 92
2.6.5.8 Synthesis of $AHH^{Cs124/Tb\text{-}Eu}$-SH (SEA ligation) 94
2.6.5.9 Synthesis of $AHH^{Cs124/Tb\text{-}Eu}$ (desulfurization) 94
2.6.5.10 Preparation of stock solutions 96
2.6.5.11 CD Spectroscopy 96
2.6.5.12 Luminescence 96
2.7 General conclusions and perspectives 97
3. Reactivity of Cu^{II}-TSCs in biological systems 99
3.1 Introduction 99
3.1.1 α-pyridyl thiosemicarbazones as anticancer drugs 99
3.1.2 Metal-binding properties of α-pyridyl TSCs 99
3.1.3 Mechanisms of action 100
3.1.4 Structure-activity relationships 101
3.2 Aim of the work 102
3.3 Interaction of TSCs and metal-TSC complexes with HSA 103
3.3.1 Introduction 103
3.3.2 Results and discussion 103
3.3.2.1 Metal-independent interaction between TSCs and HSA 104
3.3.2.2 Competition between TSCs and HSA for Cu^{II} 104
3.3.2.3 Selectivity of TSCs for HSA-bound Cu^{II} vs Zn^{II} 106
3.3.3 Experimental section 108
3.3.3.1 Materials 108
3.3.3.2 Preparation of stock solutions 108
3.3.3.3 UV-vis spectroscopy 108
3.3.3.4 EPR spectroscopy 108
3.4 ROS production by Cu^{II}-TSC complexes in the presence of GSH 109
3.4.1 Introduction 109

3.4.1.1 Mechanism of Cu^{II}-catalysed thiol oxidation ____ 109
3.4.2 Results and discussion ____ 110
3.4.2.1 ROS production by 3AP- and Dp44mT-Cu^{II} complexes ____ 110
3.4.2.2 Higher ROS production by Cu^{II}-TSC complexes at lower pH ____ 112
3.4.3 Experimental section ____ 115
3.4.3.1 Materials ____ 115
3.4.3.2 Preparation of stock solutions ____ 115
3.4.3.3 UV-vis spectroscopy ____ 115
3.4.3.4 EPR spin scavenging ____ 115
3.5 Conclusions and perspectives ____ 116
References ____ 117

Acknowledgments/Remerciements/Ringraziamenti

I would like to start this manuscript expressing my gratitude to the many people who have contributed, scientifically or not, to the achievement of this thesis and have accompanied me, from near and far, throughout the past three years, which have been at the same time the hardest and the best of my life.

First, I wish to thank Peter for making this possible and for being an outstanding supervisor. Thanks for making me feel free but never alone, as a driving instructor (with no driving license though) that let you drive autonomously but always stands by your side ready to step in when needed. Thanks for making me feel as a peer and not a subordinate. Thanks for sharing your broad scientific knowledge, for the very inspiring and stimulating discussions and for all the given opportunities for my scientific and human growth. You do represent a role model as a researcher, as an advisor, as a man.

Mon co-premier merci est pour Grand Maitre Laurent (Raibaut), pour m'avoir si bien encadré au quotidien ! Merci de m'avoir initié à la synthèse peptidique et à la ligation native, mais surtout au principe suprême du DTC. Merci de m'avoir toujours encouragé et soutenu. Merci pour l'aide dans la rédaction, surtout des parties en français, de ce manuscrit. Merci d'avoir aussi veillé, avec Vincent, à ma vie sentimentale ainsi qu'à celle scientifique. Enfin, merci aussi pour nos débats, car il n'y a pas de progrès sans confrontation.

I would like to thank Dr. Pascale Delangle, Prof. Clotilde Policar, Dr. Gilles Ulrich and Prof. Wojciech Bal for reading and evaluating this manuscript and being part of this thesis defence committee. I thank Dr. Ulrich also for useful discussions and help with fluorescence measurements. It is also thanks to you if PET and ICT are not arcane acronyms or if a fluorimeter is not a "black box" anymore. Thank you Wojciech for being also part of my mid-thesis committee, for the very helpful and inspiring discussions, and for the bibliographic support to this thesis.

I would like to warmly thank Dr. Olivier Sénèque, who somehow co-lead the main project developed during this thesis. Thanks for your valuable advice and suggestions, as well as for kindly providing fundamental synthetic building blocks.

I wish to thank also Dr. Maria Linder for interesting exchanges about α_2-Macroglobulin, small copper carrier and more generally Cu speciation in the blood.

As a thesis dealing with luminescent probes could have not been achieved without the availability of a fluorimeter, I would like to thank Dr. Loïc Charbonnière, Dr. Clemence Cheignon and Dr. Aline Nonat, as well as Prof. Paolo Samorì and Dr. Veronica Montes Garcia for the access to their fluorescence equipment and help with the luminescence measurements.

I would like to thank Dr. Bertrand Vileno, who recorded and analyzed the EPR spectra reported in this thesis. Thanks for the very pleasing EPR sessions spent together, for your dedication and endless patience. Thanks also to Nolwenn, for her kind technical support, and especially for the very nice moments spent together outside the lab.

I wish also to thank Dr. Youssef El Khoury and Prof. Petra Hellwig for FT-IR and Raman measurements. Thanks, Youssef, for introducing me into the multifaceted landscape of vibrational spectroscopies, and for your detailed and cautious analysis.

I also thank the staff of the Le Bel Federation, in particular Martine Heinrich and Noémie Bourgeois (CD, fluorescence), Maurice Coppe and Bruno Vincent (NMR) for help with the use of spectroscopic facilities. I also thank Jean-Louis Schmidt for help with HRMS and LC-MS analysis.

I thank our collaborators in Vienna, namely Dr. Christian Kowol and Phillip Fronik, Dr. Petra Heffeter and Sonja Hager, Martin Schaier and Dr. Gunda Koellensperger, for their contributions to the thiosemicarbazone project. I really enjoy our stimulating monthly online meetings and I am glad to work within such an interdisciplinary team.

Thanks also to Prof. Emilia Sicilia and Alessandra Ritacca, whose DFT calculations have been an important support for our mechanistic hypothesis about thiosemicarbazone reactivity. I hope we will soon solve the puzzle.

I am profoundly grateful to the great family that welcomed me in Strasbourg more than three years ago: the BCB group. I really enjoyed every meeting, apero, party, breakfast, picnic and trip together.

Thanks (petit) Vincentito, for your continuous "background" help and support in the lab, for the very stimulating discussions and your contagious scientific enthusiasm. Thanks for your almost excessive courtesy. I'll never forget, for instance, when on my very first day in the lab you promptly picked up the phone to complain about my bedbugs issue. I also appreciated how you cared about my mum, asking "la mamma, va bene?" every single day of the last three years.

Merci (Mme) Angélique, pour avoir été beaucoup plus qu'un membre permanent de l'équipe. Merci d'avoir toléré mes blagues insolentes et irrévérencieuses. En effet, ton esprit est plus jeune que le mien ! Merci d'avoir partagé plein de beaux concerts !

Grazie Alicina, per essere stata un punto di riferimento dentro e fuori dal gruppo. È stata davvero dura abituarsi alla tua assenza quotidiana, ma sono davvero contento che il nostro rapporto abbia resistito alla lontananza.

Thanks Paulina, for your friendliness. I regret we couldn't spend more time together. Hope we'll meet again someday.

Thanks Nina – the Wise Aunt – for your precious and patient help in the lab, even after your departure, and for disclosing the darkest sides of "Origin". Thanks for teaching me a little Polish and initiating me into vodka. Last but not least, thanks for your not-too-Polish affability.

Merci Thibaut, pour ton calme et ton amicalité. Merci à toi et Capucine pour votre générosité et hospitalité. J'ai beaucoup aimé les soirées passées chez vous. Ça a réchauffé mon cœur.

Merci Capucine – la méchante – pour notre amitié, pour tes plats délicieux et nos échanges culinaires.

Merci Maxime, parce qu'après seulement une semaine depuis ton arrivée, j'avais l'impression de te connaître depuis longtemps. Enfin, j'ai pardonné à Vincent de t'avoir choisi.

Thanks Michael, for bringing some colour, chaos, and southern warmth in the group.

Merci Merwan – le charcutier – pour toutes tes histoires chelous qui "rimarrano un ricordo indelebile nella mia memoria".

Merci à MJ – la Ministre – de donner une touche plus féminine à notre équipe et d'avoir adouci l'ambiance du bureau des étudiants.

Thanks Lucie – the grandma – for the very nice time spent together inside and outside the lab, despite your age. Happy you're staying longer in Strasbourg. Thanks also for preparing the SEA resin used in this thesis.

Merci DJ Emily, pour m'avoir appris un langage français plus « politiquement correct ». Merci aussi d'avoir animé (ou plutôt, « énervé ») la vie de notre équipe. Tu vas vraiment me manquer !

Thanks also to all the undergraduate students that worked in our lab during the past years, especially Lucie Lorusso and Mai Hoang, who contributed to the main project of this thesis.

Merci Barbara pour tous les beaux moments passés ensemble. Tu as été beaucoup plus que « la doctorante d'à côté » !

Merci Christophe d'avoir rejoint officieusement notre équipe. Tes histoires, notamment la blague du train pour Nice, m'ont fait beaucoup rire !

Thanks also to all the people from the 4th floor, especially Dennis, Elise and Morane for sharing very pleasant lunch and apero during these years.

Thanks to the OMECA group, especially Marine, Agnideep and Geordie for the very nice months spent at the 9th flood during my first year!

Grazie agli amici italiani, e non, a Strasburgo: Stefano, Pietro, Matilde, Vale, Sara, Irene, Rafa, Veronica, Nicholas, Luca, Stefania, Francesca, Gabriella, Cosimo e Aldo, per avermi fatto sentire meno solo e lontano da casa. Un grazie speciale a Stefano e Pietro, miei impareggiabili compagni di viaggio e avventure tra la Sicilia e Strasburgo.

Grazie a Giuseppe, Sebastiano e Claudio – i Biottori – per essere rimasti sempre in contatto e per i nostri incontri (pre-Covid) in giro per l'Europa.

Grazie ad Andrea, Ninni e Roberta, per essermi stati quotidianamente vicini da lontano. Grazie anche a Simone, Francesca, Daniele, Livia, Leo e Gloria. Grazie ad Alessia, per i weekend Marsigliesi e l'indimenticabile "vacanza-studio" a Lisbona.

Grazie a zie e zii, cugine e cugini, a Rosetta, Silvana, Massimo, Giorgio, Gianluigi e Riccardo, per essere stati presenti anche se lontani.

Grazie a Giuseppe – l'ingegnere – per avermi stimolato e incoraggiato a intraprendere questo percorso.

Grazie Angela, per essere la mia àncora, la mia roccia, un punto fermo su cui poter sempre contare. Senza di te, non sarei giunto fin qui.

Grazie mamma e papà, per aver accettato e supportato le mie scelte, e sopportato la nostra lontananza. Grazie per non farmi mai perdere la voglia di tornare a casa. Spero che la soddisfazione per questo traguardo ripaghi tutti i sacrifici.

Infine, grazie alla persona che forse ha più sofferto per la mia lontananza durante questi anni, a cui devo tanto di ciò che sono, e alla quale dedico questa tesi.

Declaration of Honour

I affirm that I am aware that plagiarism is a serious misconduct that may lead to administrative and disciplinary sanctions up to dismissal from the University of Strasbourg and liable to prosecution in the courts of the French Republic.

I am aware that the absence of a clear and transparent citation of a source borrowed from a third party (text, idea, reasoning or other creation) is constitutive of plagiarism.

In view of the foregoing, I hereby certify that the work described in my thesis manuscript is original work and that I have not resorted to plagiarism or any other form of fraud.

List of publications

E. Falcone, A. Sour, V. Lebrun, G. Ulrich, L. Raibaut* and P. Faller* **Reversible turn-on fluorescent Cu(II) sensors: rather dream than reality?** *Dalton Trans.,* **2019**, 48, 14233-14237 (doi: 10.1039/C9DT02864A)

E. Falcone, I. M. M. Ahmed, V. Oliveri,* F. Bellia,* B. Vileno, Y. El Khoury, P. Hellwig, P. Faller* and G. Vecchio **Acrolein and Copper as Competitive Effectors of α-Synuclein** *Chem. Eur. J.*, **2020**, 26, 1871 (doi: 10.1002/chem.201904885)

E. Falcone, P. Gonzalez, L. Lorusso, O. Sénèque, P. Faller* and L. Raibaut* **A Terbium(III) luminescent ATCUN-based peptide sensor for selective and reversible detection of Copper(II) in biological media** *Chem. Comm.,* **2020**, 56, 4797-4800 (doi: 10.1039/D0CC01007C)

E. Falcone,* M. Okafor, N. Vitale, L. Raibaut, A. Sour and P. Faller* **Extracellular Cu^{2+} pools: from current knowledge to next-generation probes** *Coord. Chem. Rev.,* **2021**, 433, 213727 (doi: 10.1016/j.ccr.2020.213727)

E. Falcone,* B. Vileno, M. Hoang, L. Raibaut and P. Faller* **A luminescent ATCUN peptide variant with enhanced properties for Copper(II) sensing in biological media**, *J. Inorg. Biochem.*, **2021**, 221, 111478 (doi: 10.1016/j.jinorgbio.2021.111478)

List of abbreviations

α_2M	α-2-macroglobulin
α-Syn	α-Synuclein
3AP	Triapine (3-aminopyridine-2-carboxaldehyde thiosemicarbazone)
AAS	Atomic absorption spectroscopy
Aβ	Amyloid β
Abs	Absorbance
AD	Alzheimer's disease
AES	Atomic emission spectroscopy
Amb	2,4-diaminobutyric acid
Alloc	Allyloxycarbonyl
AOC	Amine oxidase
APP	Amyloid precursor protein
$AscH^-$	Ascorbate
$AscH^{\bullet-}$	Ascorbyl radical
ATCUN	Amino-Terminal Copper(II) and Nickel(II)
BBB	Blood-brain barrier
BCS	Bathocuproine disulfonate
BDNF	Brain-derived neurotrophic factor
Boc	*tert*-butyloxycarbonyl
BODIPy	Boron-dipyrromethene (4,4-difluoro-4-bora-3a,4a-diaza-s-indacene)
bipy	bipyridine
CCS	Copper chaperone for SOD
CD	Circular Dichroism
CHEF	Chelation-enhanced fluorescence
CCO	Cytochrome c Oxidase
CNS	Central nervous system
Cou	Coumarin
Cp	Ceruloplasmin
Cs124	Carbostyril 124 (7-Amino-4-methyl-2-hydroxyquinoline)
CSF	Cerebrospinal fluid
Ctr	Copper transport protein
Cu_{EXC}	Exchangeable Copper
CuUF	Ultrafiltrable copper
Cys	Cysteine
Dap	2,3-diaminoproprionic acid
DBH	Dopamine β-hydroxylase
DCM	Dichloromethane
DEDTC	Diethyldithiocarbamate
DFT	Density functional theory
DIEA	*N*,*N*-diisopropylethylamine
DMF	*N*,*N*-dimethylformamide
DMSO	Dimethyl sulfoxide
DNA	Deoxyribonucleic acid
Dns	Dansyl
DOTA	1,4,7,10-tetraazacyclododecane-1,4,7,10-tetraacetic acid

DO3Apic	2,2′,2′-(10-((6-carboxypyridin-2-yl)methyl)-1,4,7,10-tetraazacyclododecane-1,4,7-triyl)triacetic acid
Dp44mT	Di-2-pyridylketone-4,4,-dimethyl-3-thiosemicarbazone
DPA	Dipicolylamine
DpC	Di-2-pyridylketone 4-cyclohexyl-4-methyl-3-thiosemicarbazone
D-Pen	D-penicillamine
EDTA	Ethylenediamine tetraacetic acid
EGFR	Epithelial growth factor receptor
EPR	Electron Paramagnetic Resonance
ERK	Extracellular signal-regulated kinases
ESI	Electrospray ionization
EtOH	Ethanol
ETR	Ethylene receptor
FBS	Fetal bovine serum
FGE	Formylglycine-generating enzyme
FGF	Fibroblast growth factor
Fluo	Fluorescein
Fmoc	Fluorenylmethyloxycarbonyl
FRET	Fluorescence Resonance Energy Transfer
GABA	gamma-aminobutyric acid
GSH	Glutathione (reduced)
GSSG	Glutathione disulfide (oxidized)
gtsm	Glyoxal-bis(N4-methyl-3-thiosemicarbazone)
HBTU	3-(bis(dimethylamino)methyliumyl)-3H-benzotriazol-1-oxide hexafluorophosphate
HCTU	O-(1H-6-Chlorobenzotriazole-1-yl)-1,1,3,3-tetramethyluronium hexafluorophosphate
HEPES	4-(2-hydroxyethyl)-1-piperazineethanesulfonic acid
Heph	Hephaestin
His	Histidine
HPLC	High performance liquid cromatrography
HSA	Human serum albumin
HSAB	Hard and Soft Acids and Bases
ICP	Inductively-coupled plasma
ICT	Internal charge transfer
K_{pH}	Condition stability constant at a given pH
LA	Laser ablation
LB	Lysogeny broth
LC	Liquid cromatography
LFSE	Ligand field stabilization energy
LMW	Low-molecular-weight
LOD	Limit of detection
LOX	Lysyl oxidase
LT	Low temperature
MAPK	Mitogen-activated protein kinase
MD	Menkes disease
Me_2NNMeN_2	3-(Dimethylamino)pyridine-2-carbaldehyde N,N-Dimethylthiosemicarbazone
MeCN	Acetonitrile
MeOH	Methanol
MES	2-morpholin-4-ylethanesulfonic acid
Met	Methionine
MOPS	3-(N-morpholino)propanesulfonic acid

MPAA	4-mercaptophenylacetic acid
MS	Mass spectrometry
MT	Metallothionein
MTF1	Metal-responsive transcription factor 1
NBD	4-Chloro-7-nitro-1,2,3-benzoxadiazole
NADH	Nicotinamide adenine dinucleotide (reduced)
NCC	Non-ceruplasmin copper
NCL	Native chemical ligation
NGF	Nerve growth factor
NHE	Normal hydrogen electrode
NMR	Nuclear magnetic resonance
NOTA	1,4,7-Triazacyclononane-1,4,7-triacetic acid
NTA	Nitriloacetic acid
Orn	Ornitine
PAM	Peptidylglycine-α-amidating monooxygenase
PB	Phosphate buffer
PBS	Phosphate buffer saline
PD	Parkinson's disease
PET	Photoinduced electron transfer
Phen	1,10-phenantroline
PHP	2-(2-(pyren-1-ylmethylene)hydrazinyl)pyridine
PIPES	Piperazine-N,N′-bis(2-ethanesulfonic acid)
PSA	Pig serum albumin
PyBOP	(Benzotriazol-1-yloxy)tripyrrolidino-phosphonium-hexafluorophosphate
REC	Relative exchangeable copper
RhoB	Rhodamine B
ROS	Reactive oxygen species
RT	Room temperature
RTK	Receptor tyrosine kinase
SCC	Small copper carrier
SEC	Size exclusion cromatography
SOD1	Superoxide dismutase 1
SEA	Bis(2-sulfanylethyl)amino
SPPS	Solid-phase Peptide Synthesis
STEAP	Six-transmembrane epithelial antigen of the prostate
*t*Bu	*tert*-butyl
TCEP	Tris(2-carboxyethyl)phosphine
TEMPOL	4-hydroxy-2,2,6,6-tetramethylpiperidin-1-oxyl
TFA	Trifluoroacetic acid
TGN	Trans Golgi network
THF	Tetrahydrofuran
TIS	Triisopropylsilane
TNBS	2,4,6-Trinitrobenzenesulfonic acid
Trien	Trientine (triethylenetetramine)
Tris	Tris(hydroxymethyl)aminomethane
Trp	Tryptophan
Trt	Trityl
TSC	Thiosemicarbazone
TTM	Tetrathiomolybdate
TYR	Tyrosinase

UV-vis	Ultraviolet-visible
VEGF	Vascular epithelial growth factor
W	Tryptophan
WD	Wilson's disease
XRF	X-ray fluorescence

Résumé

Introduction

Le cuivre (Cu) est un oligoélément essentiel pour la plupart des organismes vivants, qui l'utilisent principalement en tant que cofacteur enzymatique. En effet, grâce à ces propriétés oxydo-réductrices, c'est-à-dire l'aptitude de cet élément à échanger un électron en alternant entre les états redox Cu^{I} et Cu^{II}, les enzymes à Cu accomplissent ainsi des processus biochimiques tels que le transport d'oxygène, le transfert d'électrons, ou encore l'oxydation de substrats organiques. Pourtant, un déficit ou un excès de Cu dans l'organisme peut être toxique. En effet, en présence de dioxygène, l'activité redox du Cu peut entraîner la production d'espèces radicalaires réactives de l'oxygène (nommé ROS et principalement $O_2^{\bullet-}$, H_2O_2, $HO^{\bullet}$), qui à leur tour vont causer des dommages oxydatifs à des biomolécules essentielles (protéines, ADN, lipides, etc.). Enfin, en condition anaérobique, un excès de Cu à l'intérieur la cellule peut aussi être toxique, en substituant par exemple un autre métal comme le fer dans un *cluster* Fe-S de protéine. Pour faire face à la toxicité potentielle du Cu, l'homéostasie du Cu est finement régulée dans l'organisme par un système comprenant plusieurs transporteurs membranaires et navettes intra- et extracellulaires du Cu. Ces transporteurs (notamment extracellulaire à Cu^{II} comme l'albumine dans le sang et intracellulaire à Cu^{I} comme les metallo-chaperonnes tels que CCS, Atox1 et Cox17) ont la propriété d'être des ligands redox-inerte qui stabilisent le Cu^{II} au niveau extracellulaire et Cu^{I} au niveau intra-cellulaire, ils assurent ainsi le transport du Cu jusqu'aux endroits ciblés (organes, organelles ou enzymes).[1,2] Par conséquent, une modification génétique de deux transporteurs protéiques membranaires du Cu (ATP7A et ATP7B) est responsable des maladies de Menkes et Wilson entrainant respectivement une déficience ou une accumulation de Cu dans l'organisme. On retrouve aussi une dyshoméostasie du Cu associés aux maladies neurodégénératives d'Alzheimer et Parkinson ou à des cancers.[3,4] C'est pourquoi, les recherches actuelles dans ce domaine s'orientent de plus à plus vers la mesure spécifique de Cu et sa spéciation dans les milieux biologiques.

Le sang constitue certainement l'échantillon biologique le plus couramment utilisé pour réaliser des analyses biomédicales. Dans ce milieu, l'enzyme Céruloplasmine (Cp) lie la plupart du Cu présent (~70-95% du Cu total) à des sites de liaisons cinétiquement inertes puisqu'enfouis à l'intérieur de la protéine. A l'inverse, le Cu dans le sang peut aussi être cinétiquement labile en se liant à des chélateurs comme l'albumine sérique ou à des acides aminés libres. On parle alors d'une population de Cu dite «échangeable» car cette portion de Cu peut être échangée par des chélateurs thermodynamiquement plus stables.[5] Récemment, l'augmentation de cette population de Cu échangeable dans le sang ou dans l'urine a été proposé comme pouvant être un marqueur diagnostique pour les maladies de Wilson et d'Alzheimer.[6,7]

D'ailleurs, l'accumulation du Cu dans les tissus tumoraux peut être visée comme cible thérapeutique à travers l'utilise de ligands formant de complexe de Cu^{II} pro-oxydants, qui pourrait tuer les cellules grâce à la production de ROS. Notamment, les thiosemicarbazones (TSCs) sont une famille de ligands étudiée comme agents anticancéreux.

Ce travail de thèse a concerné deux axes de recherche, l'un adressé à la conception des sondes luminescent pour la détection du Cu^{II} échangeable dans des échantillons biologiques, et l'autre à la compréhension du mécanisme d'action des complexes Cu^{II}-TSCs comme médicaments anticancéreux.

Conception des sondes luminescentes à Cu^{II}

Pour mesurer la quantité de Cu échangeable dans un échantillon biologique, les méthodes usuelles reposent sur une étape de séparation des deux populations de Cu cinétiquement échangeable et inerte. Cependant il semble difficile de conserver la spéciation native du Cu de l'échantillon menant à des quantifications peu reproductibles.[5] C'est pourquoi l'emploi d'un chélateur sonde (émettant un signal de detection) sélectif du Cu^{II} échangeable serait utile pour réaliser une analyse directe (sans étape de séparation) d'un échantillon biologique. Tenant compte de la faible concentration du Cu dans les liquides biologiques (< 10 µM), les sondes luminescentes apparaissent adaptées pour cette quantification. En effet, grâce à leur grande sensibilité, les sondes luminescentes sont couramment utilisées dans les tests biochimiques d'immunofluorescence ou RT-PCR. Ces dernières peuvent être distinguées en deux familles de sondes dites «à allumages Off/On» (ou «*turn-on*») ou «à extinctions On/Off» (ou «*turn-off*») selon si leur signal est respectivement augmenté ou diminué par l'analyte détecté. En général, les sondes *turn-on* sont préférées aux sondes *turn-off*, car l'extinction de leur luminescence peut aussi être causée par un évènement indirect à la détection de l'analyte comme la dégradation de la sonde, le photoblanchiment du fluorophore ou encore sa faible détection due à l'effet de filtre interne (ou encore nommé « inner filter effect ») engendré par le milieu biologique. Cependant, les sondes luminescentes *turn-on* exploitant une chélation directe du Cu^{II} à un chélateur fluorescent reste complexe à concevoir car ce métal à la propriété d'induire une extinction totale de la fluorescence des chromophores organiques. Plusieurs sondes de types *turn-on* ont néanmoins été mis au point mais elles reposent sur une détection par réactivité chimique du Cu^{II} avec la sonde via des réactions d'hydrolyse, d'oxydation ou de cycloaddition d'alcyne-azoture afin de convertir un substrat non-fluorescent en un fluorophore luminescent. Toutefois, ce type de sonde *turn-on* reste pour la plupart irréversible, empêchant ainsi leur application pour détecter des fluctuations de concentration en Cu^{II} échangeable dans le temps.

Enfin, d'autres critères importants pour la conception de sonde à Cu^{II} sont aussi à considérer pour l'analyse d'échantillons biologiques (urine ou sanguin) comme :

- Une affinité appropriée de la sonde pour retirer le Cu de ses ligands biologiques (par exemple une constante d'affinité à pH 7.4 log $K_{7.4}$ > 13 pour retirer le Cu par l'albumine);
- Une sélectivité de la sonde pour le Cu^{II} face aux autres bio-métaux (en particulier au Zn^{II});
- Une détection de luminescence suffisante pour s'affranchir de l'autofluorescence du milieu biologique.

Pour répondre à ces critères, nous avons développé dans ce travail de thèse des sondes peptidiques luminescentes à lanthanides capables de réaliser une détection *turn-off* de Cu^{II} dans des échantillons biologiques grâce à un motif peptidique naturel, nommé ATCUN (Amino-Terminal Cu^{II} and Ni^{II}-binding), retrouvé sur la partie N-terminale de l'albumine.[8] Ce motif ATCUN de type *Xxx-Zzz-His* (Xxx et Zzz étant un acide aminé sauf une proline pour Zzz) a la particularité de lier sélectivement le Cu^{II} avec une grande affinité (log $K_{7.4}$ ~ 12–15) grâce à sa sphère de coordination

impliquant l'amine N-terminale, deux amidates et l'imidazole d'une histidine placée en troisième position de ce motif (Figure 1).

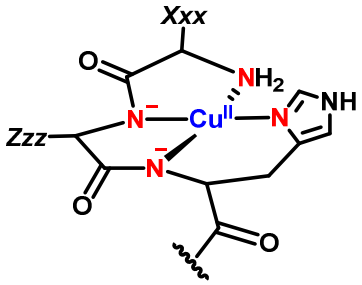

Figure 1. Structure du complexe Cu^{II}-ATCUN. Le Cu^{II} est coordonné par l'amine N-terminale, deux amidates et l'imidazole d'une histidine placée en troisième position de ce motif. *Xxx* et *Zzz* représentent deux acides aminés sauf une proline pour Zzz.

Ce motif a ensuite été combiné à un complexe luminescent de terbium (Tb^{III}) sensible au Cu^{II} qui est excité par effet d'antenne via un fluorophore. Le Tb^{III} a la propriété d'avoir un long temps de vie de luminescence (~ 2 ms) permettant ainsi de réaliser une détection résolue en temps (c'est-à-dire en introduisant un délai entre l'excitation et la détection du signal de luminescence enregistré) afin de s'affranchir de l'autofluorescence du milieu biologique. Enfin, nous avons perfectionné cette même sonde en la rendant ratiométrique grâce à l'introduction supplémentaire d'un complexe de Eu^{III} de référence peu sensible à la détection du Cu^{II} afin d'obtenir une meilleure quantification de la sonde et du Cu^{II} mesuré dans des échantillons d'urine.

Etudes sur la réactivité de complexes Cu^{II}-TSCs dans les milieux biologiques

Les TSCs, comme la Triapine (3AP) et le Dp44mT, ont longtemps été étudiés en tant que potentiels médicaments anticancéreux (Figure 2).[9] Ces molécules sont des ligands tridents qui forment des complexes 1:1 (géométrie plan carré) avec du Cu^{II} mais aussi des complexes 1:2 (géométrie octaédrique) avec le Fe et le Zn^{II}.

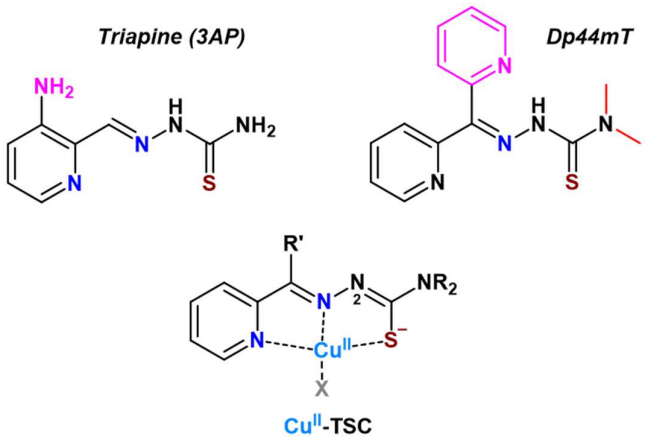

Figure 2. Structures de Triapine et Dp44mT et d'un complexe Cu^{II}-TSC.

L'activité cytotoxique de la 3AP est à la fois associée à l'inhibition de l'enzyme à fer ribonucléotide réductase (RNR) par chélation du fer ainsi qu'à une production de ROS par ce complexe. Par ailleurs, le ligand Dp44mT et d'autres dérivés de la 3AP ont aussi montré un synergisme possible avec le Cu^{II} et une cytotoxicité beaucoup plus élevée que la 3AP. C'est

pourquoi la production de ROS par des complexes Cu^{II}-TSCs a été proposé comme faisant partie du mécanisme de cytotoxicité du Dp44mT.[10]

Dans ce travail de thèse nous avons cherché à évaluer par spectroscopie d'absorption et spectroscopie RPE (résonance paramagnétique électronique) la possibilité des TSCs (tels que la 3AP et le Dp44mt) à lier du Cu^{II} dans le sang, notamment en présence de l'albumine sérique. En outre, afin de mieux comprendre la différence de cytotoxicité entre 3AP et Dp44mT, nous avons comparé leur taux de production de ROS à différents pH (cytosolique à pH 7.4 et lysosomale à pH 5).

Résultats et discussions

Conception des sondes luminescentes à Cu^{II}

Parmi les sondes luminescentes de type *turn-on* à Cu^{II} présentées dans la littérature, le composé (2-(2-(pyren-1-ylméthylène)hydrazinyl)pyridine) (nommé PHP, log $K = 4$ pour le Cu^{II}) a été décrit comme une sonde *turn-on* réversible en présence d'H_2O/MeCN (Figure 3A).[11] Dans la première partie de ce travail de thèse nous avons cherché à mieux comprendre le mécanisme de fonctionnement de cette sonde fluorescente en étudiant sa réactivité en présence de Cu^{II} par spectroscopie d'absorption UV-visible et par fluorescence. Nous avons observé que l'ajout du Cu^{II} en présence de PHP cause bien un déplacement de la bande d'absorption (de 387 nm à 346 nm) et une augmentation de fluorescence à 385 nm (Figure 3B, C).

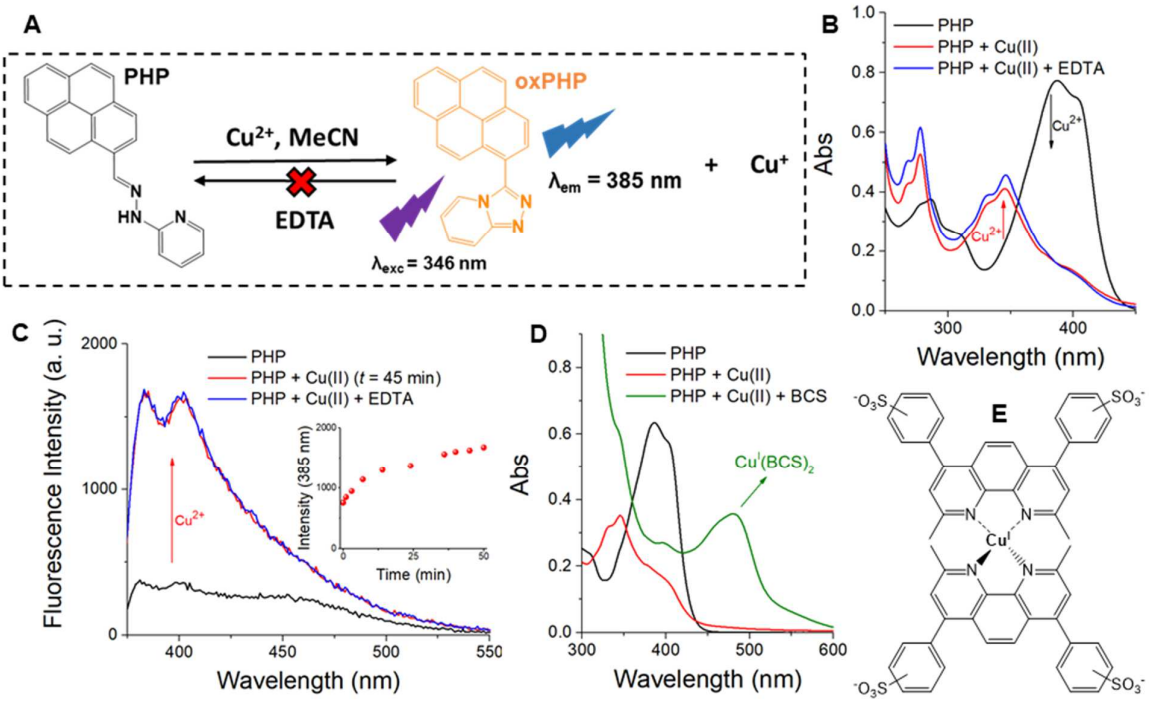

Figure 3. Interaction de la sonde PHP avec le Cu^{II}. A) Schéma du mécanisme de détection; B) Suivi de la réaction par spectroscopie d'absorption; C) Suivi de la réaction par fluorescence (λ_{exc} = 346 nm); D) Détection du Cu^{I} par BCS à la suite de la réaction entre le PHP et le Cu^{II}. E) Structure du complexe $Cu^{I}(BCS)_2$. Conditions expérimentales : B) [PHP] = 20 µM, [Cu^{II}] = 25 µM, [EDTA] = 40 µM ; C) [PHP] = 10 µM, [Cu^{II}] = 20 µM, [EDTA] = 20 µM ; D) [PHP] = 20 µM, [Cu^{II}] = 25 µM, [BCS] = 100 µM. Solvant: MeCN:HEPES 25 mM 1:1.

Pour autant, afin de tester la réversibilité de cette sonde, l'addition d'un chélateur plus fort comme l'EDTA (log $K_{7.4}$ = 15.9) n'entraine pas de changements spectroscopiques significatifs (Figure 3B, C) tendant à montrer le caractère irréversible de cette sonde.

Par ailleurs, lors de l'interaction de la sonde PHP avec le Cu^{II}, la formation de Cu^{I} a été mise en évidence par l'ajout d'un indicateur spécifique (BCS, bathocuproïne disulfonate, Figure 3D, E), ce qui a suggéré qu'une réaction d'oxydoréduction entre le PHP et le Cu^{II} devait avoir lieu. Une analyse approfondie du milieu de titrage par l'analyse HPLC-MS a montré la formation d'un produit majoritaire, qui après isolement et caractérisation par de nombreuses techniques (UV-vis, fluorescence, RMN et spectrométrie de masse) correspond en réalité à une oxydation irréversible du PHP en un composé fluorescent responsable de l'effet *turn-on* observé en présence de Cu^{II} (Figure 3A). Enfin, nous avons aussi remarqué que cette réaction d'oxydation du PHP nécessite du MeCN en tant que stabilisateur du Cu^{I} formé et reste inefficace en présence du peptide antioxydant glutathion (GSH), abondant dans nos cellules, qui réduit et lie le Cu^{I} de manière plus efficace que le PHP. Ces éléments démontrent que cette sonde PHP pourra difficilement fonctionner pour la détection de Cu^{II} dans un milieu biologique.

D'autres exemples de sondes *turn-on* supposées réversibles utilisant d'autres chélateurs ont aussi été reportées pour détecter le Cu^{II} même si dans la plupart des cas les preuves expérimentales sur leur réversibilité sont absentes ou peu détaillé.[5] La similarité structurelle et réactionnelle de ces sondes au PHP suggère qu'elles pourraient partager le même mécanisme de fonctionnement et donc être également irréversibles.

Dans une seconde partie de ce travail de thèse, nous nous sommes intéressés à la conception de sondes réversibles luminescentes *turn-off* à lanthanide (Ln^{III}) basées sur le motif peptidique ATCUN pour la détection de Cu^{II} en milieu biologique.

La première sonde réalisée, $GNH^{W/Tb}$, est composée du motif peptidique ATCUN de séquence GNH, d'un complexe Tb^{III}(DOTA) greffé en chaîne latérale d'une lysine et d'un tryptophane utilisé comme antenne pour sensibiliser le Tb^{III} (Tableau 1).

Tableau 1. Séquences peptidiques des sondes développées

SONDE	SEQUENCE PEPTIDIQUE
$GNH^{W/Tb}$	Gly-Asn-His-Trp-$Lys^{Tb(DOTA)}$-Gly-Lys-NH_2
$AHH^{W/Tb}$	Ala-His-His-Trp-$Lys^{Tb(DOTA)}$-Gly-Lys- NH_2
$AHH^{Cs124/Tb-Eu}$	Ala-His-His-Glu^{Cs124}-$Dap^{Tb(DOTA)}$-Ala-Ala-$(Pro)_6$-Glu^{Cs124}- $Dap^{Eu(DOTA)}$-Lys-NH_2

Le mécanisme de détection de cette sonde à lanthanide fonctionne sur l'excitation indirecte du complexe de Tb^{III} par effet d'antenne ici joué par le tryptophane (antenne) qui une fois excité (à 280 nm) dans son état triplet transfert son énergie vers un état excité du Tb^{III} qui par la suite pourra se désexciter en émettant à plusieurs longueurs d'onde, notamment à 487, 545, 586 et 623 nm (Figure 4A). Lors de la liaison du Cu^{II} au motif ATCUN, la présence du métal entraine une extinction de la fluorescence du tryptophane diminuant ainsi l'efficacité de transfert d'énergie au Tb^{III} engendrant aussi son extinction (Figure 4B). Par la suite, nous avons vérifié la sélectivité de cette sonde pour le Cu^{II} en présence de différents métaux (Figure 4C), de plus cette sonde a montré une limite de détection du Cu^{II} égale à 0.56 µM (utilisant fente d'excitation égale à 4 nm et fente d'émission égale à 3 nm) qui apparait appropriée pour mesurer du Cu^{II} échangeable dans le sang (0.6–1.2 µM). Afin d'illustrer la propriété de détection de luminescence en temps résolue de cette sonde, nous l'avons testé dans un milieu biologique de culture bactérienne (LB) qui donne une forte autofluorescence à la longueur d'onde d'excitation du tryptophane. Dans ce cas, la

luminescence du lanthanide ne peut pas être détectée (Figure 4D), sauf en introduisant un délai de temps (0.1 ms) entre l'excitation du tryptophane et la détection de luminescence du Tb^{III} permettant ainsi de supprimer l'autofluorescence du milieu, ce qui témoigne de l'avantage donné par le long temps de vie (~ 2 ms) de luminescence du Tb^{III} (Figure 4D, E).[12]

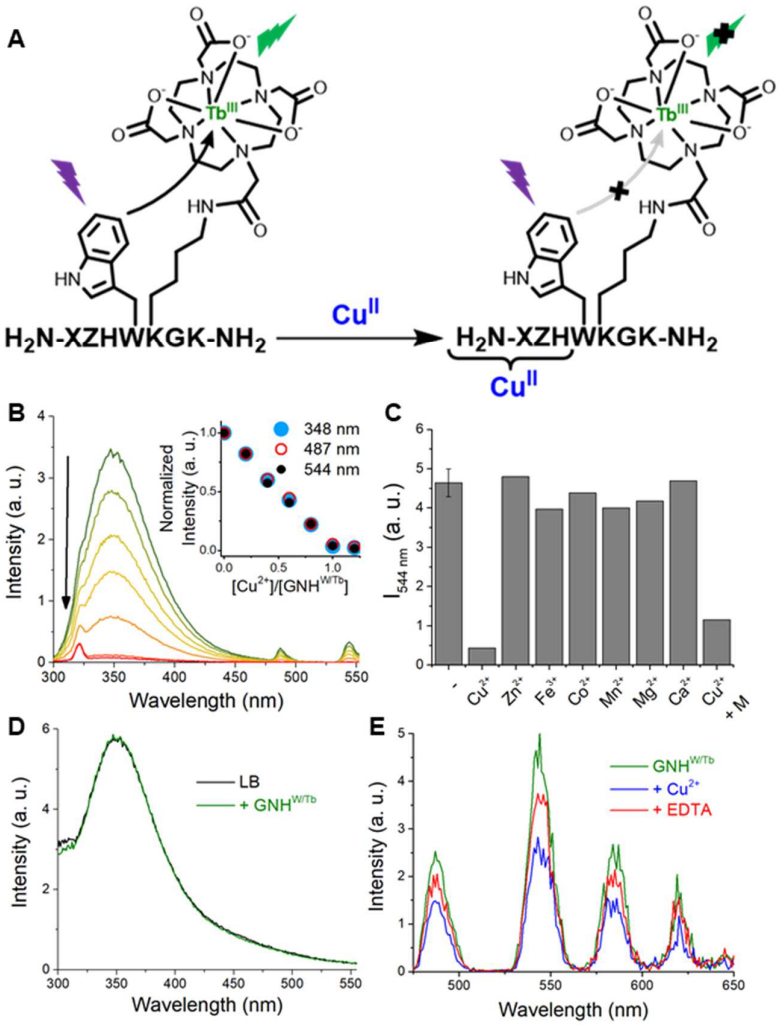

Figure 4. Caractérisation de la sonde $GNH^{W/Tb}$. A) Schéma du mécanisme de détection; B) Extinction de la fluorescence du Trp et de la luminescence du Tb^{III} par le Cu^{II}; C) Sélectivité de la sonde pour le Cu^{II} par rapport aux autres bio-métaux; D) Fluorescence de la sonde dans le milieu LB (λ_{exc} = 280 nm); E) Détection résolue dans le temps (délai = 0.1 ms) de la sonde dans le milieu LB. Conditions expérimentales : B) $[GNH^{W/Tb}]$ = 10 µM, $[Cu^{II}]$ = 10 µM, HEPES 100 mM, pH 7.4; C) $[GNH^{W/Tb}]$ = 10 µM, $[Cu^{II}]$ = $[Zn^{II}]$ = $[Fe^{III}]$ = $[Co^{II}]$ = $[Mn^{II}]$ = 10 µM, $[Mg^{II}]$ = $[Ca^{II}]$ = 2 mM, HEPES 100 mM, pH 7.4; D, E) $[GNH^{W/Tb}]$ = $[Cu^{II}]$ = 10 µM, [EDTA] = 100 µM, milieu LB 10%.

La chélation du Cu^{II} et donc le temps de réponse de cette sonde se sont cependant montrés assez lent en milieu biologique, en raison d'autres ligands du Cu^{II} potentiellement compétiteurs pouvant être présents. Afin d'améliorer la rapidité de chélation de la sonde, une variante de cette sonde, nommée $AHH^{W/Tb}$, a été réalisée en changeant la séquence du motif ATCUN GNH en AHH comprenant deux histidines. En effet, cette séquence possède une vitesse d'échange de Cu^{II} supérieure au motif ATCUN classique.[13] Nous avons alors comparé la cinétique de transfert du Cu^{II} dans différents milieux biologiques (albumine, sérum fetal bovin, milieu de culture LB)

relativement aux deux sondes $GNH^{W/Tb}$ et $AHH^{W/Tb}$ en regardant l'extinction de luminescence du Tb^{III} à 545 nm. La cinétique de capture du Cu^{II} s'est effectivement avérée plus rapide pour le peptide $AHH^{W/Tb}$ dans les différents milieux (Figure 5A, B, C), y compris sa vitesse de relargage du Cu^{II} en présence d'EDTA (Figure 5D) en suivant l'augmentation de fluorescence du Trp des sondes à 360 nm.[14] Par conséquent, le motif ATCUN AHH a été utilisé pour les sondes développées dans la suite de cette étude.

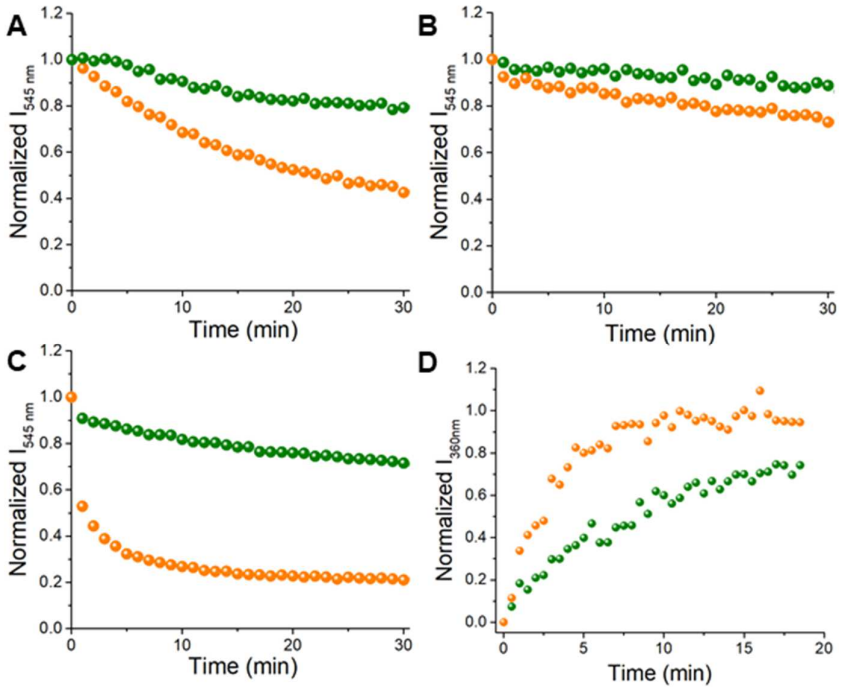

Figure 5. Cinétique de transfert de Cu^{II} par les sondes $GNH^{W/Tb}$ (vert) et $AHH^{W/Tb}$ (orange). A) Transfert du Cu^{II} par l'albumine aux sondes; B) Liaison du Cu^{II} dans le sérum fetal bovin; C) Liaison du Cu^{II} dans le milieu LB; D) Relargage du Cu^{II} par les sondes à l'EDTA. Conditions expérimentales: $[GNH^{W/Tb}] = [AHH^{W/Tb}] = 10$ µM, $[Cu^{II}] = 9$ µM, [HSA] = 10 µM (A), [EDTA] = 10 mM (D), HEPES 100 mM pH 7.4 (A,B), sérum fetal bovin 10% (B), milieu LB 10% (C).

Même si les deux sondes *turn-off* $GNH^{W/Tb}$ et $AHH^{W/Tb}$ possèdent de bonnes propriétés d'affinité, de cinétiques d'échange du Cu^{II} et de réversibilité, leur application pour des analyses quantitatives est limitée du fait de leur comportement *turn-off* car le signal de la sonde dépend à la fois de la concentration du Cu^{II} à mesurer dans l'échantillon et de la concentration de la sonde elle-même.

Afin de surmonter ce problème, nous avons développé des sondes ratiométriques en incorporant sur la sonde précédente $AHH^{W/Tb}$ un second couple antenne/complexe lanthanide à europium, Eu^{III}, qui sert de référence interne en émettant un signal de luminescence (bandes d'émission à 580, 593, 615, 653, 690 et 701 nm) peu sensible à l'influence du Cu^{II} lié à la sonde. Pour ce faire, un couple antenne/complexe de l'Eu^{III} a été placé de façon éloigné du site ATCUN AHH via un *linker* espaceur peu flexible composé de poly-prolines censé se replier en hélice poly-proline.[15] La synthèse de ce type de sondes ratiométriques à deux lanthanides (Tb^{III} et Eu^{III}) a nécessité la mise en place d'une stratégie d'assemblage par ligation chimique native de fragments peptidiques comprenant chacun un lanthanide.[16] Enfin, nous avons optimisé ces sondes en étudiant plusieurs types d'antennes pour sensibiliser simultanément le Tb^{III} ou Eu^{III} tout en regardant l'influence de la longueur de l'hélice poly-proline afin de limiter l'extinction de luminescence du complexe

l'Eu^{III} par la chélation du Cu^{II} à la sonde. La sonde ratiométrique finalisée, nommée $AHH^{Cs124/Tb-Eu}$, utilise deux couples antennes Carbostyril 124 (Cs124)/Tb^{III}(DOTA) ou Eu^{III}(DOTA) séparés par un motif espaceur de six prolines (Figure 6A).

Avantageusement, le Cs124 peut être excité à une longueur d'onde supérieure à celle du tryptophane (330 nm), ce qui favorise l'application de cette sonde dans des milieux comme l'urine et le sérum présentant une forte absorption au-dessous de ~300 nm limitant ainsi une excitation efficace d'une antenne tryptophane.

L'efficacité de la réponse de cette sonde ratiométrique pour détecter le Cu^{II} a été démontrée par extinction totale de luminescence du Tb^{III} tout en conservant un signal d'émission de l'Eu^{III} partiellement éteint (~50%) en présence d'un équivalent de Cu^{II} lié (Figure 6B).

Enfin, cette sonde ratiométrique $AHH^{Cs124/Tb-Eu}$ a pu détecter le Cu^{II} dans des échantillons d'urines issus de rats à modèle de la maladie de Wilson (excédentaire en Cu^{II} et préalablement traités par le chélateur détoxifiant D-Pen avant recueil d'urine). Notamment, l'échantillon d'urine du groupe de rats traité avec le chélateur a montré un signal de luminescence du Tb^{III} plus bas, donc une quantité de Cu^{II} plus élevée dans les urines excrétées, en comparaison de l'échantillon d'urine de rat du groupe contrôle (non traité) pour un signal de luminescence d'Eu^{III} constant dans les deux cas (Figure 6C).

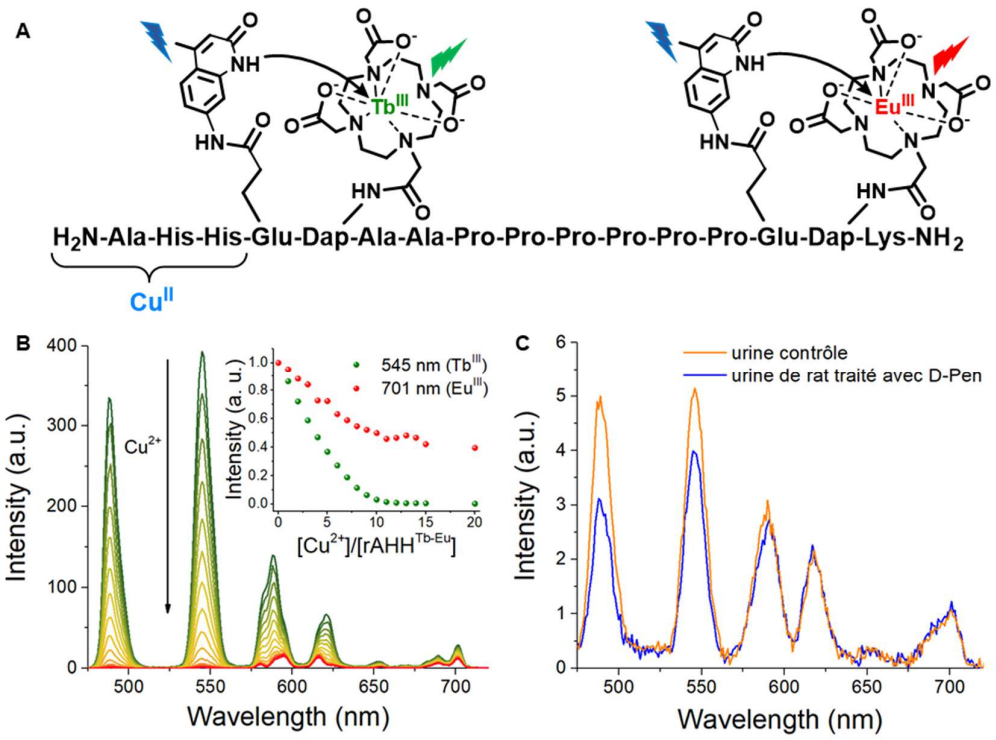

Figure 6. Caractérisation de la sonde $AHH^{Cs124/Tb-Eu}$. A) Structure schématique de la sonde; B) Extinction de la luminescence par titrage avec Cu^{II}; C) Détection du Cu^{II} dans l'urine de rats. Conditions expérimentales: B) [$AHH^{Cs124/Tb-Eu}$] = 10 µM, HEPES 100 mM, pH 7.4; C) [$AHH^{Cs124/Tb-Eu}$] = 10 µM, urine 10%.

Etudes sur la réactivité de complexes Cu^{II}-TSCs dans les milieux biologiques

Pour évaluer la stabilité des complexes de Cu^{II}-TSC dans le sang, des spectres RPE de ces complexes en présence d'albumine sérique humaine (HSA) ont été enregistrés. La Figure 7 montre que pour le ligand 3AP comme pour le ligand Dp44mT, le spectre RPE du mélange HSA-Cu^{II}-TSC (bleu) ressemble à celui du complexe Cu^{II}-TSC (rouge) mais apparait décalé pour des valeurs de *g* plus faibles. Ce résultat suggère qu'un complexe ternaire se forme entre le Cu^{II}-TSC et l'albumine. Notamment, l'expérience contrôle du complexe ternaire TSC-Cu^{II}-Imidazole (vert) montre que son spectre RPE est superposable à celui du spectre RPE du mélange HSA-Cu^{II}-TSC, ce qui signifierait que la protéine HSA lie probablement le Cu^{II} via la chaine latérale d'une histidine.

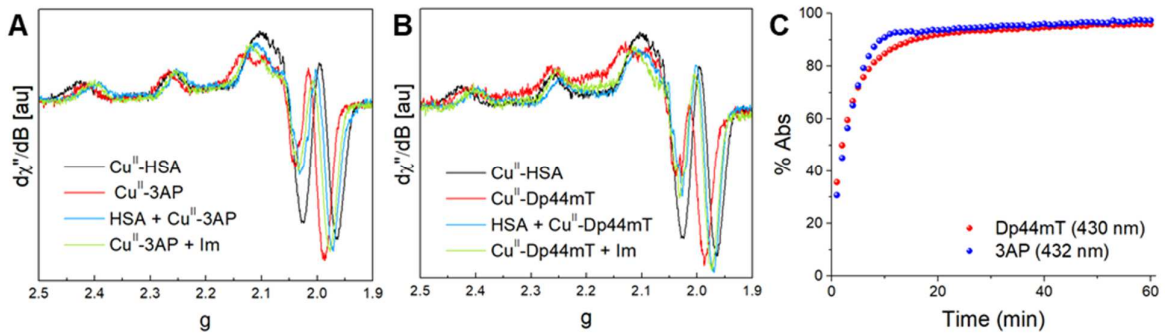

Figure 7. Réactivité de complexes Cu^{II}-TSCs vis-à-vis de l'albumine sérique étudiée par spectroscopie RPE (A, B) et d'absorption UV-vis (C). Conditions expérimentales: A, B) [TSC] = 300 µM, [Cu^{II}] = 250 µM, [HSA] = 300 µM, HEPES 50 mM pH 7.4 (DMSO ~5%), glycérol 10% (v/v), T = 100 K ; C) [TSC] = 10 µM, [Cu^{II}] = 9 µM, [HSA] = 100 µM, [TSC] = 10 µM, [Cu^{II}] = 10 µM, [HSA] = 100 µM, HEPES 500 mM pH 7.4 (DMSO 1%). T = 37 °C.

De plus, nous avons effectué un suivi par spectroscopie d'absorption de la réaction du complexe Cu^{II}-HSA vis-à-vis des ligands 3AP et Dp44mT grâce aux bandes d'absorption caractéristiques des complexes Cu^{II}-TSCs (à 422 nm pour 3AP et 412 nm pour Dp44mT).[17] Lors de l'ajout des ligands TSCs au complexe Cu^{II}-HSA nous avons observé la croissance de bandes d'absorption à environ 430 nm (Figure 7C). Ce déplacement bathochrome de la bande des complexes Cu^{II}-TSCs suggère que le Cu^{II} est transféré de l'albumine aux TSCs en formant un complexe ternaire. En particulier, la majorité du Cu^{II} est transférée en moins de 20 min à 37 °C.

En définitive, ces résultats tendent à montrer que les ligands TSCs 3AP et Dp44mT ont la capacité d'extraire le Cu^{II} de l'albumine en formant avec cette proteine un complexe ternaire stable .

Enfin, nous avons mesuré la capacité des complexes Cu^{II}-3AP et Cu^{II}-Dp44mT à produire des ROS en présence de GSH à pH cytosolique (7.4) ou à pH lysosomale (5). En effet, le Dp44mT semble être accumulé avec le Cu^{II} dans les lysosomes des cellules déclenchant ainsi l'action cytotoxique.[10] Le radical nitroxyle TEMPOL a été utilisé pour capturer les ROS produites, ce qui a pour effet d'éteindre le signal RPE du TEMPOL (Figure 8).

A pH 7.4, le complexe Cu^{II}-Dp44mT (rouge) s'est révélé être nettement plus actif pour la production de ROS que le complexe Cu^{II}-3AP (blue), dont l'activité est comparable au Cu^{II} « libre » (noir). Cela peut être expliqué par le fait que le complexe de Cu^{II} avec le 3AP est

rapidement réduit et dissocié par le GSH pour former un complexe de Cu^{I}-$(GS)_x$, alors que le Dp44mT forme lui un complexe ternaire assez stable avec le Cu^{II} et le GSH.[17]

A pH 5, les deux complexes Cu^{II}-TSCs, mais plus particulièrement le Cu^{II}-Dp44mT, ont montré une activité remarquablement plus haute qu'à pH 7.4, alors que le Cu^{II} « libre », comme attendu, montre une plus faible activité. En effet, la coordination et la réduction du Cu^{II} en Cu^{I} par le GSH implique la déprotonation de ce dernier normalement favorisée à plus haut pH.

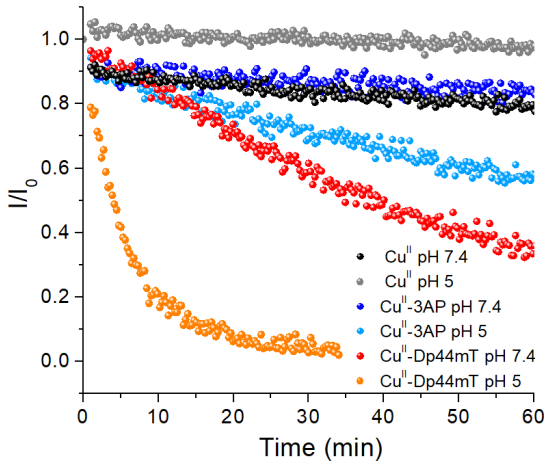

Figure 8. Disparition du signal du TEMPOL à la suite de la réaction avec les ROS produit par les complexes Cu^{II}-TSC en présence de GSH. Conditions expérimentales: [Cu^{II}] = 27 µM, [TSC] = 30 µM, [GSH] = 3 mM, [TEMPOL] = 20 µM, HEPES 100 mM pH 7.4 or MES 100 mM pH 5 (DMSO 3%).

On peut ainsi faire l'hypothèse qu'une plus grande protonation du TSC puisse causer l'effet observé à bas pH. En effet, la protonation de l'azote du groupe hydrazinique transforme le groupement thiolate en groupement thione ce qui a pour effet de réduire l'affinité du TSC pour le Cu^{II} facilitant ainsi la réduction du Cu^{II} par le GSH et par conséquent la production de ROS.

Conclusion générale

En conclusion, ce travail de thèse s'est intéressé, d'un coté, à la problématique de conception de sonde *turn-on* ou *turn-off* pour la détection et au dosage du Cu^{II} en milieu biologique et, de l'autre, à la réactivité des ligands anticancéreux vis-à-vis de l'albumine sérique et du GSH.

Nous avons développé une série de sondes luminescentes *turn-off* à lanthanides réversibles et spécifiques basées sur le motif peptidique naturel ATCUN. En particulier, grâce à ce motif nous avons montré la bonne sélectivité et l'affinité de ces sondes pour la detection de Cu^{II}. De plus, l'apport d'un complexe luminescent de Tb^{III} à long temps de vie (~ 2 ms) a permis de faire une détection de luminescence résolue en temps afin de s'affranchir de l'autofluorescence du milieu biologique lors de la détection. Enfin, le perfectionnement de ces sondes luminescentes en version ratiométriques avec deux complexes de lanthanides Tb^{III} et Eu^{III} permet maintenant de mieux contrôler à la fois la concentration de la sonde présente et de réaliser la detection de Cu^{II}. En perspectives de ces travaux, des futures optimisations de ces sondes pour la détection dans des milieux biologiques complexes comme le plasma sanguin reste à envisager.

Par ailleurs, nous avons montré que les thiosemicarbazones pourraient être capables de lier le Cu^{II} dans le sang et former ainsi des complexes ternaires avec l'albumine, ce qui pourrait moduler leur biodisponibilité dans l'organisme. De plus, nous avons aussi mis en évidence que le Dp44mT produit plus de ROS que la 3AP en présence de Cu^{II} et de GSH, justifiant ainsi sa plus grande cytotoxicité. Enfin, nous avons étudié l'influence du pH sur les complexes Cu^{II}-TSC pour la production de ROS. Nos résultats montrent un taux de production de ROS qui augmente en diminuant le pH de 7.4 à 5, ce qui apparait intriguant d'après le mécanisme de réaction supposé. Des études complémentaires restent à effectuer afin de mieux comprendre ce phénomène.

Références

(1) Festa, R. A.; Thiele, D. J. Copper: An Essential Metal in Biology. Curr. Biol. 2011, 21 (21), R877–R883. https://doi.org/10.1016/j.cub.2011.09.040.

(2) Macomber, L.; Imlay, J. A. The Iron-Sulfur Clusters of Dehydratases Are Primary Intracellular Targets of Copper Toxicity. Proc. Natl. Acad. Sci. U. S. A. 2009, 106 (20), 8344–8349. https://doi.org/10.1073/pnas.0812808106.

(3) Hordyjewska, A.; Popiołek, Ł.; Kocot, J. The Many "Faces" of Copper in Medicine and Treatment. BioMetals 2014, 27 (4), 611–621. https://doi.org/10.1007/s10534-014-9736-5.

(4) Falcone, E.; Ahmed, I. M. M.; Oliveri, V.; Bellia, F.; Vileno, B.; El Khoury, Y.; Hellwig, P.; Faller, P.; Vecchio, G. Acrolein and Copper as Competitive Effectors of α-Synuclein. Chem. - A Eur. J. 2020, 26 (8), 1871–1879. https://doi.org/10.1002/chem.201904885.

(5) Falcone, E.; Okafor, M.; Vitale, N.; Raibaut, L.; Sour, A.; Faller, P. Extracellular Cu2+ Pools and Their Detection: From Current Knowledge to next-Generation Probes. Coord. Chem. Rev. 2021, 433, 213727. https://doi.org/10.1016/j.ccr.2020.213727.

(6) El Balkhi, S.; Trocello, J. M.; Poupon, J.; Chappuis, P.; Massicot, F.; Girardot-Tinant, N.; Woimant, F. Relative Exchangeable Copper: A New Highly Sensitive and Highly Specific Biomarker for Wilson's Disease Diagnosis. Clin. Chim. Acta 2011, 412 (23–24), 2254–2260. https://doi.org/10.1016/j.cca.2011.08.019.

(7) Squitti, R.; Ghidoni, R.; Simonelli, I.; Ivanova, I. D.; Colabufo, N. A.; Zuin, M.; Benussi, L.; Binetti, G.; Cassetta, E.; Rongioletti, M.; Siotto, M. Copper Dyshomeostasis in Wilson Disease and Alzheimer's Disease as Shown by Serum and Urine Copper Indicators. J. Trace Elem. Med. Biol. 2018, 45, 181–188. https://doi.org/10.1016/j.jtemb.2017.11.005.

(8) Gonzalez, P.; Bossak, K.; Stefaniak, E.; Hureau, C.; Raibaut, L.; Bal, W.; Faller, P. N-Terminal Cu-Binding Motifs (Xxx-Zzz-His, Xxx-His) and Their Derivatives: Chemistry, Biology and Medicinal Applications. Chem. - A Eur. J. 2018, 24 (32), 8029–8041. https://doi.org/10.1002/chem.201705398.

(9) Heffeter, P.; Pape, V. F. S.; Enyedy, É. A.; Keppler, B. K.; Szakacs, G.; Kowol, C. R. Anticancer Thiosemicarbazones: Chemical Properties, Interaction with Iron

Metabolism, and Resistance Development. Antioxidants Redox Signal. 2019, 30 (8), 1062–1082. https://doi.org/10.1089/ars.2017.7487

(10) Lovejoy, D. B.; Jansson, P. J.; Brunk, U. T.; Wong, J.; Ponka, P.; Richardson, D. R. Antitumor Activity of Metal-Chelating Compound Dp44mT Is Mediated by Formation of a Redox-Active Copper Complex That Accumulates in Lysosomes. *Cancer Res.* **2011**, *71* (17), 5871–5880. https://doi.org/10.1158/0008-5472.CAN-11-1218.

(11) Venkatesan, P.; Wu, S. P. A Turn-on Fluorescent Pyrene-Based Chemosensor for Cu(II) with Live Cell Application. RSC Adv. 2015, 5 (53), 42591–42596. https://doi.org/10.1039/c5ra05440k.

(12) Falcone, E.; Gonzalez, P.; Lorusso, L.; Sénèque, O.; Faller, P.; Raibaut, L. A Terbium(III) Luminescent ATCUN-Based Peptide Sensor for Selective and Reversible Detection of Copper(II) in Biological Media. Chem. Commun. 2020, 56 (35), 4797–4800. https://doi.org/10.1039/d0cc01007c.

(13) Gonzalez, P.; Vileno, B.; Bossak, K.; El Khoury, Y.; Hellwig, P.; Bal, W.; Hureau, C.; Faller, P. Cu(II) Binding to the Peptide Ala-His-His, a Chimera of the Canonical Cu(II)-Binding Motifs Xxx-His and Xxx-Zzz-His. Inorg. Chem. 2017, 56 (24), 14870–14879. https://doi.org/10.1021/acs.inorgchem.7b01996.

(14) Falcone, E.; Vileno, B.; Hoang, M.; Raibaut, L.; Faller, P. A Luminescent ATCUN Peptide Variant with Enhanced Properties for Copper(II) Sensing in Biological Media. J. Inorg. Biochem. 2021, 221, 111478. https://doi.org/10.1016/j.jinorgbio.2021.111478.

(15) Zhang, D. Y.; Azrad, M.; Demark-Wahnefried, W.; Frederickson, C. J.; Lippard, S. J.; Radford, R. J. Peptide-Based, Two-Fluorophore, Ratiometric Probe for Quantifying Mobile Zinc in Biological Solutions. ACS Chem. Biol. 2015, 10 (2), 385–389. https://doi.org/10.1021/cb500617c.

(16) Cepeda, C.; Raibaut, L.; Fremy, G.; Eliseeva, S. V.; Romieu, A.; Pécaut, J.; Boturyn, D.; Petoud, S.; Sénèque, O. Using Native Chemical Ligation for Site-Specific Synthesis of Hetero-Bis-Lanthanide Peptide Conjugates: Application to Ratiometric Visible or Near-Infrared Detection of Zn2+. Chem. - A Eur. J. 2020, 26 (59), 13476–13483. https://doi.org/10.1002/chem.202002708.

(17) Santoro, A.; Vileno, B.; Palacios, Ò.; Peris-Díaz, M. D.; Riegel, G.; Gaiddon, C.; Krężel, A.; Faller, P. Reactivity of Cu(II)-, Zn(II)- and Fe(II)-Thiosemicarbazone Complexes with Glutathione and Metallothionein: From Stability to Dissociation to Transmetallation. Metallomics 2019, 11 (5), 994–1004. https://doi.org/10.1039/c9mt00061e.

1. Introduction

1.1 Metals in biology

Although nonmetal elements, namely O, C, H, N, P and S, account for more than 99% of the atoms in a human body, several metal ions are also essential to life. In humans, Ca is the most abundant metal element, as it is a fundamental bone component and second messenger, while Na and K are well-known electrolytes, and Mg serves mainly as an enzyme cofactor. Besides such "bulk elements", trace metals such as Fe, Zn and Cu are required in very low amounts (see Table 1). Nevertheless, they are momentous to the maintenance of life. Indeed, Fe and Cu are versatile redox-active enzyme cofactors, while Zn serves mainly as Lewis acid. Finally, humans do also need Mn, Co and Mo as co-factors of important enzymes, such as SOD2, methionine synthase and xanthine oxidase, respectively.[1]

Table 1. Amount of essential metal elements in the human body (average body weight of 70 Kg).[1]

Element	Amount (g)
Ca	1000
K	140
Na	100
Mg	30
Fe	5
Zn	2
Cu	0.1
Mn	0.016
Mo	0.005
Co	0.002

Furthermore, the role of trace metals in biochemical catalysis and the presence of those elements on prebiotic Earth have led to the plausible hypothesis that minerals or even free metal ions might have catalysed prebiotic metabolism and the synthesis of bio-macromolecules such as nucleotides and peptides.[2]

1.2 Copper: *"a veteran covered with glory"* [§]

1.2.1 Chemistry of Cu in aqueous solution: coordination and reactivity

The main oxidation states of Cu, Cu^{I} and Cu^{II}, have $[Ar]3d^{10}$ and $[Ar]3d^{9}$ electronic configurations and hence are diamagnetic and paramagnetic, respectively. In spite of the apparent higher stability of the d^{10} configuration of Cu^{I}, Cu^{II} is the most stable state in aqueous solution, as Cu^{I} is promptly oxidized by dioxygen, or it disproportionates to Cu^{0} and Cu^{II} in anaerobic conditions. Therefore, in order to survive in water, Cu^{I} should be stabilized by suitable ligands and/or co-solvents.

[§] This is how the chemist and writer Primo Levi described Copper in *Zinc,* a tale of *The Periodic Table*.

Once dissolved in water, Cu^{II} salts generate the hexaaquacopper(II) ions, $[Cu(H_2O)_6]^{2+}$, where Cu is coordinated in its typical distorted (axially-elongated) octahedral geometry (D_{4h} symmetry), according to the so-called Jahn-Teller effect (see Fig. 1).[3] Interestingly, such distortion is accountable for the position of Cu^{II} complexes on top of the Irving-Williams series, i.e. for the higher stability of Cu^{II} complexes compared to the other divalent first-row d-metal ions.[4,5]

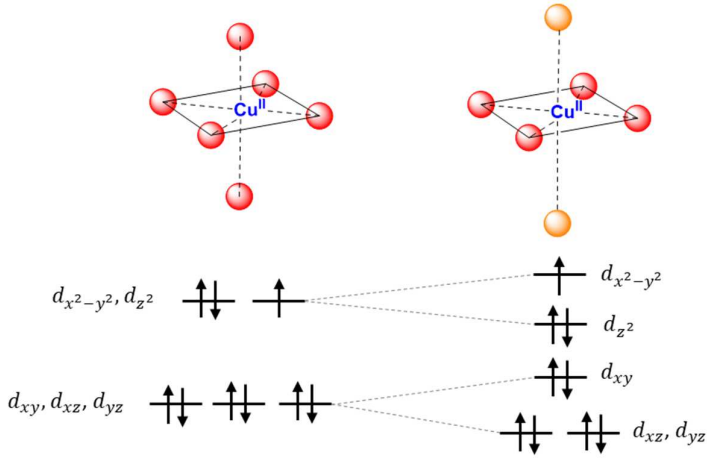

Figure 1. Jahn-Teller effect. Octahedral complexes with unevenly occupied degenerate orbitals undergo a geometrical distortion that stabilizes the system removing the degeneracy. Notably, Cu^{II} complexes typically show an axially-elongated octahedral geometry with four strongly bound equatorial ligands and up to two weakly bound axial ligands.

As the hexaaquacopper(II) has p$K_a \approx 8$, hydrolysis occurs above neutral pH with the formation of the insoluble neutral hydroxide species $Cu(OH)_2$ ($K_{sp} = 1.6 \cdot 10^{-19}$ at 25°C).[6] Likewise, Cu^{I} also forms quite insoluble hydroxide ($K_{sp} = 2 \cdot 10^{-15}$) which in turn dehydrates to cuprous oxide (Cu_2O).

The two Cu oxidation states prefer very different ligands and coordination geometry, which is mainly ascribed to their different hard/soft character and electronic configuration. Indeed, according to Pearson's HSAB (Hard and Soft Acids and Bases) theory, Lewis acids (e.g. metal cations) and bases (e.g. metal ligands) are distinguished in soft or hard basically depending on their charge-to-radius ratio, and a certain base prefers reacting with an acid of its same type (soft-soft or hard-hard).[7] Due to its big ionic radius and low charge, Cu^{I} is classified as soft acid, whereas Cu^{II} shows an intermediate character. As a result, the former prefers binding to soft ligands such as thiolates or thioethers (e.g. cysteine and methionine in proteins), while the latter prefers harder N and O donors (e.g. amines, imidazole, carboxyl group). Besides, as mentioned above, Cu^{II} favourite geometry is substantially square planar, square pyramidal or square bipyramidal depending on the extent of the axial elongation (Jahn-Teller distortion). Instead, Cu^{I} being d^{10}, it does not benefit from any ligand field stabilization energy (LFSE = 0), and hence its preferred geometries, i.e. linear, trigonal or tetrahedral, are limited to low coordination numbers due to steric factors, as soft donors are normally large.[6]

The accessibility of two oxidation states explains the exploitation of Cu by living organisms as a catalyst in electron transfer and redox reactions. However, the reduction potential of the Cu^{II}/Cu^{I} couple ($E° = 0.16$ V) also allows free Cu to catalyse the generation of harmful Reactive Oxygen Species (ROS) in the presence of dioxygen (or H_2O_2) and a suited reductant (see Fig. 2). Notably, ascorbate ($AscH^-$, $E°_{AscH^-/AscH^{\bullet}} = 0.33$ V)[8] and thiols (RSH) are recognized as the most biologically-relevant reducing agents for Cu^{II}, leading to the formation of dehydroascorbic acid or disulfides

(RSSR) via the ascorbyl ($AscH^{\bullet -}$) or thiyl ($RS^{\bullet}$) radicals, respectively. In addition, thiols are excellent ligands for Cu^{I}, and hence Cu^{I}-$(SR)_x$ complexes are often formed upon their reaction. Interestingly, the reaction of Cu^{II} and hydrogen sulfide (H_2S) yields copper sulfide (CuS), which is very insoluble ($K_{sp} = 6 \cdot 10^{-36}$).[6]

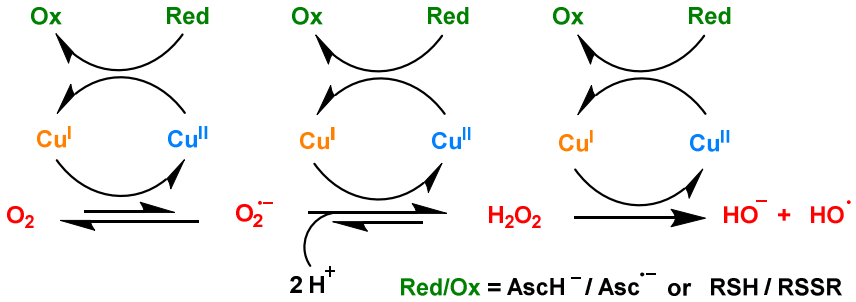

Figure 2. Mechanism of Cu-catalysed ROS production in the presence of dioxygen and a reducing agent (Red) such as $AscH^-$ or a thiol (RSH).

Importantly, coordinating ligands are able to tune the reduction potential of the Cu^{II}/Cu^{I} couple over the whole electrochemical water window, i.e. from – 0.4 to + 0.8 V at pH 7, depending on the relative association constants for the Cu^{II} and Cu^{I} complex. In particular, the reduction potential decreases if the ligand stabilizes Cu^{II} more than Cu^{I} and it increases in the opposite case. Noteworthy, considering the very different coordination preferences of Cu^{II} and Cu^{I}, it is very challenging for Cu complexes to achieve efficient redox cycling. Thus, biological Cu ligands have evolved either to suppress or to optimize the redox cycling as per the need (see section 1.2.4).

Finally, Cu complexes are mostly kinetically labile, i.e. they can undergo ligand-exchange, unless solvent/ligand accessibility is hampered by steric hindrance.

1.2.2 Cu in biological systems

1.2.2.1 An evolutionary perspective

Although mankind has known Cu for thousands of years (as also celebrated by writers and poets), it can be considered a "modern" or "young" bioelement compared to other essential trace metals. Indeed, the primordial atmosphere was reducing as it contained H_2, H_2S, and CH_4 as well as CO_2 and CO. As a result of the likely high concentration of H_2S in the primordial sea (about 1-10 mM) and the reducing conditions, Cu was found in the reduced state in the form of highly insoluble sulfide minerals, and hence it was not bioavailable to early cells. Interestingly, the profile of the cytosolic concentration of "free" transition metals ions mirrors the concentration of such ions in the primordial sea and correlates inversely with the Irving-Williams series. This suggests that the bioavailability of the metal ions in the environment was a fundamental aspect influencing the bioselection of elements by primordial living organisms. Later, the Great Oxygenation Event caused by the early photosynthetic organisms led to an oxidizing environment, and hence to the conversion of S^{2-} to SO_4^{2-}, insoluble Cu^{I} to soluble Cu^{II} and soluble Fe^{II} to insoluble Fe^{III} (in the form of hydroxide). In such an oxidizing environment, Cu^{II} met the biochemical need for a redox catalyst operating in a higher range of redox potential (0-0.8 V) and hence partially replaced, or better complemented, Fe as a biological redox catalyst.[9–12]

However, living organisms had also to cope with the potential toxicity of Cu redox chemistry, evolving complex machinery to handle the metal ion safely (see section 1.2.3). In this regard, it is

curious to observe how cells also tamed the capacity of Cu (bound in the enzyme superoxide dismutase, SOD) to catalyse superoxide ($O_2^{\bullet-}$) dismutation to fight against its very ability to produce the superoxide radical via the Fenton-type reaction.

1.2.2.2 Biological functions of Cu: from redox catalysis to neuromodulation

Cu is involved in many different physiological processes, such as cellular respiration, antioxidant defence, the production of connective tissue, the biosynthesis of neurotransmitters, peptides and pigments, as well as iron homeostasis. From the chemical point of view, all these biological functions are related to similar Cu-mediated electron transfer or redox reactions (see Table 2).

The electron transfer activity is typically encountered in proteins that are involved in energetic metabolism. For instance, Azurin serves as the electron donor to nitrite reductase in the denitrification pathway of some bacteria, Plastocyanin takes part in the photosynthetic electron transport chain between photosystems II and I, and Cu sites in NADH dehydrogenase and cytochrome c oxidase (CCO) are essential to both prokaryotic and eukaryotic respiratory chains.

Besides, the activity of cuproenzymes is closely related to dioxygen biochemistry, i.e. oxidation and oxygenation reactions. As an example, methane monooxygenase catalyses the conversion of methane in methanol, hephaestin oxidizes Fe^{II} to Fe^{III} and galactose oxidase converts the primary alcohol of the sugar in the corresponding aldehyde. Moreover, as mentioned above, the enzyme SOD1 catalyses the dismutation of the cytotoxic $O_2^{\bullet-}$ radical into O_2 and H_2O_2. Noteworthy, Cu is also found in enzymes involved in denitrification, such as N_2O reductase and the above-mentioned nitrite reductase. Finally, another Cu-protein whose function is related to O_2 is hemocyanin, which ensures O_2 transport throughout the body of some mollusc and arthropods.[13]

In addition to its main catalytic functions, an important role of Cu in signalling has been more recently recognized.[14–17] As an example, Cu modulates the binding of ethylene, a key plant hormone, to its receptor (ETR), and seems to mediate the recognition of small organosulfur metal-coordinating odorants by olfactory receptors in mammals.[18–20]

Moreover, Cu^{II} has been shown to stimulate cell proliferation via the interaction with Receptor Tyrosine Kinase (RTK), such as EGFR (epidermal growth factor receptor), and the protein MEK1 which has a key role in the mitogenic MAPK/ERK signalling pathway. In particular, Cu promotes RTK phosphorylation and the following activation of both AKT and MAPK/ERK pathways. MEK1 seems able to bind two Cu ions, which enhance its kinase activity (i.e. ERK1/2 phosphorylation) and in turn cell proliferation.[21–23]

A fundamental role of Cu in angiogenesis (i.e. the growth of blood vessels from pre-existing vessels) has also been recognized. Indeed, Cu interacts directly with several pro-angiogenic factors (e.g. FGF, VEGF and angiogenin) and promotes their secretion and expression.[24,25]

Furthermore, Cu acts as a neuromodulator in the brain. Indeed, calcium-dependent Cu trafficking from neuronal cell bodies to dendrites has been reported.[26] Upon synaptic depolarization, such Cu pool can be then released into the synaptic cleft, where it is estimated to attain about 100 μM concentration. Cu showed inhibitory activity towards neurotransmitter (glutamate, GABA and ATP) receptors.[27–30] In addition, Cu can interact with neurotrophins (e.g. NGF and BDNF) and influence their binding to TrkB and TrkA receptors, respectively.[31–34]

Table 2. Function and localization of human cuproenzymes.

Enzyme	Localization‡	Organ‡	Catalysed Reaction (Function)
Cytochrome C Oxidase (CCO)	Inner Mitochondrial Membrane	Ubiquitous	Reduction of O_2 to H_2O (H^+ translocation)
Superoxide dismutase 1 (SOD1)	Cytosol, Nucleus, Mitochondrial Intermembrane Space	Ubiquitous	Dismutation of $O_2^{\bullet-}$ to O_2 and H_2O_2 (Radical scavenging)
Superoxide dismutase 3 (SOD3)	Secretory pathway/ extracellular space	Ubiquitous	
Hephaestin (Heph)	Plasma membrane	Ubiquitous	Oxidation of Fe^{II} to Fe^{III}
Ceruloplasmin (Cp)	Secretory pathway/ extracellular space	Liver, Brain	
Peptidylglycine-α-amidating monooxygenase (PAM)	Secretory pathway/ extracellular space	Ubiquitous	Biosynthesis of C^{ter}-amidated peptides
Lysyl oxidase (LOX)	Secretory pathway/ extracellular space	Ubiquitous	Oxidation of lysyl amine to aldehyde (collagen cross-linking)
Dopamine β-hydroxylase (DBH)	Secretory pathway/ extracellular space	Brain, Adrenal gland	Hydroxylation of Dopamine to Noradrenaline
Tyrosinase (TYR)	Secretory pathway/ extracellular space	Skin, Retina	Oxidation of Tyrosine to DOPA and DOPA to DOPA-quinone (melanin biosynthesis)
Formylglycine-generating enzyme (FGE)	Endoplasmic reticulum	Ubiquitous	Conversion of cysteine to formylglycine
Amine oxidases (AOC1-3)	Secretory pathway/ extracellular space	Ubiquitous	Oxidation of primary amines to aldehydes

‡ Sources: UniProt database (www.uniprot.org) and The Human Protein Atlas (www.proteinatlas.org)

1.2.2.3 Mechanisms of Cu toxicity

By virtue of its significant roles, a deficiency of Cu appears clearly detrimental for most living organisms. Likewise, a surplus of Cu results to be poisonous. The fundamental mechanisms of such toxicity, though not thoroughly known, are ascribable to some of the above-mentioned chemical properties of Cu ions.

Firstly, the toxicity of excess Cu has been classically and almost exclusively related to its redox activity, notably through the ROS production by Cu^{II} in presence of dioxygen and reductants (see Fig. 2) or via the Fenton reaction of Cu^{I} with H_2O_2, which produces the most dangerous hydroxyl radical ($HO^{\bullet}$). ROS in turn induce oxidative damage on all types of biomolecules (protein, lipids and nucleic acids), whose structure and function is consequently impaired. In addition, redox-based Cu toxicity may arise from abnormal oxidation of protein thiols (cysteines). Likewise, due to its significant affinity to cysteine and histidine residues, excess Cu might inhibit the activity of certain proteins through the binding to essential residues. Such an interaction could also induce protein misfolding and in turn aggregation.

More recently, Cu toxicity has been also observed on bacteria grown under anaerobic conditions, suggesting that other O_2-independent mechanisms do exist. Indeed, thanks to its highest thiophilicity, Cu^I is able to inactivate iron-sulfur (Fe-S) proteins (such as fumarase, isopropylmalate dehydratase, ferredoxin, as well as the Fe-S cluster assembly machinery) via the transmetallation of Fe in solvent-exposed Fe-S clusters. Importantly, this mechanism has been also observed in eukaryotic cells.[35–38]

Very interestingly, our immune system exploits Cu toxicity to fight against bacterial pathogens. Indeed, in macrophages, Cu is pumped into the phagolysosomes where bacteria are sequestered and killed.[39–42]

1.2.3 Cu homeostasis in humans

In order to prevent the potential toxicity of loosely/mis-bound Cu ions, sophisticated machinery is charged with handling and trafficking Cu safely throughout the body.

1.2.3.1 Systemic Cu trafficking

Dietary Cu is mainly absorbed in the small intestine, from which it is then transported to the liver.[43] The latter plays a key role in maintaining systemic Cu homeostasis (see Fig. 3). Indeed, its Cu content (normally about 15-55 μg/g of dry tissue) is the highest among the organs.[15,44] Serum Cu-binding proteins (see section 1.2.3.2) are secreted from the liver in the bloodstream and ensures Cu distribution throughout the body. The liver also provides for excess Cu excretion through the bile (~ 2 mg/24 h).[45] Conversely, almost no Cu is normally found in the urine, namely < 50 μg/24 h (corresponding to < 0.5 μM assuming an average urine volume of 1.5 L in 24 h).[46]

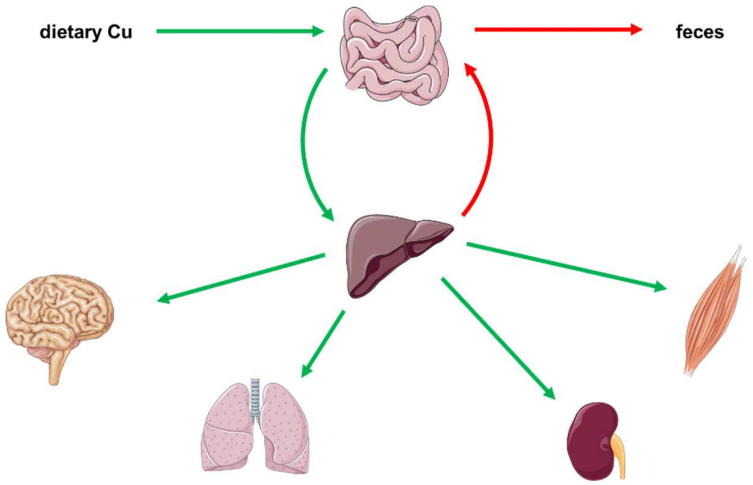

Figure 3. Systemic Cu trafficking. Dietary Cu is adsorbed by enterocytes in the small intestine and transported through the bloodstream to the liver, from which Cp is secreted and Cu is re-distributed to the whole body. Excess Cu is excreted by the liver into the bile and then discarded in the stool.

1.2.3.2 Serum Cu trafficking

In human blood, the average total Cu concentration is ~16 μM (normal values spans from 12.7 to 22.2 μM).[47,48] Several blood Cu^{II} pools can be distinguished (see Table 3). Most of serum Cu (~65-95%, ~10-15 μM) is bound to Ceruloplasmin (Cp), a cuproenzyme that oxidizes Fe^{II} to Fe^{III} contributing to its uptake and systemic distribution via Transferrin (Tf). Cp is metallated with six Cu ions in the secretory pathway of hepatic cells and then released into the bloodstream. As Cu

ions in Cp are buried and shielded by the protein structure, they appear to be kinetically inert, or better not exchangeable nor chelatable by external ligands (unless used at very high, ~10^{-2} M, concentration).[49,50] Indeed, exogenous Cu did not equilibrate with endogenous Cp-bound Cu, but it resulted bound to a kinetically labile, exchangeable pool, including Human Serum Albumin (HSA) and α_2-Macroglobulin (α_2M).[47,51]

In particular, HSA (~ 600 μM) is the main component of the exchangeable pool, as it seems to bind up to ~ 20% serum Cu (~ 3 μM) in a well-characterized redox-inert high-affinity site (see section 1.2.4.1).

α_2M is a serum antiprotease whose alleged Cu-binding has been discovered and characterized by Linder and coworkers. Although the exact Cu coordination remains unknown, it seems that α_2M might be physiologically saturated with two Cu ions per tetramer, accounting for up to ~15% serum Cu (~ 2 μM).[52,53] However, Palumaa and co-workers have recently contradicted previous findings, reporting that α_2M does not bind Cu nor competes with HSA for Cu *in vitro* and showing that no Cu was associated with α_2M in serum samples.[54] Albeit not clear, the source of such incoherent results could be ascribed to the different form of Cu used, i.e. acetate salt by Palumaa et al. or a nitrilotriacetate complex, Cu-NTA, by Linder et al. Indeed, whereas free Cu might not be able to bind directly to α_2M, Cu-NTA might form stable ternary complexes with the protein.

Finally, low-molecular-weight (LMW) molecules such as amino acids have been suggested as relevant Cu-binding ligands since long ago.[55] More recent calculations reported by Palumaa et al. suggest that < 1% of serum Cu may be bound to histidine (His) and other amino acids (Xxx) as $Cu(His)_2$ and Cu(His)(Xxx) complexes.[54] Besides, also small peptides such as GHK are potential Cu partners in the blood. Furthermore, Lutsenko et al. recently reported about an additional LMW Cu pool, called Small Cu Carrier (SCC), whose identity remains elusive.[56–58]

Table 3. Cu^{II} pools in the blood.

Pool ([Ligand]$_{tot}$)		**Cu-loading† (n° of bound Cu ions)**	**% Total Cu ([Cu-Ligand])**	**Affinity***	**Lability/Inertia**
Cp (~2.6 μM)[59]		~ 90% (6) [59]	65-95% (~ 10-15 μM) [59,60]	n/a	Inert [49]
HSA (~ 600 μM)		< 2% (1) [61]	5-20% (~ 3μM) [59,60]	13 [62]	Exchangeable ($t_{1/2,\ ON}$ < 1 sec;[63,64] $t_{1/2,\ OFF}$ ~ min [49,65])
α_2M (~3.5 μM) [66]		~ 100% (2/tetramer) [67]	5-15% (~ 2μM) [59,60]	> 13 [67]	Exchangeable [67]
LMW	His (75 μM) [68]	~ 0.01% (1)	< 5% [60]	8.4 (Cu-His) 6.3 ($Cu\text{-}His_2$) [69]	Exchangeable [70]
	GHK (0.5 μM) [71]	n/a (1)		~13 [72]	
	SCC (n/a)	n/a		n/a	

† % of ligand bound to Cu

* log $K_{7.4}$

1.2.3.3 Cellular Cu uptake

Cu cellular uptake occurs predominantly as Cu^{I} via the membrane transporter Ctr1, and to a lower extent as Cu^{II} through the non-specific divalent metal ion transporter DMT1. Ctr1 and its homolog Ctr2, which is mainly located in lysosomes and late endosomes, are trimeric membrane proteins (each monomer containing three transmembrane helices) forming a cone-shaped pore. Two triads of methionine (Met) residues at the extracellular edge of the pore form a selectivity filter that binds two Cu^{I} ions.[73–75] In addition, Ctr1 also contains an N-terminal ectodomain rich in His and Met residues that promote Cu uptake. Conversely, Ctr2 ectodomain (which is exposed to endosome lumen) is shorter and devoid of such motifs. Interestingly, Ctr1 ensures Ctr2 protein stability against proteasomal degradation, while Ctr2 promotes the formation of an N-truncated form of Ctr1 that facilitates endosomal copper mobilization.[76,77] Importantly, both Ctr1 and Ctr2 contain two distinct N-terminal Cu^{II}-binding sites that could be involved in the uptake of Cu upon reduction (see section 1.2.4.1).[78–80]

Actually, the mechanism with which extracellular Cu^{II} carriers deliver Cu to the cell is not fully understood yet. Linder et al. have shown that HSA and α_2M can deliver Cu to hepatic cells with different mechanisms.[67] In addition, it has been shown that *in vitro* HSA interacts with Ctr1 ectodomain and is able to transfer Cu^{II} to the membrane transporter.[65,81] Moreover, in spite of its kinetic inertia, Cp-bound Cu also resulted to be bioavailable and taken up by cells via an endocytosis-independent mechanism. Cu release from Cp likely require substantial conformational change induced by interaction with membrane proteins and/or Cu^{II} reduction by the reductase STEAP or small physiological reductants such as ascorbate.[82–85]

1.2.3.4 Intracellular Cu trafficking

Once internalized, Cu is kept reduced by the high abundance of reducing agents such as glutathione (GSH), ascorbate and NADPH. GSH attains 1–10 mM concentration in cells, where it is found in both reduced (thiol) and oxidized (disulfide, GSSG) form. Importantly, the GSH:GSSG ratio, which represents a key marker of cellular redox status, is > 1 in all cell compartments (in particular, > 10000:1 in the cytosol and mitochondria, while in the 1–15:1 range in the endoplasmic reticulum) and contributes to keeping intracellular Cu in the reduced Cu^{I} state (Cu^{II} exists only transiently during the redox cycling of cuproenzymes).[86] GSH is also able to tightly bind Cu^{I} in mainly tetranuclear ($[Cu_4(GS)_6]$) Cu^{I}-S^{-} clusters.[87] Accordingly, an important role of GSH in Cu uptake has been suggested.[88] However, further studies have shown that the intracellular concentration of "free" Cu is normally buffered around 1 aM, which is below the threshold for Cu-GSH cluster assembly.[89] Indeed, cytosolic Cu is placed in the charge of intracellular shuttles, called metallochaperones, that bind Cu^{I} in quite redox-inert sites (see section 1.2.4.2) and escort it safely towards specific enzymes and organelles (see Fig. 4). In particular, three cytosolic Cu-chaperones have been identified to date.

CCS (Copper Chaperone for SOD) delivers Cu to the sole cytosolic cuproenzyme, SOD1, and helps its maturation. CCS is made of three distinct domains (DI-III): DI binds Cu^{I} tightly and is required for Cu transfer to SOD1; D2, homologous to SOD1, is crucial for protein recognition; D3 is essential for the formation of a disulfide bond in SOD1 required to reach the active dimeric form of the enzyme.[90–93]

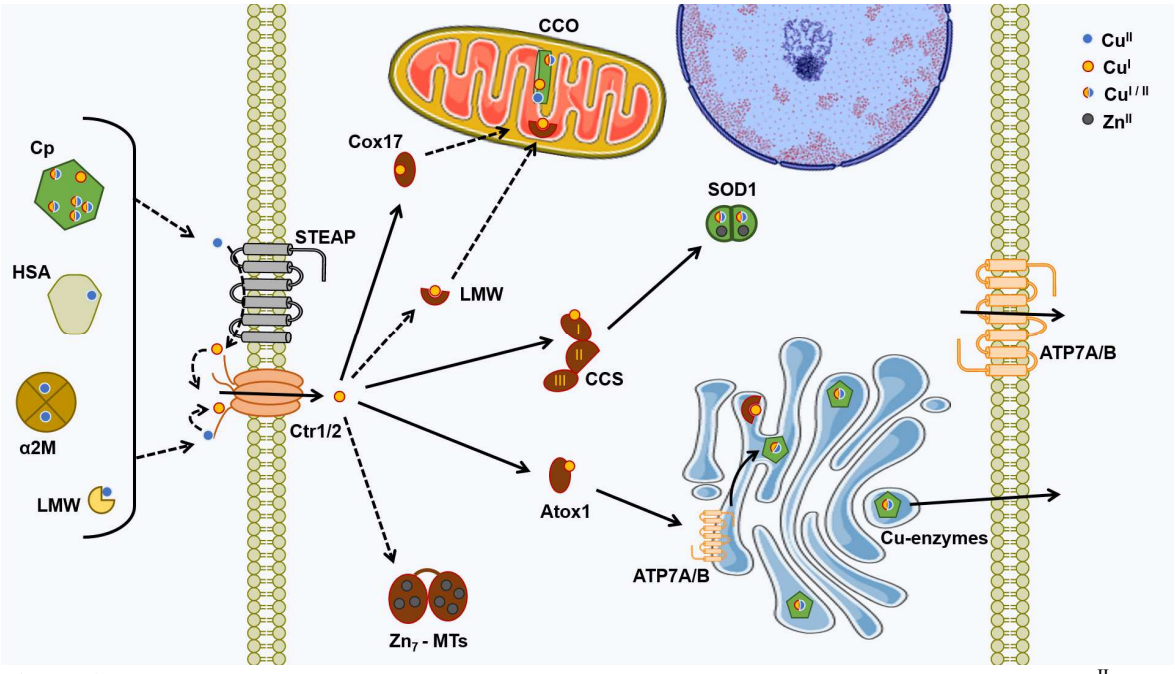

Figure 4. Cu uptake and intracellular trafficking. Extracellular Cu carriers deliver Cu either as Cu^{II} (blue circles) either upon reduction by STEAP reductases or reducing agents such as ascorbate. Ctr1 imports Cu^{+} (yellow circles), which is then shuttled by metallochaperones (and maybe by an LMW pool like GSH) to specific targets: CCS to SOD1, Cox17 to CCO, Atox1 to ATP7A/B, which in turn transport Cu^{+} in the TGN where Cu-enzymes are metalated, or export Cu in the extracellular space. Dashed arrows indicate pathways that are uncertain or occur only under Cu-overload (such as Cu-binding to MTs).

Cox17 seems to transport Cu to the mitochondria, where the important cuproenzyme cytochrome c oxidase (CCO) is located. CCO is a large transmembrane protein complex (Complex IV of the respiratory chain) composed of up to thirteen subunits. It catalyzes the reduction of dioxygen to water, which provides energy to pump protons from the matrix to the mitochondrial intermembrane space (IMS), contributing to generate the proton gradient required for ATP biosynthesis. Subunits I (COX1) and II (COX2) host two Cu-binding sites, Cu_B and Cu_A respectively, which are crucial for the enzymatic activity. In the IMS, Cox17 transfers Cu to CCO assembly proteins such as SCO1 and Cox11. In particular, Cox11 is implicated in the formation of the Cu_B site, while SCO1, together with SCO2, is involved in the formation of the Cu_A site.[94,95] In addition, SOD1 is also needed in the IMS to scavenge harmful radicals formed by the respiratory chain. As its translocation through the mitochondrial outer membrane occurs in the apo-state, CCS is also found in the IMS to ensures SOD1 maturation.[96] The source of mitochondrial Cu is not clear yet. Cox17 might shuttle Cu from the cytosol to the IMS, but it seems not to be essential for Cu transport to the mitochondria. Actually, an undefined non-proteinaceous labile Cu pool has been found in the mitochondrial matrix and it seems to be mobilized to the IMS and used for the metallation of CCO and SOD1. Such LMW ligand could be also responsible for Cu trafficking from the cytosol to the mitochondria, where Cu accumulation in the matrix is mediated by the phosphate carrier SLC25A3. Interestingly, the existence of such Cu pool in the matrix may guarantee the functionality of the mitochondrial cupro-proteome even in the face of an overall cellular Cu deficiency.[97–100]

Finally, Atox1 provides for Cu delivery to the secretory pathway via the transmembrane Cu-transporting ATPases, ATP7A and ATP7B, indirectly ensuring the metallation of most

cuproenzymes, which are located mainly extracellularly. In particular, Atox1 interacts and delivers Cu to the six ATP7A/B N-terminal Atox-like metal-binding domains (NMBDs).[101–103] On top of its chaperone activity, Atox1 has been proposed to act as a Cu-responsive transcription factor inducing the expression of genes involved in cell proliferation (Cyclin D1) and radical scavenging (SOD3).[104–107] However, a direct Atox1-DNA interaction was not supported by *in vitro* experiments. Nevertheless, Atox1 can translocate to the nucleus, where gene regulation could be mediated by several Atox-interacting proteins that have been identified in yeast.[108,109]

ATP7A/B pumps Cu into the lumen of the trans-Golgi network (TGN) or secretory vesicles, which can lead in turn to Cu export. These two transporters often show distinct localization and functions. For instance, ATP7A is found on the basolateral membrane of enterocytes and blood-brain barrier (BBB) where it ensures dietary Cu absorption and Cu import into the brain parenchyma, respectively. Instead, ATP7B mediates Cu biliary excretion in hepatocytes and expels excess Cu from the brain in the apical membrane of the BBB. In noradrenergic neurons, ATP7A also pumps Cu into secretory granules for the metallation of DBH, whereas ATP7B sequesters Cu into vesicles regulating the amount of available cytosolic Cu.[110,111] The mechanism of active (i.e. ATP-dependent) Cu transport through ATP7A/B involves a self-phosphorylation reaction: before ATP hydrolysis, Cu is bound tightly in sites exposed to the cytosol; after the autophosphorylation, Cu is released into the luminal/extracellular compartment.[94]

Curiously, nothing is known about the trafficking of Cu inside the TGN lumen and the metallation of cuproenzymes therein. In the absence of specific metallochaperones, Cu might be mainly shuttle by GSH.

Finally, an additional family of intracellular Cu-binding proteins is formed by Metallothioneins (MTs). These are small Cys-rich proteins with high metal-binding capacity due to the formation of metal-thiolate clusters. In mammals, four isoforms (MT-1 to MT-4) exist, with multiple subtypes within each isoform. While MT-1 and MT-2 are ubiquitously expressed, MT-3 and MT-4 are selectively distributed into the central nervous system (CNS) and the stratified epithelia, respectively. Although MTs show a higher affinity for Cu^{I} than Zn^{II} (in line with HSAB theory, see section 1.2.1), and the highest affinity for Cu^{I} among cytosolic cuproproteins, they seem to be mostly loaded with Zn^{II}, due to its higher bioavailability, and to bind Cu only in case of overload.[112]

This also suggests that an increasing affinity gradient (from Ctr1 to the acceptor proteins via the metallochaperones) is not the mere driving force of the directional Cu trafficking in cells.[113] Indeed, the latter is also likely kinetically controlled, e.g. via protein-protein interactions.

1.2.3.5 Regulation of cellular Cu homeostasis

Contrary to microorganisms, whose Cu sensors and regulators (e.g. CueR in bacteria and Mac1 in yeast) have been identified,[13] very little is currently known about the regulation of human Cu homeostasis.

For many years, the metal-responsive transcription factor (MTF-1) has been the sole known mediator of the cellular response to Cu excess. Notably, thanks to six DNA-binding zinc finger domains, MTF-1 is directly activated by zinc and promotes the expression of MT-I/II. Excess levels of Cu and other heavy metals ions instead activate MTF-1 indirectly by the displacement of zinc from MTs.[114,115]

More recently, other regulatory mechanisms of Cu uptake/export have been discovered.

For instance, Ctr1 is regulated at both transcriptional and post-translational levels in human cells. In particular, Ctr1 transcription is regulated by the ubiquitous transcription factor Sp1, a zinc-finger protein that recognizes the *hCtr1* gene promoter sequence. Excess Cu down-regulates Ctr1 expression via Sp1. It has been shown *in vitro* that Cu can replace Zn^{II} in the ZF domain of Sp1. Interestingly, such a metal swap induces a slight conformational change that disrupts the ability of Sp1 to bind to the *hCtr1* promoter sequence. Furthermore, Sp1 also self-regulates its own expression with the same Cu-dependent mechanism.[116–118]

Besides, mitochondria generate and transmit a redox signal that regulates cellular Cu import and export. In particular, SCO1 sustains Ctr1 expression, limiting its proteasomal degradation, and regulates ATP7A-mediated Cu efflux through the mediation of Cox19. The latter is a soluble CCO assembly factor that partitions between mitochondria and the cytosol in a Cu-dependent manner and stimulates the trafficking of ATP7A to the plasma membrane.[119,120]

1.2.3.6 Cu speciation in bodily secretions and excretions

Unlike serum Cu pools, the Cu-binding components of other extracellular fluids are not precisely known. Recently, Cu speciation in gastrointestinal fluids has been revised by Linder.[121]

In the bile, early studies showed Cu bound to LMW ligands, which might be protease-resistant Cp fragments. More recent studies also suggested the presence of Cu-MTs.

Cu is also found in the saliva at 1-10 μM concentration, where it could serve as an antimicrobial agent. For instance, the salivary peptide Histatin-5 (Hist-5) can bind Cu^{II} with high affinity and a potential role of such interaction in the physiological function of the peptide has been proposed.[122–126]

As anticipated, an exiguous amount of Cu is normally found in urine (< 0.5 μM/24h). As a consequence of the size-dependent filtering activity of the kidney, urinary Cu originates mainly from the serum LMW pool. Indeed, the elusive SCC was first discovered as the main Cu pool (> 70% total Cu) in the urine and suggested to mediate a secondary Cu excretion pathway.[70] Besides, even though protein urine content is also normally neglected (e.g. HSA concentration is < 0.3 μM/24h), a Cu/HSA ratio around 2 has been reported, suggesting that a Cu-HSA pool might exist in urine.[127,128] In addition, MTs have also been found in urine and might bind Cu therein.[129] Overall, most (if not all) urinary Cu pools seem to be labile and exchangeable.

It has also been mentioned above the remarkable role played by Cu at the synapse. In addition, Cu dyshomeostasis has been implicated in some neurodegenerative disorders (see section 1.2.5.2). Accordingly, many putative Cu-binding synaptic ligands have been proposed even though no solid evidence exists about their relevance *in vivo*. For instance, MT-3 is supposed to occur also extracellularly in the brain, where it might scavenge free Cu^{II} preventing oxidative damage.[130–132]

Besides, the cells of the choroid plexus release Cu (via ATP7A) and Cp into the cerebrospinal fluid (CSF), where their concentration is approximately 0.3-0.5 μM and 1 nM, respectively. Indeed, Cp-bound Cu is only about 35% of total Cu in the CSF, whereas HSA is the most abundant protein (about 3 μM) and likely the major Cu pool. As a result, most Cu in the CSF is exchangeable.[28,133,134]

Finally, Cp represents the major form of Cu in breast milk (70–80%), where Cu attains about 5 μM concentration. Interestingly, the metabolism of newborns is adapted to acquire Cu from Cp. HSA and casein might bind the residual Cu.[135–139]

1.2.4 Cu coordination to proteins and peptides

Hereinafter, the Cu-binding sites in the mentioned cuproproteins are described at the molecular level and on a functional basis. In particular, cuproproteins are distinguished in cuproenzymes and Cu-carriers, the latter being in turn differentiated in Cu^{II}- and Cu^{I}-carriers (transporters and chaperones).

Interestingly, the structural difference between Cu-sites in enzymes and carriers mirrors their distinct functions. Indeed, Cu in enzymes needs to be trapped and generally cycle between the $Cu^{I/II}$ states, whereas Cu-carriers have to be redox-inert (to avoid toxicity) and kinetically labile.

1.2.4.1 Cu^{II} carriers

Among the established and putative extracellular Cu^{II}-carriers, HSA, the tripeptide GHK and amino acids (especially Histidine) are those whose Cu coordination is well-known.

HSA binds Cu^{II} in an N-terminal site (NTS), involving the first three amino acids, Asp-Ala-His (DAH). This motif, NH_2-Xxx^1-Zzz^2-His^3 (XZH), where Xxx and Zzz can be any amino acid except for Pro (a secondary amine) as Zzz, is usually known as Amino-Terminal Cu^{II}- and Ni^{II}-binding (ATCUN) motif. The ATCUN motif is a tetradentate chelator that coordinates Cu^{II} via the N-terminal amine group (NH_2), the first two amidates of the peptide backbone (N^-) and the N^{π} of the His^3 imidazole ring forming a square planar complex (see Fig. 5). Such coordination mode involving four nitrogen atoms is often denoted as 4N (NH_2, N^-, N^-, N_{Im}).[72,140] In line with Cu^{II} preference for nitrogen donors and square planar coordination geometry, this site is well-adapted for Cu^{II} but not for Cu^{I}, resulting in a very low reduction potential (< –1 V) and negligible ROS production in the presence of ascorbate.[141] Moreover, the ATCUN motif also binds selectively Cu^{II} among the essential biometals, as a strong Lewis acid character is needed to induce amide deprotonation. Importantly, this site shows a quite high affinity for Cu^{II}, i.e. log $K_{7.4}$ = 12-15, which is probably the highest among the naturally occurring pure Cu^{II}-ligand currently known. The affinity depends on the identity of Xxx, Zzz and the sequence downstream, as well as the whole protein structure.[72] For instance, Cu^{II}-HSA has log $K_{7.4}$ = 13, while the simple tripeptide DAH showed log $K_{7.4}$ = 13.7.[62,142] Even though a correlation has been found between the affinity for Cu^{II} and the basicity of the N-terminal amine (pK_a), the relative affinity of different ATCUN sequences remains hardly predictable. Finally, Cu^{II}-bound to the ATCUN motif is kinetically labile, although bulky and aromatic amino acids can effectively shield the ion enhancing the kinetic stability from minutes to hours/days.[143] Noteworthy, as the name suggests, ATCUN peptides can also bind Ni^{II}, which is not an essential element for mammals. However, the affinity and binding kinetics of such ion are much lower compared to Cu^{II}.[142] Interestingly, the ATCUN motif does not occur uniquely in HSA. hCtr1 also contains an ATCUN motif, MDH, with an affinity comparable to HSA (log $K_{7.4}$ = 13), from which Ctr1 can retrieve Cu^{II}.[65] Furthermore, the ATCUN motif is also found in about 400 human protein sequences, such as human protamine-2, endostatin, the neuropeptide Neuromedin C, the hormone hepcidin and the above-mentioned Hist-5. However, it is not clear whether the ATCUN motif has a functional role in such biomolecules.[72,144]

The tripeptide GHK, containing the similar but distinct NH_2-Xxx^1-His^2 (XH) motif, represents a tridentate chelator binding Cu^{II} with a 3N (NH_2, N^-, N_{Im}) coordination mode involving the N-terminal amine, one amidate, His^2 imidazole and a fourth external ligand (see Fig. 5).

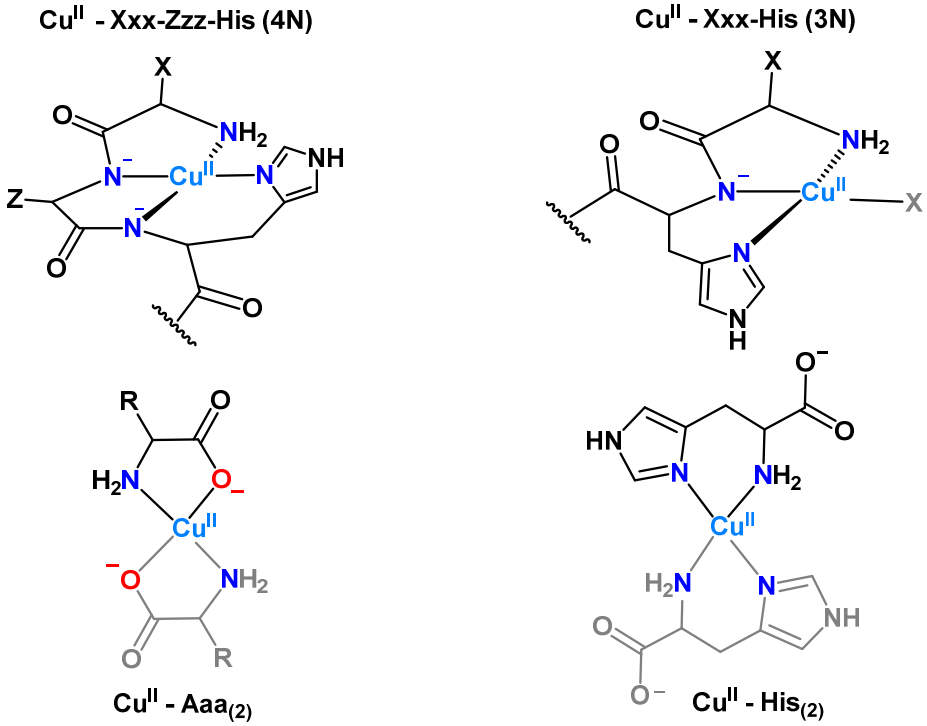

Figure 5. Structure of the Cu^{II} complexes with Xxx-Zzz-His and Xxx-His peptides, amino acids and Histidine.

GHK affinity for Cu^{II} is similar to HSA. Likewise, XH motif shows high selectivity for Cu^{II} (e.g. the log $K_{7.4}$ of AH dipeptide is ~3 for Zn^{II} and ~13 for Cu^{II}).[145] Besides, although XH motif has a higher reduction potential (~ –0.2 V), it shows poor ROS production activity.[72,140,146] Finally, the XH motif shows faster Cu^{II} exchange than XZH (< ms), as a likely result of the lower number of amidates involved (as the amide protonation seems to be the rate-limiting step) and the possibility to form 3N+L (self-)ternary complexes (see section 2.5.1.2).[63,72,140,147,148] Finally, free amino acids represent bidentate ligands coordinating via the amino group and the carboxylate with modest affinity and selectivity (e.g. log $K_{7.4}$ = 5.87 for Cu-Gly and log $K_{7.4}$ = 2.62 for Zn-Gly). Histidine can coordinate Cu also via the imidazole side-chain, forming stronger bidentate 2N (NH_2, N_{Im}) complexes (log K_1 = 8.43, log K_2 = 6.3 at pH 7.4).[69] Cu^{II}-$(His)_2$ complex can be reduced by ascorbate and cysteine in aerobic conditions forming ROS.[141,149,150]

1.2.4.2 Cu^{I} carriers

As opposed to extracellular Cu^{II} carriers, intracellular Cu^{I} transporters and chaperones stabilize Cu^{I} in linear or trigonal coordination sites involving mostly Cys or Met residues. As already mentioned, hCtr1 ectodomain has several His- and Met-rich motifs, while Cu^{I} results tricoordinated by Met residues belonging to an MX_3M motif in the second transmembrane domain of each monomer (see Fig. 6). Moreover, at the intracellular C-terminus, an HCH motif has been shown to bind and transfer Cu^{I} to Atox1 *in vitro*.[151] Most chaperones bind Cu^{I} through two Cys residues, belonging to characteristic motifs. In particular, Atox1, CCS (domain I) and the NMBDs of ATP7A/B, which all show the same ferredoxin-like fold, bind Cu^{I} via two Cys belonging to a CXXC motif. Such coordination site may be further stabilized by an additional Cys residue from a molecule of GSH.[152] Interestingly, such trigonal species are also involved in the Cu transfer between Atox1 and the NMBDs of ATP7A/B.[153] Moreover, the ability of Atox1 to form

tetracoordinated Cu-bridged dimers has been reported.[101,154] Besides, in ATP7A/B, a CXC motif found in the sixth transmembrane domain represents the Cu-translocation site.[94] Cox17, instead, coordinates Cu via two adjacent Cys residues,[155] while Cox11 dimerizes upon Cu^{I}-binding forming a tetracoordinated dinuclear Cu-S cluster.[156] A trigonal Cu-binding site involving a CX_3C motif as well as a His residue is found in SCO1/2.[157] Finally, human MTs can bind up to twelve Cu ions in Cu-thiolate clusters. The reaction of Cu with Zn_7-MT-3 yields for instance the formation of a Cu_4-S_9 cluster that is air-stable and redox-inert.[158]

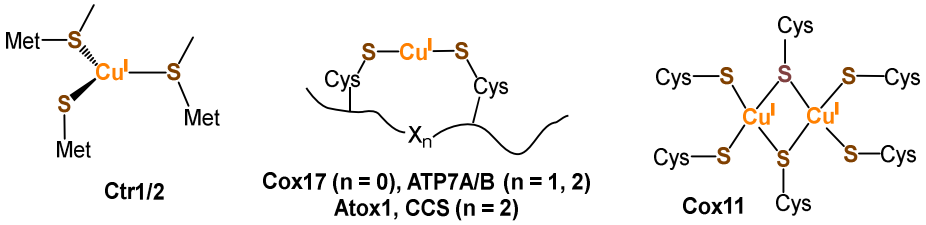

Figure 6. Structure of some Cu^{I}-binding sites in membrane transporters and metallochaperones.

1.2.4.3 Cu-enzymes

As discussed above, Cu^{I} and Cu^{II} states prefer very different ligand and coordination geometry, so much that an efficient redox cycling is rarely accomplished by Cu-complexes with simple organic ligands in biological conditions.[159] However, living systems shaped the active sites of cuproenzymes to favour their function, i.e. optimize redox cycling, accommodating $Cu^{I/II}$ in a so-called *entatic* (literally meaning "under tension") state that represents a compromise in terms of both donor type and coordination geometry.[160] In particular, the well-defined protein structure constrains Cu in mostly tetra- or penta-coordinated sites via a mix of hard, or better intermediate, and soft ligands (mainly His, Cys and Met).

Cu-binding sites in cuproenzymes are distinguished into three main types based on their structural features, which also reflect their different functions (see Table 4).

Table 4. Cu-binding sites in human cuproenzymes.

Enzyme	Type of site	Ligands
CCO	Cu_A	1 His, 1 Met, 2 bridging Cys 1 His, 1 C=O
	Cu_B	3 His
SOD1/3	T2	3-4 His
DBH, PAM	T2	3 His (Cu_H) 2 His, 1 Met (Cu_M)
Amine oxidases	T2	3 His
TYR	T3	3 His + 3 His
Cp, Heph	T1	2 His, 1 Cys, (1 Met)
	T2	2 His, H_2O
	T3	3 His + 3 His
FGE	n/a	2 Cys

In Type 1 (T1) Cu centres, which are typically found in electron-transfer proteins (known as cupredoxins), Cu is coordinated by 2 His (N^{π}) and 1 Cys forming a pseudo-trigonal plane. T1 sites are further classified based on the presence and identity of axial ligands: 1 Met (class I), a non-

methionine residue (class II), forming a distorted tetrahedral site, or 1 Met and a glycine carbonyl oxygen (class III), resulting in a distorted trigonal bipyramidal geometry. Examples of T1 Cu proteins are the above-mentioned plastocyanin (class I) and azurin (class III). In humans, T1 Cu sites are found only in multicopper proteins (see below).[6,161]

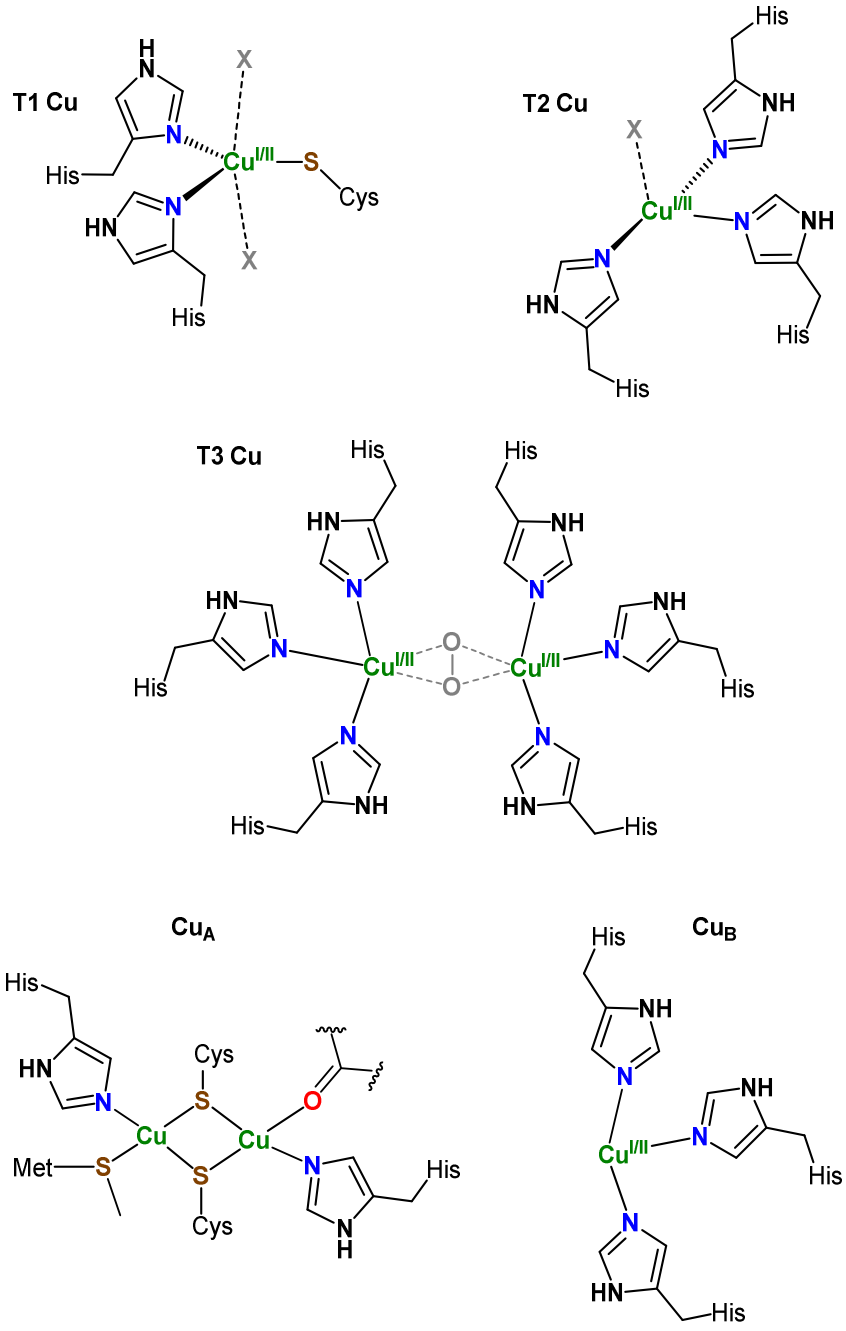

Figure 7. Structure of the main Cu-binding sites in cuproenzymes.

Type 2 (T2) Cu sites are instead tri- or tetra-coordinated mostly via His (N^{τ}) residues (Met, Glu, Gln or Tyr may complete the coordination sphere). Such site is found in SOD1/3, monooxygenases (DBH and PAM) and amine oxidases (such as LOX). In SOD1/3, for instance, Cu^{II} and Cu^{I} are

tetra- and tri-coordinated, respectively, by His residues. DBH and PAM contain two T2 sites: Cu_H, coordinated by 3 His, and Cu_M, coordinated via 2 His and 1 Met.[162]

Type 3 (T3) Cu sites are antiferromagnetically coupled dinuclear Cu centres found for instance in TYR and the O_2-transporter hemocyanin. In the absence of O_2, each Cu^I ion is coordinated by 3 His in a trigonal planar geometry. Upon dioxygen binding in a side-on bridging coordination, a distorted trigonal bipyramidal geometry is adopted.[6]

Besides, some cuproenzymes, notably multicopper oxidases (MCO), contain more than one Cu site. Members of such family are laccases, ascorbate oxidase, as well as Ceruloplasmin (Cp) and its homologue Hephaestin. All MCOs include at least 4 Cu ions arranged in a mononuclear T1 Cu site and a trinuclear Cu centre composed of a T2 Cu site and a couple of T3 ions.[163] In particular, Cp binds 6 ions arranged as three T1 Cu sites (two including a Met residue and one lacking axial ligands), one of which is permanently reduced, and a trinuclear Cu centre where dioxygen binding and activation occur.[164,165]

The two Cu sites of CCO, Cu_A and Cu_B, escape the classification described above. The Cu_A site, which is found in COX2 subunit and serves for electron transfer, is a dinuclear mixed-valence Cu centre bridged by 2 Cys residues in a tetrahedral geometry. The coordination spheres are completed by 1 His and 1 Met or 1 His and a glutamate carbonyl oxygen, respectively. The Cu_B site, found in COX1 subunit, is coordinated by 3 His in a trigonal planar geometry and faces a heme a_3 cofactor, between which dioxygen is bound and reduced (see Fig. 7).[6]

Finally, a very unconventional Cu site involving two Cys residues has been recently identified in the enzyme FGE.[166–168]

1.2.5 Cu-related human diseases

By virtue of the momentous role played by Cu and Cu-enzyme in human physiology, it seems evident that the breakdown of Cu homeostasis can lead to severe pathological conditions. Indeed, some genetic disorders related to defective cuproenzyme activity or altered Cu trafficking exist, as well as idiopathic diseases where Cu involvement has been observed but remains controversial.

1.2.5.1 Genetic disorders of Cu metabolism

Genetic defects affecting some cuproenzymes, such as SOD1, TYR and Cp, give rise to consequent diseases, such as amyotrophic lateral sclerosis, oculocutaneous albinism and aceruloplasminemia, respectively.[169–171] The latter is characterized by the lack of functionality of Cp, resulting in iron accumulation in the liver and the brain, while normal Cu transport and metabolism are observed. Interestingly, this indicates that Cp has a primary role in iron mobilization but not as a Cu carrier.

Besides, CCO deficiency can arise from mutations of the assembly cofactors SCO1 and SCO2, leading to neonatal hepatic failure and encephalocardiomyopathy.[172–174]

Actually, the impairment of Cu trafficking can affect simultaneously several biochemical functions and lead to very detrimental consequences. This is indeed illustrated by the two best-known Cu-related disorders, i.e. Menkes and Wilson diseases, which are caused by mutations in the membrane transporters ATP7A and ATP7B, respectively.

Menkes disease (MD) is an X-linked recessive disorder affecting about 1:100000-250000 newborns. As ATP7A assures Cu transport from enterocytes to the bloodstream, its impairment

entails the accumulation of Cu in the intestine and a systemic Cu deficiency with, consequently, reduced activity of cuproenzymes. As a result, MD patients show mental and growth retardation, hypopigmentation and laxity of skin and joints. The average lifespan of MD patients is about 3 years.[175,176] The diagnosis of MD is classically based on clinical manifestations and confirmed by decreased blood levels of Cu (< 11 μM) and Cp (< 200 mg/L). Interestingly, the level of plasma catecholamines, which are altered as a result of DBH deficiency, is also a selective biomarker. Parenteral Cu supplementation as Cu-His complex (see Fig. 5) represents the classical treatment, even though this often does not improve neurological manifestations due to poor penetrance in the brain.[177,178] Recently, elesclomol (see Fig. 8) appeared to be promising to overcome such limitation.[179]

Wilson's disease (WD) is an autosomal recessive disorder with an incidence of 1:30000-100000. WD is progressive and the severity of clinical manifestations is very variable, spanning from hepatic cirrhosis and chronic hepatitis to cardiomyopathy and neurological defects such as Parkinsonian features (e.g. tremor and bradykinesia).[176,180] Indeed, ATP7B dysfunction implies Cu accumulation in the liver (250 μg/g of dry weight) and the brain, as well as reduced Cp levels in the blood (< 100 mg/L).[44,48,181] Therefore, total serum Cu is usually decreased, but normal levels are also often observed.[182] This suggests an increase of the exchangeable non-Cp Cu (NCC) pool. Effectively, the level of NCC, or better the Relative Exchangeable Cu (REC), i.e. the exchangeable/total Cu ratio, correlates well with Cu overload in WD and is emerging as a relevant biomarker due to high diagnostic selectivity and specificity.[183] Curiously, high urine Cu levels (> 1 μM/24h) are also diagnostic in untreated WD patients. As an explanation, it has been recently proposed that a putative secondary SCC-mediated Cu excretion pathway in urine may be upregulated as a result of ATP7B impairment.[70] Importantly, the median life expectancy of untreated WD patients is 40 years, but almost normal expectancy is often achievable with currently available treatments. These typically consist in Cu chelation therapy using D-penicillamine (D-Pen), trientine (trien) or tetrathiomolybdate (TTM), or zinc supplementation (e.g. as zinc acetate) to inhibit Cu intestinal absorption (see Fig. 8).[180,184,185]

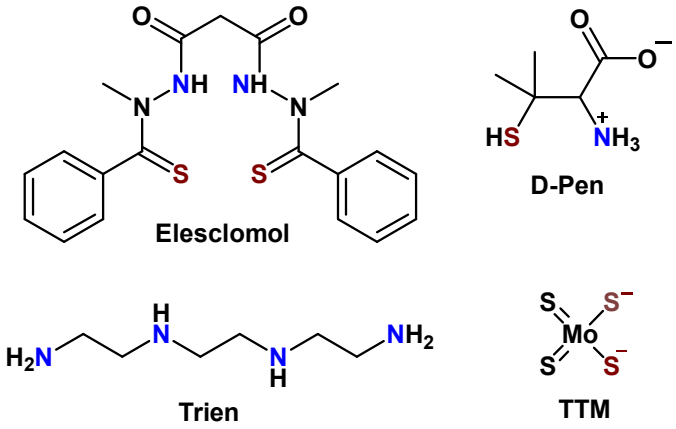

Figure 8. Ligands used or investigated as drugs to treat MD (elesclomol) and WD (D-pen. Trien, TTM). Cu-binding atoms are coloured.

1.2.5.2 Neurodegenerative diseases

The harmful effects of brain Cu dyshomeostasis are clearly demonstrated by the clinical manifestations of MD and WD. Besides, brain Cu misbalance has been also related to the most relevant neurodegenerative disorders, namely Alzheimer's disease (AD) and Parkinson's disease (PD), which share oxidative stress and proteinaceous aggregates (amyloids) as major hallmarks.[186]

AD is the most common type of dementia in western countries, currently affecting almost 50 million people worldwide. AD patients' brain is characterized by the presence of extracellular deposits, called amyloid plaques, mainly composed of the peptide(s) Amyloid-β (Aβ), and intracellular aggregates of the protein τ, known as neurofibrillary tangles (NFTs).[187]

Aβ peptides are generated by the "amyloidogenic" proteolysis of the Amyloid Precursor Protein (APP), a transmembrane neuronal protein. In particular, the sequential cleavage of APP by β- and γ-secretases originates $A\beta_{1\text{-}40}$ and $A\beta_{1\text{-}42}$ peptides, which may be further processed (e.g. by proteases such as neprilysin, angiotensin-converting enzyme and insulin-degrading enzyme) forming N-truncated Aβ species. Actually, the N-truncated $A\beta_{4\text{-}40}$ peptide is now recognized to be as abundant as $A\beta_{1\text{-}42}$ in both healthy and AD brains.[188,189]

Only a small portion (about 5%) of AD cases are hereditary, due to mutations in APP or γ-secretase subunits (presenilins). Most AD cases are instead idiopathic. According to the so-called *amyloid cascade hypothesis*, AD pathology arises from the aggregation of Aβ into soluble amorphous oligomers, now considered the most neurotoxic species, and then into insoluble fibrils, although Aβ appears also to be essential to brain physiology.[190,191]

Importantly, Cu can interact with APP, preventing its amyloidogenic processing, inducing its dimerization and trafficking to the plasma membrane. Hence, it has been speculated that APP, whose function is unknown, could play a role in Cu brain metabolism and modulate the neuromodulatory activity of Cu.[192–196] In addition, it has been shown *in vitro* that Cu can modulate the amount and the morphology of Aβ aggregates depending on the Cu/Aβ ratio.[197] Most importantly, a high amount of Cu has been found in amyloid plaques, where Cu can be bound to Aβ.[198,199] Moreover, the Cu content of the whole brain seems to be lower in AD patients than healthy controls, while increased NCC has been reported in the CSF.[200,201] Interestingly, intracellular Cu deficiency implies higher Aβ secretion.[202] AD patients also show increased levels of Cu, especially non-Cp Cu (NCC), in serum and urine. In particular, the Cu:Cp ratio has been proposed as a suitable marker.[201,203,204] Actually, few single nucleotide polymorphisms in ATP7B gene have been identified in some AD patients, which could explain the Cu misbalance observed.[205–207]

Therefore, the molecular interaction between Cu ions and Aβ peptides have been thoroughly investigated. Studies showed that $A\beta_{1\text{-}40/42}$ bind Cu^{II} and Cu^{I} with (sub)nanomolar affinity forming complexes that are competent in ROS production and, as such, could contribute to AD pathogenesis.[208,209] On the contrary, N-truncated $A\beta_{4\text{-}x}$ and $A\beta_{12\text{-}x}$ fragments bearing ATCUN motifs (see section 1.2.4.1) have even higher Cu-affinity (log $K_{7.4}$ about 14) and showed lower redox activity.[210–214] Hence, they have been postulated to act as Cu^{II} carriers or synaptic Cu^{II} scavengers.[188,215]

Similar to AD, Parkinson's disease is characterized by intracellular aggregates, known as Lewy bodies, mainly composed of the protein α-Synuclein (α-Syn).

The most affected brain regions of PD patients, i.e. substantia nigra and locus coeruleus, show lower Cu levels than healthy controls, whereas meta-analytic studies showed no significant difference of Cu levels in serum and CSF between PD patients and controls.[216,217]

The interaction of Cu with α-Syn has also been extensively studied, showing that Cu modulates α-Syn aggregation, toxicity and aggregation.[218,219] Several Cu-binding sites have been identified in α-Syn, revealing its ability in producing ROS.[220–223] However, due to moderate (micro- to nanomolar) Cu affinity, the occurrence of Cu-(α-Syn) complexes *in vivo* is questionable and not yet addressed. Notwithstanding, even a functional role of Cu-(α-Syn) as ferrireductase has been proposed.[224–226]

1.2.5.3 Cancer

The favourable role of Cu in carcinogenesis appears coherent with Cu involvement in signalling pathways promoting cell proliferation and angiogenesis (see section 1.2.2.2), a process that is essential to support tumour growth. In addition, Cu seems also to promote tumour metastasis, e.g. via the activity of LOX, which is secreted by cancer cells to remodel the extracellular matrix and allow cell migration. Thus, accumulation of Cu and the up-regulation of Cu-transporters/chaperones (e.g. Ctr1, Atox1, CCS, Cox17, SCO1 as well as ATP7A/B) in cancer cells have been reported for many tumour types. This trend is mirrored by elevated serum Cu and Cp levels, which might arise from enhanced Cu export from the liver. Interestingly, such increase correlates with disease progression and remission, suggesting the possibility that serum Cu levels may be used as a marker during cancer treatments.[25,227,228]

Consequently, Cu chelation is being explored as a strategy to halt cancer progression, for instance exploiting chelators used in WD (D-Pen, trien and TTM, see Fig. 9). On the other hand, different approaches aim at raising intracellular Cu levels to enhance its cytotoxic effects. For this purpose, Cu ionophores (i.e. ligands facilitating Cu import) such as gtsm, hydroxyquinolines (HQs) and diethyldithiocarbamate (DEDTC), as well as potentially pro-oxidant Cu-complexes (i.e. redox-active complexes able to produce ROS) of phenanthrolines (phen), bipyridine (bipy) and thiosemicarbazone (TSC) ligands are currently investigated (see Fig. 9). Interestingly, based on the higher Cu content in the tumour environment, such Cu-targeting anticancer drugs could benefit from selective toxicity towards cancer cells.[25,228–234]

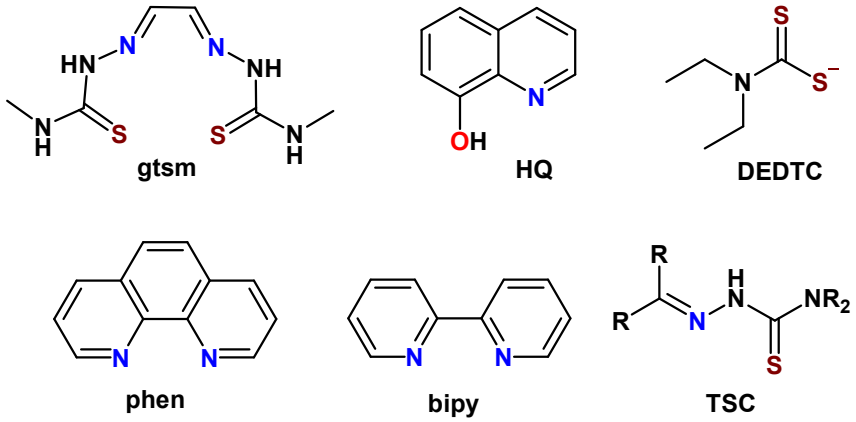

Figure 9. Ligands investigated as Cu-based anticancer drugs. Cu-binding atoms are coloured.

1.3 Aim of the thesis

The physiological functions and the pathological effects of Cu in living systems demonstrate the interest in Cu measurement in biological samples. Notably, Cu dyshomeostasis does not arise only from the alteration of total Cu levels, but it often occurs as Cu mislocalization and protein mismetallation with Cu. Therefore, besides "bulk" Cu determination, the dynamic and spatially-resolved detection of *cuprome* (i.e. Cu metallome) is equally important. Furthermore, as already mentioned, the exchangeable Cu pool in biological fluids, rather than the total Cu, has been particularly correlated with WD and AD.[183,235]

However, methods for the specific detection of the exchangeable pool are not established yet. Actually, current approaches employing elemental analysis (e.g. ICP-MS/OES or AAS) or imaging techniques (e.g. LA-ICP-MSI or XRF) are mostly insensitive to Cu speciation, unless they are coupled with separative steps or rely on a Cu-responsive chemical probe (see section 2.1).[236]

For instance, Cu-sensitive luminescent probes could be suitably designed to detect and image exchangeable Cu in biological systems. In particular, sensors based on emission enhancement upon Cu recognition, known as "turn-on", are more desirable for quantification and imaging applications than those based on luminescence quenching, denoted as "turn-off" (see section 2.2).

Several turn-on luminescent Cu^{I}-probes have been reported and used to investigate intracellular Cu^{I}-trafficking.[26,89,99,237] Conversely, a deep analysis of luminescent Cu^{II}-probes reported in the literature revealed that, at best, very few of them, may be suitable for exchangeable Cu^{II} analysis in body fluids.[236] In particular, as Cu^{II} is a well-known luminescence quencher, the design of coordination-based (hence reversible) turn-on Cu^{II}-probes appears very challenging. Notwithstanding, some examples of putative reversible turn-on Cu^{II}-probes have been reported. Thus, with the aim to develop luminescent Cu^{II} probes suited for applications in biological samples, we first examined the working mechanism of a putative reversible turn-on Cu^{II}-probe previously reported in the literature. Remarkably, we found out that this is instead based on an irreversible Cu-mediated reaction, unlikely to occur in biological conditions (see section 2.3).[238]

Therefore, in light of the very challenging *rational* design of reversible turn-on Cu^{II}-probes, we first focused on the development of turn-off luminescent chelators provided with beneficial properties for the detection of exchangeable Cu^{II} in biological media, namely suited affinity and selectivity as well as background-free detection.[239,240] Then, our efforts were directed towards the development of a ratiometric derivative in order to improve Cu^{II} quantification and enable the analysis of exchangeable Cu^{II} in urine and blood serum (see sections 2.4-2.6).

Besides, the mode of action of some putative Cu-based drug, such as anticancer thiosemicarbazones (TCSs), is not thoroughly understood yet. Notably, although synergism with Cu^{II} has been observed for some TSCs, for which Cu^{II}-mediated ROS production has been proposed as a mechanism of cytotoxicity, it is currently controversial whether TSCs form pro-oxidant Cu^{II}-complexes *in vivo*. Hence, a minor part of this work was devoted to the investigation of the stability and reactivity of some Cu^{II}-TSCs complexes in the presence of HSA or GSH, to assess the capacity of TSCs to pick up Cu^{II} in the blood and to generate ROS in the presence of GSH and dioxygen at both cytosolic and lysosomal pH (see section 3).

2. Luminescent probes for exchangeable Cu

2.1 Introduction

The measurement of non-Cp Cu (NCC), also referred to as exchangeable Cu (Cu_{EXC}) has been gaining interest as a potential diagnostic marker for WD and AD. In the following, current methods to detect and quantify the NCC/Cu_{EXC} are described highlighting their shortcomings.

2.1.1 Exchangeable Cu measurement

2.1.1.1 Drawbacks of common elemental analysis and imaging methods

Although elemental analysis techniques, such as ICP-MS (inductively-coupled plasma-mass spectrometry) or ICP-AES (inductively-coupled plasma-atomic emission spectroscopy) and AAS (atomic absorption spectroscopy), are the gold standard for bulk (total) Cu measurement in biological or environmental samples thanks to their very low detection limits (in the pM-nM range), they are not directly suited for speciation analysis. To this aim, the so-called *hyphenated* techniques are required, which combine the above-mentioned detection methods with separation techniques such as size-exclusion chromatography (SEC) or electrophoresis. These approaches have been extremely important for the study of Cu speciation in body fluids and represent the ground on which current knowledge about Cu metabolism is based. However, they require relatively fancy instrumentation and expertise, which hamper the applications in clinical analysis.[241–245]

Besides, LA-ICP-MS (laser ablation-ICP-MS) and X-ray fluorescence (XRF) are used for imaging scope, providing high sensitivity and spatial resolution (down to about 20 nm for XRF). Nevertheless, they detect total Cu and remain mostly insensitive to metal speciation.[246,247]

2.1.1.2 Indirect estimation of NCC – the *Walshe's index*

The measurement of NCC first acquired significance in the diagnosis of WD, for which purpose Walshe proposed to estimate indirectly the NCC in serum as the difference (known as Walshe's index), between total Cu (measured by elemental analysis) and Cp-bound Cu. The latter has initially been measured via immunological methods, which unfortunately do not distinguish apo- and holo-Cp, resulting in a potential overestimation of Cp-bound Cu and underestimation of NCC. Indeed, even unrealistic negative NCC values were obtained. Therefore, it was then recommended to selectively measure holo-Cp via an enzymatic assay of its oxidase activity, with the assumption that Cp is saturated with 0.3% (w/w) Cu. However, this assumption, together with the variable purity of commercial Cp standards, compromise the reliability of this method.[248–250]

2.1.1.3 Chelation-free methods – *ultrafiltrable Cu*

Due to the flaws of Walshe's index, direct methods have been developed implicating the separation of NCC from holo-Cp. Such separation is mostly achieved via ultrafiltration (UF) through size-exclusion membranes with a defined molecular weight cut-off.[60,251–255] Thus, a suitable cut-off could be used for instance to retain Cp (132 kDa) and collect the NCC in the ultrafiltrated fraction,

also referred to as *ultrafiltrable* Cu (Cu_{UF}), which can be then quantified by elemental analysis. Notably, the Cu pools present in the Cu_{UF} depend on the cut-off used.

McMillin et al. reported a method to measure non-protein-bound ("free") Cu using a filter with 30 kDa cut-off. They found Cu_{UF} lower than about 1.5 μM in more than hundred healthy people, while Cu_{UF} resulted to be at least 6-fold higher in WD patients.[254]

On the other hand, using different 50 kDa or 30 kDa cut-off membranes, negligible levels of Cu_{UF} were detected by Catalani et al., who suggested that protein clotting into the membrane could represent a source of systematic error leading to Cu_{UF} underestimation. Instead, the same authors isolated non-protein-bound Cu (0.1 – 0.8 μM) with a 100 kDa cut-off filter that evidently also retained HSA.[60]

These examples show that the amount and the speciation of Cu_{UF} strongly depend on the precise type of filter and cut-off used, undermining reproducibility and reliability.

2.1.1.4 Chelation-based methods – *exchangeable* or *chelatable Cu*

A partially different approach employs chelators to extract Cu from the labile pool. Nevertheless, most methods reported up to date still rely on the extraction or isolation of the Cu-chelator complex prior to the detection of such *exchangeable* (or *chelatable*) Cu, Cu_{EXC} (see Table 5).

Table 5. Chelation-based methods for Cu_{EXC} measurement.

Chelator	Affinity‡	Chelator Concentration (mM)	Incubation time (min)	Sample treatment	Detection method	Reference
DEDTC	11.7, 12.2 [256]	0.28	20	n/a	Colorimetry (λ_{abs} = 440 nm)	[257]
		0.16	30	Extraction of Cu-DEDTC in mineral oil	ICP-MS	[258]
His	8.4, 6.3 [69]	10-100	120	Dialysis	ICP-MS	[259]
EDTA	15.9 [54]	5	60	Ultrafiltration	ICP-MS, AAS	[183,255]
Phen	9.1, 6.8 [260]	1	60	Addition of DNA and mercaptoethanol; reaction with thiobarbituric acid in trichloroacetic acid at 100 °C; extraction in butanol	Fluorescence (λ_{ex} = 532nm λ_{em} = 553 nm)	[261]

‡ The values reported for Phen, His and EDTA are log *K* at pH 7.4; for DEDTC log *K* was determined in methanol.

For instance, Woimant and colleagues employed EDTA (5 mM, 1h incubation, log $K_{7.4}$ = 15.9, see Fig. 10) to chelate Cu_{EXC} in serum prior to ultrafiltration (30 kDa cut-off) and elemental analysis. Interestingly, the authors reported higher levels of Cu_{EXC} (0.62 – 1.15 μM) compared to Cu_{UF} (0.07 – 0.16 μM), coherently with the ability of EDTA to extract HSA-bound Cu, which should not be

found instead in Cu_{UF}.[255,262] Overall, Woimant et al. showed higher short-term (24h) stability of Cu_{EXC} compared to Cu_{UF} and proposed the Cu_{EXC}/Cu_{TOT} ratio, called Relative Exchangeable Cu (REC), as a promising biomarker with high selectivity and specificity for WD diagnosis.[183]

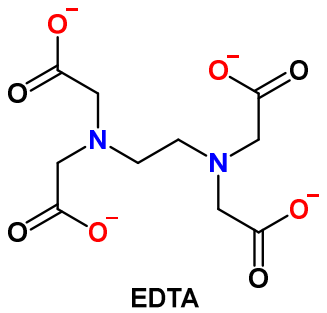

Figure 10. Structure of the hexadentate chelator EDTA. Cu-binding atoms are coloured.

However, speciation analysis recently revealed the presence of protein-bound Cu (Cu-HSA and Cu-Cp) in Cu_{UF} obtained after incubation of blood serum with EDTA and ultrafiltration with 30 kDa cut-off. Furthermore, very poor reproducibility was found even using filters of the same lot.[263] This underlines once more the flaws related to the use of ultrafiltration devices.

Another interesting strategy to detect the Cu-chelator complex, known as "phenanthroline assay", was introduced by Gutteridge in 1984 using the bidentate ligand 1,10-phenanthroline (phen, log K_1 = 9.1, log K_2 = 6.8 for Cu^{II}). The quantification of the formed $Cu(phen)_2$ complex is achieved thanks to its pro-oxidant activity towards DNA. $Cu(phen)_2$ is indeed very competent in catalysing the production of ROS in the presence of a reductant such as β-mercaptoethanol. The generated ROS can in turn degrade DNA forming intermediate thiobarbituric acid-reactive species that become fluorescent and can be detected upon reaction with thiobarbituric acid.[261] It is noteworthy that, even though the assay relies on the redox activity of $Cu(phen)_2$, the endogenous Cu chelated by phen is not necessarily a redox-active or pro-oxidant form of Cu, as often falsely claimed. Gutteridge et al. applied this assay to measure labile Cu in serum, CSF, sweat and brain tissue.[264–268] Interestingly, Gutteridge also found no chelatable Cu in fresh serum samples and suggested that the levels of NCC could be altered by Cu release from Cp upon sample storage and freezing.[269]

Although the reactivity-based phenanthroline assay benefits from catalytic amplification, it is also more susceptible because interferences can be also amplified. In addition, even though ultrafiltration is not required, the assay needs additional reactants (β-mercaptoethanol, DNA, thiobarbituric acid), harsh reaction conditions (100 °C) and a liquid-liquid extraction step. Hence, a more direct read-out of the catalytic activity would be desirable.

Overall, most current methods rely on elemental analysis to detect Cu_{UF} or Cu_{EXC}. As a cheaper and faster alternative, Squitti and colleagues recently used a fluorescent Cu probe to detect Cu_{UF}.[249] In this vein, a suitable luminescent chelator used as a probe for Cu would also enable the direct measurement of Cu_{EXC} in biological samples without sample treatments nor separative steps. However, for this purpose, the probe has to fulfil some demanding criteria that are discussed in the following.

2.1.2 Requisites for application of a Cu^{II}-probe in Cu_{EXC} measurement

The requisites that must be fulfilled to apply a luminescent Cu^{II}-probe in biological samples concern both the chelator (e.g. affinity, selectivity) and the luminophore moieties (e.g. absorption/emission wavelength, brightness).

2.1.2.1 Affinity

In order to chelate, even partially, the Cu_{EXC}, a chelator must compete thermodynamically with the endogenous Cu-ligands. The exact affinity needed depends primarily on the affinity and concentration of endogenous ligands, as well as on the chelator concentration used.

To get insight into the affinity needed by a probe, we can focus, for the sake of simplicity, on the equilibria occurring in a simplified system mimicking the blood, i.e. containing 500 µM HSA and 3 µM HSA-bound Cu.

By definition

$$K^{HSA} = \frac{[CuHSA]}{[Cu][HSA]} \qquad \text{Eq. 1}$$

and

$$K^{P} = \frac{[CuP]}{[Cu][P]} \qquad \text{Eq. 2}$$

are the thermodynamic stability constant of Cu complexes with HSA and the probe P, respectively.

At the equilibrium,

$$K^{P} = K^{HSA}\frac{[HSA]}{[CuHSA]}\frac{[CuP]}{[P]} \qquad \text{Eq. 3}$$

As [CuHSA] = $[CuHSA]_0$ – [CuP], [HSA] = $[HSA]_0$ – [CuHSA] (where $[CuHSA]_0$ is the concentration of CuHSA in absence of P, and $[HSA]_0$ the total concentration of HSA) and [P] = $[P]_0$ – [CuP] (where $[P]_0$ is the total concentration of the probe), Eq. (A.3) becomes:

$$K^{P} = K^{HSA}\frac{[HSA]_0 - ([CuHSA]_0 - [CuP])}{([CuHSA]_0 - [CuP])}\frac{[CuP]}{([P]_0 - [CuP])} \qquad \text{Eq. 4}$$

Finally, defining l as the Cu-loading of P, [CuP] = $l\cdot[P]_0$, ($0 \le l \le 1$) the following equation is obtained:

$$K^{P} = K^{HSA}\frac{([HSA]_0 - [CuHSA]_0 + l[P]_0)}{([CuHSA]_0 - l[P]_0)}\frac{l}{(1-l)} \qquad \text{Eq. 5}$$

Assuming $[CuHSA]_0$ = 3 µM and $[HSA]_0$ = 500 µM and considering that the stability constant of Cu-HSA is log $K_{7.4}$ = 13, a chelator added in very high excess, e.g. at 5 mM concentration such as EDTA in the method reported by Woimant et al., needs an affinity of log K ~14 to withdraw 99% of Cu_{EXC} (2.97 µM), but only log K ~ 12 to chelate 50% of Cu_{EXC} (1.5 µM). Interestingly, as EDTA has log K ~ 16, it is able to bind substantially all Cu_{EXC}, representing an *outcompeting* chelator.

However, luminescence measurements are normally performed at much lower probe concentration, i.e. < 10 µM. Actually, such low chelator concentration is also needed to achieve a significant Cu-loading and hence a detectable signal change. Thus, a chelator added at 1 µM

concentration must have instead log K = 15.3 in order to achieve 50% Cu-loading, whereas log K ~ 14 would be enough to accomplish 10% loading. Remarkably, such affinity values are quite independent from the total chelator concentration below 10 µM, but depends more on the Cu-loading desired, and hence on the detection limit and sensitivity of the probe (see Fig. 11A).

Overall, a chelator at concentration < 10 µM needs a log K > 13 (that is the log K of HSA) to bind a portion of Cu_{EXC}. Moreover, an upper-affinity threshold has to be considered to avoid the probe saturation and hence allow a dose-dependent response to Cu. In particular, both the probe affinity and concentration must be conveniently tuned to this aim. As an example, a probe with log K = 18 ideally shows a dose-dependent Cu response in the range 0.5-10 µM at 10 µM concentration (black dots, Fig. 11B) and in the range 0.1-1 µM at 1 µM concentration (red dots, see Fig. 11B).

These interesting, albeit simplistic, thermodynamically-based considerations reveals that the affinity of the chelator must be suitably chosen as a function of the specific application sought. Indeed, an excess of an *outcompeting* chelator, such as EDTA, allows the quantitative determination of Cu_{EXC}, but it could be detrimental if used for *in vivo* applications as it would considerably perturb Cu homeostasis. Conversely, a *competing* probe that binds only a portion of the Cu_{EXC} cannot achieve a precise quantification unless all the thermodynamic (and kinetic) parameters of the system analyzed are known. Notwithstanding, it allows to compare different samples and also to detect dynamic changes of Cu levels.

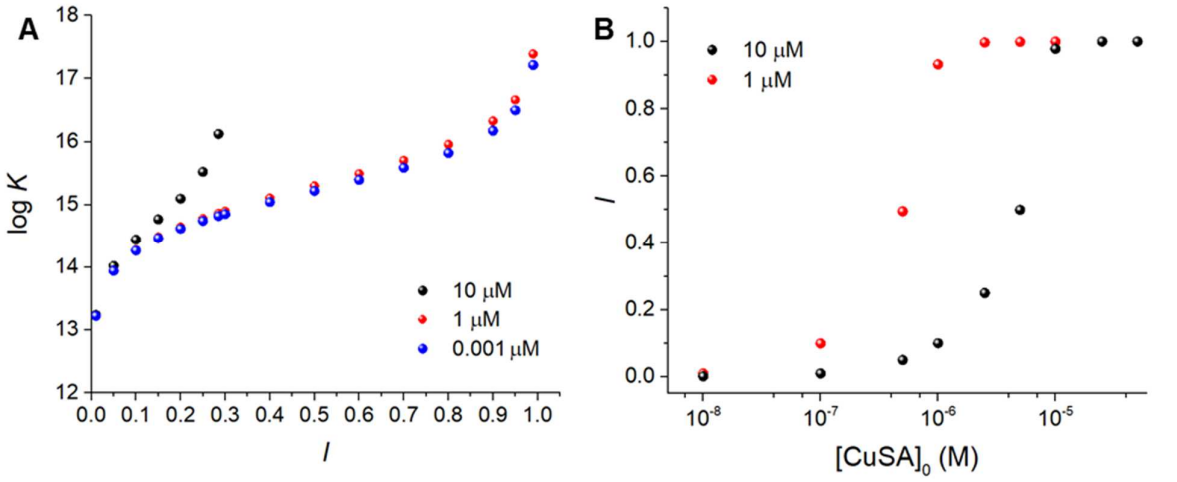

Figure 11. Thermodynamic criteria to design and apply a chelator for the measurement of Cu_{EXC}. A) Relation between the stability constant (log K) of a probe at different concentrations (black dots, 10 µM; red dots, 1 µM; blue dots, 0.001 µM) and its Cu^{II} loading l in the presence of $[HSA]_0$ = 500 µM and $[CuHSA]_0$ = 3 µM; B) the loading of a probe with log K = 18 at 10 µM (black dots) or 1 µM (red dots) concentration as a function of the Cu_{EXC} concentration ($[CuHSA]_0$).

2.1.2.2 Reversibility

The real-time monitoring of Cu fluctuations in a biological system also requires the reversibility of the probe, that is the ability to bind but also release Cu if the medium becomes more competitive (e.g. if Cu is translocated or the concentration of endogenous ligands increases). In order to be reversible, a probe has not to be an outcompeting chelator, i.e. it must have a not too high affinity (see above). In addition, the Cu-chelator complex has also to be kinetically labile and, notably, it should undergo Cu-exchange reactions faster than the timeframe in which Cu fluctuations occur. It is noteworthy that the dissociation rate constant (k_{off}) of a chelator with affinity log K > 13 may be very low (e.g. if the association rate is diffusion-limited, i.e. $k_{on} = 10^9$ $M^{-1}s^{-1}$, $k_{off} < 10^{-4}$ s^{-1},

which implies half-time of hours) to ensure a fast transfer via a pure dissociative mechanism. Hence, the ability of the chelator to form (even transient or low populated) ternary complexes enhancing the Cu transfer via an associative mechanism could be beneficial (see section 2.5).

2.1.2.3 Selectivity

Another fundamental aspect to consider in the chelator choice or design is the selectivity for Cu^{II} over the other biological cations. In particular, selectivity is not a concern when a very large excess of an outcompeting chelator is used, especially if the complex is detected by elemental analysis, such as in the methods described above. On the contrary, the selectivity of a luminescent probe, used at (sub)micromolar concentration, must be taken into account. Notably, the selectivity of a probe for Cu^{II} may arise from either (i) the selective binding of Cu^{II} or (ii) the selective response (e.g. fluorescence quenching) of the probe in response to Cu^{II}. However, although a probe based on a non-selective chelator but with a selective response could be able to detect qualitative Cu fluctuations, it would not be recommended for quantification purposes as the signal may also change indirectly due to the binding equilibria involving the competing cations. Therefore, an intrinsically selective chelator is preferable.

It could be erroneously argued that the selectivity of a ligand for Cu^{II} is guaranteed by virtue of the Irving-Williams series (see section 1.2.1), which actually compares the affinity of equivalent concentrations of divalent cations to a unique ligand. However, in a biological system, many ligands and cations co-exist at different concentrations. Hence, the real selectivity of a chelator in a biological medium depends on the concentrations and affinity of all the competing ligands and cations.

Among essential biometals, only Zn^{II} practically represents a relevant issue for the selectivity of a ligand for Cu^{II}. Indeed, Zn^{II} is the most similar ion to Cu^{II} in terms of intermediate hard/soft character and position in the Irving-Williams series. In particular, Irving and Williams showed that the log (K_{Cu}/K_{Zn}), which we can use as a selectivity parameter, spans from ~ 1 to ~ 6 for different types of common ligands.[4,5] Roughly, this also means that such ligands are selective for Cu^{II} in the presence of ~ 10- to 10^6-fold excess of Zn^{II}.

Overall, in order to compete with a ligand for Cu^{II} but not Zn^{II}, a chelator needs higher selectivity for Cu^{II}, i.e. higher log (K_{Cu}/K_{Zn}), and in particular higher log K_{Cu} but lower log K_{Zn} compared to the competing ligand. As an example, in blood serum, where ~12 μM Zn^{II} (~ 75–90% of total serum Zn) is bound to HSA (in a different site than Cu^{II}) with log K_{Zn} = 7,[61,270] the probe needs log K_{Zn} < 7 and log K_{Cu} > 13, thus a log (K_{Cu}/K_{Zn}) > 6. Such requisite is quite demanding and not fulfilled by most ligands, including those used so far in the measurement of Cu_{EXC} (see Table 6).

Notwithstanding, chelators forming square-planar complexes involving at least one amidate donor can be sufficiently selective for Cu^{II} over Zn^{II}, as the latter is normally not acidic enough to foster amide deprotonation. Remarkably, this is the case of the naturally-occurring N-terminal Xxx-His and Xxx-Zzz-His (ATCUN) peptide motifs already described (see section 1.2.4.1). In addition, aminomethyl-phenolate ligands (see L2 in Fig. 12) have shown a suitable selectivity owing to the phenolate donors.[271] Furthermore, although aza-crown ethers such as cyclam and cyclen (see Fig. 12) have higher Cu vs Zn selectivity than HSA (i.e. log (K_{Cu}/K_{Zn}) > 6), they would also bind a significant portion of Zn^{II} as their log K_{Zn} >> 7.[272]

Table 6. Selectivity of some chelators for Cu^{II} against Zn^{II}.

CHELATOR	log K_{Cu} ˙	log K_{Zn} ˙	log (K_{Cu}/K_{Zn})
HSA	13 [62]	7 [61] ‡	6
His	18.3 [273]	12 [274]	6.3
EDTA	15.9 [49]	13.6 [275]	2.3
Phen	15.4 [276]	11.9 [276]	3.5
Xxx-Zzz-His	12-15 [72]	(n/a)	(12-15)
Xxx-His	12-13 [72]	3 [145]	9-10
L2	13.8 [272]	6.1 [272]	7.7
Cyclam	23.8 [272]	12.6 [272]	11.1
Cyclen	21.1 [272]	12.7 [272]	8.4

˙ Values are log $K_{7.4}$ for all chelators except for His and Phen, for which log β_2 values are considered.
‡ Note that HSA binds Zn^{II} in a different site than Cu^{II}.

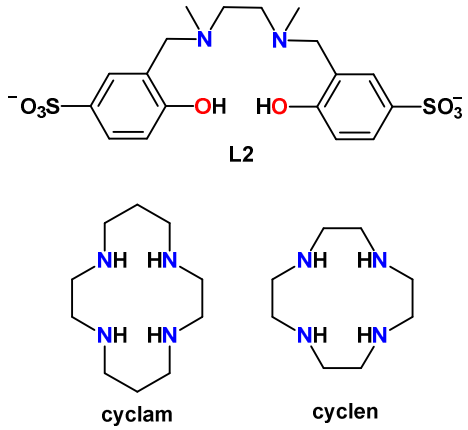

Figure 12. Ligands showing high selectivity for Cu^{II} over Zn^{II}. Metal-binding atoms are coloured.

Finally, the selectivity can be also compromised by a kinetic competition between Cu^{II} and Zn^{II} transfer from endogenous ligands to the probe. For instance, the dissociation of Cu^{II} from HSA may be relatively slow while Zn^{II} is more readily released (see section 3.3).

2.1.2.4 Detectability

Besides the requisites concerning the Cu^{II}-binding site of a luminescent probe, the luminescent moiety must also comply with some requirements in order to be applied in biological systems. First, its limit of detection (LOD) should be lower than the Cu_{EXC} concentration whose measurement is sought. Among the several factors influencing the LOD, the brightness (i.e. the product of the molar extinction coefficient, ε, and the quantum yield, Φ) of the luminophore is clearly paramount.

Besides, luminescence detection in biological media is particularly challenged by the "inner-filter effect" and autofluorescence. Indeed, several biomolecules, such as aromatic amino acids (Trp, Tyr and Phe), heme groups and flavins, absorb light in the UV-visible spectral region. Consequently, autofluorescent emission is observed when fluorescent biomolecules are photoexcited. As the biological medium constitutes the largest portion of a sample to which a luminescent probe is added, it can absorb a considerable portion of the exciting light, representing a "inner-filter" that hamper the efficient excitation, and in turn the emission, of the probe. Likewise, autofluorescence can represent a non-negligible background in the detection of the

probe signal. To circumvent such issues, suitable brightness and excitation/emission wavelengths are required, which have to be adapted to the medium of interest.

On balance, the spectral regions from the far red to the near-infrared (NIR), i.e. 650-950 nm (NIR-I) and 1000-1700 nm (NIR-II), where blood and water absorption are minimal, represent the most "transparent" windows in biological tissues. As a result of low absorption and scattering, red/NIR light also shows a maximal depth of penetration in biological tissues (~ 5 mm), appearing ideal for *in vivo* bioimaging. Therefore, red/NIR-absorbing luminophores are the most suited for applications in biological media and are the focus of intense research.[277–280] In this respect, an emerging approach is represented by two-photon excitation, which exploits the simultaneous (within fs) absorption of two NIR photons by fluorophores that emit in the visible region.[281,282]

Furthermore, to get rid of the autofluorescent background, which is characterized by short lifetime (up to few ns), luminophores presenting higher emission lifetime, such as lanthanides ions, can be used (see section 2.4.1.2).[283,284]

2.2 Luminescent probes for Cu^{II} – State of the art

In the following, luminescent Cu^{II} probes are classified depending on their response and mechanism and described highlighting their pros and cons.

2.2.1 Turn-off probes

Turn-off probes for Cu^{II} can be developed straightforwardly due to the widely-known ability of Cu^{II} to quench fluorescence emission via ultrafast non-radiative decay and spin-orbit coupling.[285,286] Turn-off probes are typically coordination-based, i.e. designed via the combination of a Cu^{II}-ligand and a luminophore located close to each other to optimize the quenching by Cu^{II} (which depends on the distance).

Many kinds of ligands have been used so far, most of which are poorly selective for Cu^{II}. In this case, the selectivity may arise from the Cu^{II}-specific quenching activity. In principle, coordination-based probes benefit from the reversibility of Cu^{II}-binding, as long as ligands with suited affinity and kinetic lability are used (see section 2.1.2).

As regards the emitting moiety, many diverse luminophores have been exploited, mostly organic dyes covering the UV to NIR spectral regions (e.g. pyrene, anthracene, dansyl, fluorescein, cyanine and BODIPY) but also luminescent inorganic complexes of transition metal ions such as Ru^{II} and Ir^{III} or lanthanides such as Tb^{III} and Eu^{III} (see section 2.4.1.2).[286–291]

Overall, albeit easily designed, turn-off luminescent sensors are flawed because the emission quenching could also arise by inner-filter effect by the medium, degradation of the probe and undesired off-target interactions.

2.2.2 Turn-on probes

Due to the shortcomings of turn-off probes, turn-on sensors are generally preferred, as they are also easier to quantify and allow for higher spatial resolution in the case of imaging applications.[287] However, as Cu^{II} is an effective quencher, the design of coordination-based turn-on sensors appears very challenging.

Actually, turn-on Cu^{II}-probes have been successfully developed using a reactivity-based approach, i.e. exploiting a Cu^{II}-induced reaction that enhances the fluorescence emission.

2.2.2.1 Reactivity-based chemodosimeters

Reactivity-based probes, also known as chemodosimeters, generally rely on the peculiar Lewis acidity or redox activity of Cu^{II}, from which selectivity also stems. Thus, the main reactions exploited are Cu^{II}-induced hydrolysis or oxidation of a "pre-fluorophore" that turns into an emitting compound. Nevertheless, the coordination of the pre-fluorophore to Cu^{II} seems to be at least partially required for the reaction to occur (unless in case of an outer-sphere oxidoreduction) and hence a suitable affinity is also required. In particular, common substrates of Cu^{II}-promoted hydrolysis are hydrazine, hydrazide, or hydrazone derivatives. Indeed, many chemodosimeters are non-fluorescent Rhodamine B or fluorescein spirolactam derivatives that undergo Cu^{II}-promoted spirolactam ring-opening and following hydrolysis of a hydrazine, hydrazide, or hydrazone group, with the release of the fluorescent moiety (see Fig. 13A).[286,287,289] Interestingly, some of these reactions are reversible. Finally, it is worth pointing out that stimuli other than Cu, such as low pH, can also trigger the opening of spirolactam rings or the hydrolysis of hydrazones, and hence chemodosimeter are also vulnerable to off-target response.[287] Besides, oxidoreduction-based chemodosimeters usually undergo a Cu^{II} induced oxidative cyclization or oxidation of an imine group to a carboxylic acid.[292–296] Furthermore, the "click" Cu-catalysed azide/alkyne cycloaddition (CuAAC) has been also used to develop Cu-selective reactivity-based sensors (see Fig. 13 B).[297–302] Importantly, to be detectable via a CuAAC-based probe, Cu^{II} has to be reducible (generally by $AscH^-$) and only partially and transiently coordinated by the substrates. Interestingly, among physiological Cu^{II}-complexes, only Cu-His has been shown to catalyse the CuAAC up to date.[303] Overall, as a consequence of relative long reaction time and common chemical irreversibility, chemodosimeters are not ideal for the real-time monitoring of Cu fluctuations.

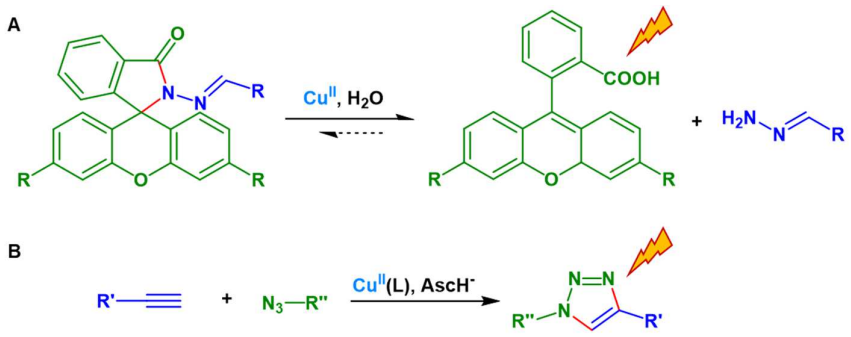

Figure 13. Mechanisms of reactivity-based Cu^{II}-probes. A) Cu^{II}-promoted spirolactam ring-opening and hydrolysis of Rhodamine B/fluorescein derivatives; B) Cu^{II}-catalysed azide/alkyne cycloaddition.

2.2.2.2 Putative coordination-based turn-on probes

Although Cu^{II} normally quenches the emission of luminescent ligands, some putative coordination-based turn-on probes have also been reported (see Table 7 and Fig. 15).[304–318] The observed fluorescence enhancement has been mostly attributed to the modulation of photoinduced electron transfer (PET) or internal charge transfer (ICT). Besides, a poorly defined chelation-enhanced fluorescence (CHEF) mechanism is also claimed for certain probes.

Table 7. Putative coordination-based turn-on Cu^{II} probes.

Probe	Mechanism	Reversibility	Solvent	Reference
1	PET	Yes (EDTA) No (EDTA)[238]	MeCN:PBS 6:4 pH 7.4	314
2		n/a	MeCN:HEPES 1:1 pH 7.0	304
3		n/a	MeCN:HEPES 3:1 pH 7.0	311
4		n/a	MeOH:HEPES 7:3 pH 7.0	305
5		n/a	MeCN:MOPS 7:3 pH 7.0	312
6		n/a	MeCN:H_2O	316
7		Yes (EDTA)	MeCN:Tris-HCl 1:1 pH 7.4	309
8	ICT	n/a	MeCN	306
9		Yes ($C_2O_4^{2-}$, EDTA, CN^-, PO_4^{3-}, S^{2-})	DMSO:H_2O 2:1 pH 8.0	307
10		n/a	MeCN:H_2O 3:1	310
11	CHEF	n/a	MeCN:HEPES 7:3 pH 7.5	313
12		n/a	MeCN:HEPES7:3 pH = 7.4	315
13		Yes (EDTA)	MeCN:Universal buffer 9:1 pH 6.8	317
14		Yes (EDTA)	MeCN:H_2O 1:1 pH 7.2	318
15	n/a	n/a	MeCN	308

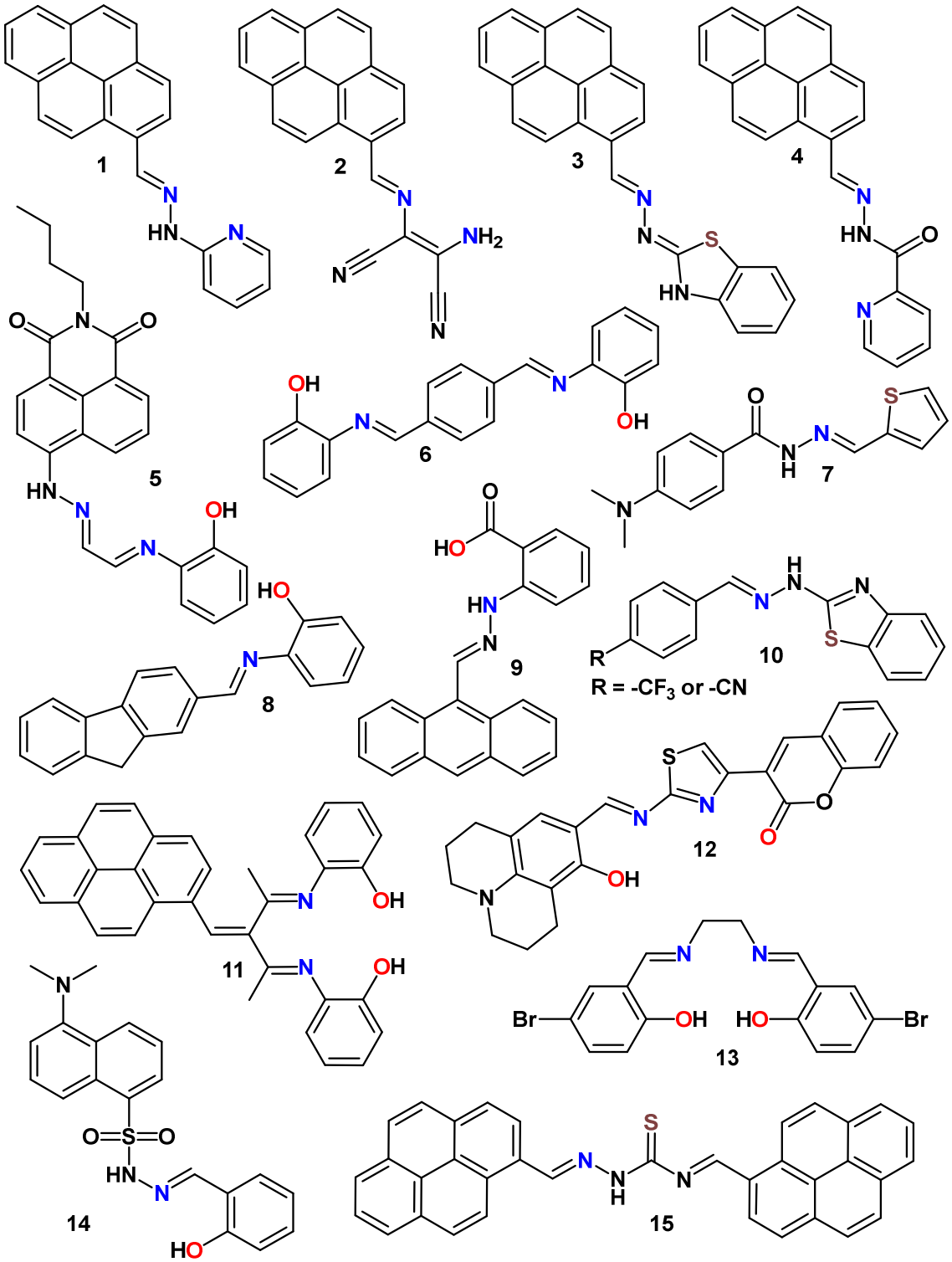

Figure 15. Structures of putative coordination-based turn-on Cu^{II} probes **1**-**15**. Cu-binding atoms are coloured.

In a (reductive) PET-based turn-on sensor, the ligand (L) moiety quenches the photo-excited fluorophore (F*) group via an intramolecular electron transfer, provided that the HOMO of the ligand ($HOMO_L$) has higher energy than the HOMO of the fluorophore ($HOMO_F$). The binding of an analyte to the ligand decreases the energy of its HOMO below that of the fluorophore so that the PET cannot occur, enabling the fluorescence emission (see Fig. 14). Importantly, the existence of PET should be proven via time-resolved spectroscopies.[319,320] ICT instead pertains to π-conjugated systems with electron-rich and electron-poor (donor and acceptor) groups at opposite ends of the molecule, such that a dipole is generated upon photo-excitation, which can be modulated by the binding of an analyte. Notably, if the analyte binding destabilizes the excited state with respect to the ground state, a blue-shift of absorption and fluorescence emission are observed, while a red-shift occurs when the excited state results stabilized (see Fig. 14).[321]

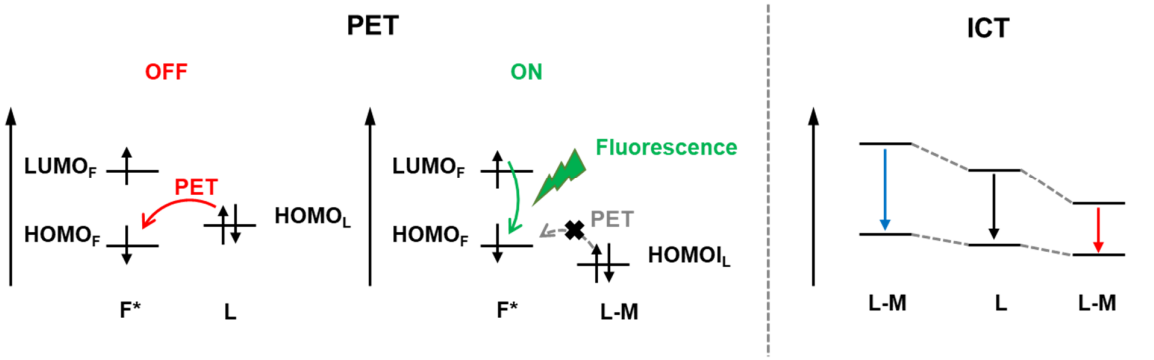

Figure 14. Schematic mechanism of PET and ICT. In PET, the metal binding stabilizes the ligand HOMO so that the PET between the ligand HOMO and the Fluorophore is prevented and fluorescence emission allowed. In ICT, the metal binding either stabilizes or destabilizes the excited state with respect to the ground state causing a blue or red shift, respectively.

Overall, many of these probes shared common structural features, such as a hydrazone group linking the luminescent moiety and the Cu^{II}-binding site, and behaviour (see Fig. 15 and Table 7): for instance, they showed selective response for Cu^{II} despite the non-selectivity of the Cu^{II}-binding site, they have been only shown to work in the presence of acetonitrile (MeCN) and, last but not least, the reversibility has not usually been verified. Therefore, the mechanism behind the turn-on of such probes appears to be puzzling and questionable.

2.2.3 Ratiometric probes

Intensiometric probes (i.e. based on the intensity change of one signal), especially if turn-off, does not seem ideal for quantification and imaging purposes. Indeed, in biological systems, the signal could be not only a function of Cu concentration but also of the probe concentration, which in turn depends on the local partitioning and the potential degradation. In addition, off-target interactions altering the probe response to Cu^{II} cannot be ruled out for both turn-off and turn-on systems. Therefore, ratiometric probes based on the measurement of the *ratio* of two signals appear more advantageous, as they are less sensitive to external factors. Hence, selectivity and quantifiability result improved.[287]

A simple kind of ratiometric probe (here called "type I") is composed of two luminescent moieties, one that is sensitive to the analyte while the other serves as an analyte-insensitive "reference" signal (see Table 8). Type I ratiometric probes are normally turn-off, as the Cu-responsive luminophore is quenched while the "reference" fluorophore is not perturbed or quenched to a lower extent.[322,323] Alternatively, a ratiometric probe can be conceived based on a system emitting two related analyte-sensitive reversible signals ("type II", see Table 8). In particular, the analyte can trigger the disappearance of a signal and the appearance of the second, for instance via ICT and/or FRET (Fluorescence Resonance Energy Transfer).[324,325] Type II probes are typically ICT-based naphthalimide derivatives that undergo a blue shift upon Cu^{II}-binding to aromatic amine donors.[326–328] Noteworthy, a red-shift can be instead obtained if Cu^{II} triggers the deprotonation of such amines (as for probe **20**).[329] Interestingly, these type II sensors show a *coordination-based* ratiometric turn-on response. In addition, ratiometric sensors can be developed on a reactivity-based mechanism, for instance coupling a chemodosimeter with a non-reactive fluorophore.[325,330]

Overall, none of the reported ratiometric Cu^{II}-probes has a suitable affinity to compete with endogenous ligands in biological systems such as blood plasma. In particular, the need for aromatic donors to develop ICT-based "type II" ratiometric sensors may clash with the requirement of high affinity for application in biological media. Besides, the ligands found in such ratiometric probes show also weak selectivity, so much that dipicolylamine (DPA) ligand found in probes **16** and **22**, for instance, is commonly used in zinc sensors.[331–334]

Table 8. Ratiometric probes for Cu^{II} reported in the literature.

Probe	Type	Affinity	Solvent	λ_{ex} (nm)	λ_{em} (nm)	Reference
16	I	4.8	PIPES	342	486 (ref) 648 (down)	[322]
17		4.5	HEPES	395	435 (ref) 526 (down)	[323]
18	II (coordination-based)	6.1	EtOH:HEPES 4:6	451	475 (up) 525 (down)	[326]
19		7.5	MOPS	455	477 (up) 535 (down)	[328]
20		n/a	EtOH:HEPES 6:4	420 510	518(down) 592(up)	[329]
21		n/a	THF:HEPES 9:1	350	435 (up) 510 (down)	[327]
22		4.9	MeCN:Tris-HCl 9:1	405	460 (up) 555 (down)	[324]
23	II (spirolactam ring-opening + hydrolysis)	n/a	MeCN:Tris-HCl 20:1	420	577 (up) 535 (down)	[330]
24		n/a	MeCN:HEPES 2:8	410	481 (down) 581 (up)	[325]

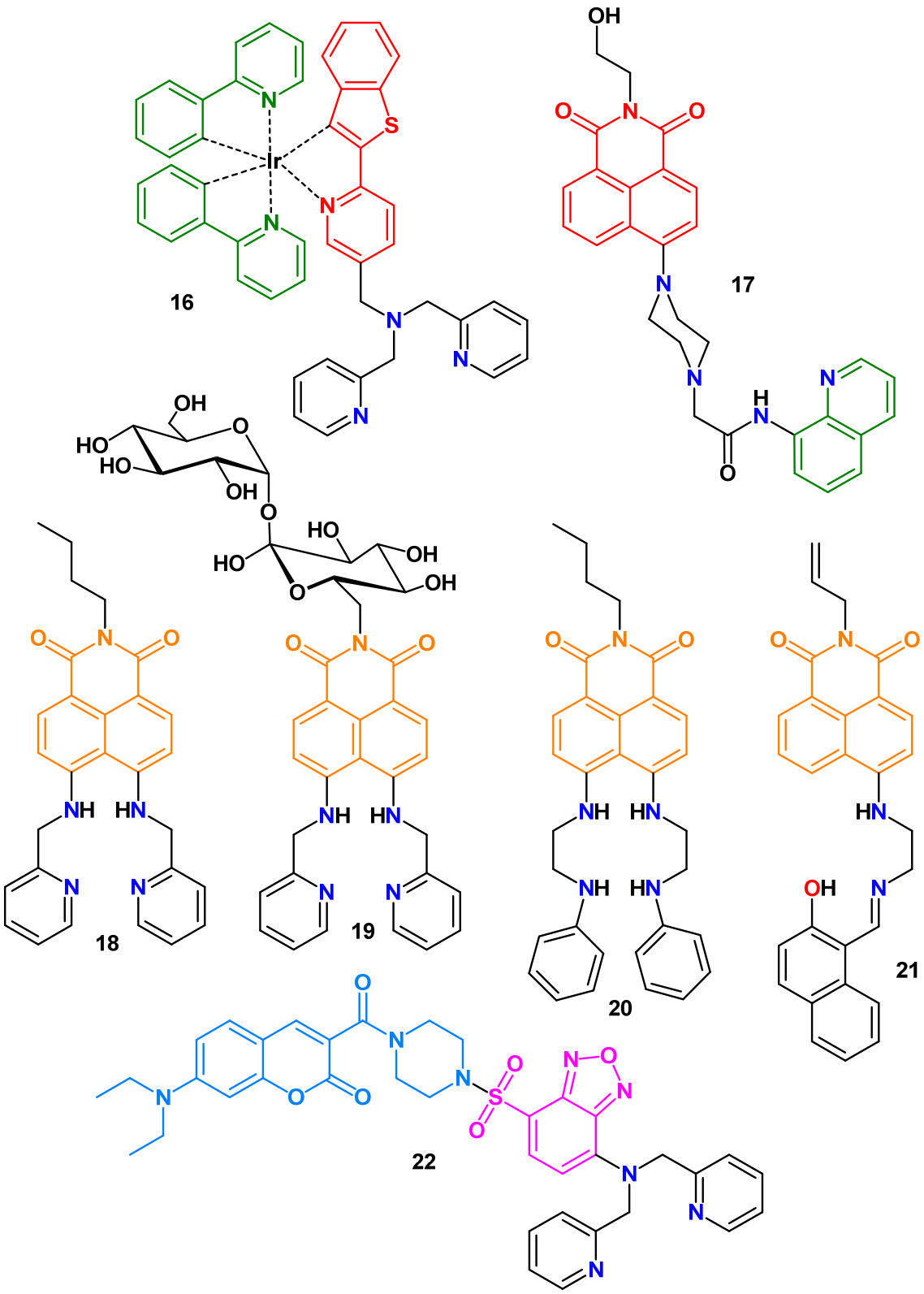

Figure 16. Structures of coordination-based ratiometric Cu^{II} probes **16**-**22**. Cu-binding atoms are coloured. For type I ratiometric probes, "reference" fluorophores are coloured in green and quenched fluorophores in red. The naphtalimide core of type II ratiometric probes is coloured in orange. In probe **22**, the donor and acceptor of a FRET couple are coloured in light blue and pink, respectively.

2.2.4 Applications of Cu^{II}-probes in biological media

Among the hundreds of luminescent Cu^{II} probes developed to date, only a few have been applied for the *in vitro* measurement of Cu^{II} in body fluids or in cell culture (see Table 9 and Fig. 17). In this regard, it seems very surprising how many Cu^{II} sensors, either turn-off/on or ratiometric, have been claimed to allegedly detect intracellular Cu^{II}. As previously described, in the intracellular environment Cu^{II} state occurs only in the transient redox cycling of Cu-enzymes, whose sites are buried and inert, while Cu is trafficked in the Cu^{I} state bound to metallochaperones due to very reducing conditions (e.g. 1-10 mM levels of GSH). Clearly, any probe for intracellular Cu should have a very high affinity (log K > 17-20) to compete with intracellular ligands, which is a condition fulfilled by very few Cu^{I} chelators so far.[335] Overall, the observation of a putative Cu^{II}-responsive signal inside cells is doubtful and rather points towards a non-specific or indirect response. For instance, low pH microenvironments could trigger reactions, and hence a response, similar to Cu^{II} ions.[287] Alternatively, the Cu^{II}-related signal inside cells could arise indirectly, e.g. via oxidative processes involving Cu^{II}-induced ROS.

Besides, all the probes listed in Table 9 show one or more shortcomings for the measurement of Cu_{EXC} in biological samples and none of them fulfils the whole set of requisites that have been defined in section 2.1.2. In particular, all the probes used in blood samples do not have a suitable affinity to detect endogenous Cu_{EXC}. [249,300,302,336–342] Instead, a couple of low-affinity sensors seemed to detect micromolar levels of Cu in brain dialysates, where the affinity required to compete with endogenous ligands is likely lower than in the blood.[343,344] Interestingly, the probe **19** was able to detect a portion (about 25%) of the Cu_{EXC} released by synaptosomes upon depolarization.[345] Only the genetically-encoded ATCUN-based probe **40**, which was applied in the detection of extracellular Cu^{II} in cell culture, was shown to compete with HSA for Cu^{II} via a competition assay, even though its apparent affinity determined by fluorescence measurements appeared to be unsuited. Moreover, among the sensors listed in Table 9, only this ATCUN-based probe benefits from a highly Cu^{II}-selective ligand.[346] Importantly, the assessment of a probe selectivity for Cu^{II} against equimolar or low excess of competing ions in buffered solution, as usually reported in the literature, is absolutely not real proof of selectivity in biological systems, since the availability of the other cations is often much higher (e.g., selectivity for Cu^{II} over Zn^{II} in the blood should be theoretically proven in the presence of > 10^6-fold excess of Zn^{II}).

Concerning the luminescent moiety, most probes were equipped with green-emitting dyes, while very few examples exhibit the more favourable red/NIR emission. Finally, even if a Tb^{III} coordination polymer appears among the sensors reported, the time-delayed detection of Tb^{III} long lifetime emission was not exploited to overcome the autofluorescent background.

In conclusion, it seems evident that current probes lack suitable affinity, selectivity, and luminescent signals for the application in biological fluids, especially in blood, which is the most challenging sample with regard to both the competition with endogenous ligands and the luminescence detection.

Table 9. Cu^{II} probes applied in Cu^{II} detection in biological systems.

Probe	Mechanism	Affinity	Reversibility	λ_{ex} (nm)	λ_{em} (nm)	Sample	Detection range (μM)	Ref.
25	Turn-Off	4.9	n/a	430	490	Human blood (spiked)	1-10	[336]
26	Turn-Off	n/a	Yes (I^-)	270	310		~ 0.009-2.5	[337]
27	Turn-Off	n/a	n/a	340	412, 518		1-10	[338]
28	Turn-Off	n/a	n/a	704	786	Mouse blood (spiked)	0.45-36.3	[339]
29	Turn-Off	n/a	Yes (EDTA)	500	727	Human blood	16-23	[340]
30	Turn-On (CuAAC)	n/a	No	395	471		~ 4	[300]
31	Turn-On (CuAAC)	n/a	No	450	520		18-30	[302]
32	Turn-On (hydrolysis)	n/a	NO (EDTA)	452	482		1-5	[341]
33	Turn-Off	5	n/a	380	495		0-3	[249,342]
34	Turn-Off	n/a	Yes (Cys, His)	450	527	Human urine (spiked)	3-6	[347]
35	Turn-On (CuAAC)	n/a	No	488	525	Human urine	~ 0.13-9.9	[301]
36	Turn-Off	n/a	n/a	328	550	Rat brain dialysate	2	[343]
37	Turn-Off	n/a	Yes	365	450		2-5	[344]
38	Turn-Off	5.6	Yes	414	645	Synaptosomes	0.2-25	[345]
19	Ratiometric Turn-On	n/a	n/a	455	477/535	Cell culture	n/a	[328]
39	Ratiometric Turn-Off	n/a	Yes (EDTA)	517/432	595/510		n/a	[348]
40	Turn-Off	8	Yes (EDTA)	480	510		n/a	[346]

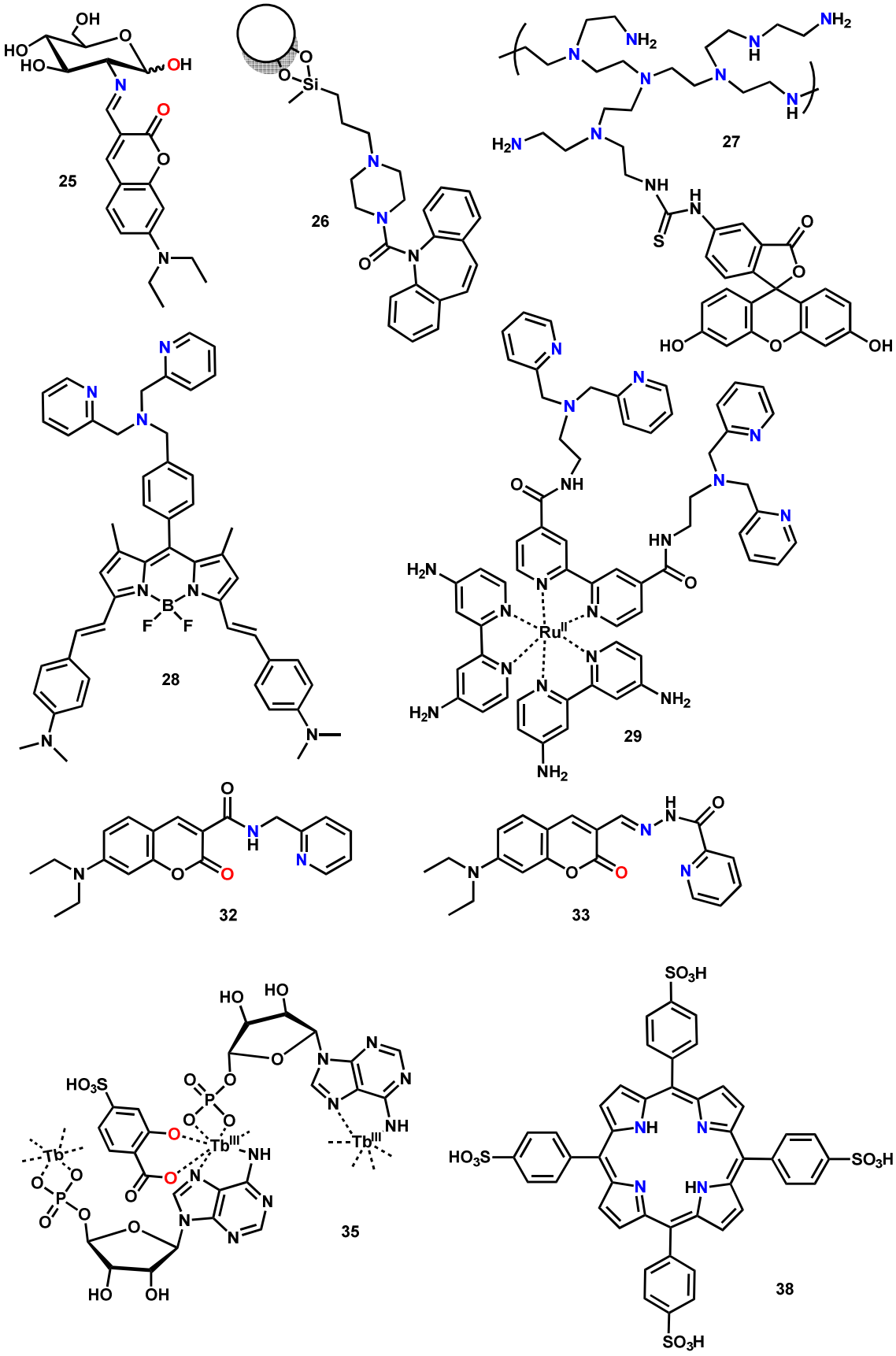

Figure 17. Structures of some coordination-based probes applied in extracellular Cu^{II} detection.

2.3 Insights into the mechanism of a putative reversible turn-on probe

2.3.1 Introduction

In section 2.2.2.2, we have questioned the coordination-based behaviour of some putative turn-on probes reported in the literature (see Table 7). To get insight into the mechanism of such kinds of probes, we choose the hydrazone 2-(2-(pyren-1-ylmethylene)hydrazinyl)pyridine, PHP, as a representative case study owing to its straightforward preparation.

PHP is composed of a pyrene group as the fluorescent unit and a hydrazinyl-pyridine as Cu^{II}-binding moiety (see Fig. 18). Such compound was shown to be weakly fluorescent, supposedly due to PET occurring between the imine nitrogen and the pyrene group, as computationally suggested by DFT (density-functional theory) calculations. Similar to most probes listed in Table 7, PHP is a promiscuous ligand whose selective turn-on response to Cu^{II} was supposed to occur upon metal binding to PHP imine and pyridine nitrogens (red in Fig. 18). This was shown in the presence of MeCN (in particular in MeCN:PBS 10 mM 4:6) due to limited water solubility. However, MeCN is not an "innocent" solvent for Cu^{II}-binding/reactivity studies, at it is known to stabilize Cu^{I} via coordination (e.g. $[Cu^{I}(MeCN)_4]^+$ salts are commonly used as Cu^{I} source).[349] Moreover, the reversibility of PHP was also shown by means of the stronger chelator EDTA (log $K_{7.4}$ = 15.9).[314]

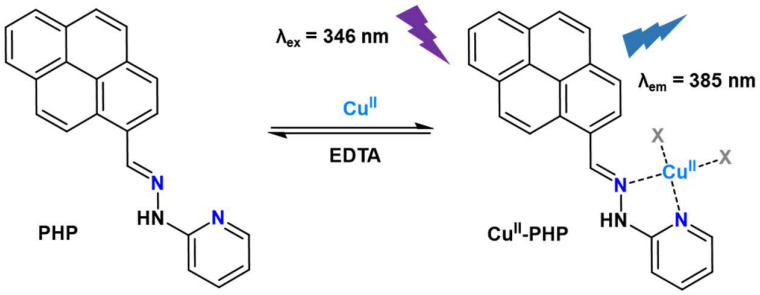

Figure 18. Scheme of the putative mechanism of Cu^{II} detection by the turn-on probe PHP. Cu^{II} is supposed to bind to the probe via imine and pyridine nitrogen donors (blue) eliciting a reversible turn-on response via suppression of PET.

2.3.2 Results and discussion

We started our re-investigation monitoring the interaction of PHP with Cu^{II} in a MeCN:HEPES 25 mM 1:1 (pH 7.4) by UV-vis absorption spectroscopy. PHP showed an absorption band at 387 nm that underwent a progressive decrease upon the addition of Cu^{II} while a new blue-shifted band appeared at 346 nm (see Fig. 19A). Besides, upon excitation at 346 nm, an increase of the fluorescence emission (see Fig. 19B) was observed. These findings resulted in agreement with the previous report. However, we realized that the absorption shift and the related fluorescence enhancement were occurring slowly, i.e. within ~ 1h (see Fig. 19B, inset). Furthermore, the addition of excess EDTA surprisingly did not reverse the effect of Cu^{II} (blue curves, Fig. 19). These results seem not compatible with a mere Cu^{II}-binding to PHP, which should be fast and reversible, but rather pointed towards the development of an irreversible chemical reaction. In this case, Cu^{II} reactivity rather than coordination should be accountable for the reported probe selectivity.

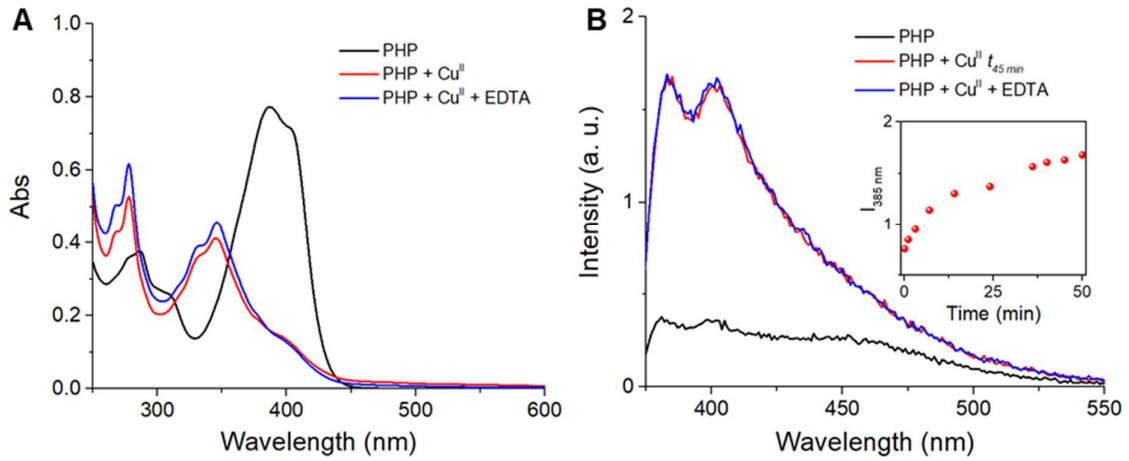

Figure 19. Spectroscopic analysis of the interaction between PHP and Cu^{II}. A) UV-vis absorption spectra and B) fluorescence spectra. Inset: evolution of the fluorescence emission (at 385 nm) over time upon addition of Cu^{II}. Conditions: A) [PHP] = 20 μM, [Cu^{II}] = 25 μM, [EDTA] = 40 μM; B) [PHP] = 10 μM, [Cu^{II}] = 20 μM, [EDTA] = 20 μM; solvent: MeCN:HEPES (25 mM, pH 7.4) 1:1.

For instance, Cu^{II} reduction to Cu^{I} and the following Cu^{I}-binding to the probe could be a likely mechanism to support the turn-on response observed, since coordination-based probes for Cu^{I} are conceivable. Hence, we assessed whether Cu^{II} undergoes reduction during the interaction with PHP. To this aim, the Cu^{I}-specific chromophore bathocuproine sulfonate (BCS) was added, showing the appearance of a characteristic band at 483 nm due to the formation of $Cu^{I}(BCS)_2$ complex and proving the formation of Cu^{I} during Cu^{II} *reaction* with PHP (see Fig. 20A). Besides, in light of the Cu^{I}-stabilizing capacity of MeCN, we tested whether such co-solvent had a role in the reaction. Interestingly, when MeCN was replaced by dimethyl sulfoxide (DMSO), no absorption band at 346 nm appeared, suggesting that the reaction was not taking place and that MeCN seems to be essential to promote the reaction via Cu^{I}-stabilization (see Fig. 20B). Furthermore, to check whether Cu^{I} binding was responsible for the turn-on behaviour, $[Cu^{I}(MeCN)_4]^{+}$ was added to PHP in MeCN. No significant change of the PHP absorption band (see Fig. 20C) was observed, suggesting that the absorption shift and fluorescent turn-on observed were not due to Cu^{I}-binding but rather to a chemical modification of the PHP molecule.

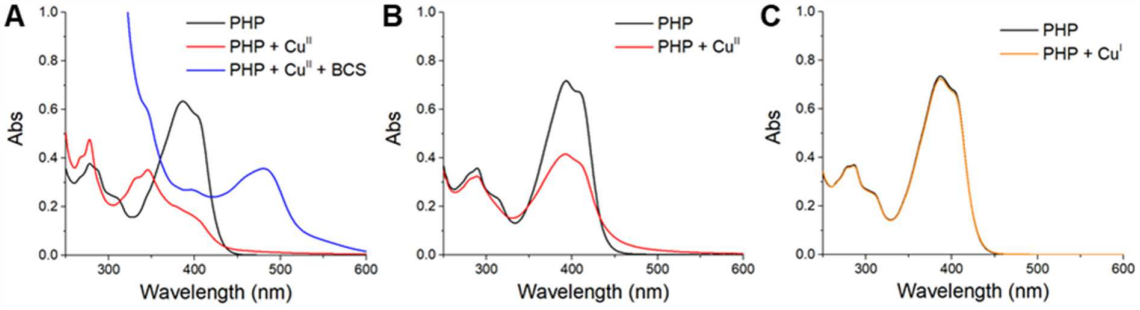

Figure 20. Evidence for the reduction of Cu^{II} to Cu^{I} by PHP in the presence of MeCN. A) The formation of $Cu^{I}(BCS)_2$ (band at 483 nm) upon addition of BCS proves the reduction of Cu^{II} to Cu^{I}; B) the replacement of MeCN with DMSO halt the reaction as no band at 346 nm appears; C) Cu^{I} does not interact with PHP. Conditions: A) [PHP] = 20 μM, [Cu^{II}] = 25 μM, [BCS] = 100 μM, MeCN:HEPES (25 mM, pH 7.4) 1:1; B) [PHP] = 20 μM, [Cu^{II}] = 25 μM, DMSO:HEPES (25 mM, pH 7.4) 1:1; C) [PHP] = 20 μM, [Cu^{I}] = 20 μM, MeCN.

Indeed, HPLC-DAD (diode array detector) analysis of the reaction mixture demonstrated the formation of several products absorbing at 345 nm, i.e. the excitation wavelength of the Cu^{II}-induced fluorescent species (see Fig. 21A). Moreover, the analysis of the UV-vis spectra corresponding to each peak revealed that the major product, **1**, showed an absorption spectrum (red curve in Fig. 21B) very similar to the excitation spectrum (light green curve in Fig. 21B) of the PHP after interaction with Cu^{II}, suggesting that the formation of product **1** is accountable for the turn-on effect.

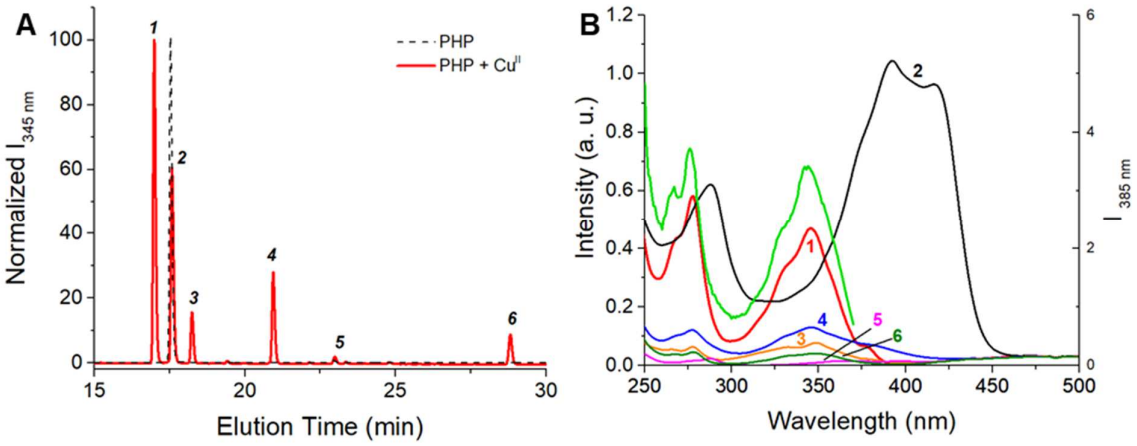

Figure 21. HPLC-DAD analysis of the reaction mixture PHP-Cu^{II}. A) Chromatograms of PHP and PHP-Cu^{II} mixture; B) DAD spectra of HPLC peaks 1-6 and excitation spectrum (light green) of PHP after reaction with Cu^{II}.

Therefore, this product was isolated by preparative TLC and characterized by ESI-HRMS and ^{1}H-NMR. Interestingly, the MS spectrum showed a peak of m/z = 320.1182 (z =1) having about 2 units lower mass than the PHP (m/z = 322.1344), which can be interpreted as the product of a $2H^+/2e^-$ oxidation. Besides, the major differences in the ^{1}H-NMR spectra of PHP and the fluorescent product concerned the hydrazone protons (δ_{NH} = 11.09 ppm and δ_{CH} = 9.13 ppm), which disappeared upon PHP oxidation (see Fig. 22A). Hence, we postulated that the reaction between Cu^{II} and PHP gives rise to the oxidative cyclisation of PHP to 3-(pyren-1-yl)-[1,2,4]triazolo[4,3-a]pyridine via the attachment of the pyridine nitrogen to the hydrazone carbon atom (see Fig. 22B). In support of this hypothesis, Cu^{II} has been shown to oxidise heterocyclic hydrazones forming 1,2,4-triazolo[4,3-a]pyridines,[350] and 3-aryl-[1,2,4]triazolo[4,3-a]pyridines have been built as deep-blue (350-450 nm) emitting fluorophores.[351] Moreover, some existing Cu^{II} turn-on chemodosimeters are actually based on Cu-promoted oxidative cyclisation of N-acyl-hydrazones, thiosemicarbazones and azo-anilines.[292,293,352,353]

Overall, we showed that PHP is not a reversible coordination-based probe for Cu^{II}, but rather an irreversible chemodosimeter based on a Cu^{II}-induced oxidative cyclisation likely forming a fluorescent triazolopyridine. With this respect, it appears unclear how PHP showed a reversible behaviour with EDTA in the original report.

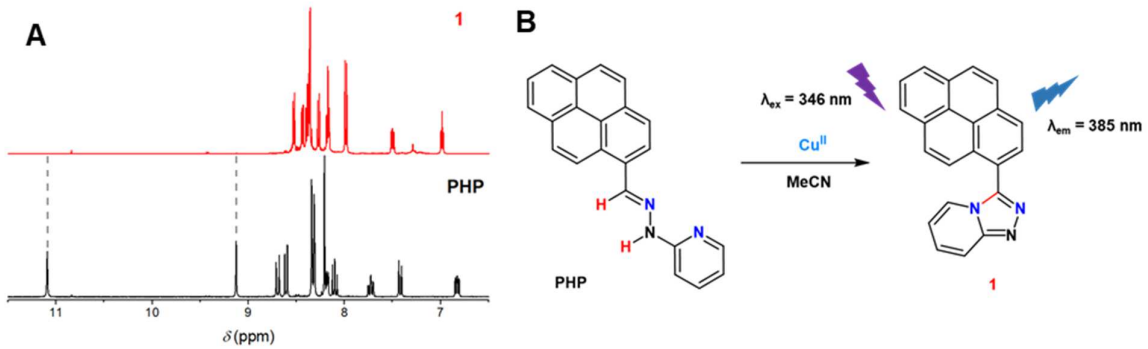

Figure 22. Characterization of compound 1. A) ^{1}H-NMR spectra of PHP (black) and compound 1 (red) show the disappearance of the hydrazone protons (grey dashed lines, δ_{NH} = 11.09 ppm and δ_{CH} = 9.13 ppm, red in B) upon reaction with Cu^{II} suggesting the formation of a 3-(pyren-1-yl)-[1,2,4]triazolo[4,3-a]pyridine (B).

Besides, we also proved that the reaction takes place only in the presence of a Cu^{I}-stabilizing agent such as acetonitrile. For this reason, we also tested whether physiological Cu^{I}-binding molecules such as glutathione (GSH), could exert the same role in the absence of acetonitrile. Indeed, GSH is able to reduce Cu^{II} and bind Cu^{I} strongly forming Cu-S clusters. Hence, we added GSH at a physiologically relevant concentration to a solution of Cu and PHP in DMSO:HEPES. While Cu^{II} induced a decrease of the PHP band in DMSO, which might be due to Cu^{II}-binding to the ligand, the addition of GSH produced a more intense and slightly red-shifted band which could be attributed to a ternary PHP-Cu-GSH complex (see Fig. 23). However, no band at 346 nm was observed and hence the PHP did not result oxidised by Cu^{II} in the presence of GSH. Interestingly, the same, red-shifted band was observed when PHP was added to a $Cu^{I}(GS)_x$ solution. Hence, it seems that GSH reduces Cu^{II} more efficiently than PHP, preventing its oxidation, and maybe form ternary complexes.

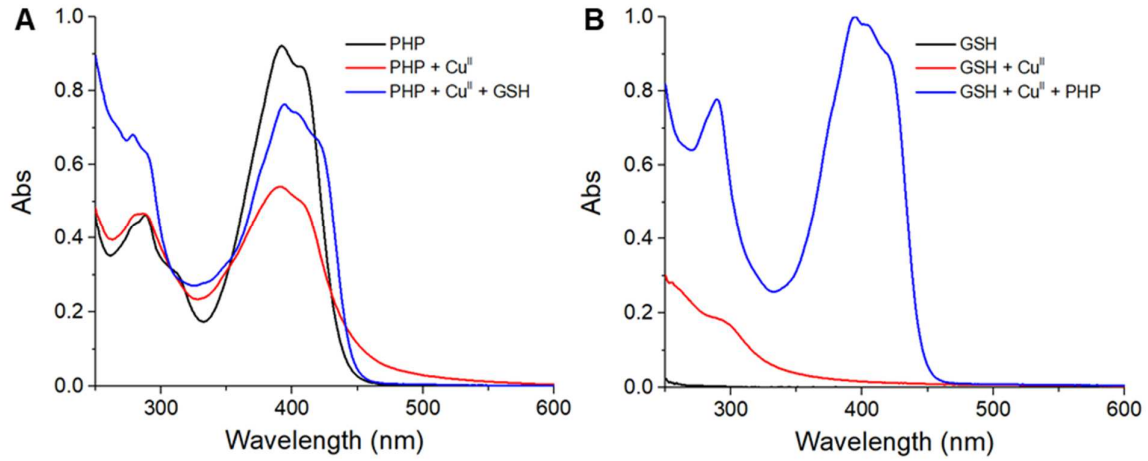

Figure 23. Interaction of PHP and Cu^{II} in the presence of GSH. A) Addition of GSH to PHP-Cu^{II}; B) addition of PHP to $CuI(GS)_x$. Conditions: [PHP] = 25 μM, [Cu^{II}] = 30 μM, [GSH] = 5 mM, DMSO:HEPES (25 mM, pH 7.4) 1:1.

2.3.3 Conclusions

Overall, our examination of PHP-Cu interaction revealed that, contrary to previous suggestions, this probe is an irreversible chemodosimeter with a slow response rather than a reversible turn-on sensor. Moreover, as the reaction occurred in the presence of acetonitrile but not in the presence of physiologically relevant thiol such as GSH, PHP appears not to be suited for Cu^{II} sensing in biological media. Furthermore, although we have discovered such an oxidation-based mechanism for PHP only, it can be speculated that the similar probes listed in Table 7 share the same or a similar reactivity-based mechanism.

In general, some issues should be taken into account and assessed during the development of a turn-on sensor to prove its real nature and mechanism. Notably, the response of the probe to Cu^{II} should be fast, i.e. complete in the mixing time in buffer, and reversible to be related with mere Cu^{II}-binding; otherwise, a chemical reaction is likely to occur. To (dis)prove this, HPLC analysis of the probe before and after interaction with Cu^{II} is recommended. In this context, care should be also taken in the analysis of NMR spectra to study the interaction of PHP with Cu^{II}. Actually, as paramagnetic Cu^{II} broadens NMR signals due to paramagnetic relaxation enhancement, the interpretation of NMR peak disappearance as Cu^{II}-binding to the corresponding atoms can be misleading, hiding a potential chemical modification. Hence, it is advised to record NMR spectra also after the removal of Cu^{II} from the mixture.

Finally, the Cu^{II}-selective response of turn-on probes based on a promiscuous ligand should be suspicious. For instance, while the characteristic Cu^{II} quenching ability can be conceived as the source of a specific turn-off response by non-specific ligands, a turn-on response due to the suppression of PET (as initially proposed for PHP) in a non-specific ligand should be also observed for metals others than Cu^{II}, as demonstrated by the existence of many PET-based Zn^{II}- and pH-responsive probes.[319,320] Otherwise, the peculiar (redox) catalytic activity of Cu^{II} could be envisioned as the basis for the selective response.

Overall, our study showed that the *rational* design of reversible coordination-based turn-on Cu^{II} probes, as well as the application of turn-on chemodosimeters in biological samples, remain very challenging.

2.3.4 Experimental section

2.3.4.1 Materials

Commercially available chemicals were used without further purification. Thin layer chromatography (TLC) was carried out on Merck silica gel 60 F254 coated aluminium plates and visualization when required was achieved using UV light. ^{1}H NMR measurements were performed in DMSO-d_6 on a Bruker Avance III 300 MHz spectrometer. ESI-HRMS spectra were acquired on an Exactive Plus EMR Orbitrap (Thermo Fischer) spectrometer.

2.3.4.2 Synthesis of PHP

PHP was prepared by adapting the procedure reported in the literature: 1-pyrenecarboxaldehyde (230 mg, 1.0 mmol) and 2-hydrazinopyridine (126 mg, 1.1 mmol) were mixed in 10 mL ethanol solution and the reaction mixture was refluxed overnight. The resulting yellow precipitate was isolated by filtration and washed with ethanol and hot ethyl acetate to give a yellow solid (315 mg, 98% yield). ESI-HRMS: calculated m/z for $C_{22}H_{16}N_3$ ($[M+H]^+$) 322.1344, found m/z = 322.1338.

^{1}H-NMR (300 MHz, DMSO-d_6): δ 11.09 (s, 1H), 9.13 (s, 1H), 8.70 (d, 1H, 9.3 Hz), 8.62 (d, 1H, 8.2 Hz), 8.31-8.34 (m, 4H), 8.16-8.21 (m, 3H), 8.10 (t, 1H, 7.5 Hz), 7.73 (t, 1H, 6.9 Hz), 7.43 (d, 1H, 8.4 Hz), 6.83 (t, 1H, 5 Hz).

2.3.4.3 Preparation of stock solutions

Stock solutions were prepared in ultrapure water (ρ = 18.2 MΩ·cm^{-1}). HEPES (4-(2-hydroxyethyl)-1-piperazineethanesulfonic acid) buffer (500 mM, pH 7.4) was prepared by dissolving HEPES (free acid) powder and adjusting the pH with NaOH. Cu^{II} (50 mM) was prepared from $CuCl_2 \cdot 2H_2O$ and the concentration was verified by UV-Vis Spectroscopy via the Cu^{II} d-d band at 780 nm (ε = 12 M^{-1}cm^{-1}). A solution of Cu^{I} (50 mM) was prepared in MeCN from tetrakis(acetonitrile)copper(I) hexafluorophosphate, $[Cu(MeCN)_4]PF_6$. PHP stock solutions were prepared either in MeCN (200 µM) or DMSO (3 mM).

2.3.4.4 Spectroscopic analysis

UV-vis spectra were recorded on a Cary 60 spectrophotometer using a 1 cm path cuvette. Fluorescence emission (λex = 346 nm) and excitation (λem = 385 nm) spectra of the reaction mixture were recorded on a HORIBA "Fluorolog FL3-22" fluorimeter.

2.3.4.5 HPLC-DAD analysis

HPLC-DAD analysis was performed using a Hitachi Primaide instrument on a C18 column (XBridge Peptide BEH C18 column from Waters, 4.6 mm x 150 mm, pore size 300 Å, particle size 3.5 µm) with a step gradient from 95% solvent A (0.1% TFA in water) and 5% solvent B (90% MeCN and 0.1% TFA in water) to 100% solvent B in 30 min.

2.3.4.6 Isolation of the fluorescent product

PHP (3.5 mg, 11 µmol) was dissolved in MeCN (100 mL) and mixed with a $CuCl_2 \cdot 2H_2O$ solution (300 µL, 16.5 µmol). The mixture volume was reduced under vacuum and the warmed solution was charged on a TLC plate. After elution in MeCN, the oxPHP-containing spot was scratched off and dissolved in hot DMSO. ESI-HRMS: calculated m/z for $C_{22}H_{14}N_3$ ($[M+H]^+$) 320.1182; found m/z = 320.1183. ^{1}H-NMR (300 MHz, DMSO-d_6): δ 8.54 (d, 1H, 7.9 Hz), 8.45 (d, 1H, 7.5 Hz), 8.36-8.42 (m, 4H), 8.29 (d, 1H, 9.2 Hz), 8.17-8.20 (m, 2H), 8.00 (d, 2H, 9.2 Hz), 7.52 (dd, 1H, 6.5 Hz, 9.2 Hz), 7.00 (dd, 1H, 6.5 Hz, 6.5 Hz).

2.4 Development of turn-off ATCUN/Ln^{III} probes for Cu^{II}

2.4.1 Introduction

As the design of selective and reversible coordination-based turn-on probes for biological applications emerged to be very challenging, we rather focused on the development of turn-off probes in an effort to fulfill the affinity, selectivity and detectability criteria stated in section 2.1.2.

To this aim, we choose the ATCUN peptide motif as Cu^{II}-chelator thanks to the high selectivity and tunable affinity in a suited range, i.e. $13 < \log K_{7.4} < 15$, to compete with the most abundant and competitive component of the exchangeable pool in the blood, HSA.

2.4.1.1 ATCUN-based Cu^{II}-probes – State of the art

Besides the ATCUN-engineered fluorescent protein presented in section 2.2.4, few short ATCUN peptides have also been developed as fluorescent sensors for Cu^{II} by conjugation with mostly green-emitting dyes (see Table 10 and Fig. 24).

It is noteworthy that the presence of a free amino-terminus in the peptide is crucial for the binding of Cu^{II} in the 4N ATCUN-type coordination mode (see section 1.2.4.1). Hence, to preserve the affinity and the selectivity of the ATCUN site, the conjugation of the fluorophores should be carefully oriented towards sites other than the N-terminus. For instance, N-terminal acetylation (i.e. amidation) is known to suppress the ATCUN-like coordination and affect the high affinity.[354,355] Likewise, a similar effect can be postulated when the terminal alkyl-amino group is converted into an aromatic amine (e.g. in probe **50**).

Overall, none of the reported ATCUN-peptide probes was applied in biological samples, and hence there is no evidence about their effective applicability and detectability in the presence of a biological background, which instead could be likely ensured by red/NIR-emitting fluorophores (see section 2.1.2.4).

Besides, as the autofluorescent background has short lifetime emission (in the ns range), it can be circumvented by resorting to long-lifetime emitting luminophores, such as lanthanide ions.

Table 10. ATCUN-based Cu^{II} probes reported in the literature.

Probe	ATCUN Sequence ⁂	N-terminus	Fluorophore	λ_{ex} (nm)	λ_{em} (nm)	Ref.
41	Dap^{Dns}-Gly-His-Ser-Ser	Amine	Dansyl	333	550	356
42	Amb^{Dns}-Gly-His-Ser-Ser					
43	Orn^{Dns}-Gly-His-Ser-Ser					
44	Dap^{RhoB}-Gly-His-Ser-Ser		Rhodamine B	n/a	~ 580	357
45	Dap^{Dns}-Gly-His-Ser-Ser		Dansyl	n/a	~ 550	
46	Dap^{Fluo}-Gly-His-Ser-Ser		Fluorescein	n/a	~ 520	
47	Asp-Ala-His-Lys^{BODIPy}		BODIPy	495	507	358
48	^{Cou}Gly-Gly-His	Amide	Coumarin	420	470	359
49	^{Dns}Gly-Gly-His	Sulphonamide	Dansyl	340	558	360
50	^{NBD}Ser-Ser-His	Aromatic amine	NBD	469	525	361

⁂ Dap: 2,3-diaminoproprionic acid; Amb: 2,4-diaminobutyric acid; Orn: ornitine; Dns: dansyl; RhoB: Rhodamine B; Fluo: fluorescein; Cou: coumarin ; NBD: nitrobenzo-2-oxa-1,3-diazol.

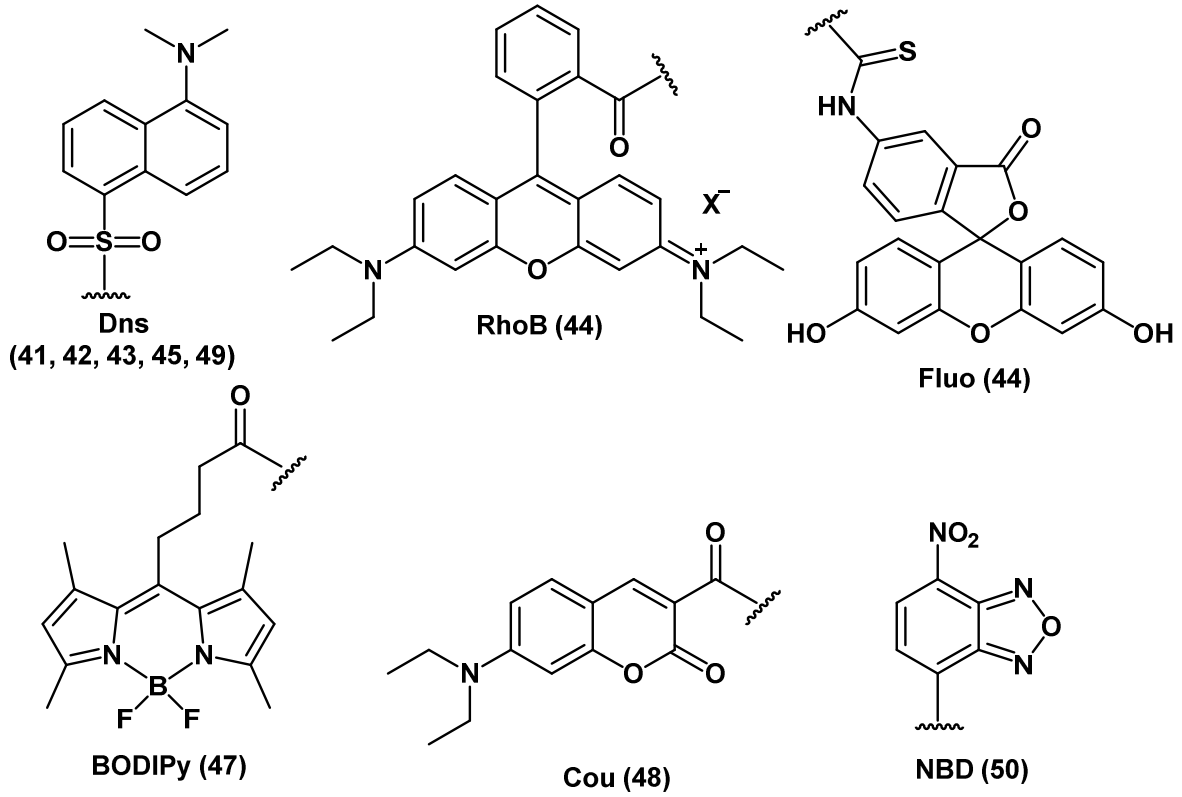

Figure 24. Fluorescent units found in ATCUN-based probes for Cu^{II}.

2.4.1.2 Lanthanides

Lanthanides (Lns) form the first-row of the f-block, characterized by the filling of the 4f orbitals (except for the eponym lanthanum). As the most common oxidation state for Ln ions is +3, with electronic configuration $[Xe]4f^n$ (n = 0-14), Ln^{III} ions are hard Lewis acids preferring hard donors such as (charged) oxygen and nitrogen atoms. Interestingly, all the Ln^{III} ions show a common chemical behaviour, quite independent of the atomic number, which mainly stems from the high penetration (i.e. the proximity to the nucleus) of f-electrons. Hence, the interaction of Ln and ligands orbitals are mostly electrostatic and isotropic, and the coordination number and the geometry of Ln complexes are mainly dictated by the electrostatic and steric repulsion between the ligands. As Ln ions have quite high ionic radii (about 100 pm), high coordination numbers, i.e. 8 and 9, are accessible and preferred.[362]

In order to form stable complexes with high coordination number, polydentate chelators such as acyclic and cyclic polyaminocarboxylate ligands (e.g. DTPA and DOTA, log K > 21) are commonly used. Remarkably, such complexes can attain very high kinetic inertia, which is paramount to ensure stability and avoid the transmetallation.[363–366]

It is also noteworthy that as a result of the very similar chemical behaviour, ligands show poor selectivity for different Ln^{III}.

Ln^{III} ions also have peculiar and remarkable spectroscopic features. In particular, they generally show several sharp but weak (ε = 1-10 $M^{-1}cm^{-1}$) absorption bands, at wavelengths characteristic of each Ln^{III} ion but largely independent from the coordination sphere. Indeed, many electronic f-

f transitions can be conceived owing to many microstates existing for each electronic configuration, although they are forbidden by the Laporte rule. The narrow bandwidth and the coordination-independent absorption wavelength stem instead from the poor overlap between f- and ligand orbitals. For the same reasons, most Ln^{III} ions (all but La^{III} and Lu^{III}) show also long-lived luminescent emission at invariable wavelengths. Indeed, the weak interaction with the ligands also prevents the coupling of electronic transitions with molecular vibrations and the nonradiative decays from the excited states.[367,368] For instance, Tb^{III} and Eu^{III} emit in the visible region (green to red) with a lifetime in the ms range, while Nd^{III} and Yb^{III} emit in the NIR with a lifetime in the μs range. Actually, Ln^{III} emission, especially in the NIR, is affected by the non-radiative deactivation by high-energy water vibration modes.[369] As a consequence, it is important to minimize the number of water molecules bound to the ion (hydration number) to maximize the emission intensity.

Furthermore, the low extinction coefficients hamper the efficient direct excitation of Ln^{III} ions. This issue is usually overcome via the so-called antenna effect, that is the indirect sensitization of Ln^{III} through the excitation of a suited chromophore and the following energy transfer to the Ln^{III}.[370] Generally, the chromophore first absorbs the light populating an excited singlet state, then, the energy is transferred to a triplet state via inter-system crossing and finally transferred to an excited level of the Ln from which emission occurs. The efficiency of the energy transfer is a function of the energy gap between the antenna triplet state and the Ln excited state, and of the antenna-Ln distance. Hence, antennas that directly coordinate the Ln^{III} ion are more efficient.[371,372] Generally, very few antennas are able to sensitize efficiently different Ln^{III}.[373] For instance, Cs124 and naphthalene can sensitize both Tb^{III} and Eu^{III}, and anthracene both Nd^{III} and Yb^{III}.[374–377] Overall, Ln show very favourable features for applications in bio-imaging. In particular, as they are not essential ions, they allow for a background-free detection, also thanks to their long-lifetime emission enabling time-delayed measurements.

2.4.1.3 Ln-based Cu^{II}-probes – State of the art

Few Ln-based probes for Cu^{II} have been reported in the literature using Tb^{III} or Eu^{III} ions (see Table 11 and Fig. 25).[378–384]

Such probes are normally composed of a Ln complex, an antenna, and an attached Cu^{II}-binding ligand, which can be the antenna itself. The quenching of Ln emission may occur directly or indirectly, through the quenching of the antenna and the impairment of the energy transfer. As already remarked for other sensors, most of the reported Ln-based probes are not equipped with high-affinity and selective ligands, but they generally show suitable LOD for potential applications in the measurement of Cu_{EXC}.

Interestingly, a probe based on the Cu-enzyme azurin was reported very recently. In particular, a lanthanide-binding tag (LBT), i.e. a short peptide sequence (15-20 amino acid) that bind Tb^{III} with high affinity and includes a Trp as the antenna for Tb^{III} sensitization,[385,386] was engineered as a loop into the protein structure, close to the Cu-binding site.[387] Although azurin-LBT represents the sole protein/Ln-based sensor for Cu^{II}, several peptide/Ln-based probes for Cu^{I} and Zn^{II} have been developed.[388–391] Besides LBTs, non-peptidic Ln^{III} complexes can be conjugated to the peptide via grafting on the amino-acid side chains. Concerning the antenna, it can be part of the Ln^{III} chelator or the peptide scaffold. In the latter case, Trp (ε_{280} = 5690 $M^{-1}cm^{-1}$, Φ = 0.12) has been commonly used to sensitize Tb^{III}, while other chromophore-derivatized amino acids have been used to excite other Ln^{III} ions.

Table 11. Lanthanide-based Cu^{II} probes reported in the literature.

Probe	Cu-ligand	Ln	Antenna	λ_{ex} (nm)	LOD (μM)	Reference
51	Phen	Eu	Phen	~ 270	n/a	[378]
52	Aromatic iminodiacetate	Tb	phenyl	285	n/a	[379]
53	Pyridine/aza-18-crown-6 ether	Eu	Pyridine derivative	325	n/a	[380]
54	DPA	Eu	Pyridine derivative	350	9.6	[381]
55	DPA	Eu	*o*-terphenyl	337	0.0037	[382]
56	DPA	Tb	Pyridine derivative	260	0.130	[383]
57	NOTA	Tb	Cs124	330	0.0017	[384]
58	Azurin	Tb	Trp	280	0.65	[387]

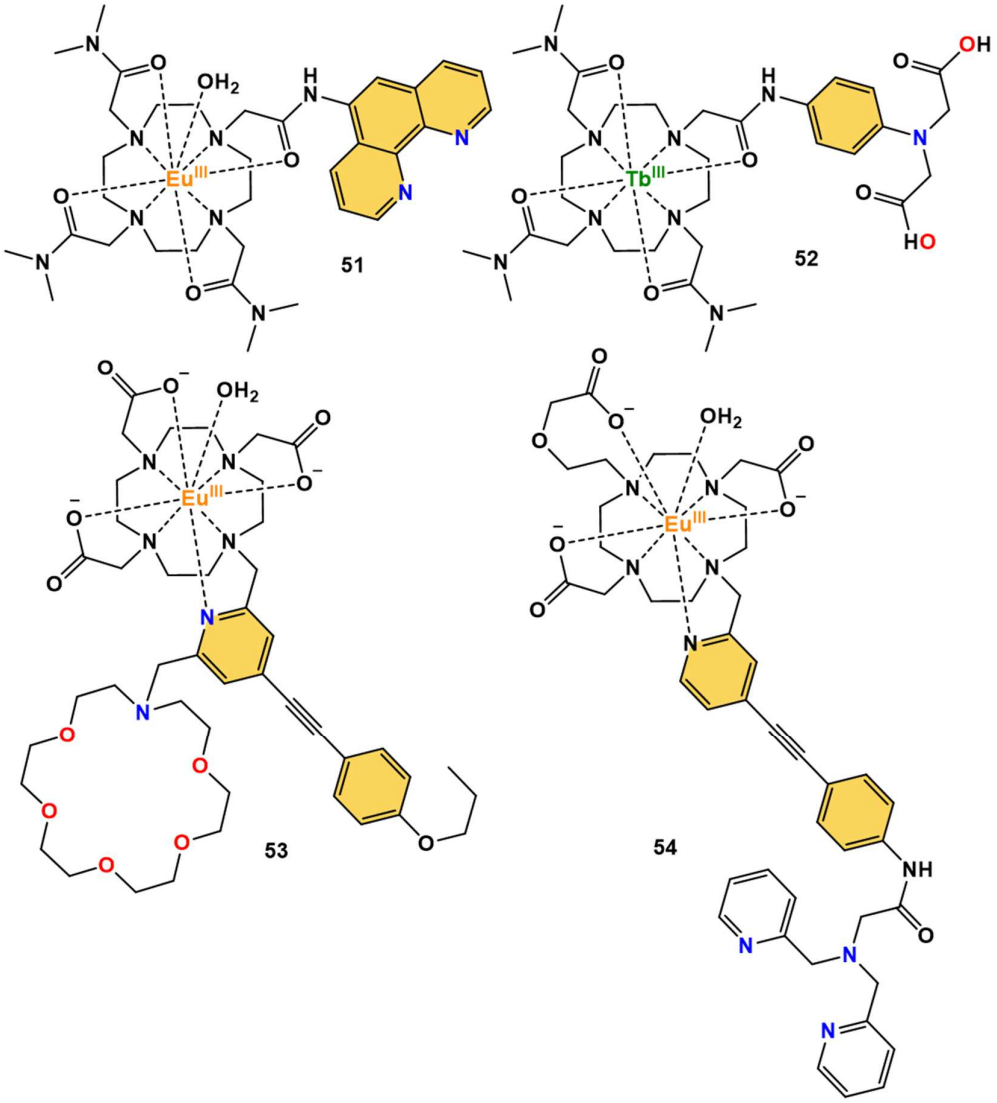

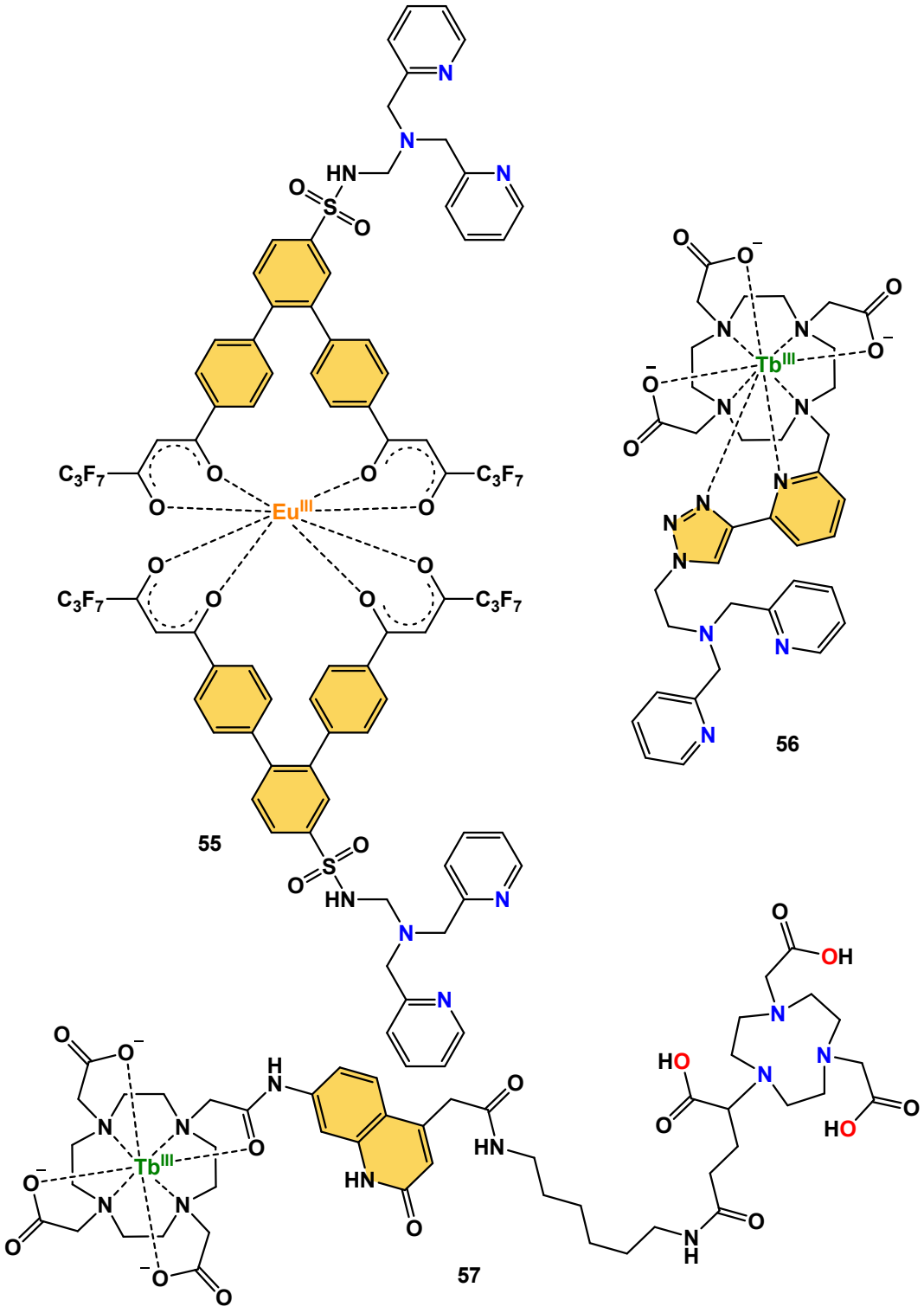

Figure 25. Structure of Ln-based Cu^{II} probes. Cu^{II}-binding atoms are coloured. Tb^{III} and Eu^{III} ions are coloured in green and orange, respectively. Lanthanide antennas are highlighted in yellow.

2.4.1.4 Design of an ATCUN/Tb^{III}-based probe for Cu^{II}

In the light of the advantageous properties of ATCUN peptides as Cu^{II}-selective chelators and lanthanide ions as long-lifetime luminophores, we decided to explore the employment of a Tb^{III} complex as the luminescent moiety in an ATCUN peptide probe for Cu^{II} detection in biological media. As explained above, a suited antenna is also needed to ensure the efficient excitation of the lanthanide. In this respect, the amino acid Trp (W) was first chosen as the antenna by virtue of its straightforward insertion into the peptide scaffold.[391–394] For this reason, we chose the ATCUN motif found in the neuropeptide Neuromedin C, which contains a Trp residue in the fourth position, i.e. Gly-Asn-His-Trp (GNHW) and showed affinity (log $K_{7.4}$ = 13.6) higher than HSA.[395,396] Interestingly, it has been shown in the literature that a Trp in such position is efficiently quenched upon Cu^{II}-binding and even a cation-π interaction between Cu^{II} and Trp^4 has been suggested to occur in the Cu-NMC complex.[63,147,396,397] Hence, a consequent quenching of Tb^{III} emission was conceivable. A Tb^{III}-chelating DOTA unit was grafted onto the side-chain of a Lys residue adjacent to Trp^4 (see Fig. 26).

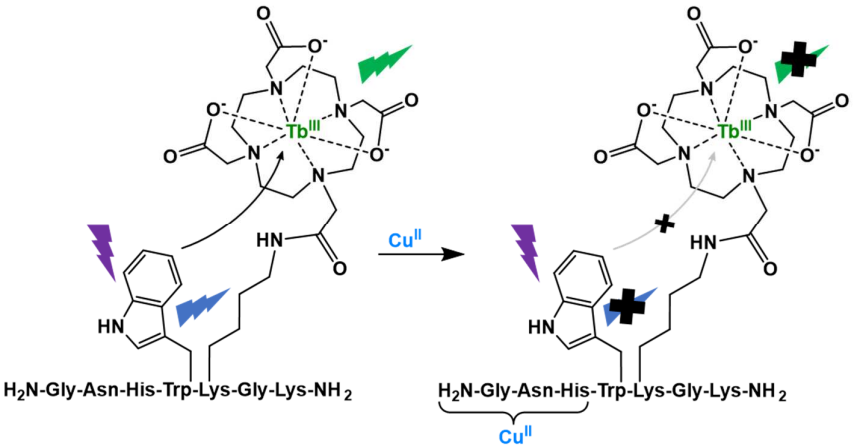

Figure 26. Structure of $GNH^{W/Tb}$ and mechanism of Cu^{II} detection: in absence of Cu^{II}, Trp excitation (violet flash) gives rise to Trp (blue flash) emission, and also Tb^{III} (green flash) emission via antenna effect, i.e. energy transfer (ET, black/grey arrow); upon Cu^{II}-binding to the peptide ATCUN motif, both Trp and Tb^{III} luminescence are quenched.

2.4.2 Results and discussion

The peptide $GNH^{W/Tb}$ (H_2N-GNHW$K^{DOTA(Tb)}$GK-NH_2) was synthesized according to a standard Fmoc/*t*Bu Solid-phase Peptide Synthesis (SPPS) protocol. The DOTA unit was grafted as DOTA-tris(*t*Bu) ester upon deprotection of an allyloxycarbonyl-protected Lys residue, and the Tb^{III} was coordinated to the DOTA after peptide cleavage and side-chain/DOTA deprotection (see section 2.4.4.2).

The fluorescence spectrum of the probe upon Trp excitation (λ_{ex} = 280 nm) shows Trp (348 nm) and Tb^{III} emission bands (487 and 545 nm), showing that partial energy transfer occurs between the amino acid and the lanthanide. As a consequence, Tb^{III} bands emerge out of the tail of Trp band, which may represent a non-negligible background (see Fig. 27A). In addition, the time-delayed excitation spectrum of Tb^{III} emission (545 nm, 100 µs) resembles Trp absorption spectrum, confirming the antenna effect (see Fig. 27B) Furthermore, the Tb^{III} lifetime resulted to be ~ 1.97 ms, in agreement with previous reports.[389]

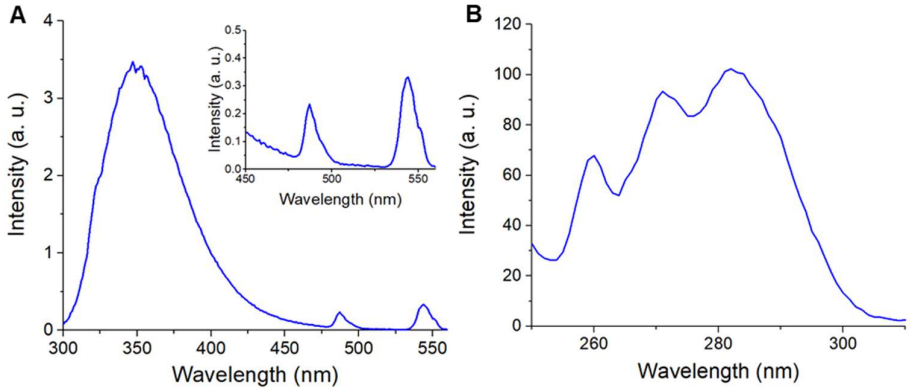

Figure 27. Characterization of $GNH^{W/Tb}$ luminescence. A) Emission spectrum upon Trp excitation (280 nm): inset: Tb^{III} emission bands; B) time-delayed (τ = 0.1 ms) excitation spectrum (545 nm). Conditions: $[GNH^{W/Tb}]$ = 10 µM, HEPES 100 mM, pH 7.4.

Then, the response of $GNH^{W/Tb}$ to Cu^{II} upon Trp excitation (λ_{ex} = 280 nm) was examined via a fluorometric titration, which showed a progressive quenching of both Trp and Tb^{III} emission bands until saturation at 1:1 Cu^{II}:$GNH^{W/Tb}$ stoichiometric ratio (see Fig. 28A). Besides, Tb^{III} lifetime was not affected by Cu^{II} addition, suggesting that Tb^{III} quenching may arise indirectly from the quenching of Trp. Moreover, the calibration curve showed good linearity between 0.05 and 10 µM and revealed a LOD of about 0.56 µM in the conditions used (see section 2.4.4.4).

Furthermore, the probe also demonstrated to be selective in the presence of physiologically-relevant extracellular concentrations of other cations (Zn^{II}, Fe^{III}, Co^{II}, Mn^{II} 10 µM, Mg^{II} and Ca^{II} 2 mM), as no significant quenching was observed when the probe was incubated with each of these ions, while Cu^{II} quenched the signal even in presence of all the other cations (see Fig. 28B).

Interestingly, Ni^{II} also quenched efficiently the signal (see Fig. 28C). However, this does not represent an issue since Ni^{II} is not an essential ion for mammals and it binds to ATCUN motifs with a much lower affinity and rate than Cu^{II}.[142,396]

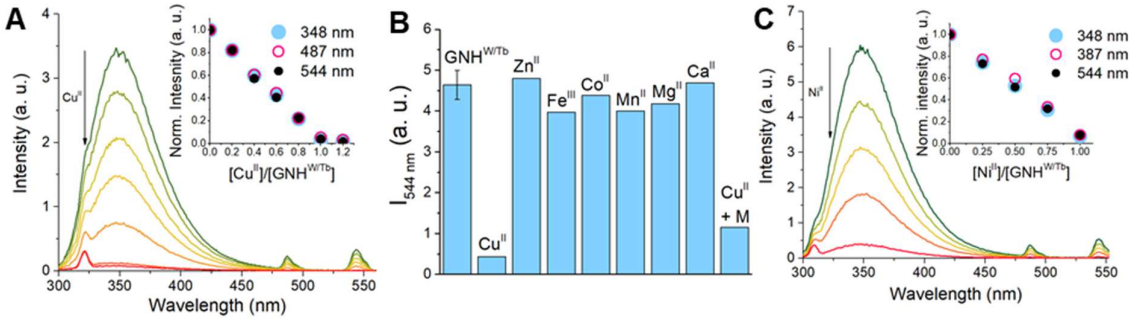

Figure 28. Luminescence response of $GNH^{W/Tb}$ to Cu^{II} and other cations. A) Quenching of $GNH^{W/Tb}$ emission upon titration with Cu^{II}; B) Diagram of $GNH^{W/Tb}$ selectivity for Cu^{II} against the other essential cations (M denotes the sum of all cations); C) Quenching of $GNH^{W/Tb}$ emission by Ni^{II}. Conditions: A) $[GNH^{W/Tb}]$ = 10 µM, HEPES 100 mM pH 7.4; B) $[GNH^{W/Tb}]$ = 10 µM, $[Cu^{II}]$ = $[Zn^{II}]$ = $[Fe^{III}]$ = $[Co^{II}]$ = $[Mn^{II}]$ = 10 µM, $[Mg^{II}]$ = $[Ca^{II}]$ = 2 mM, HEPES 100 mM pH 7.4; C) $[GNH^{W/Tb}]$ = 10 µM, $[Ni^{II}]$ = 2.5 µM (light green), 5 µM (yellow), 7.5 µM (orange), 10 µM (red), HEPES 100 mM pH 8.2, after 3h incubation.

Thus, we tested whether the probe could detect Cu^{II} in the presence of a fluorescent biomolecule. To this aim, we chose Porcine Serum Albumin (PSA), which binds Cu^{II} weakly (as it does not contain an ATCUN motif) and contain many fluorescent aromatic residues. Notably, the Cu^{II} transfer from PSA to the probe can be monitored over time via the progressive quenching of the

probe emission. The fluorescent spectrum of the Cu^{II}-PSA complex showed an intense and broad band centred at ~ 335 nm, which can be attributed to the aromatic amino acid in the protein (Trp, Phe and Tyr). Remarkably, when the probe was added to the mixture, no change was observed within 1h (see Fig. 29A), suggesting that neither Trp nor Tb^{III} bands could be detected against PSA fluorescent background. Hence, we resorted to time-delayed detection of Tb^{III} luminescence to get rid of such background. In this condition, the four characteristic emission bands of Tb^{III} (at 487, 544, 585 and 623 nm) were detected and a progressive quenching was observed. Importantly, the addition of the stronger chelator EDTA caused a slow and almost complete recovery of the signal, proving the reversibility of the sensor (see Fig. 29B).

Then, the probe was challenged in the detection of Cu^{II} in a more complex medium, such as the lysogeny broth (LB) used for bacterial culture growth. This is composed of tryptone and yeast extract, hence it is rich in peptides and protein fragments that may represent relevant competitors for Cu^{II}. Similar to the case of PSA, the probe $GNH^{W/Tb}$ could not be detected in the presence of 10% LB medium due to the high background (see Fig. 29C). Instead, the time-delayed detection allowed the measurement of Tb^{III} emission. Interestingly, the addition of Cu^{II} produced a rather slow and partial quenching of the signal. Analogously, the addition of EDTA slowly recovered the signal (see Fig. 29D).

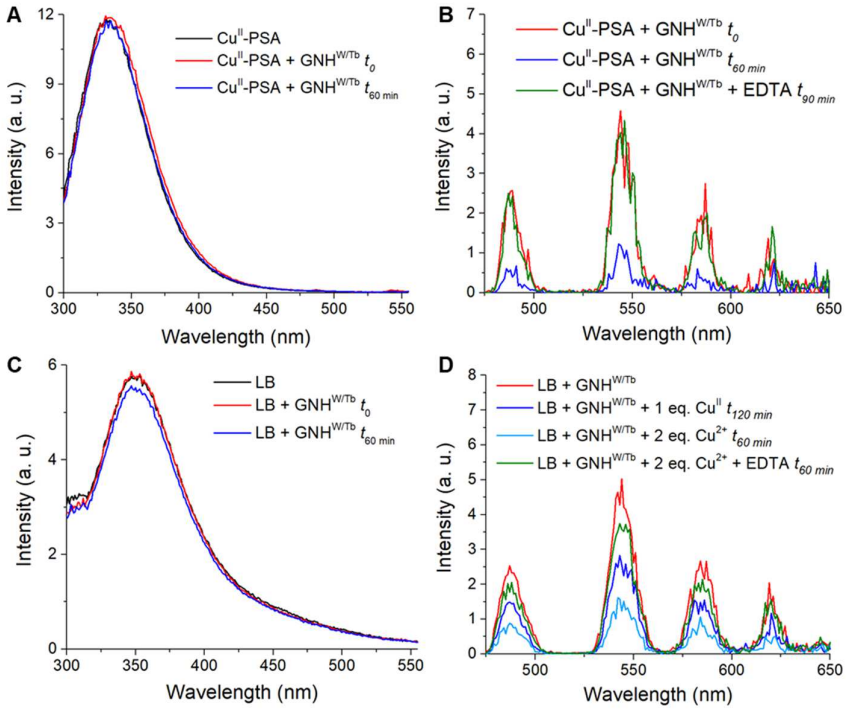

Figure 29. Luminescence response of $GNH^{W/Tb}$ to Cu^{II} in the presence of a biological autofluorescence medium. A, B) Cu^{II} transfer from PSA to $GNH^{W/Tb}$ and from $GNH^{W/Tb}$ to EDTA monitored by fluorescence (A) and time-delayed luminescence (B). C, D) Reversible detection of Cu^{II} in LB medium monitored by fluorescence (C) and time-delayed luminescence (D). Conditions: A, B) [PSA] = 10 μM, [Cu^{II}] = 9 μM, [**$GNH^{W/Tb}$**] = 10 μM, [EDTA] = 35 μM, HEPES 50 mM pH 7.4; C, D) [**$GNH^{W/Tb}$**] = 10 μM, [Cu^{II}] = 10 μM (blue), 20 μM (cyan), [EDTA] = 100 μM, LB 10 %; τ = 0.1 ms (B, D).

On balance, the probe showed a reversible binding/sensing of Cu^{II} even in a complex medium containing potential competing ligands. However, the kinetics of the response appeared to be surprisingly slower than in buffer, where the Cu^{II}-binding/response is achieved within the mixing

time. To explain such behaviour, we speculate that even though $GNH^{W/Tb}$ has likely suitable affinity to bind Cu^{II} in the LB medium, the latter also kinetically competes with the probe. Namely, it is likely that the Cu^{II} spiked into the LB medium containing $GNH^{W/Tb}$ is first caught by kinetically-favoured ligands that slowly release Cu^{II} to the probe. This may be due to the fact that the Cu^{II}-binding to the amide groups of the ATCUN motif requires their slow deprotonation.[148]

2.4.3 Conclusions

Overall, the novel probe $GNH^{W/Tb}$ revealed to detect Cu^{II} selectively and reversibly, and to be responsive to Cu_{EXC} fluctuations in a biological-like medium such as 10% LB. In addition, the time-delayed detection of the Tb^{III} long-lifetime emission was required to detect the probe and hence Cu^{II} in the presence of a biologically-relevant fluorescent background, which demonstrate the advantageous use of the lanthanide as luminescent moiety. However, the response of the probe appeared to be remarkably slow. Such kinetics issue, which seems unprecedented in the literature, has been addressed in the following.

2.4.4 Experimental section

2.4.4.1 Materials

Commercially available reagents were used without further purification. LB medium was prepared from LB broth (Lennox) powder (Carl Roth), enriched with 5 g/L of yeast extract (Carl Roth). Analytical HPLC was performed using a Hitachi Primaide instrument on a C18 column (XBridge Peptide BEH C18 column from Waters, 4.6 mm x 150 mm, pore size 300 Å, particle size 3.5 µm). MS spectra were recorded on an LCQ Fleet Ion Trap mass spectrometer (Thermo Fischer). Preparative HPLC was carried out using a LaPrep Sigma (VWR International) instrument. Spectrophotometric titrations were performed on a Cary 60 UV-vis spectrophotometer using a 1 cm path quartz cuvette. Luminescence spectra were recorded on a Fluorolog FL3-22 or a FluoroMax-4 spectrometer from HORIBA JobinYvon using a 1 cm path quartz cuvette.

2.4.4.2 Peptide synthesis

$GNH^{W/Tb}$ (H_2N-GNHWK$^{DOTA(Tb)}$GK-NH_2) was synthesized manually through a standard Fmoc/*t*Bu SPPS protocol in a syringe with filter frit (see Fig. 30). Fmoc-Rink amide aminomethyl-polystyrene resin (Fmoc-Rink-Amid AM Resin from Iris Biotech, 0.74 mmol/g loading, 100-200 mesh) was used to obtain C-terminal amidation. Coupling reactions (1h under shaking) were performed using 4 equivalents of Fmoc-protected amino acids, 3.9 equivalents of HBTU (3-[Bis(dimethylamino)methyliumyl]-3H-benzotriazol-1-oxide hexafluorophosphate) as coupling agent, 8 equivalents of DIEA (diisopropylethylamine) as the base and DMF (N,N-dimethylformamide) as the solvent. After coupling, the presence of unreacted N-terminal free amine was checked with TNBS (2,4,6-Trinitrobenzenesulfonic acid) reagent, and the coupling was repeated in case of a positive test. Capping of the unreacted free amine group was carried out using 5% acetic anhydride (Ac_2O) and 10% DIEA in DMF for 5 min. N-terminal Fmoc deprotection was carried out using 20% piperidine in DMF. The peptide N-terminus was Boc-protected adding 4 equivalents of di-tert-butyl dicarbonate (Boc_2O) and 2 equivalents of DIEA in DMF for 1 hour. Deprotection of the alloc-protected side-chain of the Lys^5 residue was performed using $Pd(PPh_3)_4$ (0.05 mmol, 0.5 eq., 58 mg) and phenylsilane (2.4 mmol, 24 eq., 0.3 mL) in degassed anhydrous DCM in the dark (2x1h). The resin was then washed with DCM (2×2 min), DMF (2×2 min), 1% H_2O in DMF (2×2 min), DMF (2×2 min), 1% DIEA in DMF (2×2 min), DMF (2×2 min), sodium diethyldithiocarbamate in DMF (0.12 M, 2×5 min) and DMF (2×2 min). The DOTA unit was grafted adding DOTA-tris(*t*Bu) ester (0.1 mmol, 57 mg, 1 eq.), PyBOP (0.2 mmol, 104 mg, 2 eq.) and then DIEA (0.8 mmol, 140 µL, 8 eq.) in DMF overnight. Resin cleavage and side-chain deprotection were performed treating with 95% TFA (trifluoroacetic acid), 2.5% H_2O and 2.5% TIS (triisopropylsilane) for 90 min. The crude was precipitated with cold ether and purified by HPLC on a C18 column (XBridge Peptide BEH C18 OBD Prep Column from Waters, 19 mm x 150 mm, pore size 130 Å, particle size 5 µm). The Tb^{III} complex was prepared by overnight incubation of a solution of the peptide in H_2O with a solution of $TbCl_3 \cdot 6H_2O$ in H_2O (5 eq.) at pH ~ 6.3. The purity and identity of the peptides were assessed by HPLC and LC-MS (see Fig. 30). $[GNH^{W}+H]^+$: experimental m/z = 1211.77, calculated m/z = 1211.63; $[GNH^{W/Tb}+H]^+$: experimental m/z = 1367.55 , calculated m/z = 1367.52. Yield: $GNH^{W/Tb} \cdot (CF_3COO^-)_3$ = 12% (4.5 mg).

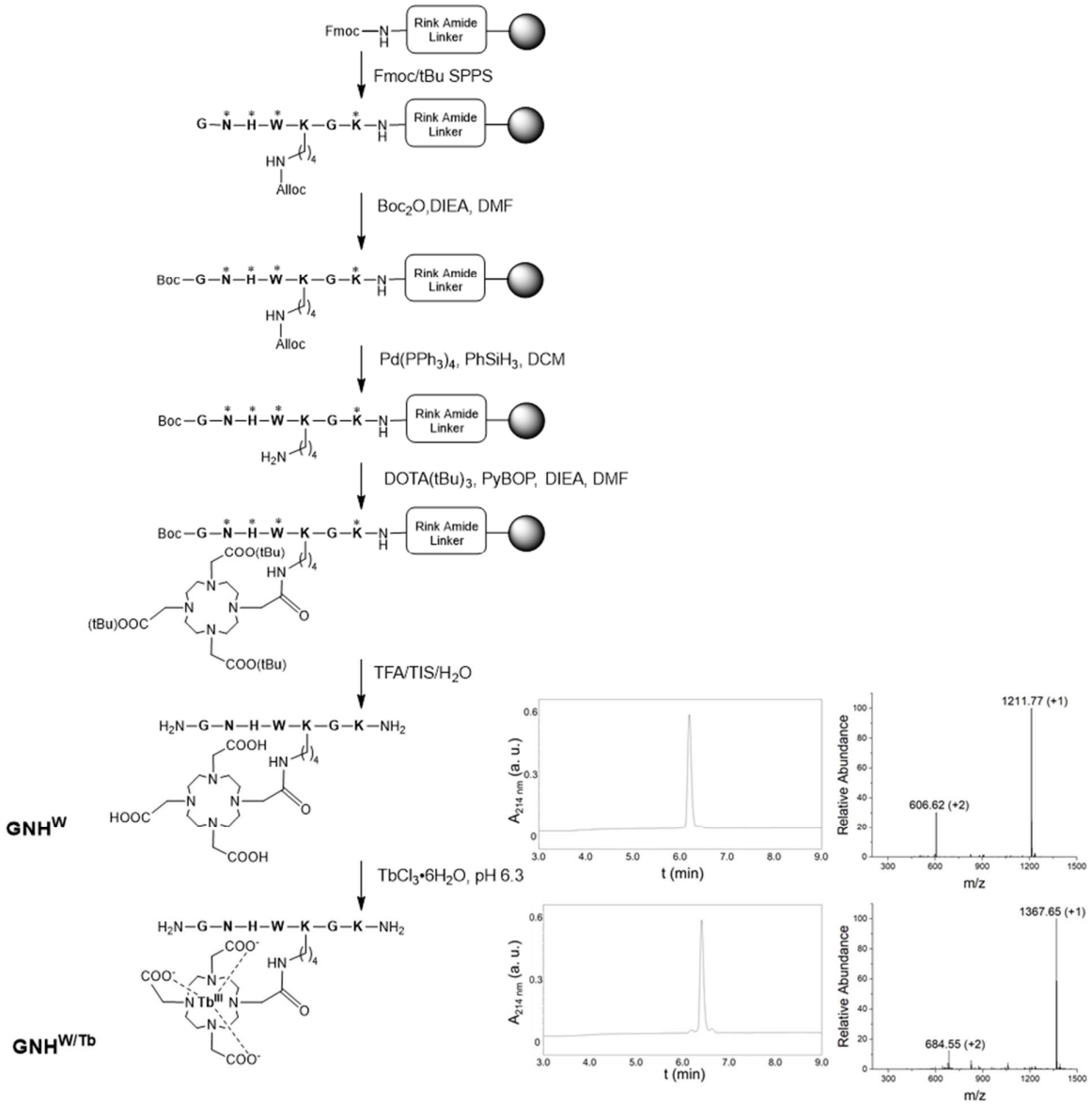

Figure 30. Synthetic pathway of $GNH^{W/Tb}$. Amino acids are labelled in bold and standard side chain protecting groups are denoted as * (Boc for Lys and Trp, Trt for His and Asn). HPLC chromatograms and ESI-MS spectra of purified GNH^{W} and $GNH^{W/Tb}$ are also reported.

2.4.4.3 Preparation of stock solutions

Stock solutions were prepared in ultrapure water (ρ = 18.2 $M\Omega \cdot cm^{-1}$). The concentration of peptide solution was determined by tryptophan UV-vis absorption (ε_{280} = 5690 $M^{-1}cm^{-1}$) and UV-vis titration with Cu^{II} monitoring the increase of the d-d band at 525 nm. HEPES buffer (500 mM, pH 7.4) was prepared by dissolving the free acid powder and adjusting the pH with NaOH. The metal salts used were $CuCl_2 \cdot 2H_2O$, $NiCl_2 \cdot 6H_2O$, $ZnSO_4 \cdot 7H_2O$, $Fe(NO_3)_3 \cdot 9H_2O$, $CoCl_2$, $MnCl_2 \cdot 4H_2O$, $MgSO_4$, $CaCl_2$, KCl. The concentration of $CuCl_2 \cdot 2H_2O$ stock solution was verified by UV-Vis spectroscopy (ε_{780} = 12 M^{-1} cm^{-1}). The concentration of the PSA solution was determined by UV-vis absorption spectroscopy (ε_{280} = 43824 $M^{-1}cm^{-1}$).

2.4.4.4 Luminescence measurements

All spectra were obtained using λ_{ex}=280 nm and time-delayed luminescence spectra were recorded with 100 µs time delay. The time-delayed excitation spectrum was recorded using λ_{em} = 544 nm.

Luminescence lifetimes were determined by fitting a single-exponential decay curve to the data (the values reported are averages of three independent measurements).

The limit of detection (LOD = $3\sigma/k$, where is the standard deviation of the blank measured over three different peptide samples, and k is the slope of the linear regression line of the luminescence quenching, $\Delta I = I_0 - I$, as a function of Cu^{II} concentration) was evaluated at 10 µM probe concentration in HEPES buffer (100 mM, pH 7.4) using excitation slit = 4 nm, emission slit = 3 nm.

The probe selectivity was assessed adding (i) the potentially competing cations individually or (ii) Cu^{II} together with the mix of all the other ions to the peptide in HEPES. The impact of Ni^{II} on the luminescence was incubating (for 3h) the peptide (10 µM) and $NiCl_2 \cdot 6H_2O$ at different molar ratios in HEPES 100 mM (pH 8.2).

2.5 Improvement of the kinetic responsiveness of ATCUN/Tb^{III}-based probes

2.5.1 Introduction

In order to overcome the slow responsiveness of the probe $GNH^{W/Tb}$ in a complex biological medium, we resorted to an ATCUN motif variant, NH_2-Xxx^1-His^2-His^3 (XHH) that has previously shown higher Cu^{II} exchange rate.

2.5.1.1 The Ala-His-His motif

The coordination of Cu^{II} by Ala-His-His (AHH) peptide has been recently studied by our group.[398,399] Analogously to the XZH (Z ≠ H) motif, AHH binds Cu^{II} with the characteristic 4N (NH_2, N^-, N^-, N_{Im}) coordination mode at pH 7.4. At lower pH (< 5.5), while the protonation of even one amidate (pK_a ~17) in the XZH motif triggers the release of Cu^{II} owing to the loss of two out of three chelate rings, Cu^{II} can be bound to the AHH motif with a 3N (NH_2, N^-, N_{Im}) mode typical of XH peptides (such as GHK, see section 1.2.4.1) thanks to a rearrangement (in which the imidazole ring of His^2 replaces His^3 amidate) that keeps two chelate rings (see Fig. 31A). For instance, about 95% Cu^{II} is bound to AHH peptide at pH 5 (log K ~ 7) as the sum of 3N (~72%) and 4N (~22%) species, whereas only 50% is bound to the 4N AAH (log K ~ 5) at the same pH (see Fig. 31B).[398,400]

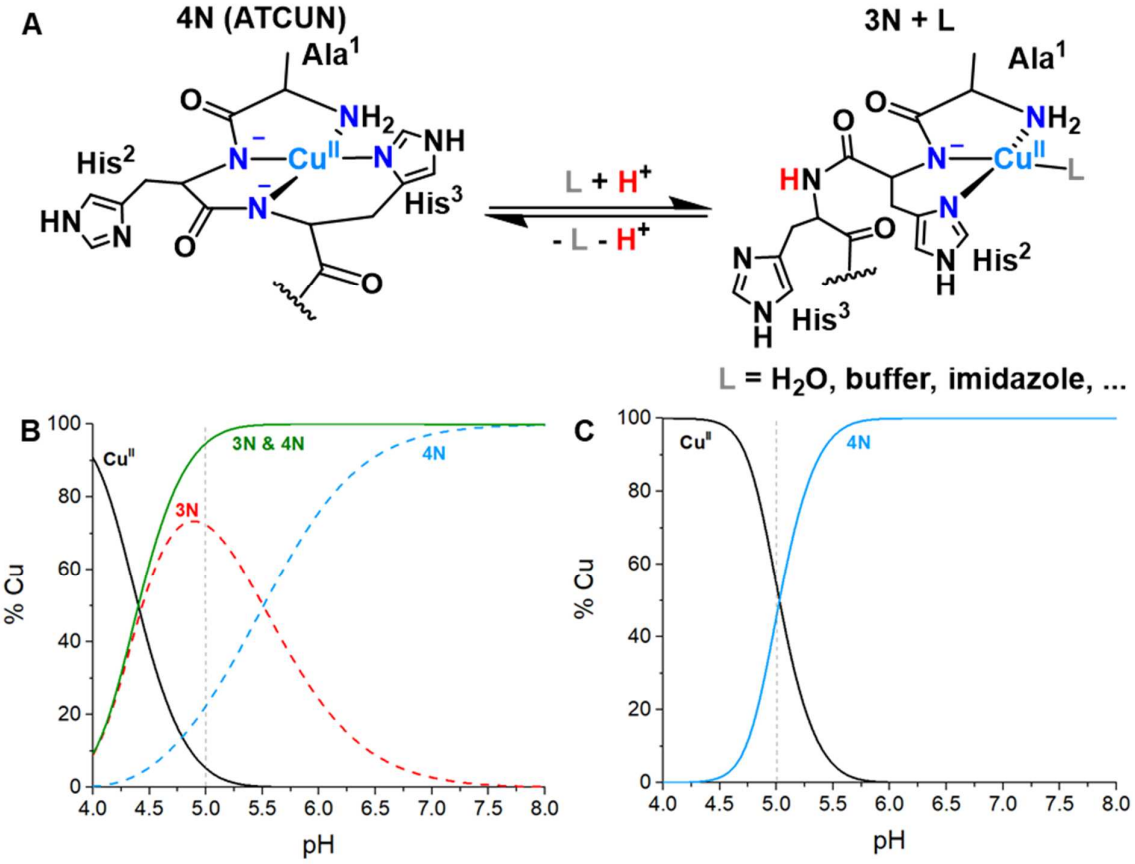

Figure 31. pH- and external ligand (L)-dependent speciation of the Cu^{II}-AHH complex. A) Structures of the 4N (ATCUN-type) and 3N(+L) coordination modes; B, C) Species distribution diagrams for Cu^{II}-($AHH\text{-}NH_2$) (B) and Cu^{II}-($AAH\text{-}NH_2$) (C) complexes, modeled at [peptide] = 10 μM, [Cu^{II}] = 9 μM using the stability constant reported in the literature.[398,400]

Remarkably, in the presence of excess peptide or external ligands (L), a certain portion of 3N(+L)-type ternary complexes co-exists with the major 4N form of the AHH peptide at pH 7.4. Interestingly, although the percentage of such ternary complexes can be very low (< 1%) at micromolar peptide concentration, the large number of external ligands in a complex biological medium (e.g. amino acids, His residues in peptides and proteins, etc.) could considerably increase the population of the 3N+L species (e.g. comparable amount of 4N and 3N+L species are obtained in the presence of imidazole at mM concentration). By virtue of this bimodal speciation, AHH benefits from the high selectivity and affinity (log $K_{7.4}$ = 13.7) of the conventional XZH motif, but also from the faster Cu^{II} exchange showed by the XH motif.[63,147,398,401]

2.5.1.2 Mechanism of Cu^{II}-exchange/transfer by ATCUN peptides

To date, the rationale behind the faster Cu^{II} exchange shown by XH and XHH has not been unambiguously ascertained. As the Cu^{II} release from XH and XZH motifs implies the protonation of amidate groups, the different exchange rate has been classically explained via the lower number of amidate donors implicated in Cu-XH (1) compared to Cu-XZH (2).[148] Besides, as the Cu^{II} transfer between XZH peptides and external ligands seems to occur via an associative mechanism, the potential of XH(H) to form 3N+L ternary complexes can be also responsible for the higher exchange rate.[402] Indeed, recent investigations showed that a 2N (NH_2, N_{Im}) intermediate is formed during the self-exchange of Cu^{II} by ATCUN peptides. Moreover, as the conversion between the 2N and 4N species showed poor pH-dependence, the rearrangement of the ligand from such 2N complex to the final 4N mode was suggested as the rate-limiting step rather than the amidate protonation.[64] Overall, we may speculate that a (2N)-Cu-L transition state forms during the Cu^{II} transfer from an ATCUN peptide and a ligand L. In such a scenario, we can envision that the reorganization from a (3N)-Cu-L complex to the hypothesized transition state requires lower activation energy compared to a (4N)-Cu complex. Hence, even if low populated, ternary 3N+L species could enhance the Cu^{II}-transfer.

2.5.2 Results and discussion

In order to improve the kinetic responsiveness of the former $GNH^{W/Tb}$ probe, the $AHH^{W/Tb}$ variant was designed and synthesised analogously (see section 2.5.4.2). $AHH^{W/Tb}$ also showed similar quenching behaviour (see Fig. 32) and dose-dependent response to Cu^{II} with a LOD of 0.28 μM (similar to $GNH^{W/Tb}$, for which LOD resulted to be 0.35 μM in the current experimental conditions, see Table 12).

Then, the response of $GNH^{W/Tb}$ and $AHH^{W/Tb}$ to Cu^{II} was compared in the presence of biological-like media such as 10% LB and fetal bovine serum (FBS), where, due to higher absorption background, the LOD of Cu^{II} resulted to be about 1 μM or higher (note that even if LOD for $GNH^{W/Tb}$ in FBS resulted to be 0.46 μM due to low standard deviation of the blank, the calibration curve showed poor linearity below 1 μM).

Table 12. LOD (μM) of Cu^{II} with $GNH^{W/Tb}$ and $AHH^{W/Tb}$ in HEPES and biological media.

	HEPES 100 mM pH 7.4	**LB 10%**	**FBS 10%**
$GNH^{W/Tb}$	0.35	1.22	0.46
$AHH^{W/Tb}$	0.28	1.23	0.97

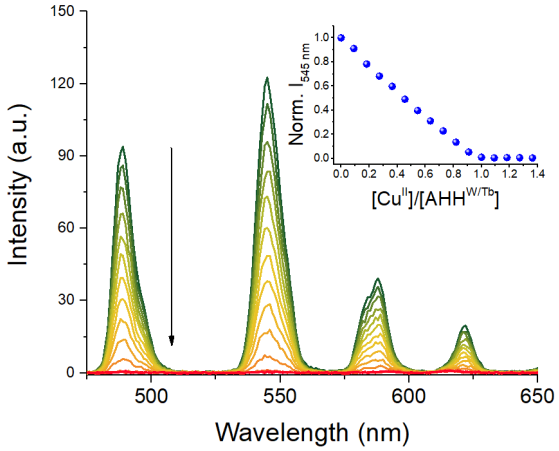

Figure 32. Quenching of $AHH^{W/Tb}$ time-delayed luminescence by Cu^{II}. Conditions: [$\mathbf{AHH^{W/Tb}}$] = 10 µM, HEPES 50 mM pH 7.4; τ = 0.1 ms.

2.5.2.1 Kinetics of Cu^{II} transfer in biological media

The kinetics of Cu^{II}-binding to the probes was tested in the presence of LB medium (10%) and fetal bovine serum (FBS, 10%), which is a common supplement for cell culture growth and resembles the composition of human serum (see Fig. 33A/B). Noteworthy, as $AHH^{W/Tb}$ and $GNH^{W/Tb}$ likely have both different affinities and Cu^{II}-exchange rates, the measurement of the luminescent quenching as a function of the time represents only apparent Cu^{II}-binding/transfer rates that depend on both affinity and binding rates.

In both cases, $AHH^{W/Tb}$ demonstrated a faster response (quenching/time) to the addition of exogenous Cu^{II} than $GNH^{W/Tb}$. However, contrary to the LB medium, where a significant portion of Cu^{II} was bound by both peptides, FBS appeared to be much more competitive, i.e. a lower amount of Cu^{II} was available for complexation by the probes in the same timespan. Likely, this results from the presence of an excess of thermodynamically-competing ligands, such as bovine serum albumin, in FBS.

Thus, to assess whether the probes are able to compete with the main Cu_{EXC} pool in human blood, i.e. HSA, we monitored the Cu^{II}-transfer from pre-complexed HSA to each probe at 1:1 HSA:probe ratio (see Fig. 33C). Interestingly, both peptides competed with HSA, and $AHH^{W/Tb}$ showed again larger Cu^{II}-binding than $GNH^{W/Tb}$ (e.g. 60% vs 20% after 30 min).

Besides, the ability of the probes to release Cu^{II}, which is sought to detect time-dependent Cu^{II} fluctuations, was examined using EDTA (see Fig. 33D). The de-quenching observed upon the addition of EDTA to the Cu-probe complexes indicated that the dissociation of Cu^{II} from $AHH^{W/Tb}$ was faster than from $GNH^{W/Tb}$. Interestingly, such behaviour was observed when a concentration of EDTA as high as 10 mM was used, whereas no significant difference was observed for the two probes with 100 µM chelator.

This could suggest that a significant enhancement of the Cu^{II}-exchange by $AHH^{W/Tb}$ is obtained only if the concentration of external ligands is such that ternary complexes are formed.

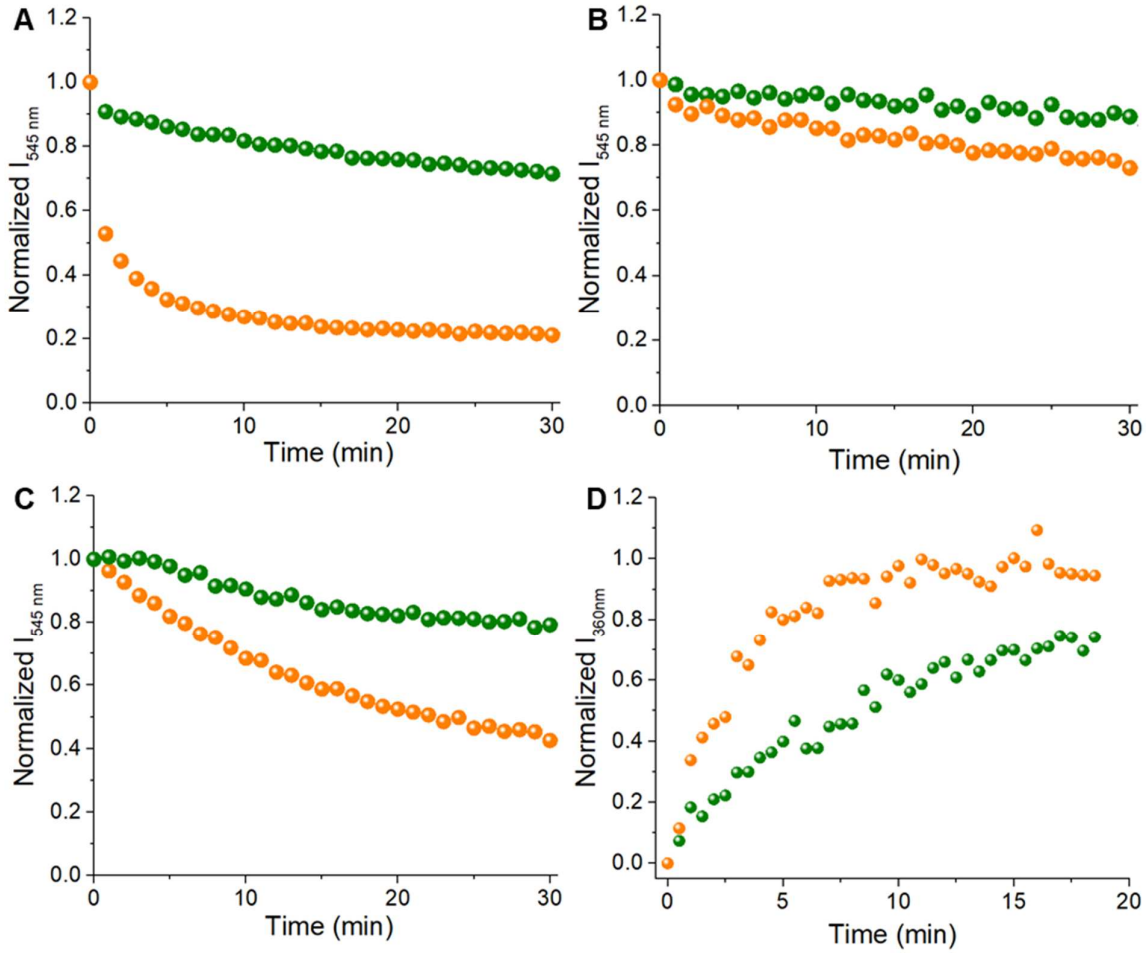

Figure 33. Comparison of $GNH^{W/Tb}$ (green dots) and $AHH^{W/Tb}$ (orange dots) Cu^{II} transfer kinetics. A) Cu^{II} binding in 10% LB medium; B) Cu^{II} binding to the peptides in 10% FBS; C) Cu^{II} transfer from HSA; D) Cu^{II} release to EDTA. Conditions: A) $[GNH^{W/Tb}] = [AHH^{W/Tb}] = 10\ \mu M$, $[Cu^{II}] = 9\ \mu M$, LB 10%; B) $[GNH^{W/Tb}] = [AHH^{W/Tb}] = 10\ \mu M$, $[Cu^{II}] = 9\ \mu M$, FBS 10%; C) $[GNH^{W/Tb}] = [AHH^{W/Tb}] = [HSA] = 10\ \mu M$, $[Cu^{II}] = 9\ \mu M$, HEPES 50 mM pH 7.4; D) $[GNH^{W/Tb}] = [AHH^{W/Tb}] = 10\ \mu M$, $[Cu^{II}] = 9\ \mu M$, [EDTA] = 10 mM, HEPES 100 mM pH 7.4; $\lambda_{ex} = 280$ nm, $\tau = 0.1$ ms (A, B, C), $\lambda_{ex} = 295$ nm (D).

2.5.2.2 Ternary complexes

Hence, we assessed the formation of potential ternary complexes by Cu^{II}-$AHH^{W/Tb}$ in the presence of HSA, LB or FBS by means of spectroscopic techniques.

In particular, a switch between the 4N and the 3N+L coordination modes can be suggested by a red-shift of the d-d band in the UV-vis absorption spectrum as well as by the increase of the *g* factors in the EPR (electron paramagnetic resonance) spectrum.[398,399]

Noticeably, Cu-$AHH^{W/Tb}$ and Cu-HSA complexes show barely distinguishable d-d bands and low-temperature (LT) EPR spectrum, as they have the very same coordination sphere (at pH 7.4).

After 1 h incubation of Cu-HSA with $AHH^{W/Tb}$, the LT-EPR spectrum looked almost identical to that of Cu-$AHH^{W/Tb}$ and Cu-HSA complexes (see Fig. 34A), meaning that Cu^{II} is bound in a 4N ATCUN-type coordination sphere, and no detectable amounts of ternary complexes were formed. Besides, to confirm that Cu^{II} was bound to $AHH^{W/Tb}$, we resorted to room-temperature (RT) EPR,

which allows to differentiate complexes having the same coordination sphere but different tumbling rates, as it is the case for HSA (66 kDa) and $AHH^{W/Tb}$ (~ 1 kDa).[62] Thus, the Cu^{II}-HSA-$AHH^{W/Tb}$ mixture showed a signal very similar to that of Cu^{II}-$AHH^{W/Tb}$ (see Fig. 34B), confirming that $AHH^{W/Tb}$ takes out Cu^{II} from HSA, as observed by the luminescence quenching.

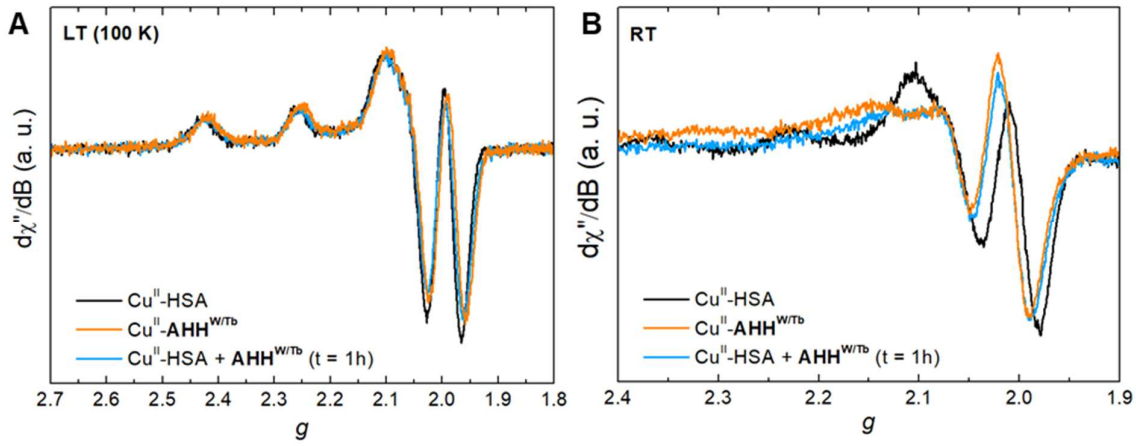

Figure 34. EPR spectra recorded at 100 K (A) or at RT (B) of Cu^{II}-HSA (black), Cu^{II}-$AHH^{W/Tb}$ (orange) and after 1h incubation of Cu^{II}-HSA with $AHH^{W/Tb}$ (blue). Conditions: [HSA] = [$AHH^{W/Tb}$] = 320 µM, [Cu^{2+}] = 300 µM, 100 mM HEPES pH 7.4. LT samples were supplemented by 10% (v/v) glycerol.

The potential formation of ternary species in LB medium and FBS (10%) was instead explored via UV-vis absorption spectroscopy. Again, no significant shift of d-d bands of Cu^{II}-$AHH^{W/Tb}$ was observed in the media compared the complex in HEPES buffer (50 mM, pH 7.4), suggesting that no more ternary complexes than those potentially found in the buffer are found in the biological samples.

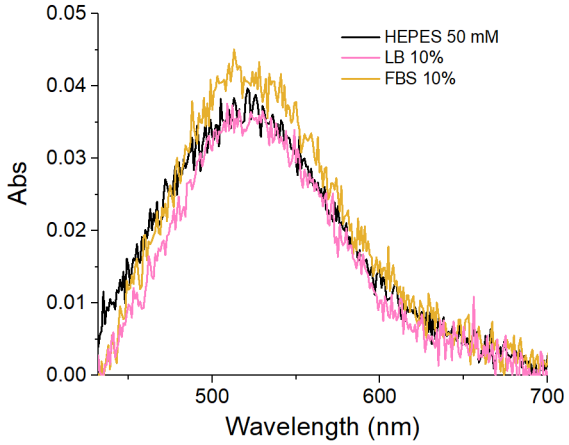

Figure 35. Visible spectra (d-d bands) of Cu^{II}-$AHH^{W/Tb}$ in HEPES 50 mM pH 7.4 (black), 10% LB medium (pink) and 10% FBS (yellow). Conditions: [$AHH^{W/Tb}$] = 500 µM, [Cu^{II}] = 450 µM.

These findings point towards the potential formation of very low levels of ternary complexes that are not detectable via the techniques used. Moreover, such ternary complexes could be even short-lived transient intermediates rather than stable species.

2.5.2.3 pH-dependence of the luminescence response

As mentioned above, the Cu^{II} complexes of XH(H) peptides benefit from higher stability than XZH at pH < 5.5. For this reason, we explored the possibility to apply the probe $AHH^{W/Tb}$ in a lower pH range than $GNH^{W/Tb}$. To study the pH dependence of the luminescent response, pH titrations of the Cu^{II}-probe complexes were performed**.**

The emission of Cu-$GNH^{W/Tb}$ was constant between pH 7.5 and 6, but it increased (2-fold) at pH 5 (see Fig. 36A). Instead, the signal of Cu-$AHH^{W/Tb}$ remained unchanged down to pH 5, increasing (2-fold) at pH 4.5 (see Fig. 36B). This indicates that $GNH^{W/Tb}$ could be applied down to pH 6, while $AHH^{W/Tb}$ can be used to detect Cu^{II} even at pH 5. This could be useful for application in slightly acidic body fluids such as urine.

However, while the luminescence of the Cu-free $GNH^{W/Tb}$ showed negligible pH-dependence, the emission of $AHH^{W/Tb}$ decreased by about 25% when lowering the pH from 7 to 4.5 (see Fig. 36C/ D). To explain this effect, it could be speculated that the protonation of a vicinal His affects Trp fluorescence and in turn Tb^{III} emission. This implies that care should be taken in the application of $AHH^{W/Tb}$ in samples with different pH.

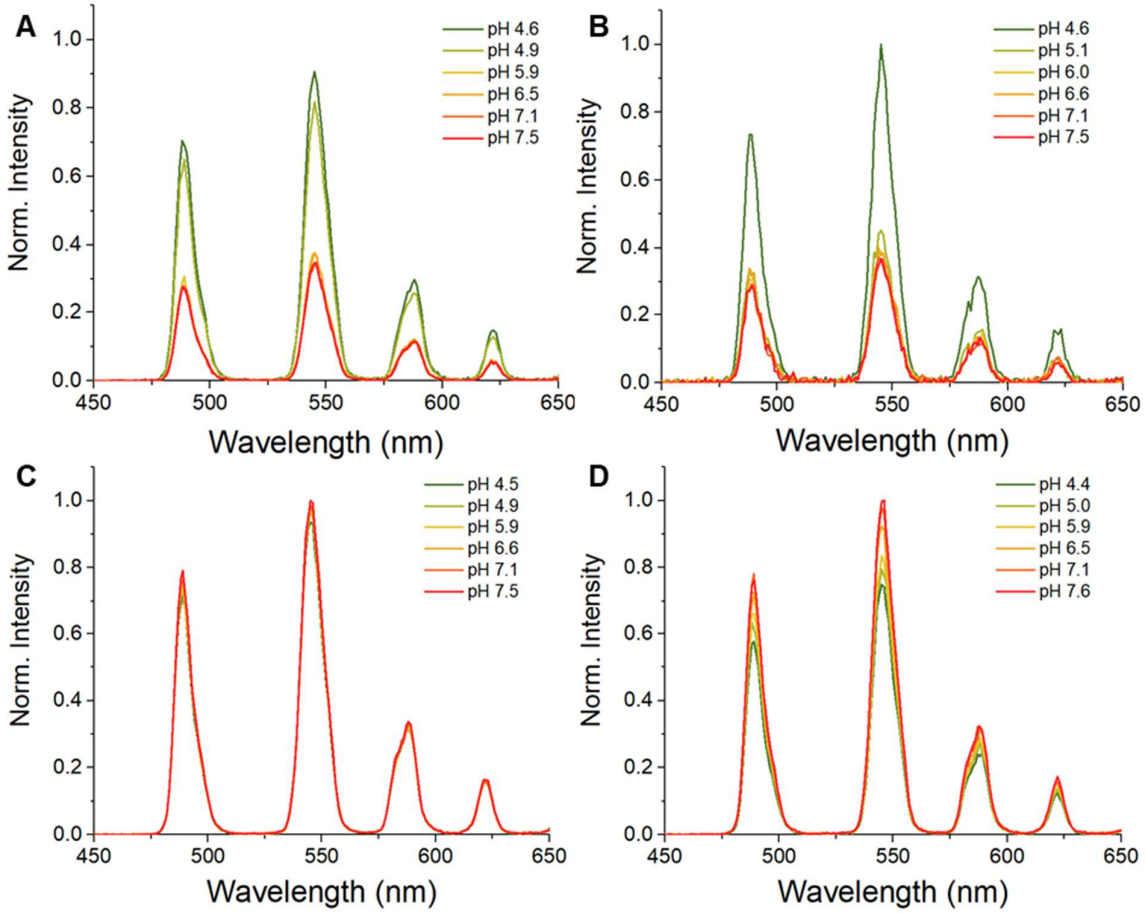

Figure 36. pH dependent time-delayed luminescence of A) Cu^{II}-$GNH^{W/Tb}$, B) Cu^{II}-$AHH^{W/Tb}$, C) $GNH^{W/Tb}$ and D) $AHH^{W/Tb}$. Conditions: A) [$GNH^{W/Tb}$] = 10 µM, [Cu^{2+}] = 9 µM; B) [$AHH^{W/Tb}$] = 10 µM, [Cu^{2+}] = 9 µM; C) [$GNH^{W/Tb}$] = 10 µM; D) [$AHH^{W/Tb}$] = 10 µM.

2.5.3 Conclusions

In conclusion, $AHH^{W/Tb}$ demonstrated enhanced kinetic responsiveness to Cu^{II} in biological media and to be competitive against HSA, which probably represents the most challenging competitor in body fluids.

Moreover, the ternary complexes that are held accountable for the faster Cu^{II} transfer seem to form in very low (undetectable) amounts and/or only transiently.

Finally, $AHH^{W/Tb}$ can be potentially applied at lower pH than $GNH^{W/Tb}$ (down to pH 5), although a pH-dependent calibration seems to be needed to compare samples at different pH.

Overall, this study highlighted that the apparent Cu^{II}-binding kinetics in biological media can be much slower than in a simple buffer solution and differ considerably from a medium to another depending on its composition. Therefore, the Cu^{II}-binding kinetics to a probe in a certain sample should be carefully assessed during the development of an analytic protocol in order to define the suitable timespan in which the analysis has to be performed.

2.5.4 Experimental section

2.5.4.1 Materials

Commercially available reagents were used unless otherwise stated. Essentially fatty acid-free HSA (Sigma) was used without further purification. LB medium was prepared from LB broth (Lennox) powder (Carl Roth), enriched with 5 g/L of yeast extract (Carl Roth). Analytical HPLC was performed using a Hitachi Primaide instrument on a C18 column (XBridge Peptide BEH C18 column from Waters, 4.6 mm x 150 mm, pore size 300 Å, particle size 3.5 µm). MS spectra were recorded on an LCQ Fleet Ion Trap mass spectrometer (Thermo Fischer). Preparative HPLC was carried out using a LaPrep Sigma (VWR International) instrument. Spectrophotometric titrations were performed on a Cary 60 UV-vis spectrophotometer using a 1 cm path quartz cuvette.

2.5.4.2 Peptide synthesis

$AHH^{W/Tb}$ (H_2N-AHHW$K^{DOTA(Tb)}$GK-NH_2) was synthesized manually through a standard Fmoc/*t*Bu SPPS protocol (see Fig. 37) in a syringe with filter frit. Fmoc-Rink amide aminomethyl-polystyrene resin (Fmoc-Rink-Amid AM Resin from Iris Biotech, 0.74 mmol/g loading, 100-200 mesh) was used to obtain C-terminal amidation. Coupling reactions (1h under shaking) were performed using 4 equivalents of Fmoc-protected amino acids, 3.9 equivalents of HCTU (O-(1H-6-Chlorobenzotriazole-1-yl)-1,1,3,3-tetramethyluronium hexafluorophosphate) as coupling agent, 8 equivalents of DIEA as the base and DMF as the solvent. After coupling, the presence of unreacted N-terminal free amine was checked with TNBS reagent, and the coupling was repeated in case of a positive test. Capping of the unreacted free amine group was carried out using 5% acetic anhydride and 10% DIEA in DMF for 5 min. N-terminal Fmoc deprotection was carried out using 20% piperidine in DMF. The N-terminal Ala residue was introduced as tert-butyloxycarbonyl-protected amino acid (Boc-Ala-OH) to ensure orthogonal deprotection of the Lys^5(Alloc). Removal of the N^{ε}-Alloc protecting group was performed using $Pd(PPh_3)_4$ (0.05 mmol, 0.5 eq., 58 mg) and phenylsilane (2.4 mmol, 24 eq., 0.3 mL) in degassed anhydrous dichloromethane (DCM) in the dark (2x1h). The resin was then washed with DCM (2×2 min), DMF (2×2 min), 1% H_2O in DMF (2×2 min), DMF (2×2 min), 1% DIEA in DMF (2×2 min), DMF (2×2 min), sodium diethyldithiocarbamate in DMF (0.12 M, 2×5 min) and DMF (2×2 min). The DOTA unit was grafted adding DOTA-tris(*t*Bu) ester (0.1 mmol, 57 mg, 1 eq.), PyBOP (0.2 mmol, 104 mg, 2 eq.) and then DIEA (0.8 mmol, 140 µL, 8 eq.) in DMF overnight. Resin cleavage and side-chain deprotection were performed treating with 95% TFA, 2.5% H_2O and 2.5% TIS for 90 min. The peptide was cleaved and acid-labile side-chain deprotected by treatment with TFA/TIS/H_2O (95:2.5:2.5) for 90 min. The crude was precipitated with cold ether and purified by reverse-phase HPLC on a C18 column (XBridge Peptide BEH C18 OBD Prep Column from Waters, 19 mm x 150 mm, pore size 130 Å, particle size 5 µm). Tb^{III} complex was prepared by overnight incubation of the peptide with $TbCl_3 \cdot 6H_2O$ (5 eq.) in H_2O at pH ≈ 6.3. The purity and identity of the peptide were assessed by analytical HPLC and LC-MS. $[AHH^{W}+H]^+$: experimental m/z = 1248.87, calculated m/z = 1248.84; $[GNH^{W/Tb}+H]$, experimental m/z = 1404.82, calculated m/z = 1404.76. Yield $AHH^{W/Tb} \cdot (CF_3COO^-)_3$: 27% (15.2 mg).

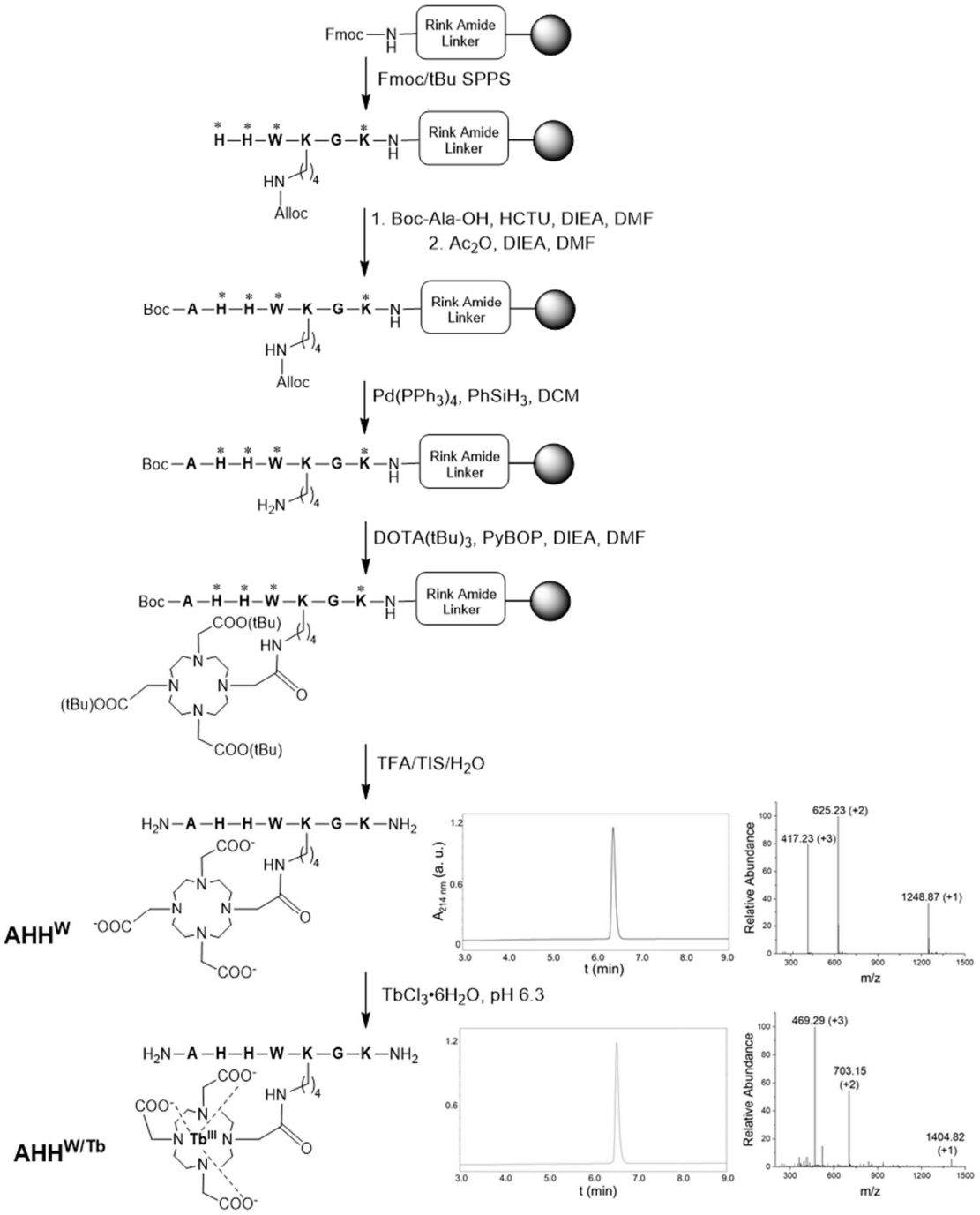

Figure 37. Synthetic pathway of $AHH^{W/Tb}$. Amino acids are labelled in bold and standard side chain protecting groups are denoted as * (Boc for Lys and Trp, Trt for His). HPLC chromatograms and ESI-MS spectra of purified AHH^{W} and $AHH^{W/Tb}$ are also reported.

2.5.4.3 Preparation of stock solutions

Stock solutions were prepared in ultrapure water (ρ = 18.2 M$\Omega \cdot cm^{-1}$). The concentration of peptide stock solutions was determined by tryptophan UV-vis absorption (ε_{280} = 5690 $M^{-1}cm^{-1}$) and spectrophotometric titration with Cu^{II}. A stock solution of HEPES buffer (500 mM, pH 7.4) was prepared by dissolving free acid powder and by adjusting the pH with NaOH. The concentration of $CuCl_2 \cdot 2H_2O$ stock solution was verified by UV-Vis spectroscopy (ε_{780} = 12 $M^{-1}cm^{-1}$). As the N-terminus of commercial HSA stock is partially truncated (and hence Cu^{II} binding to the ATCUN site is abolished),[403] the concentration of the ATCUN-bearing HSA was measured via spectrophotometric titration with Cu^{II}.

2.5.4.4 Luminescence measurements

Luminescence spectra were recorded on a Cary Eclipse (Agilent) fluorescence spectrophotometer using a 1 cm path quartz cuvette, λ_{ex} = 280 nm and 100 µs time delay.

Cu^{II}-binding kinetics in LB medium and FBS were measured by adding exogenous Cu^{2+} to a solution of the peptides in the media.

Calibration curves have been obtained by adding the pre-formed Cu^{II}-complexes (at 10 µM final concentration of the peptides and Cu^{II} concentration varying from 0.1 to 10 µM) to the buffer/media solution. Luminescence intensity was measured using the following parameters: excitation slit 20 nm, emission slit 10 nm, averaging time 0.1 s. The average intensity at 545 nm over five measurements was plotted versus the Cu^{II} concentration and fitted using linear regression ($y = k\ x$) with fixed intercept (the average intensity of the blank, i.e. the peptides in absence of Cu^{II}). The limit of detection (LOD) was calculated based on $3\sigma/k$ (where σ is the standard deviation of the blank measurements and k is the slope of the linear regression line).

pH titrations were performed adding small aliquots of a concentrated NaOH solution to the peptides/complexes solutions in water.

Kinetics of Cu^{II}-binding in LB medium was monitored via time-delayed luminescence using a Spark (Tecan) plate reader inside a 384 wells microplate.

Kinetics of Cu^{II} release to EDTA was monitored via tryptophan fluorescence emission using a CLARIOStar Plus (GMB Biotech) plate reader inside a 384 wells microplate, with λ_{ex} = 295 nm and λ_{em} = 360 nm.

2.5.4.5 UV-vis spectroscopy

UV-vis spectra were recorded on a Cary 60 spectrophotometer using a 1 cm path quartz cuvette. Spectra of Cu^{II}-$AHH^{W/Tb}$ in biological media were obtained adding the pre-formed complex to the medium.

2.5.4.6 EPR spectroscopy

EPR spectra were recorded on a continuous-wave EPR X-band spectrometer (EMXplus, Bruker Biospin GmbH, Germany) equipped with a high sensitivity resonator (4119HS-W1, Bruker) at both room (RT, T = 295 K ± 1 K) and low temperature (LT, T = 100 K), which was achieved by a continuous flow liquid nitrogen cryostat.

The principal RT experimental parameters were: modulation amplitude 10 G, microwave power 10 mW, time constant ~ 80 ms, conversion time ~ 375 ms. 1000 G were swept in 5 minutes and 5

scans were accumulated. A blank sample (100 mM HEPES at pH 7.4) was used to baseline all spectra.

The principal LT experimental parameters were: modulation amplitude 5 G, microwave power 0.1 mW, time constant ~ 80 ms, conversion time ~ 200 ms. 1500 G were swept in 5 minutes and 6 scans were accumulated.

Samples were prepared in 100 mM HEPES (pH 7.4) at 320 μM concentration of the ligands and 300 μM Cu^{II}. RT samples were transferred into 25 μL glass capillaries (Hirschmann) and sealed on both ends. LT samples were supplemented by 10 % v/v glycerol to ensure a good glassy sample once freeze-quenched in 3 mm ID quartz tubes (Wilmad LabGlass).

2.6 From intensiometric to ratiometric ATCUN/Ln^{III} probes

The general shortcomings of turn-off probes have been described above. Above all, they suffer from inaccurate quantification, since the probe signal may change also due to a change in the concentration of the probe itself, for instance, because of degradation, or due to off-target interactions, especially in a complex biological medium. Therefore, ratiometric probes are preferred as the ratio between two signals is less sensitive to external factors. For instance, "type I" ratiometric probes (see section 2.2.3) includes a non-responsive luminophore acting as an internal "reference" for the calibration of the probe response.

As seen in section 2.2.3, current ratiometric Cu^{II} probes do not show suitable affinity and selectivity for applications in biological media, although probe **19** was applied to detect extracellular Cu in cell culture.[328] Hence, novel ratiometric sensors for Cu^{II} are needed in order to measure Cu_{EXC} in biological samples.

As already observed, "type II" ratiometric probes seem to involve aromatic donors which undermine the affinity and the selectivity for Cu^{II}. On the other hand, the design of "type I" ratiometric probes appears more straightforward, as it can be envisioned that a luminophore placed far from the Cu^{II} binding site would be less affected by the quenching effect.

2.6.1 Assessment of a poly-Proline spacer

Thus, with the aim to develop an ATCUN peptide-based ratiometric sensor, we first focused our attention on the choice of an appropriate spacer to distance the Cu^{II}-responsive and the Cu^{II}-binding site. Although well-folded protein structures could ensure a defined spatial detachment between two appended entities such as fluorophores, the design of a rigid linker using short peptides is hampered by their tendency to be intrinsically disordered and hence very flexible.

Browsing the literature about peptide-based ratiometric probes, we encountered a ratiometric two-fluorophore Zn^{II} sensor build on a peptide scaffold.[404] Notably, the authors employed a poly-proline (poly-Pro) scaffold to separate the two fluorophores, i.e. a Zn^{II}-insensitive hydroxycoumarin conjugated at the peptide N-terminus and a Zn^{II}-responsive DPA-fluorescein derivative grafted on the side-chain of the C-terminal Lysine.

Indeed, poly-Pro sequences can assume well-defined helical secondary structures thanks to the unique properties of proline (Pro), which is a (cyclic) secondary amine, and hence forms tertiary amide bonds when polymerized. Contrary to most peptide bonds, which predominantly exist in the *trans* conformation due to the lower steric repulsion between the amide hydrogen and the preceding C_α, the *trans* and *cis* conformers of Xxx-Pro peptide bonds show considerably lower energy difference owing to the cyclic nature of Pro side-chain (see Fig. 38A).[405] Notwithstanding, by virtue of the high constrain brought by the bulky side-chain, the preferred folding of oligoprolines is the so-called poly-proline helix II (PPII), which is a left-handed helix composed of *trans* peptide bonds (see Fig. 38B). PPII is characterized by backbone dihedral angles ϕ = -75° and ψ = 150° and a pitch of about 9 Å with 3 residues per turn. Interestingly, due to the lack of amide hydrogens, the PPII helix is not stabilized by intramolecular hydrogen bonds, unlike α-helices and β-sheets, but rather by van der Waals interactions between adjacent amide bonds.[406–408]

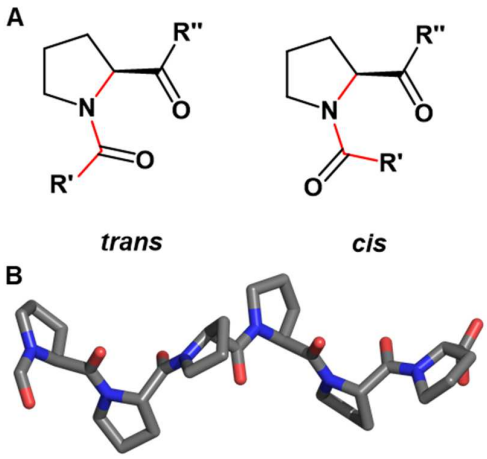

Figure 38. Structure of *trans* and *cis* conformers of Proline peptide bonds (A) and PPII helix (B).

Oligoprolines have been recognized for a long time for their structural rigidity, thanks to which they have been used as "molecular rulers", for instance, to calibrate FRET efficiency measurements or to modulate the distance between groups attached at the poly-Pro termini.[408–411]

Thus, we examined whether the adoption of a poly-Pro spacer could be suited to build an ATCUN-based ratiometric Cu^{II} sensor. For this purpose, we designed a proof-of-principle peptide, $RTH^{W\text{-}NBD}$, bearing a high-affinity ATCUN motif (RTH, log $K_{7.4}$ = 14.5),[412] a Trp residue as Cu^{II}-responsive fluorophore, a hexa-proline spacer, and an NBD dye grafted onto a Lys side-chain as "reference" fluorophore (see Fig. 39).

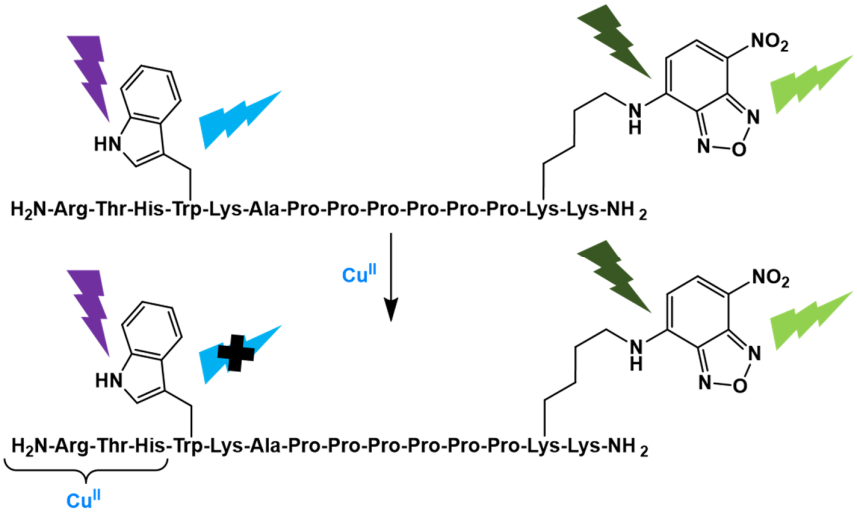

Figure 39. Mechanism of ratiometric Cu^{II} detection by $RTH^{W\text{-}NBD}$: Cu^{II} quenches efficiently Trp emission due to its proximity to the ATCUN motif, while ideally it does not affect NBD emission, which acts as a "reference" fluorophore.

2.6.1.1 Results and discussion

The peptide $RTH^{W\text{-}NBD}$ (H_2N-RTHWKAPPPPPPK^{NBD}K-NH_2) was synthesized via automatized SPPS followed by manual deprotection of alloc-protected lysine and coupling of NBD on the side-chain (see section 2.6.5.2). First, the peptide structure was assessed via circular dichroism (CD)

spectroscopy, which showed a spectrum with a minimum at ~220 nm and a maximum at ~230 nm (see Fig. 40), attributable to a PPII helix.[413–415]

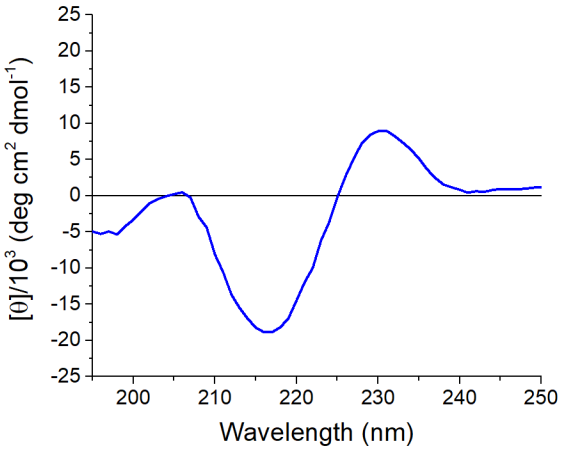

Figure 40. Far-UV CD spectrum of $RTH^{W\text{-}NBD}$. Conditions: [$RTH^{W\text{-}NBD}$] = 20 μM, HEPES 2 mM pH 7.4.

Then, the fluorescent response of $RTH^{W\text{-}NBD}$ to Cu^{II} was studied via fluorometric titration (see Fig. 41A). Trp and NBD fluorescent emission were recorded exciting at 280 nm and 480 nm, respectively. Remarkably, while Trp emission (at 348 nm) showed about 80% quenching at 1:1 Cu:$RTH^{W\text{-}NBD}$ ratio, the signal of the distal NBD group (at 560 nm) was quenched only by about 20%. Moreover, unlike Trp, the plot of NBD emission as a function of the Cu:$RTH^{W\text{-}NBD}$ ratio did not show a breakpoint at 1:1 ratio, suggesting that its quenching does not directly arise from the binding of Cu^{II} to the ATCUN motif (see Fig. 41B). Hence, the ratiometric response, i.e. I_{348}/I_{560}, represents a corrected version of Trp signal that takes into account external factors contributing to the fluorescence quenching.

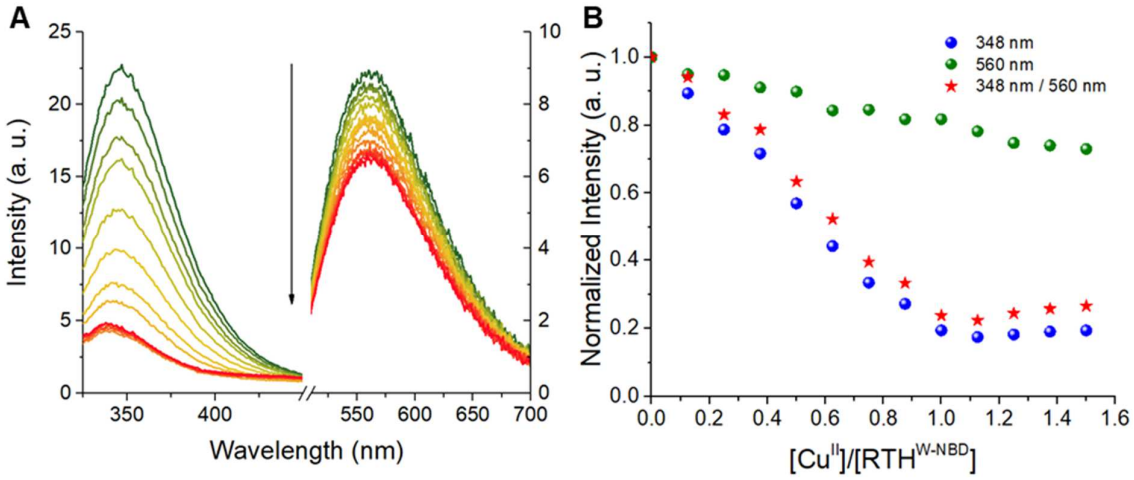

Figure 41. Fluorometric Cu^{II} titration of $RTH^{W\text{-}NBD}$. A) Fluorescence spectra of Trp (λ_{ex} = 280 nm, λ_{em} = 348 nm) and NBD (λ_{ex} = 480 nm, λ_{em} = 560 nm) emission upon gradual addition of Cu^{II}. B) Titration curves and plot of the ratiometric response (red stars). Conditions: [$RTH^{W\text{-}NBD}$] = 2 μM, HEPES 100 mM pH 7.4.

Overall, the ratiometric behaviour observed using a poly-Pro spacer appeared satisfactory and promising for the development of two-fluorophore peptide-based ratiometric Cu^{II} probes.

2.6.2 Development of ratiometric probes for Cu^{II} using the Tb^{III}/Eu^{III} couple

2.6.2.1 Tb^{III}/Eu^{III}-based ratiometric sensors

In order to improve the detection and quantification of the turn-off ATCUN/Ln^{III}-based probes reported previously, we focused our efforts on designing peptide-based ratiometric probes composed of the ATCUN motif, two different luminescent Ln^{III} complexes and a poly-Pro spacer.

The Tb^{III}-Eu^{III} couple is often used to build Ln^{III}-based ratiometric sensors.[416–420] Indeed, although Tb^{III} and Eu^{III} emission bands partially overlap in the 560-670 nm spectral range, they also show distinct bands at ~490 and 545 nm (Tb^{III}) and 700 nm (Eu^{III}).

As the two Ln^{III} complexes need to be far away in the case of a Cu^{II} sensor, two antenna units have to be used. Conveniently, Tb^{III} and Eu^{III} can be sensitised by the same chromophore (e.g. naphthalene) or by different antennas that can be excited at the same wavelength.

However, as Ln^{III} ions share common coordination preferences, and ligands selective for a certain Ln^{III} ion do not exist, the regiospecific metalation of even distinct Ln^{III} chelator appears very challenging and very few strategies have been developed so far. For instance, Sames et al. exploited the different kinetic lability of the macrocyclic DOTA (more inert) and the linear DTPA (more labile) ligands to achieve the site-specific metalation with Tb^{III} and Eu^{III}.[421] Later, Faulkner et al. reported a different approach based on the selective (acid vs. basic) deprotection of differently carboxy-protected (*t*-butyl vs. ethyl) DOTA esters.[422] Another strategy introduced by Faulkner et al. consists in the conjugation of previously metalated inert Ln^{III} complexes.[416,423,424] Likewise, Sénèque et al. recently used bis(2-sulfanylethyl)amino (SEA) Native Chemical Ligation (NCL) to assemble peptide building blocks bearing distinct Ln^{III}-DOTA complexes forming hetero-bis-lanthanide ratiometric Zn^{II} probes.[425]

2.6.2.2 SEA ligation

In 1994, bioinspired by the mechanism of protein splicing, Kent et al. developed the Native Chemical Ligation (NCL) as a tool to link two deprotected peptidic fragments forming a native peptidic bond between a peptide thioester and a cysteinyl peptide in aqueous solution at neutral pH (see Fig. 42).[426,427] In particular, this approach includes the trans-thioesterification between the cysteinyl peptide (green) and the peptide thioester (red), followed by an intramolecular *S,N*-acyl shift between the amino group of Cys (orange) and the thioester group (green). Due to the instability of thioesters linkers during the standard Fmoc/*t*Bu SPPS protocols (notably under the basic conditions of Fmoc deprotection), it is preferable to generate the thioester moiety in solution, after the peptide cleavage from the resin. In 2010, Melnyk et al. developed an SPPS strategy to prepare a stable peptide thioester precursor, that can be converted to the active thioester via a reverse *N,S*-acyl shift.[428,429] Such precursor is the bis(2-sulfanylethyl)amino (SEA) group, which can be attached to a chloro-trityl resin on which SPPS is performed and then cleaved forming a "SEA-peptide" bearing a C-terminal bis(2-sulfanylethyl)amido moiety. In addition, the thiol groups of the "SEA^{on}" peptide can be further stabilized and inactivated by oxidation to the disulfide "SEA^{off}" form (see Fig. 43). Hence, the SEA ligation protocol involves the reduction of the SEA sulfide by tris(2-carboxyethyl)phosphine (TCEP) in the presence of 4-mercaptophenylacetic acid (MPAA), which catalyses the ligation via trans-thioesterification.

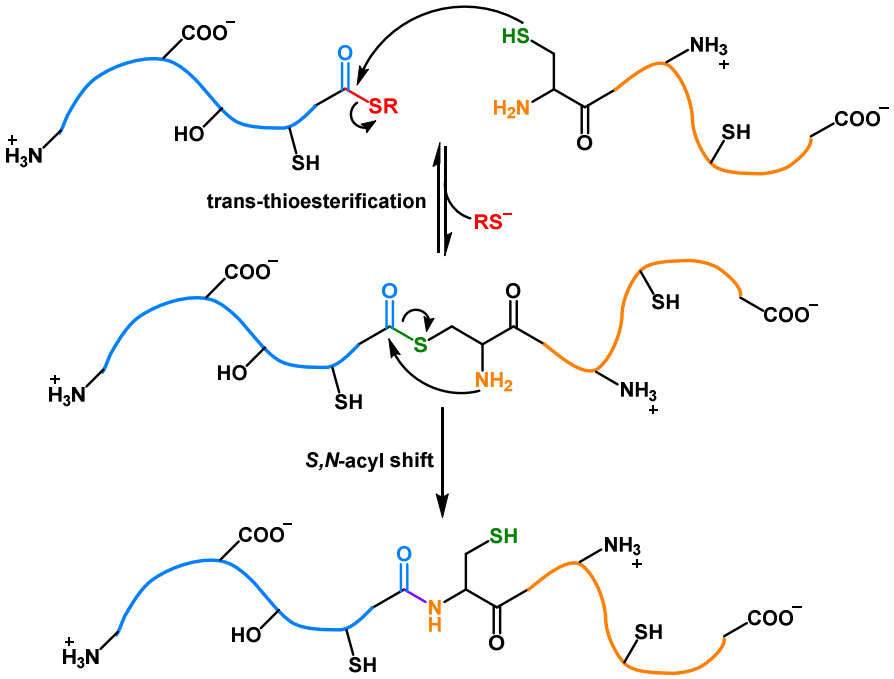

Figure 42. Mechanism of Native Chemical Ligation between a peptide thioester (blue) and a cysteinyl-peptide (orange). First, a trans-thioesterification occurs between the thiol group (green) of the N-terminal cysteine and the thioester group (red). Then, the newly formed thioester undergoes a *S,N*-acyl shift forming a native peptidic bond (purple).

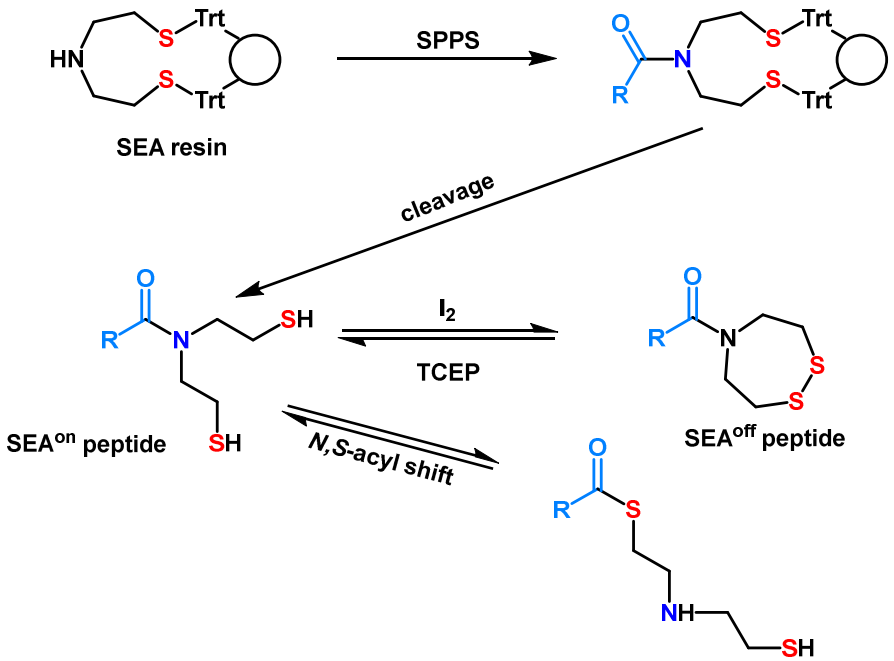

Figure 43. Synthesis of a SEA-peptide bearing a "latent" N-terminal peptide thioester group. A bis(2-sulfanylethyl)amino (SEA) resin is used for the elongation of the SEA-peptide sequence. After the cleavage from the resin, the SEA peptide is oxidised using I_2 to the more stable disulfide form. The reduction of such compound by TCEP and a reverse *N,S*-acyl shift produces the sought peptide thioester.

2.6.2.3 Design of an ATCUN/Tb^{III}/Eu^{III}-based ratiometric probe

Here, we adopted an NCL approach to develop an ATCUN hetero-bis-lanthanide (Tb^{III}/Eu^{III}) ratiometric probes for Cu^{II}, $AHH^{W/Tb\text{-}pic/Eu}$. In particular, we assembled the N-terminal peptide fragment $AHH^{W/Tb}$-SEA (AHHWK$^{DOTA(Tb)}$A-SEA) containing the AHH motif and the Trp-Tb^{III}(DOTA) couple as Cu^{II}-responsive luminescent unit, and the C-terminal fragment $CP_9^{pic/Eu}$ (CPPPPPPPPPK$^{DO3Apic(Eu)}$K-NH_2) containing the poly-Pro spacer and a Eu^{III}-DO3Apic (2,2′,2′-(10-((6-carboxypyridin-2-yl)methyl)-1,4,7,10-tetraazacyclododecane-1,4,7-triyl)triacetic acid) complex as "reference" luminescent unit. The DO3Apic unit (see Fig. 44) contains a picolinate group serving as a very efficient intra-ligand antenna for Eu^{III} that can be excited at the same wavelength as Trp (280 nm). In addition, thanks to the binding of the picolinate unit to the Eu^{III}, DO3Apic represents a nonadentate ligand that prevents water-binding to Eu^{III} enhancing its signal.[430] Moreover, the intra-ligand picolinate antenna has lower flexibility than Trp, reducing the possibility to get closer to the Cu^{II}-binding site. Finally, envisaging a lower quenching by Cu^{II} at a longer distance, a nona-proline spacer was used for this probe.

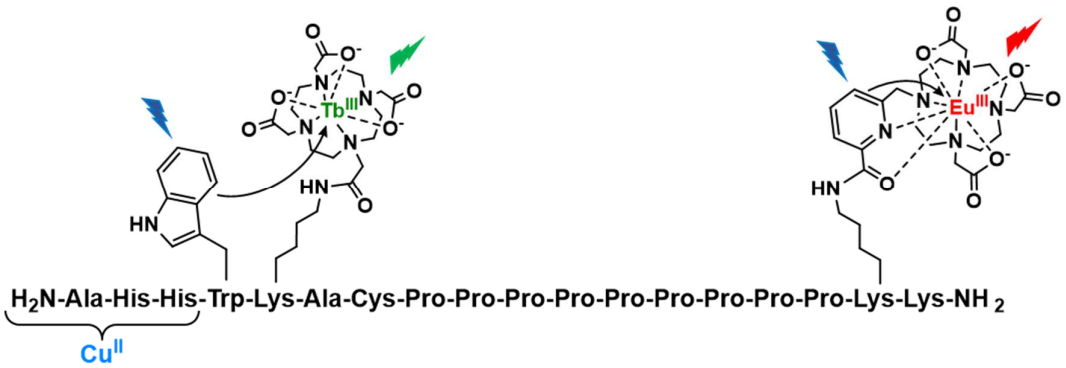

Figure 44. Structure of the ratiometric probe $AHH^{W/Tb\text{-}pic/Eu}$.

2.6.2.4 Results and discussion

The peptide fragments $AHH^{W/Tb}$-SEA and $CP_9^{pic/Eu}$ were synthetized by standard SPPS and metalated similarly to the previously described probes. The SEA ligation of $AHH^{W/Tb}$-SEA and $CP_9^{pic/Eu}$ was accomplished obtaining the probe $AHH^{W/Tb\text{-}pic/Eu}$ (see sections 2.6.5.3-2.6.5.5).

As the intra-ligand picolinate is a far better antenna for Eu^{III} than Trp for Tb^{III}, the intensity of Eu^{III} is expected to be higher than Tb^{III}.[430] Nevertheless, as Tb^{III} has a higher lifetime than Eu^{III}, the ratio between the intensity of their bands can be modulated by tuning the time delay applied. Therefore, in order to select a time-delay yielding comparable Tb^{III} and Eu^{III} signals and keeping a good signal-to-noise ratio, the decay of Tb^{III} and Eu^{III} luminescence at 487 and 700 nm, respectively, was recorded (see Fig. 45A). The lifetimes resulted to be 1.96 and 1.16 ms for Tb^{III} and Eu^{III}, respectively, in agreement with previous reports, and a time delay of 3 ms was chosen to record the time-delayed luminescence spectrum (see Fig. 45B). Thus, all bands can be observed with a good signal-to-noise ratio. Notably, the band at 487 and 545 nm arise from Tb^{III} transitions and the bands at a wavelength higher than 675 nm arise from Eu^{III} transitions, while the bands in the 575-675 spectral range bands include a contribution from both Tb^{III} and Eu^{III}.

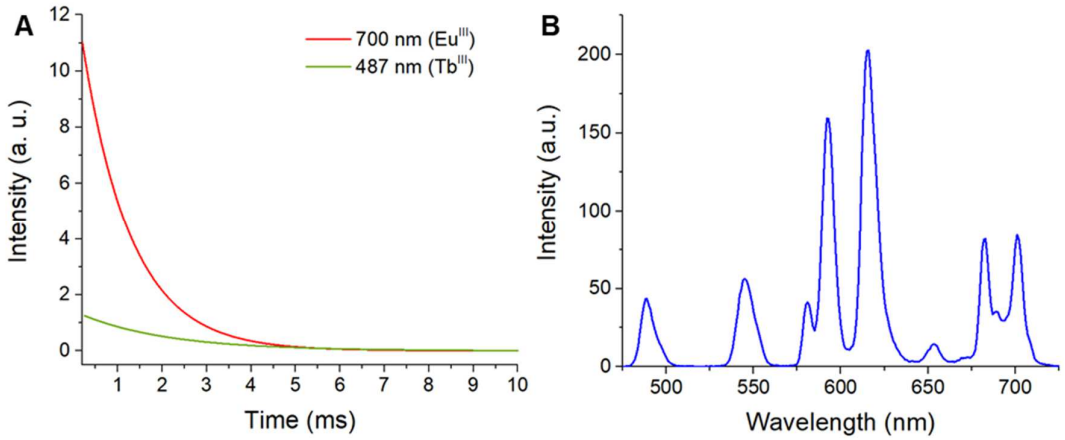

Figure 45. Characterisation of AHH$^{W/Tb\text{-}pic/Eu}$ luminescence. A) Decay of Tb^{III} (green, 487 nm) and Eu^{III} luminescence (red, 700 nm); B) time-delayed luminescence spectra of AHH$^{W/Tb\text{-}pic/Eu}$ with 3 ms time delay.

The luminescent response was hence assessed titrating AHH$^{W/Tb\text{-}pic/Eu}$ with Cu^{II} (see Fig. 46A), which quenched Eu^{III} emission of a lower extent, about 70%, than Tb^{III} (about 100%). As a result, the spectrum observed after the addition of one equivalent of Cu^{II} (red) shows only Eu^{III} bands. Moreover, the plot of both Tb^{III} and Eu^{III} signals as a function of the Cu^{II}:AHH$^{W/Tb\text{-}pic/Eu}$ show a breakpoint at 1:1 ratio suggesting that both Ln^{III} are responsive to the binding of Cu^{II} to the ATCUN motif (see Fig. 46A, inset). Besides, Eu^{III} quenching resulted surprisingly higher compared to the analogous NBD in RTH$^{W\text{-}NBD}$ (20% quenching). Such unexpected behaviour seems even more surprising considering that AHH$^{W/Tb\text{-}pic/Eu}$, compared to RTH$^{W\text{-}NBD}$, contains 9 rather than 6 prolines.

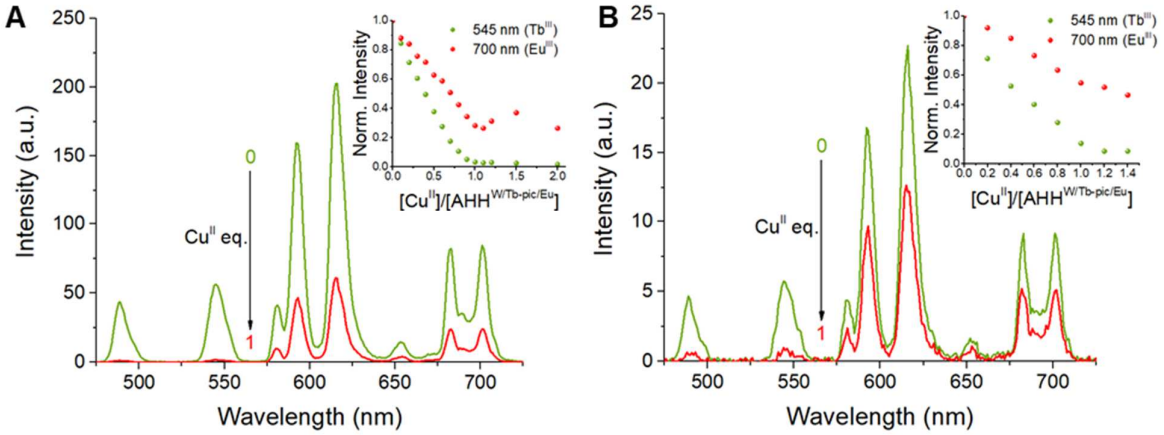

Figure 46. Luminescence response of AHH$^{W/Tb\text{-}pic/Eu}$ to Cu^{II}. A, B) Time-delayed luminescence spectrum of AHH$^{W/Tb\text{-}pic/Eu}$ without (green curve) and with 1 eq. of Cu^{II} (red curve); insets: titration curves. Conditions: [AHH$^{W/Tb\text{-}pic/Eu}$] = 10 μM (A) or 1 μM (B), HEPES 50 mM pH 7.4 (A, B).

On balance, the poly-Pro length is not the only difference between RTH$^{W\text{-}NBD}$ and AHH$^{W/Tb\text{-}pic/Eu}$. Indeed, the grafted Ln^{III} complexes and the additional Cys residue (required for the SEA ligation) in AHH$^{W/Tb\text{-}pic/Eu}$ could, for instance, perturb the helical folding of the poly-Pro that should keep Eu^{III} far from the ATCUN site. In addition, the known tendency of poly-Pro sequence to self-assemble,[407,431,432] as well as the Cu^{II}-catalysed cysteine oxidation with consequent formation of disulfide-bridged dimers, could be accountable for the increased quenching effect. Hence, we investigated these aspects.

The potential contribution of peptide assembly was assessed by titrating the peptide at 10-fold lower concentration (1 μM, see Fig. 46B). In these conditions, Eu^{III} band was quenched to a lower extent than at 10 μM concentration (see insets), revealing that some intermolecular interaction could indeed partially contribute to the observed behaviour.

Besides, the peptide structure was verified by CD (see Fig. 47). Interestingly, although the C-terminal proline-rich fragment CP_9 (H_2N-CPPPPPPPPPKK-NH_2) showed an enhanced CD signal compared to the hexa-proline containing $RTH^{W\text{-}NBD}$ peptide, the full-length $AHH^{W/Tb\text{-}pic/Eu}$ peptide presented a lower PPII helical character. Indeed, the decrease of the positive band at 230 nm, which is the most diagnostic of a PPII helix, as well as the additional negative band at about 240 nm, revealed that the flaking amino acids and the pendant complexes perturb the folding of the spacer, implying higher flexibility of the peptide scaffold that intensify the quenching of Eu^{III}, as it can get closer to the Cu^{II} site.

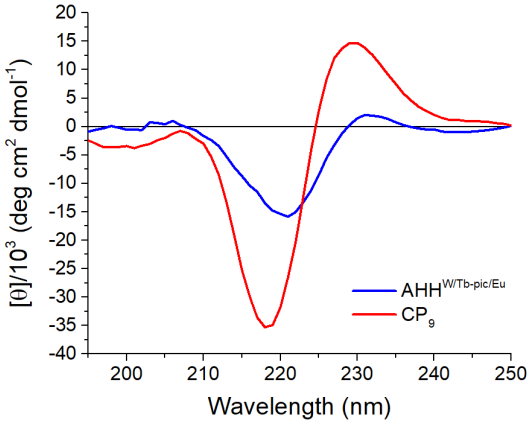

Figure 47. Far-UV CD spectrum of $AHH^{W/Tb\text{-}pic/Eu}$ (blue) and CP_6 (red). Conditions: [$AHH^{W/Tb\text{-}pic/Eu}$] or [CP_9] = 30 μM, HEPES 5 mM pH 7.4.

Furthermore, we assessed whether Cu^{II} oxidized the peptide Cys forming disulfide-bridged dimers. For this purpose, $AHH^{W/Tb\text{-}pic/Eu}$ (10 μM) was incubated with Cu^{II} (0.9 eq.) in HEPES (100 mM, pH 7.4). After 30 minutes, the LC-ESI-MS spectrum of the solution shows new peaks (m/z = 1255.23, z =5; m/z = 897.06, z = 7, red spectrum in Fig. 48) compared to the $AHH^{W/Tb\text{-}pic/Eu}$ peptide in absence of Cu^{II} (blue spectrum in Fig. 48), which can be ascribed to the formation of a disulfide bridged dimer (see table in Fig. 48).

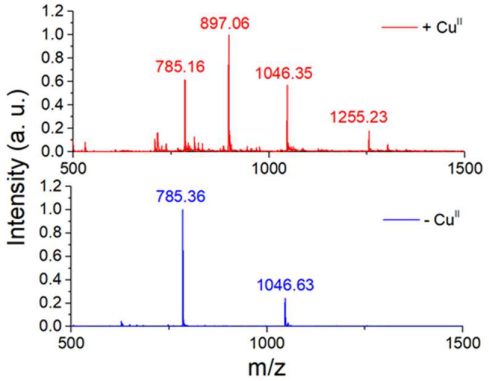

z	$AHH^{W/Tb\text{-}pic/Eu}$ (MW = 3136.14)	$AHH^{W/Tb\text{-}pic/Eu}$ dimer (MW = 6270.27)
+3	1046.38	/
+4	785.04	/
+5	/	1255.05
+6	/	1046.05
+7	/	896.75
+8	/	784.78

Figure 48. LC-ESI-MS spectra of $AHH^{W/Tb\text{-}pic/Eu}$ before (blue) and after (red) incubation (30 min) with Cu^{II}. Conditions: [$AHH^{W/Tb\text{-}pic/Eu}$] = 10 μM, [Cu^{II}] = 9 μM, HEPES 100 mM pH 7.4. The expected m/z of the ions deriving from $AHH^{W/Tb\text{-}pic/Eu}$ monomer or dimer are reported in the table.

Overall, the nona-proline spacer appeared to be not very suited to build the two-Ln^{III} ratiometric Cu^{II}-probe sought. Actually, an unexpected lower PPII helix content and the tendency of such poly-Pro segment to self-assemble seem partially accountable for the worse response compared to the $RTH^{W\text{-}NBD}$ probe.[413–415,433] Therefore, a hexa-proline spacer might be more convenient. Besides, the Cu^{II}-induced dimerization of $AHH^{W/Tb\text{-}pic/Eu}$ via disulfide bridge formation also potentially undermines the ratiometric behaviour and the applicability in biological media, where disulfide bridges could be formed with endogenous biomolecules. Consequently, the removal or the protection of the reactive Cys thiol group appears to be needed to prevent disulfides formation.

2.6.3 Optimization of ATCUN/Tb^{III}/Eu^{III}-based probe for biological applications

In the attempt to improve the response of the previous construct, another Tb^{III}/Eu^{III}-based probe was conceived. First, as for the promising $RTH^{W\text{-}NBD}$, we decided to adopt a 6- rather than 9-residue poly-Pro spacer. Besides, in order to remove the potential interference of the free Cys thiol, Cys was desulfurized after the SEA ligation.

Furthermore, we tackled another flaw of the ATCUN/Ln^{III}-based probe developed, namely the excitation in the UV region. Indeed, the antenna we employed so far for Tb^{III} and Eu^{III} sensitization, i.e. Trp and picolinate, were excited at 280 nm. As discussed above, the inner-filter effect exerted by biomolecules in such spectral region is very high and challenges the excitation of exogenous fluorophores. Remarkably, although the excitation at 280 nm, together with a time-delay, enabled the detection of $GNH^{W/Tb}$ and $AHH^{W/Tb}$ in diluted biological media such as 10% LB and FBS, we failed to record Tb^{III} emission from the $AHH^{W/Tb}$ peptide in rat urine samples. This brought out the need to use another antenna, suitable for both Tb^{III} and Eu^{III}, that can be excited at a higher wavelength.

In this regard, the carbostyril derivative Cs124 (Carbostyril 124, 7-Amino-4-methyl-2-hydroxyquinoline), which can be excited at 330 nm (ε_{327} = 12000 $M^{-1}cm^{-1}$, Φ = 0.97) , has been shown to sensitize both Tb^{III} and Eu^{III} (but with different efficiency).[434] Moreover, Cs124 conjugates with Glu amino acid (Fmoc-Glu(Cs124)-OH, see Fig. 49) have been successfully used as a building block to insert a Cs124 unit into peptide scaffolds.[377,425,435] Therefore, we chose to use Cs124 as the antenna for Tb^{III} and Eu^{III}, bound to DOTA ligands.

Finally, we also decided to reduce the flexibility of the appended Ln^{III} complexes grafting the DOTA units on the shorter Dap amino acid rather than Lys. Indeed, approaching the Ln^{III} complexes to the peptide backbone could be beneficial for the energy transfer between Cs124 and the Ln^{III} ions, and also to hamper potential interactions between the "reference" Eu^{III} complex and Cu^{II}.

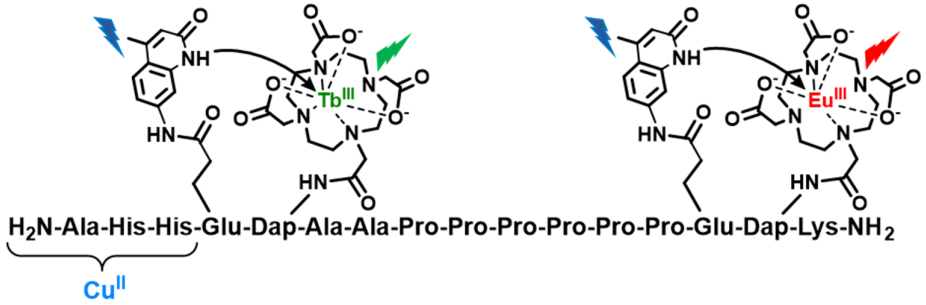

Figure 49. Structure of the ratiometric probe $AHH^{Cs124/Tb\text{-}Eu}$.

2.6.3.1 Results and discussion

Based on these principles, the probe AHH$^{Cs124/Tb-Eu}$-SH was synthetized assembling the N-terminal peptide AHH$^{Cs124/Tb}$ (AHHE^{Cs124}Dap$^{DOTA(Tb)}$A-SEA) and the C-terminal fragment CP$_6^{Cs124/Eu}$ (CPPPPPPE^{Cs124}Dap$^{DOTA(Eu)}$K-NH$_2$). AHH$^{Cs124/Tb-Eu}$-SH was then desulfurized obtaining AHH$^{Cs124/Tb-Eu}$ (see sections 2.6.5.6-2.6.5.9).

Curiously, the CD analysis of the native and desulfurized peptides showed distinct signatures (see Fig. 50). In particular, AHH$^{Cs124/Tb-Eu}$-SH (red) showed a minimum around 215 nm but no positive band at 230 nm. However, the apparent absence of this positive band might be due to an undesired baseline drift. The thiol-free AHH$^{Cs124/Tb-Eu}$ peptide (blue) showed a similar but weaker negative peak at 215 nm and a positive band around 240 nm. Interestingly, according to the literature, such a red-shift of the positive band in oligoprolines could be induced by aromatic-proline interactions.[436] Here, this could suggest that an interaction between prolines and the aromatic Cs124 occurs. Overall, the CD spectra recorded revealed that desulfurization impacts the peptide structure. Besides, they did not confirm unambiguously, but they also did not disprove, the formation of a PPII helix.

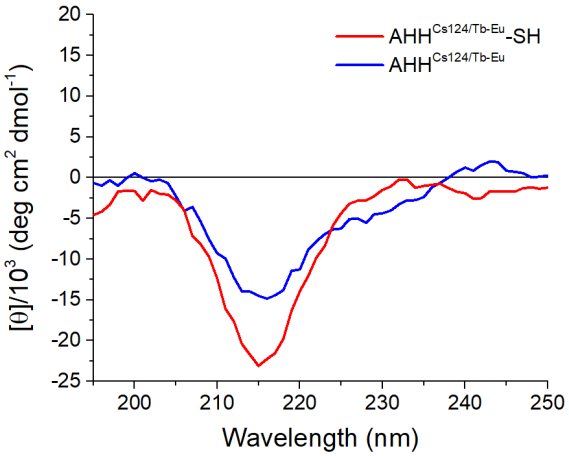

Figure 50. Far-UV CD spectrum of AHH$^{Cs124/Tb-Eu}$-SH (blue) and AHH$^{Cs124/Tb-Eu}$ (red). Conditions: [AHH$^{Cs124/Tb-Eu}$-SH] or [AHH$^{Cs124/Tb-Eu}$] = 20 μM, HEPES 2 mM pH 7.4.

The characterization of AHH$^{Cs124/Tb-Eu}$-SH time-delayed emission showed that, as reported in the literature, Cs124 sensitizes Tb^{III} better than Eu^{III}, as the latter show much less intense bands than the former (see Fig. 51A, green curve).[434]

The titration of AHH$^{Cs124/Tb-Eu}$-SH with Cu^{II} revealed that Tb^{III} and Eu^{III} luminescence were quenched at about 100% and 50%, respectively. Hence, it seems that the newly designed scaffold ensures a lower interaction between Eu^{III} and Cu^{II} compared to AHH$^{W/Tb-pic/Eu}$.

Then, we assessed the impact of the free Cys thiol on the luminescent response to Cu^{II} titrating the desulfurized variant AHH$^{Cs124/Tb-Eu}$ (see Fig. 51B). Remarkably, this did not behave differently from its parent AHH$^{Cs124/Tb-Eu}$-SH, suggesting that the peptide dimerization does not alter the response significantly, or that non-covalent dimerization occurs independently from the disulfide bridge.

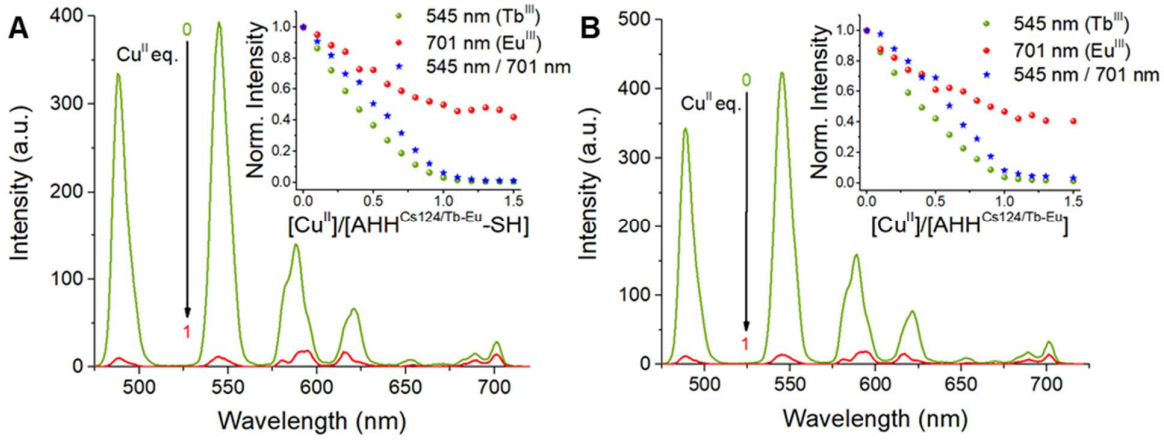

Figure 51. Luminescence response of AHH$^{Cs124/Tb\text{-}Eu}$-SH (A) and AHH$^{Cs124/Tb\text{-}Eu}$ (B) to Cu^{II}. Conditions: [AHH$^{Cs124/Tb\text{-}Eu}$-SH] = 10 μM (A) or [AHH$^{Cs124/Tb\text{-}Eu}$] = 10 μM (B), HEPES 100 mM pH 7.4.

Finally, we evaluated whether the Cs124 antenna enables the detection in urine. Thus, we recorded time-delayed luminescence spectra of AHH$^{Cs124/Tb\text{-}Eu}$-SH in urine samples collected from LEC (Long–Evans Cinnamon) rats, which are studied as an animal model of Wilson's disease.[437] In particular, we analysed the samples collected from a rat treated with the Cu-chelator D-Pen (see Fig. 8) with an untreated control. Of note, the administration of D-Pen increases urinary Cu levels.[438,439] Remarkably, both Tb^{III} and Eu^{III} signals were detected (see Fig. 52). Moreover, the treated rat sample showed a lower intensity of Tb^{III} bands than the control, consistent with a higher Cu content, while Eu^{III} bands showed no difference. Therefore, these preliminary data demonstrate that a ratiometric, albeit only qualitative at present, Cu^{II} detection is achievable in real biological samples such as urine.

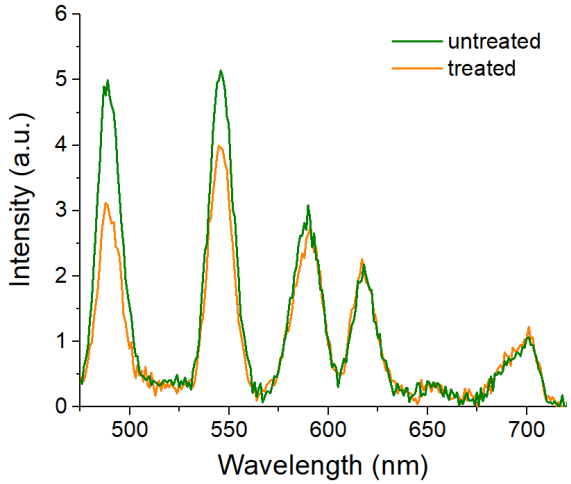

Figure 52. Ratiometric Cu^{II} detection by AHH$^{Cs124/Tb\text{-}Eu}$-SH in urine samples collected from a D-Pen-treated (orange) LEC rat and an untreated control (green). Conditions: [AHH$^{Cs124/Tb\text{-}Eu}$-SH] = 10 μM, urine 10%.

2.6.4 Conclusions

As the turn-off response impairs a proper quantification of the probe and hence of Cu^{II}, we attempted to develop a ratiometric probe that is less sensitive to external factors and artefacts. For this aim, we designed a proof-of-concept dual-lanthanide ATCUN-based probe exploiting an oligoprolines sequence as the spacer between a Cu^{II}-responsive Tb^{III} complex proximal to the ATCUN motif and an ideally "reference" Eu^{III} complex. In such a probe, Cu^{II} quenched completely Tb^{III}, but only partially Eu^{III}. Therefore, a ratiometric response could be obtained. However, the spacer used did not ensure a complete quenching of the "reference" fluorophore, which would be desirable. Overall, the flexibility of the peptide scaffold and side-chain-grafted luminophores, as well as a certain propensity of the peptide to self-assemble, seems to be responsible for such behaviour. These issues have to be certainly addressed to further optimize the probe prototypes realized in this work.

Besides, the use of Cs124, rather than Trp or picolinate, as the antenna, enabled the detection of the probe in urine samples. Hence, our investigations also highlight that the choice (e.g. Trp/pic vs Cs124) and the placement (e.g. intra-ligand vs external) of the antenna are crucial to obtain a comparable intensity of Tb^{III} and Eu^{III} signals and ensure the detection in biological media.

2.6.5 Experimental section

2.6.5.1 Materials

Commercially available reagents were used without further purification. SEA resin was prepared by Dr. Lucia Borkova following a previously reported procedure.[429] DO3Apic-tris(allyl)ester and Fmoc-Glu(Cs124)-OH were prepared according to literature procedures and kindly provided by Dr. Olivier Sénèque (CEA, Grenoble).[377,430] Analytical HPLC was performed using a Hitachi Primaide instrument on a C18 column (XBridge Peptide BEH C18 column from Waters, 4.6 mm x 150 mm, pore size 300 Å, particle size 3.5 µm). LC-MS spectra were recorded on an LTQ-XL mass spectrometer coupled to a Dionex UltiMate3000 Ultra-HPLC system (Thermo Scientific). Preparative HPLC was carried out using a LaPrep Sigma (VWR International) instrument. Spectrophotometric titrations were performed on a Cary 60 UV-vis spectrophotometer using a 1 cm path quartz cuvette.

2.6.5.2 Synthesis of $RTH^{W\text{-}NBD}$

$RTH^{W\text{-}NBD}$ (H_2N-RTHWKAPPPPPPK^{NBD}K-NH_2) was synthetized via standard Fmoc/*t*Bu SPPS protocol using an automated peptide synthesizer (Biotage Iniziator+ Alstra) on a Tentagel XV RAM resin (0.24 mmol/g loading, particle size 100-200 µm). Amino acid coupling was performed using 4 eq. of Fmoc-protected amino acids and 3.8 eq. of DIC/Oxyma (0.5 M) as coupling agents in DMF. Microwave heating (5 min, 75 °C) was applied except for the three N-terminal amino acids (60 min, rt) to prevent His racemization. Capping of the unreacted free amine group was carried out using 0.16 M (Ac_2O and 1M DIEA in NMP/DMF 4:1 for 2 min. Fmoc deprotection (3×5 min) was carried out using 20% piperidine in DMF. The peptide N-terminus was Boc-protected adding 4 equivalents of Boc_2O and 2 equivalents of DIEA in DMF for 1 hour. Deprotection of the alloc-protected side-chain of the Lys^{13} residue was performed using $Pd(PPh_3)_4$ (0.05 mmol, 0.5 eq., 58 mg) and phenylsilane (2.4 mmol, 24 eq., 0.3 mL) in degassed anhydrous

DCM in the dark (2x1h). The resin was then washed with DCM (2×2 min), DMF (2×2 min), 1% H_2O in DMF (2×2 min), DMF (2×2 min), 1% DIEA in DMF (2×2 min), DMF (2×2 min), sodium diethyldithiocarbamate in DMF (0.12 M, 2×5 min) and DMF (2×2 min). 4-Chloro-7-nitro-1,2,3-benzoxadiazole (NBD-Cl, 0.05 mmol, 10 mg, 5 eq.) was coupled overnight in the dark in the presence of DIEA (0.01 mmol, 20 µL, 10 eq.) in DMF. Resin cleavage and side-chain deprotection were performed treating with TFA/H_2O/TIS (95:2.5:2.5) for 90 min. The crude was precipitated with cold ether and purified by HPLC on a C18 column (XBridge Peptide BEH C18 OBD Prep Column from Waters, 19 mm x 150 mm, pore size 130 Å, particle size 5 µm). The purity and identity of the peptides were assessed by HPLC and LC-MS (see Fig. 53). Deconvoluted mass: 1798.60, expected mass: 1799.08. Yield: $RTH^{W\text{-}NBD}\cdot(CF_3COO^-)_5$ ~ 5% (5.5 mg).

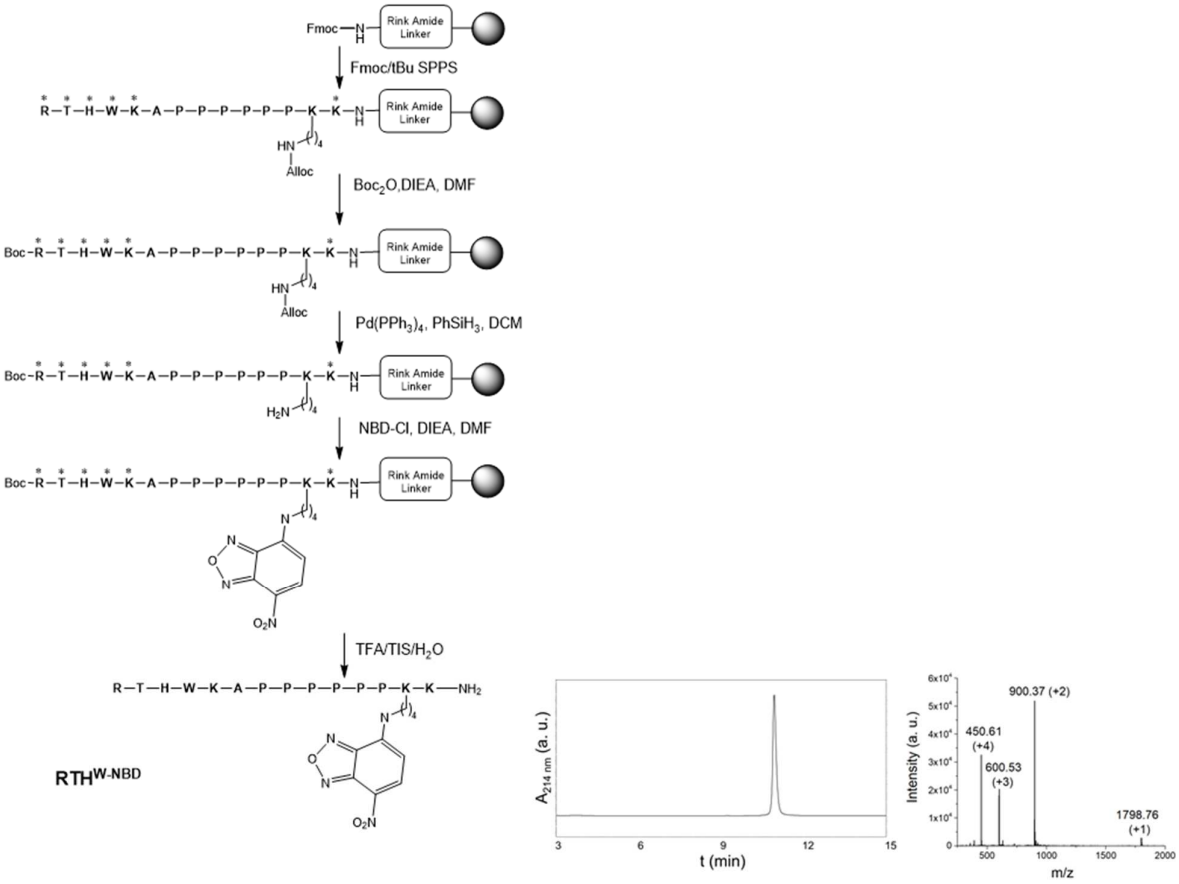

Figure 53. Synthetic pathway of $RTH^{W\text{-}NBD}$. Amino acids are labelled in bold and standard side chain protecting groups are denoted as * (Pbf for Arg, *t*Bu for Thr, Trt for His, Boc for Trp and Lys). HPLC chromatograms and ESI-MS spectrum of purified $RTH^{W\text{-}NBD}$ are reported.

2.6.5.3 Synthesis of $AHH^{W/Tb}$-SEA^{off}

$AHH^{W/Tb}$-SEA^{off} (H_2N-$AHHWK^{DOTA(Tb)}A$-SEA^{off}) was synthesized manually via standard Fmoc/*t*Bu SPPS protocol on a SEA resin (0.12 mmol/g loading). Amino acids couplings (2×45-60 min) was performed using 4 eq. of Fmoc-protected amino acids, 3.9 equivalents of HCTU and 8 eq. of DIEA in DMF, except for the first coupling where double amounts of reactants were used (8 eq. Fmoc-Ala-OH, 8 eq. HCTU, 16 eq. DIEA). Capping of the unreacted free amine group was carried out using 5% acetic anhydride (Ac_2O) and 10% DIEA in DMF for 5 min. Fmoc deprotection was carried out using 20% piperidine in DMF. The N-terminal Ala residue was introduced as tert-butyloxycarbonyl-protected amino acid (Boc-Ala-OH) to ensure orthogonal deprotection of the Lys^5(Alloc), which was performed using $Pd(PPh_3)_4$ (0.05 mmol, 0.5 eq., 58 mg) and phenylsilane (2.4 mmol, 24 eq., 0.3 mL) in degassed anhydrous dichloromethane (DCM) in the dark (2x1h). The resin was then washed with DCM (2×2 min), DMF (2×2 min), 1% H_2O in DMF (2×2 min), DMF (2×2 min), 1% DIEA in DMF (2×2 min), DMF (2×2 min), sodium diethyldithiocarbamate in DMF (0.12 M, 2×5 min) and DMF (2×2 min). The DOTA unit was grafted adding DOTA-tris(*t*Bu) ester (0.1 mmol, 57 mg, 1 eq.), PyBOP (0.2 mmol, 104 mg, 2 eq.) and then DIEA (0.8 mmol, 140 µL, 8 eq.) in DMF overnight. Resin cleavage and side-chain deprotection were performed treating with TFA/H_2O/TIS/DTT/thioanisole (90:2.5:2.5:2.5) for 90 min. The crude was precipitated with cold ether, dissolved in 0.1 % aq. TFA and lyophilized. Oxidation of the SEA thiol groups was achieved by dissolving the lyophilized powder in 10% acetic acid and adding I_2 dropwise until the solution became orangish. DTT was added to quench the excess of I_2. The SEA-peptide was then purified by HPLC on a C18 column (XBridge Peptide BEH C18 OBD Prep Column from Waters, 19 mm x 150 mm, pore size 130 Å, particle size 5 µm). Tb^{III} complex was prepared analogously to $AHH^{W/Tb}$ (see section 2.5.4.2). The purity and identity of the peptides were assessed by HPLC and LC-MS (see Fig. 54). Deconvoluted mass AHH^{W}-SEA: 1252.65, expected mass AHH^{W}-SEA: 1252.48; deconvoluted mass $AHH^{W/Tb}$-SEA^{off}: 1408.42, expected mass $AHH^{W/Tb}$-SEA^{off}: 1408.38. Yield: AHH^{W}-SEA·$(CF_3COO^-)_3$ ~8% (5 mg).

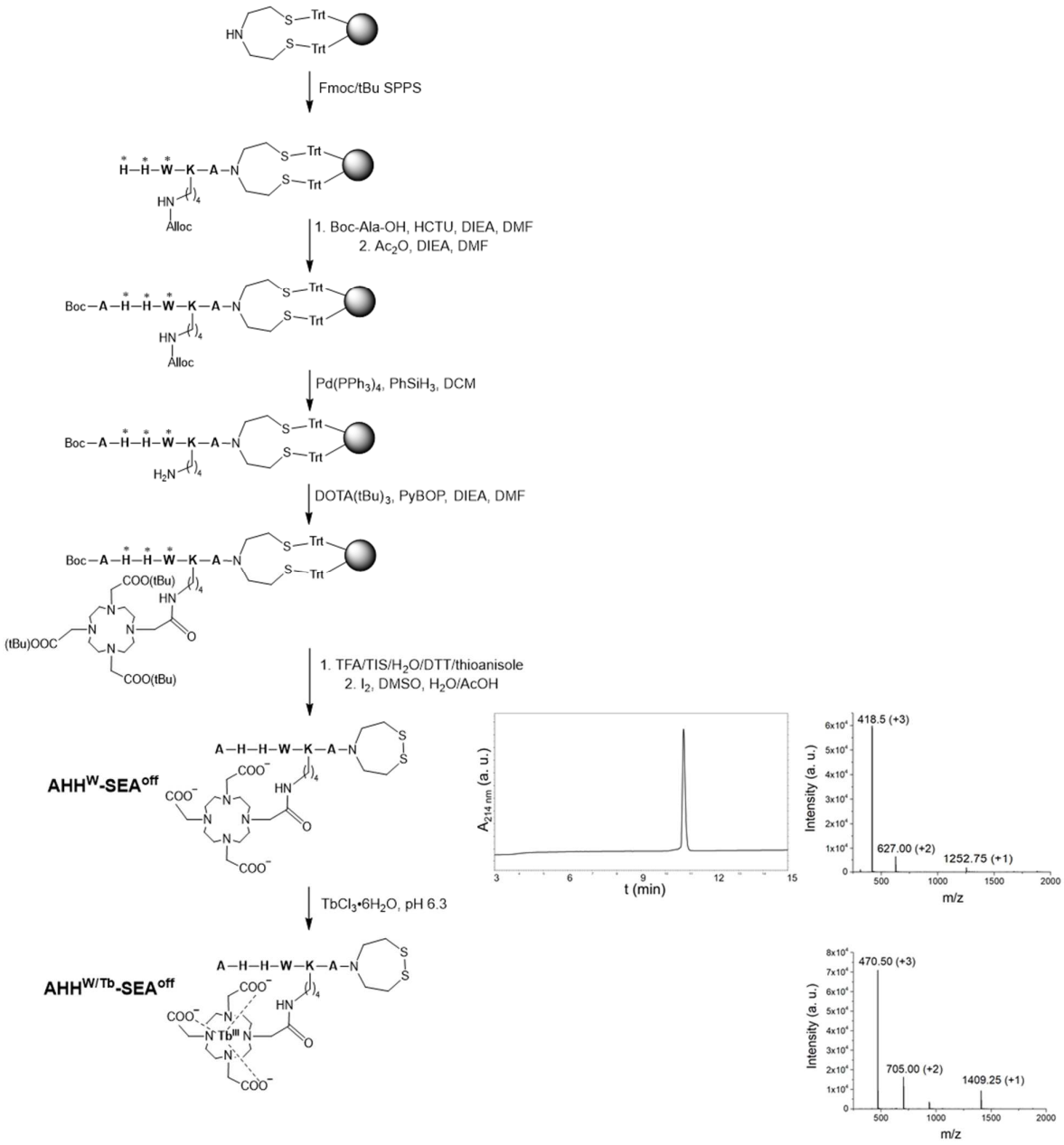

Figure 54. Synthetic pathway of AHH$^{W/Tb}$-SEA^{off}. Amino acids are labelled in bold and standard side chain protecting groups are denoted as * (Trt for His, Boc for Trp). HPLC chromatogram and/or ESI-MS spectrum of AHH^{W}-SEA^{off} and AHH$^{W/Tb}$-SEA^{off} are reported.

2.6.5.4 Synthesis of $CP_9^{pic/Eu}$

$CP_9^{pic/Eu}$ (H_2N-CPPPPPPPPPK$^{DO3Apic(Eu)}$K-NH_2) was synthetized via standard Fmoc/*t*Bu SPPS protocol on a Tentagel XV RAM resin (0.24 mmol/g loading, particle size 100-200 µm). All amino acids but Cys were coupled with an automated peptide synthesizer (Biotage Iniziator+ Alstra) using 4 eq. of Fmoc-protected amino acids and 3.8 eq. of DIC/Oxyma (0.5 M) in DMF under microwave heating (5 min, 75 °C). Capping of the unreacted free amine group was carried out using 0.16 M (Ac_2O and 1M DIEA in NMP/DMF 4:1 for 2 min. Fmoc deprotection (3×5 min) was carried out using 20% piperidine in DMF. N-terminal Cys was coupled (3×30 min) manually using 4 eq. of Fmoc-Cys(Trt)-OH, 4 eq. of PyBOP as the activator and 8 eq. of DIEA in DMF. The peptide N-terminus was Boc-protected adding 4 eq. of Boc_2O and 2 eq. of DIEA in DMF for 1 hour. Deprotection of the alloc-protected side-chain of the Lys^{11} residue was performed using $Pd(PPh_3)_4$ (0.05 mmol, 0.5 eq., 58 mg) and phenylsilane (2.4 mmol, 24 eq., 0.3 mL) in degassed anhydrous DCM in the dark (2x1h). The resin was then washed with DCM (2×2 min), DMF (2×2 min), 1% H_2O in DMF (2×2 min), DMF (2×2 min), 1% DIEA in DMF (2×2 min), DMF (2×2 min), sodium diethyldithiocarbamate in DMF (0.12 M, 2×5 min) and DMF (2×2 min). DO3Apic-tris(allyl)ester (0.045 mmol, 30 mg, 1 eq.) was coupled overnight using PyBOP (0.09 mmol, 52 mg, 2 eq.) and DIEA (0.36 mmol, 70 µL, 8 eq.) in DMF. Deprotection of allyl esters was performed as described above for alloc-Lys. Resin cleavage and side-chain deprotection were performed treating with TFA/H_2O/TIS (95:2.5:2.5) and DTT (200 mg) for 90 min. The crude was precipitated with cold ether and purified by HPLC on a C18 column (XBridge Peptide BEH C18 OBD Prep Column from Waters, 19 mm x 150 mm, pore size 130 Å, particle size 5 µm). The DO3Apic unit was metalated with Eu^{III} adding $EuCl_3 \cdot 6H_2O$ (7 eq.) in H_2O at pH 6.2 overnight. The purity and identity of the peptide were assessed by analytical HPLC and LC-MS (see Fig. 55). Deconvoluted mass CP_9^{pic}: 1714.08, expected mass CP_9^{pic}: 1714.06; deconvoluted mass $CP_9^{pic/Eu}$: 1862.21, expected mass $CP_9^{pic/Eu}$: 1863.00. Yield $CP_9^{pic} \cdot (CF_3COO^-)_2$ ~2% (3.6 mg).

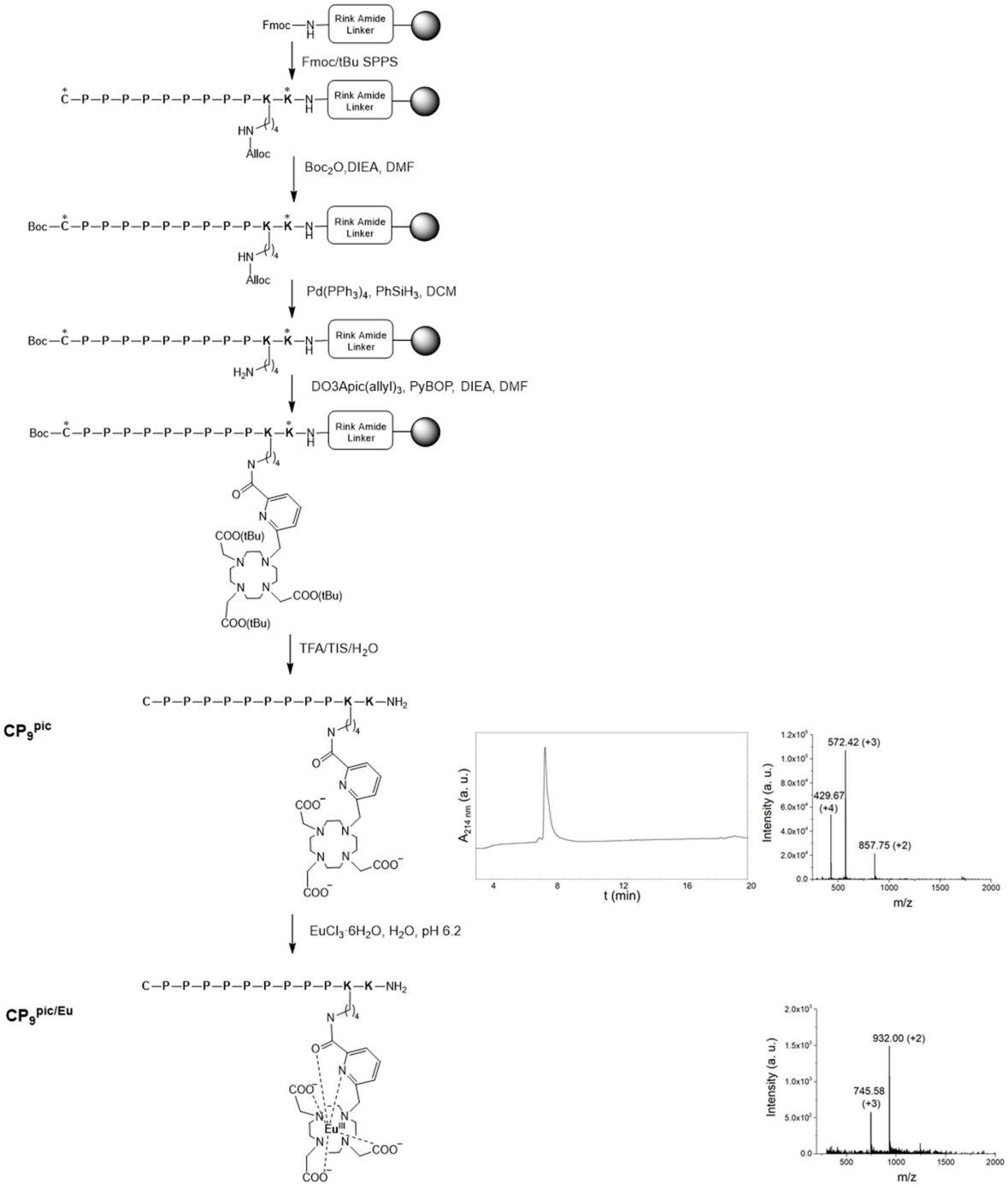

Figure 55. Synthetic pathway of $CP_9^{pic/Eu}$. Amino acids are labelled in bold and standard side chain protecting groups are denoted as * (Trt for Cys, Boc for Lys). HPLC chromatogram and/or ESI-MS spectrum of CP_9^{pic} and $CP_9^{pic/Eu}$ are reported.

2.6.5.5 Synthesis of $AHH^{W/Tb\text{-}pic/Eu}$ (SEA ligation)

A solution of TCEP and MPAA was prepared by dissolving TCEP·HCl (114.7 mg) and MPAA (33.6 mg) in 1 mL phosphate buffer 100 mM pH 7.4. The pH of such solution was adjusted to pH 6.5 with NaOH 5M. After degassing under Ar for about 15 min, the TCEP/MPAA solution (450 µL) was used to dissolve the mixture of peptides $AHH^{W/Tb}$-SEA (3 mg, 2 µmol) and $CP_9^{pic/Eu}$ (3.6 mg, 2 µmol) at ~4 mM final peptide concentrations. The SEA ligation was performed overnight at 37°C under shaking. At the end, the reaction mixture was diluted with 0.1% aq. TFA, and MPAA was extracted with diethyl ether. The peptide was purified by HPLC on a C18 column (XBridge Peptide BEH C18 OBD Prep Column from Waters, 19 mm x 150 mm, pore size 130 Å, particle size 5 µm). The purity and identity of the peptide were assessed by analytical HPLC and LC-MS (see Fig. 56). Deconvoluted mass $AHH^{W/Tb\text{-}pic/Eu}$: 3135.67, expected mass $AHH^{W/Tb\text{-}pic/Eu}$: 3136.14. Yield $AHH^{W/Tb\text{-}pic/Eu} \cdot (CF_3COO^-)_4$ ~ 8% (0.5 mg).

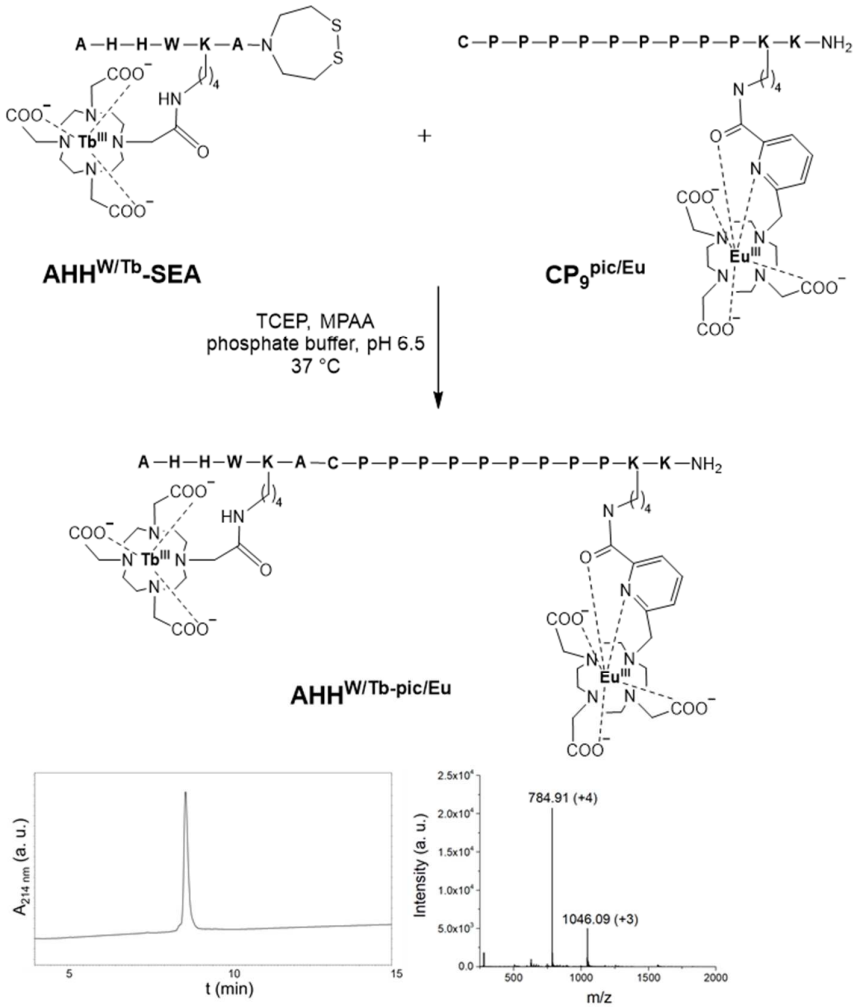

Figure 56. Synthetic pathway of $AHH^{W/Tb\text{-}pic/Eu}$. HPLC chromatogram and ESI-MS spectrum are reported.

2.6.5.6 Synthesis of AHH$^{Cs124/Tb}$-SEA^{off}

AHH$^{Cs124/Tb}$-SEA^{off} (H_2N-AHHE^{Cs124}Dap$^{DOTA(Tb)}$A-SEA^{off}) was synthesized manually via standard Fmoc/*t*Bu SPPS protocol on a SEA resin (0.12 mmol/g loading). Amino acids couplings (2×30-45 min) was generally performed using 4 eq. of Fmoc-protected amino acids, 3.9 equivalents of HCTU and 8 eq. of DIEA in DMF, except for the first coupling where double amounts of reactants were used (8 eq. Fmoc-Ala-OH, 8 eq. HCTU, 16 eq. DIEA). Glu^{Cs124} was coupled adding 2 eq. of Fmoc-Glu(Cs124)-OH, 2 eq. PyBOP and 4 eq. DIEA in DMF. The N-terminal Ala residue was introduced as *tert*-butyloxycarbonyl-protected amino acid (Boc-Ala-OH) to ensure orthogonal deprotection of the Dap(Alloc). Capping of the unreacted free amine group was carried out using 5% acetic anhydride (Ac_2O) and 10% DIEA in DMF for 5 min. Fmoc deprotection was carried out using 20% piperidine in DMF. Alloc deprotection was performed using $Pd(PPh_3)_4$ (0.05 mmol, 0.5 eq., 58 mg) and phenylsilane (2.4 mmol, 24 eq., 0.3 mL) in degassed anhydrous dichloromethane (DCM) in the dark (2x1h). The resin was then washed with DCM (2×2 min), DMF (2×2 min), 1% H_2O in DMF (2×2 min), DMF (2×2 min), 1% DIEA in DMF (2×2 min), DMF (2×2 min), sodium diethyldithiocarbamate in DMF (0.12 M, 2×5 min) and DMF (2×2 min). The DOTA unit was grafted adding DOTA-tris(*t*Bu) ester (0.1 mmol, 57 mg, 1 eq.), PyBOP (0.2 mmol, 104 mg, 2 eq.) and then DIEA (0.8 mmol, 140 µL, 8 eq.) in DMF overnight. Resin cleavage and side-chain deprotection were performed treating with TFA/H_2O/TIS/DTT/thioanisole (90:2.5:2.5:2.5:2.5) for 90 min followed by pure TFA treatment for 60 min. The crude was precipitated with cold ether, dissolved in 0.1 % aq. TFA and lyophilized. Oxidation of the SEA thiol groups was achieved by dissolving the lyophilized powder in 10% acetic acid and adding I_2 dropwise until the solution became orangish. DTT was added to quench the excess of I_2. The SEA-peptide was then purified by HPLC on a C18 column (XBridge Peptide BEH C18 OBD Prep Column from Waters, 19 mm x 150 mm, pore size 130 Å, particle size 5 µm). Tb^{III} complex was prepared analogously to AHH$^{W/Tb}$ (see section 2.5.4.2). The purity and identity of the peptides were assessed by HPLC and LC-MS (see Fig. 57). Deconvoluted mass AHH^{Cs124}-SEA: 1309.68, expected mass AHH^{Cs124}-SEA: 1309.49; deconvoluted mass AHH$^{Cs124/Tb}$-SEA^{off}: 1465.58, expected mass AHH$^{Cs124/Tb}$-SEA^{off}: 1465.39. Yield: AHH^{Cs124}-SEA·$(CF_3COO^-)_3$ ~ 4% (5.4 mg).

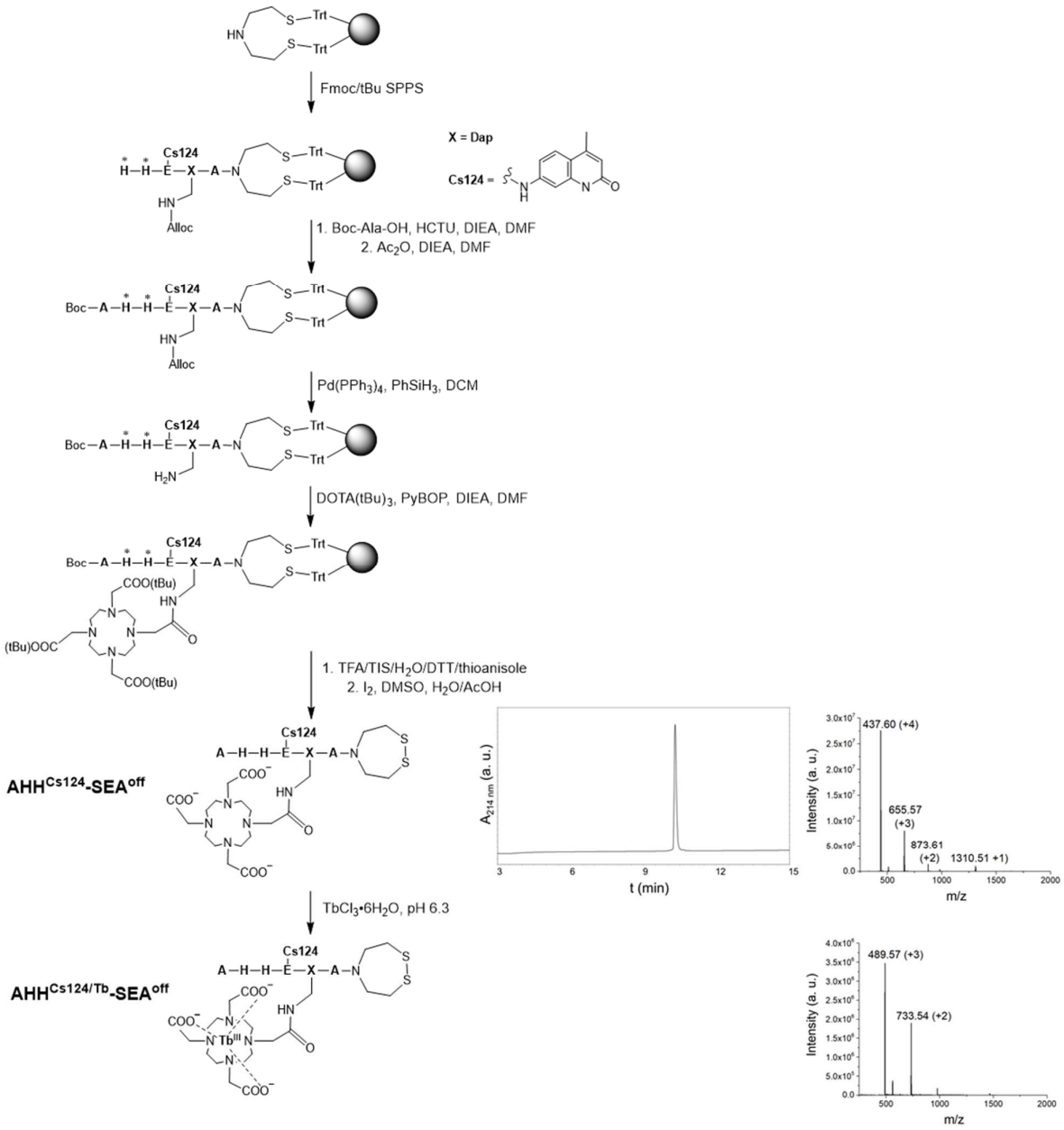

Figure 57. Synthetic pathway of AHH$^{Cs124/Tb}$-SEA^{off}. Amino acids are labelled in bold and standard side chain protecting groups are denoted as * (Trt for His). HPLC chromatogram and/or ESI-MS spectrum of AHH^{Cs124}-SEA^{off} and AHH$^{Cs124/Tb}$-SEA^{off} are reported.

2.6.5.7 Synthesis of $CP_6^{Cs124/Eu}$

$CP_6^{Cs124/Eu}$ (H_2N-CPPPPPPE^{Cs124}Dap$^{DOTA(Eu)}$K-NH_2) was synthetized via standard Fmoc/*t*Bu SPPS protocol on a Tentagel XV RAM resin (0.24 mmol/g, particle size 100-200 µm). Pro residues were coupled on an automated peptide synthesizer (Biotage Iniziator+ Alstra) using 4 eq. of Fmoc-protected amino acids and 3.8 eq. of DIC/Oxyma (0.5 M) in DMF under microwave heating (5 min, 75 °C). Dap and Lys were coupled manually (2×30-45 min) using 4 eq. of Fmoc-protected amino acid, 3.9 eq. of HCTU as the activator and 8 eq. of DIEA in DMF, while Cys and Glu^{Cs124} were coupled using 4 eq. Fmoc-Cys(S*t*Bu)-OH, 4 eq. of PyBOP and 8 eq. DIEA in DMF or 2 eq. of Fmoc-Glu(Cs124)-OH, 2 eq. PyBOP and 4 eq. DIEA in DMF, respectively. Capping of the unreacted free amine group was carried out using 5% acetic anhydride (Ac_2O) and 10% DIEA in DMF for 5 min. Fmoc deprotection was carried out using 20% piperidine in DMF. The peptide N-terminus was Boc-protected adding 4 eq. of Boc_2O and 2 eq. of DIEA in DMF for 1 hour. Deprotection of the alloc-protected side-chain of Dap was performed using $Pd(PPh_3)_4$ (0.05 mmol, 0.5 eq., 58 mg) and phenylsilane (2.4 mmol, 24 eq., 0.3 mL) in degassed anhydrous DCM in the dark (2x1h). The resin was then washed with DCM (2×2 min), DMF (2×2 min), 1% H_2O in DMF (2×2 min), DMF (2×2 min), 1% DIEA in DMF (2×2 min), DMF (2×2 min), sodium diethyldithiocarbamate in DMF (0.12 M, 2×5 min) and DMF (2×2 min). The DOTA unit was grafted adding DOTA-tris(*t*Bu) ester (0.1 mmol, 57 mg, 1 eq.), PyBOP (0.2 mmol, 104 mg, 2 eq.) and then DIEA (0.8 mmol, 140 µL, 8 eq.) in DMF overnight. Resin cleavage and side-chain deprotection were performed treating with TFA/H_2O/TIS (95:2.5:2.5) for 90 min followed by pure TFA treatment for 30 min. The crude was precipitated with cold ether and purified by HPLC on a C18 column (XBridge Peptide BEH C18 OBD Prep Column from Waters, 19 mm x 150 mm, pore size 130 Å, particle size 5 µm). The Eu^{III} complex was prepared as described for $CP_9^{pic/Eu}$. The purity and identity of the peptide were assessed by analytical HPLC and LC-MS (see Fig. 58). Deconvoluted mass CP_6^{Cs124}: 1677.32, expected mass CP_6^{Cs124}: 1677.02; Deconvoluted mass $CP_6^{Cs124/Eu}$: 1826.42, expected mass $CP_6^{Cs124/Eu}$: 1825.96. Yield $CP_6^{Cs124}\cdot(CF_3COO^-)_2$ ~7% (7.5 mg).

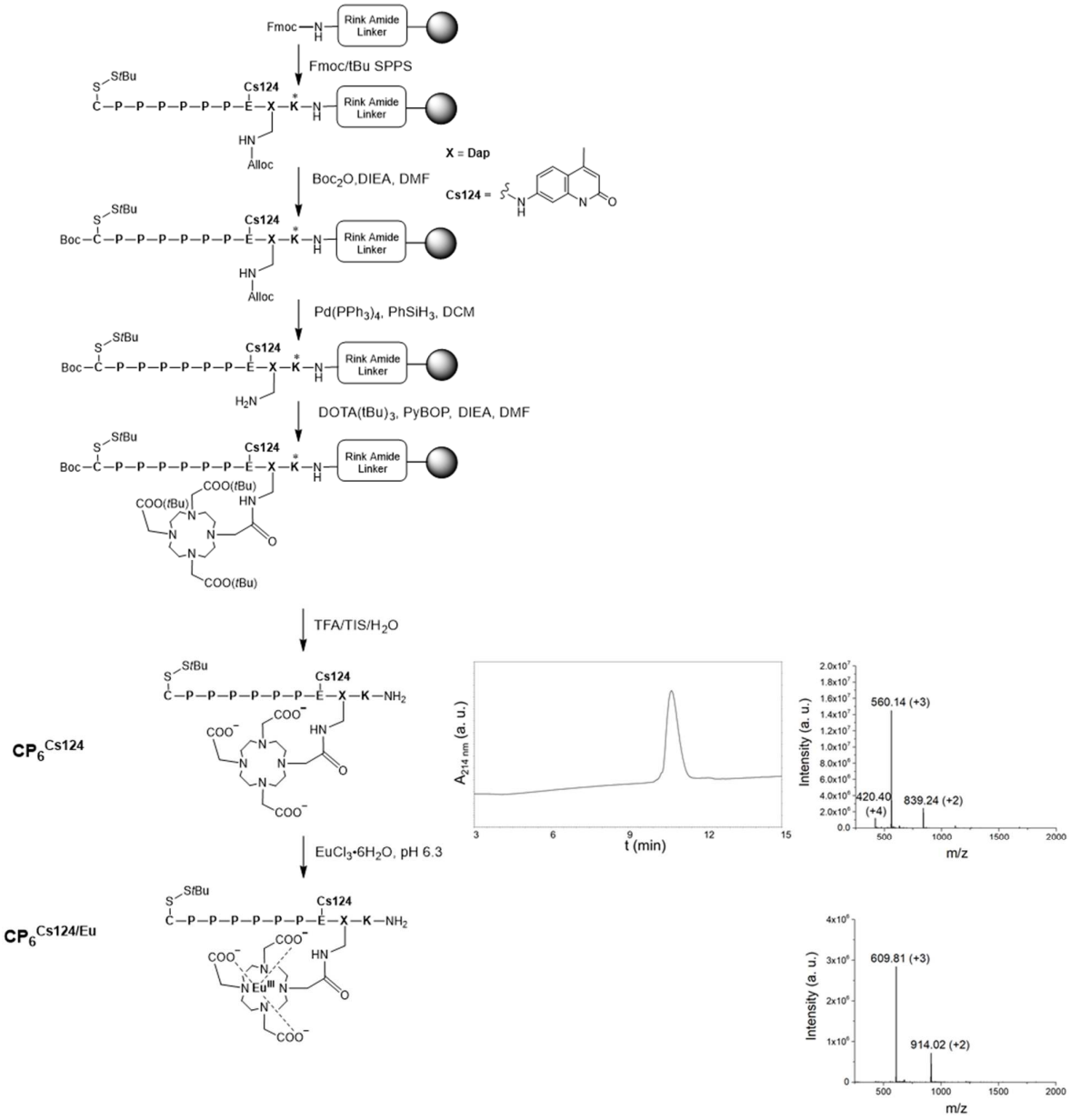

Figure 58. Synthetic pathway of $CP_6^{Cs124/Eu}$. Amino acids are labelled in bold and standard side chain protecting groups are denoted as * (Boc for Lys). HPLC chromatogram and/or ESI-MS spectrum of CP_6^{Cs124} and $CP_6^{Cs124/Eu}$ are reported.

2.6.5.8 Synthesis of AHH$^{Cs124/Tb-Eu}$-SH (SEA ligation)

A solution of TCEP and MPAA was prepared by dissolving TCEP·HCl (43 mg, 50 eq.) and MPAA (25 mg, 50 eq.) in 1 mL phosphate buffer 100 mM pH 7.4. The pH of such solution was adjusted to pH 6.6 with NaOH 5M. After degassing under Ar for about 15 min, the TCEP/MPAA solution (1 mL) and a solution of guanidine hydrochloride 6 M in phosphate buffer 100 mM (1 mL) were added to the powder of peptides AHH$^{Cs124/Tb}$-SEA (5.4 mg, 3 µmol) and CP$_6^{Cs124/Eu}$ (7.5 mg, 3.6 µmol) at 2.5 mM final peptide concentrations. The SEA ligation was performed at 37°C under shaking and monitored by HPLC. After 70 hours, the reaction mixture was diluted with 0.1 % aq. TFA (2 mL), and MPAA was extracted with diethyl ether. The peptide was purified by HPLC on a C18 column (XBridge Peptide BEH C18 OBD Prep Column from Waters, 19 mm x 150 mm, pore size 130 Å, particle size 5 µm). The purity and identity of the peptide were assessed by analytical HPLC and LC-MS (see Fig. 59). Deconvoluted mass AHH$^{Cs124/Tb-Eu}$-SH: 3068.78, expected mass AHH$^{Cs124/Tb-Eu}$-SH: 3067.93. Yield AHH$^{Cs124/Tb-Eu}$-SH·$(CF_3COO^-)_4$ ~77% (8.2 mg).

2.6.5.9 Synthesis of AHH$^{Cs124/Tb-Eu}$ (desulfurization)

The desulfurization was performed adapting a protocol reported in the literature.[440,441] AHH$^{Cs124/Tb-Eu}$-SH (3 mg, 1 mM final concentration) was dissolved in a solution containing TCEP·HCl 200 mM, glutathione (GSH) 50 mM and VA-044 (2,2'-azobis[2-(2-imidazolin-2-yl)propane]dihydrochloride) 20 mM in phosphate buffer 100 mM at pH 7.2 (adjusted manually with NaOH 5 mM). The reaction was carried out at 25 °C under shaking and monitored by HPLC. After 6 hours, the reaction mixture was diluted with 0.1% aq. TFA and purified on a C18 column (XBridge Peptide BEH C18 OBD Prep Column from Waters, 19 mm x 150 mm, pore size 130 Å, particle size 5 µm). The purity and identity of the peptide were assessed by analytical HPLC and LC-MS (see Fig. 59). Deconvoluted mass AHH$^{Cs124/Tb-Eu}$: 3036.60, expected mass AHH$^{Cs124/Tb-Eu}$: 3035.87. Yield AHH$^{Cs124/Tb-Eu}$ ·$(CF_3COO^-)_4$ ~34% (1 mg).

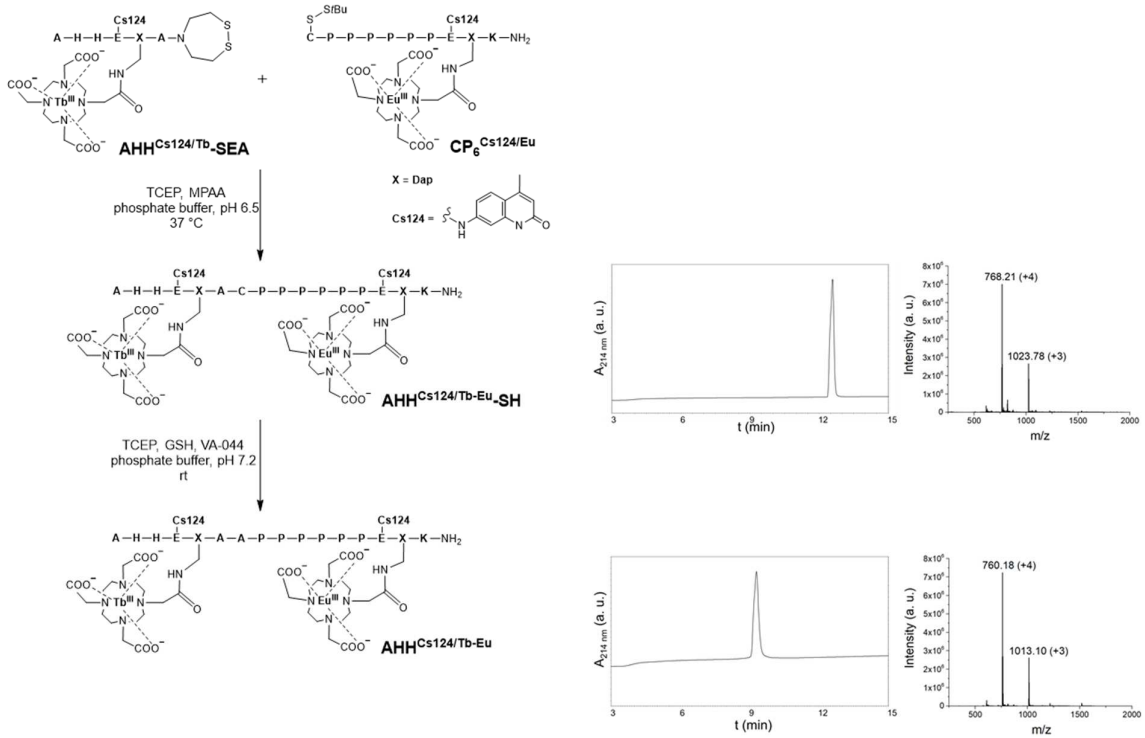

Figure 59. Synthetic pathway of AHH$^{Cs124/Tb-Eu.}$ HPLC chromatograms and ESI-MS spectra of AHH$^{Cs124/Tb-Eu}$-SH and AHH$^{Cs124/Tb-Eu}$ are reported.

2.6.5.10 Preparation of stock solutions

Stock solutions were prepared in ultrapure water ($\rho = 18.2\ M\Omega \cdot cm^{-1}$). A stock solution of HEPES buffer (500 mM, pH 7.4) was prepared by dissolving free acid powder and adjusting the pH with NaOH. The concentration of $CuCl_2 \cdot 2H_2O$ stock solution was verified by UV-Vis spectroscopy ($\varepsilon_{780} = 12\ M^{-1}cm^{-1}$). A stock solution of phosphate buffer (500 mM, pH 7.4) was prepared by dissolving K_2HPO_4 and KH_2PO_4 and adjusting the pH with NaOH. The concentration of peptide stock solutions was estimated by UV-vis absorption spectroscopy and, if possible, via spectrophotometric titration with Cu^{II} (monitoring the increase of the d-d band at ~520 nm). In particular, $RTH^{W\text{-}NBD}$ concentration was estimated in HEPES 50 mM pH 7.4 using $\varepsilon_{480} = 26000\ M^{-1}cm^{-1}$.[442] $AHH^{W/Tb\text{-}pic/Eu}$ concentration was estimated in water using $\varepsilon_{280} = (\varepsilon_{280,Trp} + \varepsilon_{280,DO3Apic(Eu)}) = (5690 + 3050)\ M^{-1}cm^{-1} = 8740\ M^{-1}cm^{-1}$.[63,443] The concentration of $AHH^{Cs124/Tb\text{-}Eu}$-SH and $AHH^{Cs124/Tb\text{-}Eu}$ stock solutions were estimated using $\varepsilon_{327} = 2 \cdot \varepsilon_{327,Cs124} = 2 \cdot (12000)\ M^{-1}cm^{-1} = 24000$.[374]

2.6.5.11 CD Spectroscopy

Far-UV (190-250 nm) CD spectra were recorded in a 1 cm path cuvette with a Jasco J-180 CD spectropolarimeter using a scanning speed of 20 nm/min and 3 accumulations. After blank (buffer) subtraction, CD spectra were smoothed using the Savitzy-Golay method.

2.6.5.12 Luminescence

Fluorescence spectra of $RTH^{W\text{-}NBD}$ were recorded on a Fluorolog FL3-22 spectrometer (HORIBA JobinYvon) using a 1 cm path quartz cuvette. Luminescence decay was measured on an FLS1000 Photoluminescence Spectrometer (Edinburgh Instruments) and lifetimes were determined by fitting a single-exponential decay curve to the data. Time-delayed luminescence spectra were recorded on a Cary Eclipse (Agilent) fluorescence spectrophotometer using a 1 cm path quartz cuvette.

2.7 General conclusions and perspectives

In this project, we aimed at developing Cu^{II}-responsive luminescent probes suited for the measurement of the exchangeable Cu pool in biological samples.

In this context, we first assessed the dubious mechanism of a putative reversible turn-on probe reported in the literature, unveiling that it actually acts as an irreversible chemodosimeter that could not be applied in biological systems. This finding calls into question the reversibility of other structurally similar putative turn-on probes and, more generally, the feasibility of a coordination-based turn-on probe for Cu^{II}, which appear at least very hard to conceive.

Hence, focusing on the realization of turn-off probes, we chose the naturally-occurring Xxx-Zzz-His ATCUN peptide motif as Cu^{II}-binding site, chiefly because of high selectivity for Cu^{II} against other physiological metal ions, and affinity (log $K_{7.4}$ = 12-15) in the range of the most competitive endogenous ligands, namely HSA. Indeed, our simulation of simplistic equilibria occurring in a serum-like system containing HSA and a probe revealed that a rather high affinity of the probe for Cu^{II} (log $K_{7.4}$ > 13) is needed to compete with HSA (log $K_{7.4}$ = 13).

Our studies showed that the GNHW- and AHHW- motifs are indeed able to retrieve Cu^{II} from equimolar HSA and bind Cu^{II} in a cell culture medium such as LB. However, very low/slow Cu^{II}-binding was observed in even diluted serum (10% FBS), where albumin is in excess, revealing that faster and higher affinity motifs are needed for applications in blood serum. In order to keep the kinetic lability of the Xxx-His-His motif, sequences with higher affinity could be identified via the screening of a peptide library bearing different Xxx residues. In this respect, the screening could be also extended to non-proteinogenic and non-natural amino acids. Indeed, the tripeptide Hms-Hms-His-NH_2 containing the non-proteinogenic amino acid α-hydroxymethylserine (Hms) seems to be the strongest ATCUN motif known to date (log $K_{7.4}$ ~17).[444] Besides, as the affinity of different ATCUN motifs has been correlated to the basicity of their N-terminal amino group,[143] it could be envisioned to replace the N-terminal amine with an electron-poor heterocycle such as pyridine (pK_a ~5).

Concerning the probe detection, we demonstrated that the time-delayed detection of lanthanide ions is advantageous, or even essential, to suppress the autofluorescent background and to enable the measurement in biological samples. However, the inner-filter effect remains a major issue to overcome, especially for turn-off probes. For this reason, the choice of an antenna with a suited absorption (and hence excitation) wavelength and extinction coefficient is crucial for the applicability of Ln^{III}-complexes as luminophores. For instance, Cs124 but not Trp allowed the detection of Tb^{III} (and Eu^{III}) in urine samples, and it is also expected to decrease the LOD of the probe $AHH^{Cs124/Tb\text{-}Eu}$ compared to $AHH^{W/Tb\text{-}pic/Eu}$. Moreover, the antenna effect, and hence the Ln^{III} signal, could also be optimized by approaching the antenna and the lanthanide, for instance using Ln^{III}-complexes bearing an intra-ligand antenna (as for DO3Apic). Finally, the use of NIR-emitting Ln^{III} ions such as Nd^{III} and Yb^{III} can be also envisaged.

Besides, we attempted to improve the quantifiability through a ratiometric detection, which can circumvent for instance the variability of the medium absorption (and hence of the inner-filter effect) among different samples thanks to a Cu^{II}-independent reference signal. Noteworthy, in order that the reference signal represents a correction factor for the inner-filter effect, the same excitation wavelength should be used for the responsive and reference fluorophores. Interestingly, this can be simply achieved for two Ln^{III} ions using the same antenna as for our $AHH^{Cs124/Tb\text{-}Eu}$.

The major challenge for the design of a type-I ratiometric probe for Cu^{II} was to set up a suitable peptidic platform allowing for the optimal detachment between the Cu^{II}-binding site and the reference luminescent moiety. Actually, poly-proline spacers did not seem really suited to achieve the sought response. As an alternative, a rigid spacer may be build using stapled peptides, which are short peptides constrained in a somehow rigid (typically α-helical) conformation by a covalent linker between two amino acid side-chains.[445] Furthermore, albeit synthetically harder, the use of a larger well-folded protein scaffold could be envisioned, as in this case the reference fluorophore could be grafted into a position that is certainly far from the N-terminal Cu^{II}-binding site (as long as the proper folding is guaranteed). Indeed, NCL strategies enable nowadays the total chemical synthesis of proteins up to 150 amino acid residues.[446]

In conclusion, this work laid the basis for the development of luminescent Cu^{II}-responsive probes which could be beneficial for direct measurement of the Cu_{EXC} in biological fluids, especially in the blood. Our results highlighted several challenges that have still to be faced and warrant further investigations in order to improve and optimize the proofs of concept presented.

3. Reactivity of Cu^{II}-TSCs in biological systems

3.1 Introduction

3.1.1 α-pyridyl thiosemicarbazones as anticancer drugs

Since the 1950s, α-pyridyl thiosemicarbazones (TSCs) have been emerging as promising anticancer drugs. The first TSC undergoing a clinical trial as an anticancer agent was Triapine (3-aminopyridine-2-carboxaldehyde thiosemicarbazone, 3AP), which has been tested in more than 30 clinical phase I and II trials so far. However, it eventually showed some adverse effects that hampered its applicability. To overcome 3AP limitations, also including inappropriate pharmacokinetic properties and drug resistance, further research led to the development of more potent and better-tolerated di-2-pyridylketone TSCs, such as Dp44mT (di-2-pyridylketone 4,4-dimethyl-3-thiosemicarbazone) and DpC (di-2-pyridylketone 4-cyclohexyl-4-methyl-3-thiosemicarbazone), which showed cytotoxicity at nanomolar rather than micromolar concentration (see Fig. 60).[232,233,447]

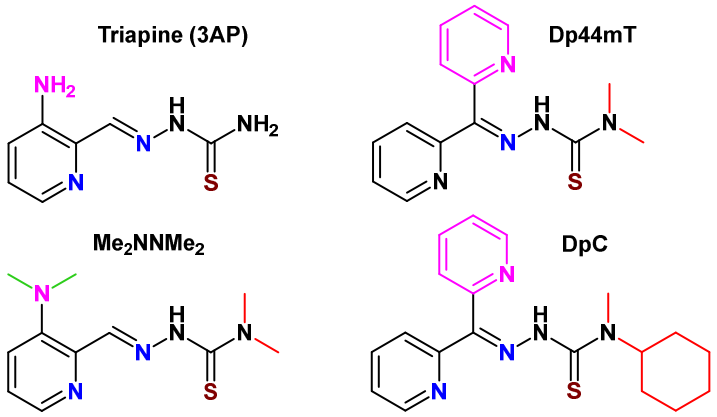

Figure 60. Structures of clinically-relevant TSCs. Structural differences are highlighted in pink, red and green.

3.1.2 Metal-binding properties of α-pyridyl TSCs

α-pyridyl TSCs are tridentate promiscuous ligands that coordinate via a (N_{py}, N, S^-) donor set, implying the deprotonation of both pyridine (pK_a ~ 3-4) and thiol moiety (pK_a ~ 10.5-11.5), which is accessible through the thione-thiol tautomerism (see Fig. 61A/B). In particular, the formation of octahedral 1:2 (metal:ligand) complexes is favoured by $Fe^{II/III}$ and Zn^{II} ions, while Cu^{II} prefers 1:1 stoichiometry forming square planar (ternary) complexes involving a fourth external donor (see Fig. 61C). Due to the square planar geometry imposed, TSCs are very weak Cu^{I} chelators, and hence Cu^{II}-TSCs complexes show negative reduction potentials (about -0.2 V).[448,449] Interestingly, while Zn^{II} forms the least stable complexes, Fe^{II} complexes are somewhat stronger than Cu^{II} ones. Besides, TSCs may exist as both E and Z isomers about the C=N double bond. Moreover, a so-called E' isomer, characterized by intramolecular hydrogen bonds, can be sometimes distinguished (see Fig. 61D). [447,450,451]

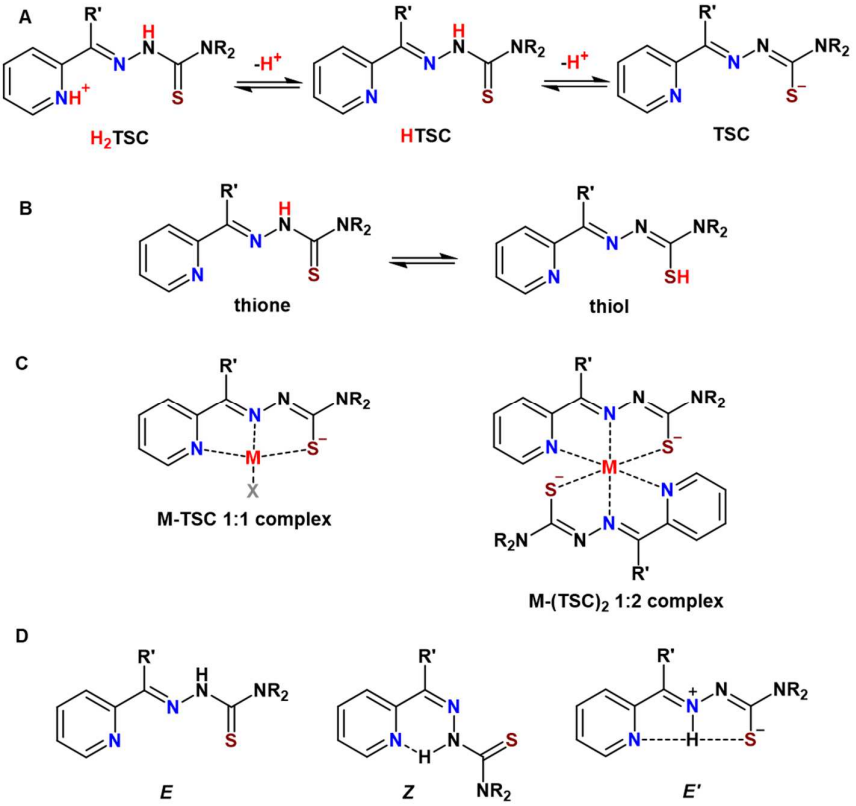

Figure 61. TSCs and their metal complexes. A) Deprotonation steps of TSCs; B) thione-thiol tautomerism; C) 1:1 and 1:2 metal-TSC complexes; D) *E*/*Z* isomerism.

3.1.3 Mechanisms of action

The anti-proliferative activity of TSCs has been traditionally ascribed to the inhibition of the iron-dependent enzyme Ribonucleotide Reductase (RNR), which is fundamental for DNA synthesis. Initially, such activity was related to iron depletion thanks to the metal-binding ability of TSCs, even though the iron-binding ability in cell culture has never been proven. Besides, as the redox-active Fe^{II}-3AP complex was shown to inhibit RNR more efficiently than the free ligand *in vitro*, an indirect ROS-dependent mechanism was proposed, e.g. affecting the intracellular thiol homeostasis (involving for instance GSH and thioredoxin reductase) that is also crucial for RNR catalytic cycle.[232,452]

Besides, contrary to 3AP, Dp44mT and its derivatives also showed a pronounced synergism with Cu^{II} salts, which suggested the involvement of Cu chelation and Cu-promoted ROS production in their mode of action. Indeed, Cu^{II}-Dp44mT (10 μM) was shown to produce ROS in the presence of cysteine (100 μM) *in vitro* and reduce the GSH/GSSG ratio in cells, whereas weak ROS generation was observed for Cu^{II}-3AP in intracellular conditions.[447,453,454]

Moreover, it was shown that Cu^{II} and Dp44mT co-accumulates in lysosomes, resulting in lysosomal membrane permeabilization (LMP) and, in turn, in apoptosis via the mitochondrial pathway. In particular, the lysosomal P-glycoprotein pump is accountable for Dp44mT transport into lysosomes, where the ligand is trapped owing to the positive charge acquired by the protonation of one pyridine at lysosomal pH (~5). LMP could be caused by Cu^{II}-binding to

Dp44mT and following ROS formation, which has indeed been demonstrated in lysosomal-like conditions (cysteine 100 μM, pH 5).[455,456]

Finally, Heffeter et al. have recently shown that, unlike 3AP, its double-dimethylated derivative Me_2NNMe_2 (see Fig. 60) exerts its cytotoxic activity through paraptosis, which is also characterized by the breakdown of ER (endoplasmic reticulum) homeostasis. Notably, Me_2NNMe_2 was detected in ER-derived vesicles, wherein Protein Disulfide Isomerase (PDI) was identified as a potential target of the Cu^{II}-Me_2NNMe_2 complex. In particular, the Cu^{II} complexes of Me_2NNMe_2, Dp44mT and DpC, but not the free ligands nor Cu^{II}-3AP, appeared to be able to inhibit PDI. PDI catalyses the oxidation, reduction, and isomerization of disulfide bonds of nascent proteins assisting their folding, and it might also bind Cu ions. Overall, the inhibition of PDI by Cu^{II}-TSC complexes could involve essential cysteine residues, which might be oxidized or blocked via the formation of a ternary complex with Cu^{II}-TSCs.[457]

3.1.4 Structure-activity relationships

To get insight into the distinct behaviour of 3AP and Dp44mT (and their respective analogues), several studies about structure-activity relationships have been conducted.

In 2009, Kowol et al. first identified the dimethylation of the terminal amino group (red in Fig. 60) as a factor that improves the cytotoxicity from the micromolar to the nanomolar range.[458] Later, the same authors evaluated the role of the stepwise methylation of pyridyl- (green in Fig. 60) and terminal-amino groups in 3AP on the cytotoxicity and the synergism with Cu^{II}. Interestingly, the dimethylation of at least one amino group led to synergism with Cu^{II}. Instead, only the methylation of both 3AP amino groups in the compound Me_2NNMe_2 led to the enhancement from micromolar to nanomolar cytotoxicity.[459] Noteworthy, the N-terminal dimethylation also increase the affinity of TSCs for Cu^{II}.

More recently, the cytotoxicity of several TSCs of the 3AP and Dp44mT families has been correlated to the thermodynamic stability and reducibility of their Cu^{II} complexes.[450,460] In particular, nanomolar-active TSCs showed higher affinity for Cu^{II} and much slower anaerobic reduction by GSH than micromolar-active analogues, such as 3AP.

Furthermore, our group also recently assessed the stability of metal-TSCs complexes in intracellular-like conditions, i.e. in the presence of biologically relevant concentrations of GSH (1-10 mM) and MTs (0.003-1 mM). Indeed, GSH and MTs are known for their ability to reduce Cu^{II} and bind to Cu^{I}. Interestingly, Cu^{II} complexes of 3AP and Dp44mT showed very different reactivity towards GSH and MT-1. Notably, in the presence of GSH only, Cu^{II}-3AP underwent quick reduction and dissociation forming $Cu^{I}(GS^{-})_x$, whereas Cu^{II}-Dp44mT formed kinetically stable ternary Cu^{II}-Dp44mT-(GS^{-}) complexes. When Zn_7-MT-1 was also present, both Cu^{II}-3AP and Cu^{II}-Dp44mT were dissociated. Besides, Dp44mT was able to bind the Zn^{II} released from MT-1, while GSH outcompeted 3AP for Zn^{II}.[461] On balance, Cu^{II}-Dp44mT but not Cu^{II}-3AP appeared to be sufficiently stable to survive for a certain time in the reducing and competing intracellular environment.

3.2 Aim of the work

Although synergism with Cu^{II} has been observed for certain TSCs, poor evidence exists to date about the formation of Cu^{II}-TSC complexes *in vivo*.

Of note, the same criteria described for probes in section 2.1.2, such as suited affinity and selectivity, must be fulfilled by any ligand to act as a Cu-based drug. As described above, the intracellular stability of Cu^{II}-TSC complexes is challenged by the GSH/MT system, which has been shown to inactivate several clinically relevant Cu^{II} complexes (e.g. with clioquinol and phenanthroline).[159] Notwithstanding, the kinetic stability of some Cu^{II}-TSCs might be sufficient to exert a cytotoxic activity.

As the investigated ligands/drugs are normally administered in the extracellular space (either in the blood or in cell culture medium), where Cu^{II}-drug complexes are most likely formed, the competition between the drug and the endogenous extracellular ligands should be examined. In this vein, in order to assess whether TSCs bind Cu^{II} and Cu^{II}-TSC complexes are stable in the extracellular milieu, we investigated the competition between HSA and some TSC for Cu^{II} as well as the stability of Cu^{II}-TSC complexes in the presence of HSA. Moreover, as TSCs also bind Zn^{II}, and the latter is more "available" than Cu^{II} in the blood, the selectivity and the competition between Cu^{II}- and Zn^{II}-binding in the presence of HSA were also studied (see section 3.3).

Besides, the mode of action of the putative Cu^{II}-TSCs complexes is not fully understood. In particular, the relevance of ROS generation by Cu^{II}-TSCs remains especially controversial.[453–455,457,462] To get insight into this aspect, we compared the capacity of 3AP and Dp44mT to generate ROS in the presence of GSH, in both cytosolic (pH 7.4) and lysosomal (pH ~5) conditions (see section 3.4).

3.3 Interaction of TSCs and metal-TSC complexes with HSA

3.3.1 Introduction

HSA serves as a carrier of metal ions and many endogenous compounds, such as fatty acids, monosaccharides and hormones. Likewise, it can bind and transport several exogenous drugs, such as warfarin, ibuprofen and diazepam, improving their pharmacokinetics (e.g. increasing their half-life in plasma). Interestingly, as a result of enhanced permeation and retention, HSA (as well as other proteins > 40 kDa) accumulates in the tumour interstitium and hence it may improve anticancer drug delivery.[463–465]

Concerning TSCs, Richardson et al. showed that Dp44mT interacts with HSA and that the latter potentiates the cellular uptake and decrease the efflux of Dp44mT in a variety of neoplastic and normal cell types, resulting in an increased anti-proliferative and apoptotic activity.[466] Moreover, exploiting surface-exposed His residues, HSA has been used to build ternary complexes with some Cu^{II}-TSCs acting as pro-drugs. Notably, the Cu^{II}-TSC complex can be released upon protonation of the His residue of HSA in the lysosomal compartment, where HSA can be internalized.[467–469]

Accordingly, it seems that at least some TSCs can bind Cu^{II} in the presence of HSA and even form Cu^{II}-bridged ternary complex via His residues. Noteworthy, some Cu^{II}-TSCs also interacts with HSA only via ligand-protein interaction, i.e. with no change of the first coordination sphere of Cu^{II}.[467]

In this work, we resorted to UV-vis and EPR spectroscopy to study (i) the competition between HSA and few medicinally-relevant TSCs, namely 3AP, Dp44mT and Me_2NNMe_2, for Cu^{II} and Zn^{II}, and (ii) the stability of the pre-formed complexes in the presence of HSA.

3.3.2 Results and discussion

The UV-vis spectra of 3AP, Dp44mT and Me_2NNMe_2 and their complexes have already been characterized in the literature.[450,451,460,461] In particular, charge transfer (CT) bands arise upon metal-binding to TSCs, likely stemming from thiolate-to-metal CT transitions (see Fig. 62).

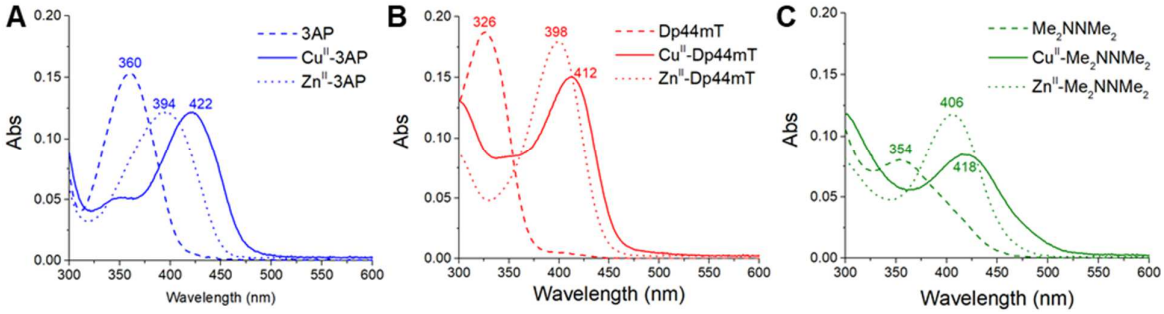

Figure 62. UV-vis spectra of TSCs (dashed lines) and their Zn^{II}- (dotted lines) and Cu^{II}- (full line) complexes. A) 3AP (blue); B) Dp44mT (red); C) Me_2NNMe_2 (green). Conditions: [TSC] = 10 μM, [Cu^{II}] = 10 μM, [Zn^{II}] = 25 μM (A) or 10 μM (B,C), HEPES 50 mM pH 7.4 (DMSO 1%).

3.3.2.1 Metal-independent interaction between TSCs and HSA

As metal-free protein-ligand may be formed, we first investigated the interaction of HSA and TSCs in absence of metal ions (see Fig. 63).

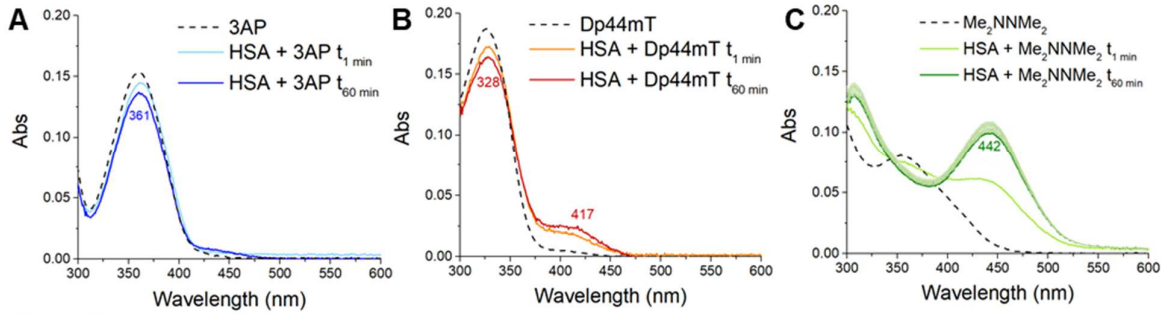

Figure 63. Interaction of TSCs with HSA. A) 3AP (blue); B) Dp44mT (red); C) Me_2NNMe_2 (green). Conditions: [TSC] = 10 μM, [HSA] = 100 μM, HEPES 50 mM pH 7.4 (DMSO 1%). T = 37 °C.

Monitoring over time the HSA-TSC mixtures, all systems showed a decrease of the ligand band (black, dashed lines), concomitant with the appearance of a red-shifted band above 400 nm, which suggests an interaction with HSA. However, the intensity of the new bands and hence the extent of such interaction differs considerably among the three compounds, notably in the order 3AP < Dp44mT < Me_2NNMe_2. Interestingly, this trend partially correlates with the compound lipophilicity, which is indeed consistent with the TSC binding to hydrophobic pockets in HSA.[459] However, the band shift observed (~90 nm) seems surprisingly large to be merely due to such hydrophobic interactions. Actually, similar bathochromic shifts have been observed for other TSCs in non-aqueous solvents (e.g. DMSO, methanol, chloroform, etc.) and attributed to the increase of the amount of the E' isomer, which has a more extended conjugated electron system.[451] This suggests that the TSC undergo a rearrangement upon interaction with HSA. Moreover, a very fast interconversion between Me_2NNMe_2 isomers has been reported, which could explain the easier rearrangement and interaction with the protein.[459]

3.3.2.2 Competition between TSCs and HSA for Cu^{II}

Then, the ability of TSCs to take out Cu^{II} from HSA was assessed by incubating the ligands with the pre-formed Cu^{II}-HSA complex at 37 °C (see Fig. 64A/B/C). After mixing, new bands (light blue, orange and light green lines) appeared and increased over time, likely as a consequence of the Cu^{II} transfer from HSA to TSCs. Moreover, the new bands were red-shifted compared to those of the Cu^{II}-TSCs complexes in absence of HSA, suggesting the formation of ternary TSC-Cu^{II}-HSA complexes. Interestingly, almost coincident spectra were obtained when the pre-formed Cu^{II}-TSCs complexes were added to HSA (see Fig. 64D/E/F). In particular, for Cu^{II}-3AP and Cu^{II}-Dp44mT, no temporal evolution was observed over 60 min, suggesting that these complexes are stable in the presence of HSA. Conversely, the band observed for Me_2NNMe_2-Cu^{II}-HSA underwent a slight red-shift from ~435 nm to ~443 nm (see fig. F). Remarkably, this wavelength corresponds to that observed upon metal-free interaction of Cu^{II}-Me_2NNMe_2 with HSA (see Fig. 63C), questioning whether such band stems from Cu^{II}-binding to Me_2NNMe_2 or Cu^{II}-independent Me_2NNMe_2-HSA interaction.

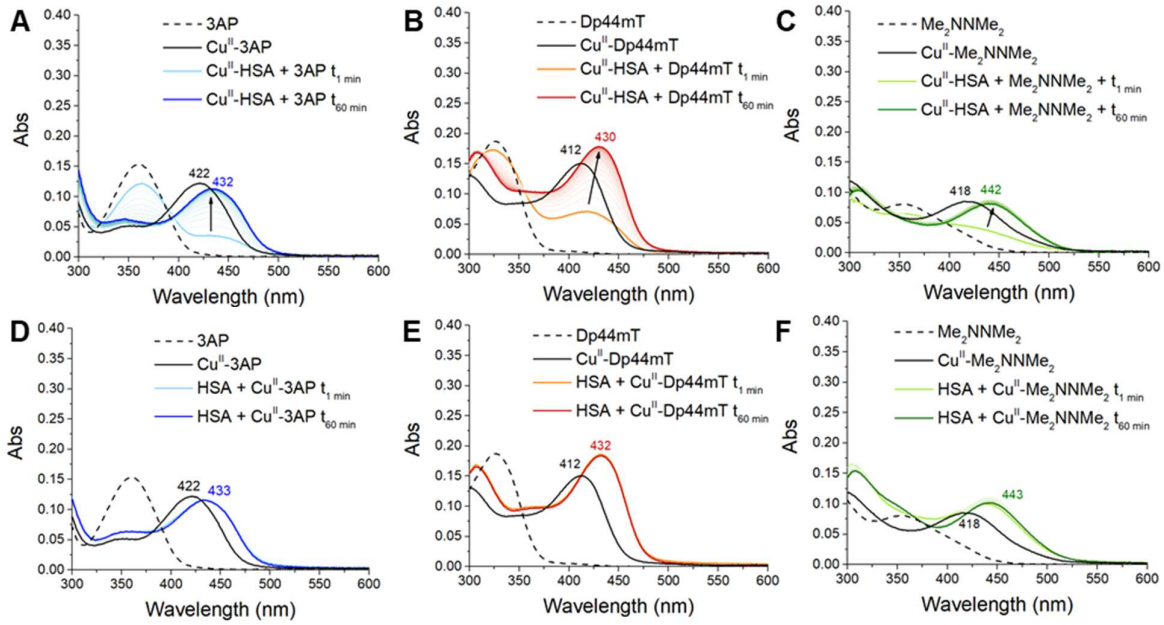

Figure 64. Competition of TSC and HSA for Cu^{II} (A, B, C) and interaction of pre-formed Cu^{II}-TSCs with HSA (D, E, F). A, D) 3AP (blue); B, E) Dp44mT (red); C, F) Me_2NNMe_2 (green). Conditions: [TSC] = 10 μM, [Cu^{II}] = 10 μM, [HSA] = 100 μM, HEPES 500 mM pH 7.4 (DMSO 1%). T = 37 °C.

To overcome the ambiguity and verify the Cu^{II} transfer as well as the formation of ternary TSC-Cu^{II}-HSA species, we recorded EPR spectra of Cu^{II}-TSCs, Cu^{II}-HSA and Cu^{II}-TSCs added to HSA, which are sensitive to Cu^{II} coordination sphere and not influenced by ligand-protein interactions (see Fig. 65). Preliminary analysis of EPR spectra (spectra simulation to obtain EPR parameters is currently ongoing) revealed that the Cu^{II} coordination in HSA/Cu^{II}-TSC mixtures (blue) results closer to those of Cu^{II}-TSCs (red) rather than to Cu^{II}-HSA (black). Besides, the shift of the spectra towards lower g values points towards the formation of ternary HSA-Cu^{II}-TSC complexes. In particular, the similarity of the spectra of such ternary complexes with those of ternary complexes with imidazole (Im, green) suggests that the fourth ligand provided by HSA is a His residue.

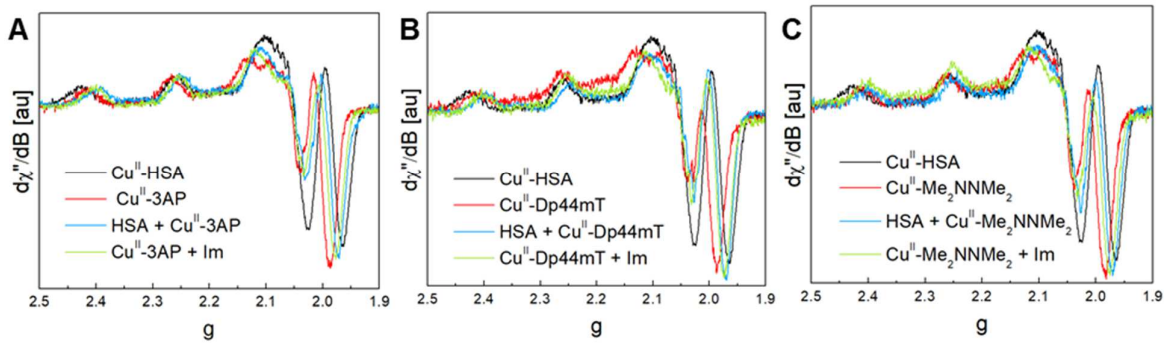

Figure 65. EPR spectra of Cu^{II}-HSA (black), Cu^{II}-TSCs (red), HSA/Cu^{II}-TSC mixtures (blue) and TSC-Cu^{II}-Im ternary complexes (green). Conditions: [TSC] = 300 μM, [Cu^{II}] = 250 μM, [HSA] = 300 μM, HEPES 50 mM pH 7.4 (DMSO ~5%), glycerol 10% (v/v), T = 100 K.

Overall, all TSCs appeared to be competitive with a 10-fold excess of HSA and form ternary complexes with protein His residues. Notably, assuming that no dissociation occurs when adding pre-formed Cu^{II}-TSC to HSA, more than 95% Cu^{II} results to be transferred from HSA to 3AP and

Dp44mT with very similar kinetics, while Me_2NNMe_2 kinetics cannot be directly compared with the former since the Cu^{II}-Me_2NNMe_2 complex added to HSA seems to re-arrange over time (see Fig. 66). Noteworthy, these data do not allow the relative quantification of "free" and HSA-bound Cu^{II}-TSCs.

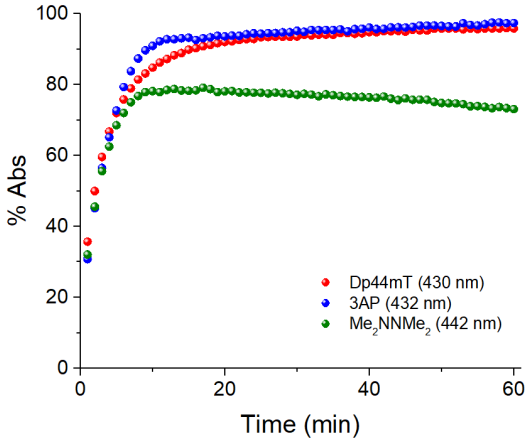

Figure 66. Kinetics of Cu^{II} transfer from HSA to TSCs: 3AP (blue dots), Dp44mT (red dots), Me_2NNMe_2 (green dots). Data were obtained normalizing absorbance values in Fig. 64A/B/C by the absorbance at t_1 in Fig. 64D/E for 3AP and Dp44mt, or t_{60} in Fig. 64F for Me_2NNMe_2.

3.3.2.3 Selectivity of TSCs for HSA-bound Cu^{II} vs Zn^{II}

As TSCs can also bind Zn^{II}, and HSA binds Zn^{II} with lower affinity than Cu^{II} (log K_{Zn} = 7, log K_{Cu} = 13), we also evaluated the ability of TSCs to retrieve Zn^{II} from HSA (see Fig. 67). Notably, 3AP was not able to withdraw Zn^{II} from HSA (see Fig. 67A), and Zn^{II}-3AP dissociates within the mixing time in the presence of HSA (see Fig. 67D). Instead, both Dp44mT and Me_2NNMe_2 seem to retrieve Zn^{II} from HSA also forming ternary complexes, as suggested by the red shift of the CT band in the presence of HSA (see Fig. 67B/C/E/F).

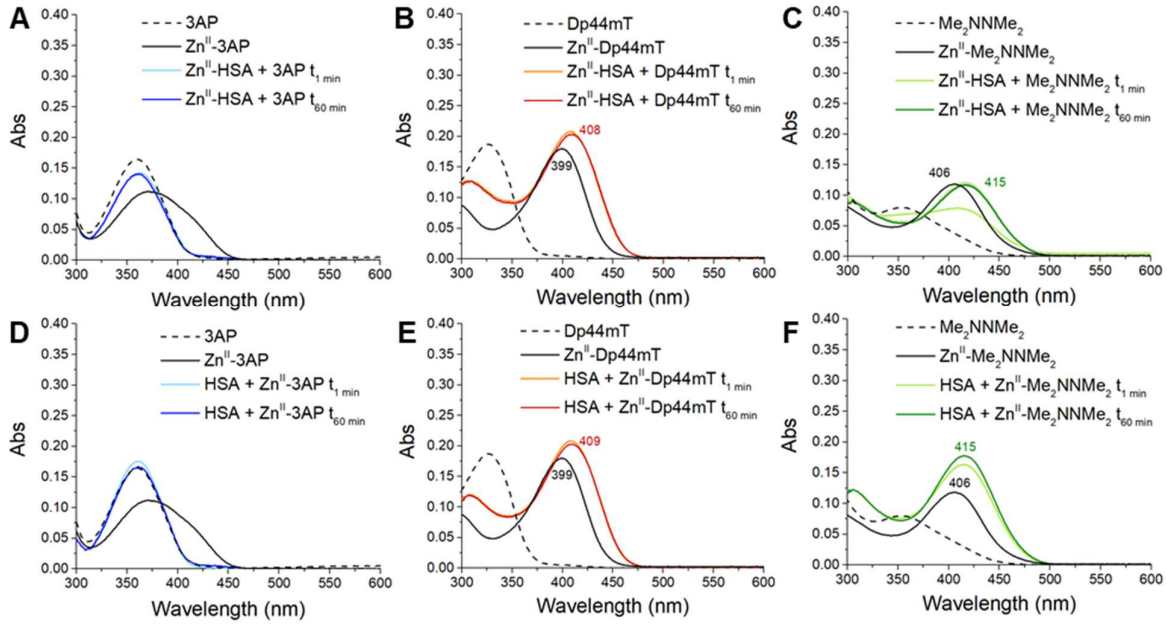

Figure 67. Competition of TSC and HSA for Zn^{II} (A, B, C) and interaction of pre-formed Zn^{II}-TSCs with HSA (D, E, F). A, D) 3AP (blue); B, E) Dp44mT (red); C, F) Me_2NNMe_2 (green). Conditions: [TSC] = 10 μM, [Zn^{II}] = 10 μM, [HSA] = 100 μM, HEPES 50 mM pH 7.4 (DMSO 1%). T = 37 °C.

Nevertheless, while Dp44mT immediately (within the mixing time) bound substantially all Zn^{II}, a slower and uncomplete (~70%) transfer was observed for Me_2NNMe_2. Of note, HSA released Zn^{II} much faster than Cu^{II} to Dp44mT, suggesting that Zn^{II} could also compete kinetically with Cu^{II} for binding to an exogenous ligand (e.g. a probe or a drug).

Hence, consistently with previous findings,[461] 3AP demonstrated rather weak Zn^{II}-binding (of note, more than one equivalent of Zn^{II} is needed to saturate the ligand), notably weaker than HSA and its derivatives Dp44mT and Me_2NNMe_2. This suggests that, although higher Cu^{II} affinity has been reported for the N-terminal dimethylated TSCs, 3AP might be more selective for Cu^{II} (vs Zn^{II}) in the blood.

Finally, to assess whether Zn^{II} competes with Cu^{II} for Dp44mT and Me_2NNMe_2, we examined the reaction between these TSCs and the pre-formed Cu^{II}, Zn^{II}-HSA complex (see Fig. 68).

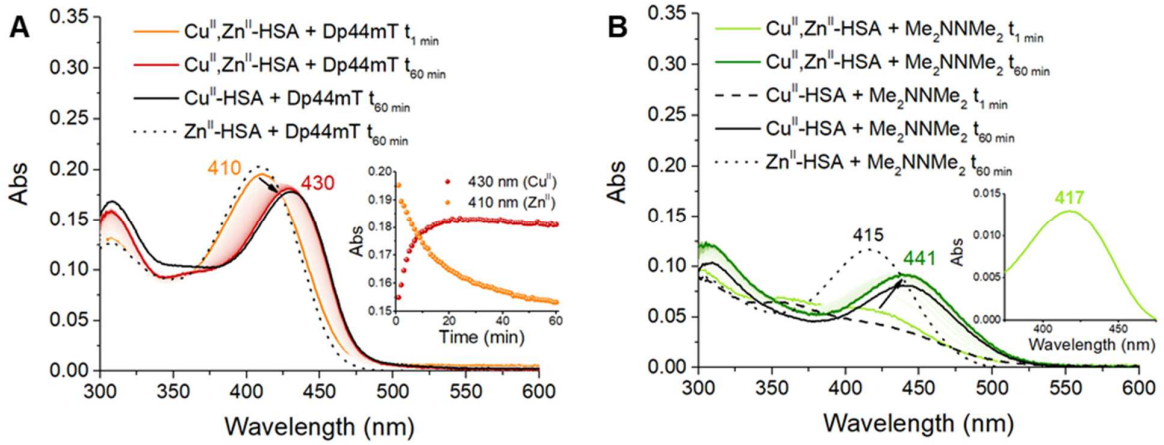

Figure 68. Competition between HSA-bound Cu^{II} and Zn^{II} for TSC-binding. A) Dp44mT (red) B) Me_2NNMe_2 (green). Conditions: [Cu^{II}] = [Zn^{II}] = 10 μM, [HSA] = 100 μM, [TSC] = 10 μM, HEPES 50 mM pH 7.4 (DMSO 1%). T = 37 °C.

In the case of Dp44mT (see Fig. 68A), the ternary Dp44mT-Zn^{II}-HSA complex was readily formed after mixing (black dashed and orange curves), but transmetallation gradually occurred with the eventual formation of the Dp44mT-Cu^{II}-HSA complex (black and red curves). Noteworthy, Zn^{II} did not significantly slow down the formation of the Cu^{II} complex. As regards Me_2NNMe_2, Zn^{II} seems to be less competitive against Cu^{II} than for Dp44mT (see Fig. 68B). Notwithstanding, the initial formation of a Me_2NNMe_2-Zn^{II}-HSA complex was unveiled by the difference spectrum (see Fig. 68B, inset) between the initial spectra in the presence (light green curve) or absence (black dashed curve) of Zn^{II}, which showed a maximum (417 nm) close to that of the Me_2NNMe_2-Zn^{II}-HSA complex (415 nm, black dotted curve). Overall, Zn^{II} does not seem to considerably interfere with the transfer of Cu^{II} from HSA to TSCs in the conditions studied, i.e. at 1:1 Cu^{II}:Zn^{II} ratio. However, HSA physiologically binds ~12 μM Zn^{II} (log K = 7) but less than 3 μM Cu^{II} (log K = 13) and hence Zn^{II} could represent a stronger competitor in the blood.

3.3.3 Experimental section

3.3.3.1 Materials

All solvents and reagents obtained from commercial suppliers were used without further purification. TSCs were purchased from Sigma Aldrich or provided by the group of Dr. C. Kowol (University of Vienna).

3.3.3.2 Preparation of stock solutions

Cu^{II} and Zn^{II} stock solutions were prepared by dissolving $CuCl_2 \cdot 2H_2O$ and $ZnSO_4 \cdot 7H_2O$ in ultrapure water ($\rho = 18.2\ M\Omega \cdot cm^{-1}$). The concentration of $CuCl_2 \cdot 2H_2O$ stock solution was verified by UV-vis spectroscopy ($\varepsilon_{780} = 12\ M^{-1}cm^{-1}$). A stock solution of HEPES buffer (500 mM, pH 7.4) was prepared by dissolving free acid powder in ultrapure water and adjusting the pH with NaOH. TSC stock solutions were prepared in DMSO, and their concentration was verified via spectrophotometric Cu^{II} titrations. HSA stock solution was prepared in ultrapure water and its concentration was determined via spectrophotometric Cu^{II} titration. Concentrated solutions of Cu^{II}/Zn^{II}-TSC complexes were prepared in DMSO/HEPES (50 mM pH 7.4) 80:20 mixtures.

3.3.3.3 UV-vis spectroscopy

UV-vis spectra were recorded in 1 cm path quartz cuvettes using a Cary 60 spectrophotometer equipped with a thermostatted (37 °C) multicell holder. A 1 μL aliquot of metal-free TSC or pre-formed Cu^{II}/Zn^{II}-TSC complex was added to HSA or to the pre-formed Cu^{II}/Zn^{II}-HSA complex in HEPES 50 mM pH 7.4.

3.3.3.4 EPR spectroscopy

Continuous-wave EPR spectra were recorded on an EMX-plus (Bruker Biospin GmbH, Germany) X-band EPR spectrometer equipped with a high sensitivity resonator (4119HS-W1, Bruker). The g factor was calibrated in the experimental conditions using the Bruker strong pitch (g = 2.0028). The principal experimental parameters values were microwave frequency of ~9.4 GHz, microwave power 0.1 mW, modulation amplitude 5 G, time constant of ~80 ms conversion time of ~200 ms. 4 scans were accumulated to achieve reasonable signal-to-noise (S/N) ratio, resulting in ~20 mins of acquisition time per spectrum. Samples were supplemented by 10% v/v glycerol to ensure homogeneous peptide distributions and avoid water crystallization-induced phase separation. Then, they were introduced into 4 mm outer diameter quartz tubes (Wilmad-Labglass) and freeze-quenched into liquid nitrogen prior to their introduction into the precooled cavity (T = 100 K, achieved by continuous flow liquid nitrogen cryostat).

3.4 ROS production by Cu^{II}-TSC complexes in the presence of GSH

3.4.1 Introduction

The Cu^{II}-mediated generation of ROS has been claimed to be, at least partially, accountable for the cytotoxic activity of some TSCs. In particular, the ROS production by Cu^{II}-Dp44mT/DpC in lysosomes, i.e. at low pH (~5), has been suggested as the basis of its mode of action.[455,470] Conversely, ROS seem to have only a minor role in the anticancer activity of 3AP and Me_2NNMe_2.[454,457] Nevertheless, a direct comparison of Cu^{II}-catalysed ROS production by 3AP and Dp44mT in the presence of GSH has never been reported. Likewise, the pH dependence of such activity has not been evaluated. Here, we addressed these aspects measuring the kinetics of ROS production via EPR using TEMPOL (4-Hydroxy-2,2,6,6-tetramethylpiperidin-1-oxyl) as a radical scavenger. Indeed, TEMPOL is a stable nitroxyl radical whose EPR signal is quenched upon reaction with hydroxyl radicals ($HO^{\bullet}$) forming an oxoammonium cation and/or an N-hydroperoxide (see Fig. 69).[471–473]

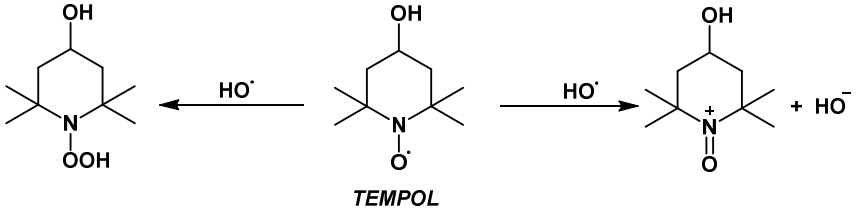

Figure 69. Reaction of TEMPOL with hydroxyl radicals.

3.4.1.1 Mechanism of Cu^{II}-catalysed thiol oxidation

The ability of Cu^{II} to produce ROS in the presence of thiols such as Cys and GSH is well known, although the mechanism of Cu^{II}-catalysed thiol oxidation (to disulfide) is not fully understood.[474] Generally, the supposed mechanism implies (i) the formation of a thiolate-Cu^{II} (RS-Cu^{II}) complex (accompanied by thiol deprotonation), (ii) the inner-sphere electron transfer from the thiol to Cu^{II}, forming Cu^{I} and a thiyl radical ($RS^{\bullet}$), and (iii) the re-oxidation of Cu^{I} to Cu^{II} by dioxygen with the formation of ROS ($O_2^{\bullet-}$, H_2O_2, $HO^{\bullet}$). Finally, two $RS^{\bullet}$ radicals can react to form the corresponding RSSR disulfide (see Fig. 70). Moreover, the formed Cu^{I} may be bound by the thiol.[475–478]

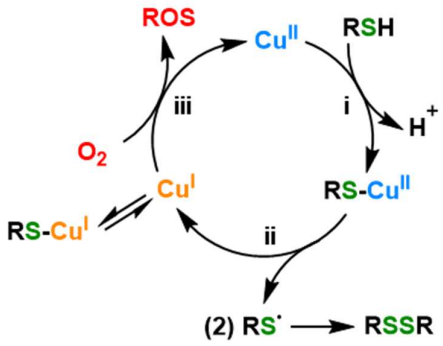

Figure 70. Putative mechanism of the Cu^{II}-catalysed thiol (RSH) oxidation by dioxygen (O_2) to disulfide (RSSR). (i) Formation of an RS-Cu^{II}; (ii) reduction of Cu^{II} to Cu^{I} and oxidation of RS^{-} to $RS^{\bullet}$; (iii) reoxidation of Cu^{I} to Cu^{II} and formation of ROS. The combination of two thiyl radicals yields the disulfide.

Overall, the reaction rate depends on the nature of the thiol. Indeed, as the binding to Cu^{II} involves the thiol deprotonation, step (i) is influenced by the thiol pK_a, and hence by the portion of deprotonated thiol at a given pH. Noteworthy, for the same reason, the reaction is pH-dependent, notably faster at higher pH. In addition, the relative affinity of the thiol for Cu^{I} and Cu^{II}, namely the reduction potential of the Cu-RS complex, impacts step (iii), i.e. the reoxidation of Cu^{I}. Accordingly, Cu^{II} oxidizes Cys (pK_a= 8.2) faster than GSH (pK_a = 9.2) as a result of lower pK_a and higher affinity for Cu^{II} than GSH.[475]

Furthermore, when Cu^{II} is complexed to a ligand, the latter modulates the redox potential and the accessibility of the thiol to the metal, and hence influence the thiol oxidation and ROS production.

3.4.2 Results and discussion

3.4.2.1 ROS production by 3AP- and Dp44mT-Cu^{II} complexes

In order to compare the ability of 3AP and Dp44mT Cu^{II}-complexes in the generation of ROS, we measured the decay of TEMPOL EPR signal in the presence of Cu^{II} or Cu^{II}-TSC complexes and GSH (see Fig. 71). Remarkably, Cu^{II}-Dp44mT (red dots) elicited a (~3-fold) faster reduction of TEMPOL, and hence a higher rate of ROS production, compared to Cu^{II}-3AP (blue dots), which substantially showed the same activity of the Cu^{I}-$(GS)_x$ complex (black dots).

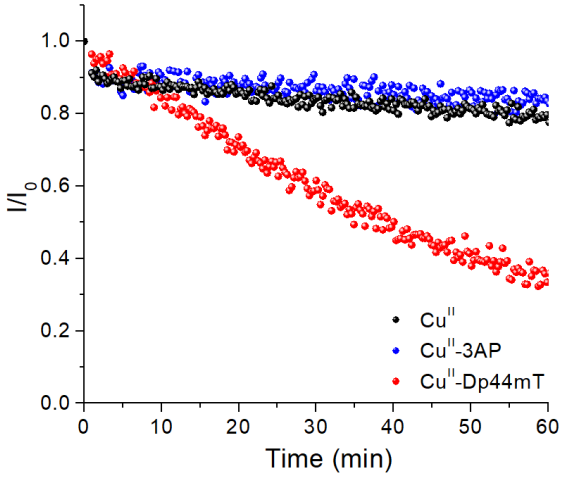

Figure 71. Decay of TEMPOL EPR signal in the presence of Cu^{II} (black dots), Cu^{II}-3AP (blue dots) or Cu^{II}-Dp44mT (red dots) and GSH. Conditions: [Cu^{II}] = 27 µM, [TSC] = 30 µM, [GSH] = 3 mM, [TEMPOL] = 20 µM, HEPES 100 mM pH 7.4 (DMSO 3%).

These findings can be explained by the different reactivity between 3AP and Dp44mT towards GSH, which has been previously described by our group (see Fig. 72).[461] Indeed, while 3AP-bound Cu^{II} is quickly reduced and dissociated forming Cu^{I}-$(GS)_x$ (see Fig. 72A), Cu^{II}-Dp44mT forms a stable ternary complex with GSH. Indeed, upon the addition of GSH to Cu^{II}-Dp44mT, the CT band slightly red-shifted but remained constant over time (see Fig. 72B). Notwithstanding, some spectral change, namely an increase of the absorbance, can be observed around 260 nm, where disulfide bonds absorb.[479] Hence, this reveals that, despite the apparent stability, the Dp44mT-Cu^{II}-GS complex is able to catalyse the oxidation of GSH to GSSG, with the concomitant production of ROS (see Fig. 70). Actually, the stability of the Cu^{II}-related absorption band is likely due to the fact that, during the catalytic redox cycle, the reoxidation is faster than the reduction, so that Cu^{II} is observed as the steady-state.

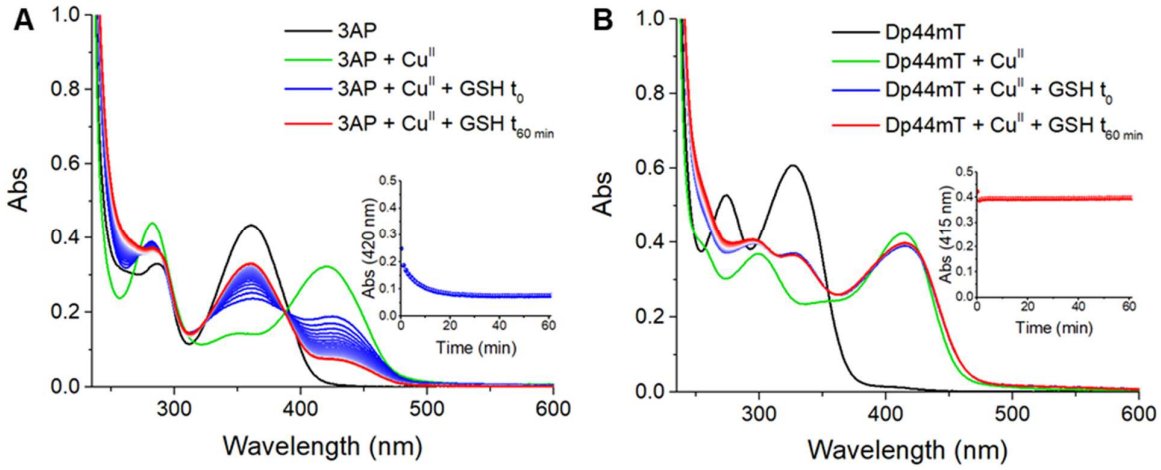

Figure 72. Reaction of Cu^{II}-3AP (A) and Cu^{II}-Dp44mT (B) with GSH at pH 7.4 monitored by UV-vis absorption spectroscopy. Conditions: [Cu^{II}] = 27 μM, [TSC] = 30 μM, [GSH] = 3 mM, HEPES 100 mM pH 7.4 (DMSO 2%).

Overall, the different behaviour of 3AP and Dp44mT can be related to the kinetics of reduction and oxidation of their Cu^{II}-complexes. The anaerobic reduction of Cu^{II}-TSC has been shown in the literature to be much faster for 3AP than the N-terminal methylated Dp44mT and Me_2NNMe_2.[460] Here, we studied the oxidation of Cu^{I}-$(GS)_x$ (prepared anaerobically adding $Cu^{I}(MeCN)_4$ to GSH) in the presence of 3AP or Dp44mT and dioxygen (see Fig. 73). The addition of the TSC in anaerobic conditions (solution fluxed with Ar in a sealed cuvette) did not cause any spectral change in the case of 3AP, whereas with Dp44mT a weak band assigned to Cu^{II}-Dp44mT immediately appeared and remained constant. This could be due to the oxidation of Cu^{I}-$(GS)_x$ to Cu^{II}-Dp44mT by adventitious O_2 added along with Dp44mT. Interestingly, upon opening of the cuvette and exposition to air, the band of Cu^{II}-Dp44mT gradually increased reaching a plateau after about 40 min. Instead, a very weak increase of the Cu^{II}-3AP band was observed within two hours. However, a much higher signal was recorded after overnight incubation.

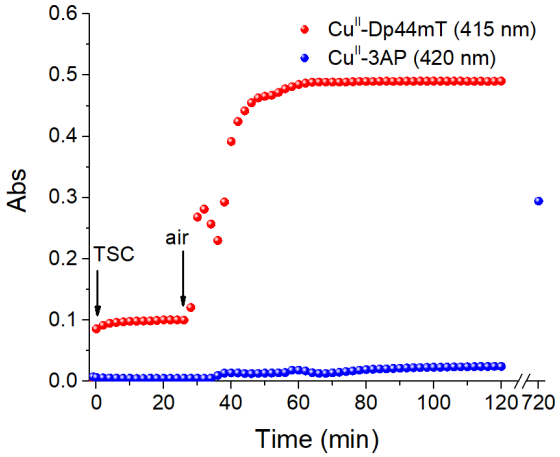

Figure 73. Reaction of Cu^{I}-$(GS)_x$ with 3AP (blue dots) or Dp44mT (red dots) in the presence of O_2 monitored by UV-vis absorption spectroscopy. Conditions: [GSH] = 3 mM, [$Cu^{I}(MeCN)_4PF_6$] = 27 μM, [TSC] = 30 μM, HEPES 100 mM pH 7.4 (DMSO, MeCN < 1%).

Thus, Cu^{I}-$(GS)_x$ proved to be much more prone to oxidation by O_2 in the presence of Dp44mT than 3AP, as the former can form a relatively strong ternary complex with Cu^{II} and GSH. Conversely, the Cu^{II}-3AP complex appeared only after all GSH was oxidized to GSSG.

On balance, the Dp44mT-Cu^{II}(-GS) complex seems favoured compared to Cu^{I}-$(GS)_x$, which is, in turn, more stable than Cu^{II}-3AP as long as excess GSH is present. Therefore, these observations point towards a scenario in which the relative affinity between Cu^{II}-TSC and Cu^{I}-$(GS)_x$ determines the fate and pro-oxidant activity of the Cu-TSC complex.

3.4.2.2 Higher ROS production by Cu^{II}-TSC complexes at lower pH

As Dp44mT also demonstrated pro-oxidant activity in lysosomal-like conditions, i.e. at pH 5, we compared the ROS production of Cu^{II}-TSC complexes in the presence of GSH at pH 7.4 and 5 (see Fig. 74) through the radical scavenging activity of TEMPOL. Remarkably, while "free" Cu^{II} normally showed lower activity at lower pH, TEMPOL reduction in the presence of Cu^{II}-TSC complexes was faster at pH 5 than at pH 7.4. In particular, such effect was more pronounced for Dp44mT (~10-fold faster) than 3AP (~ 1.5-fold faster).

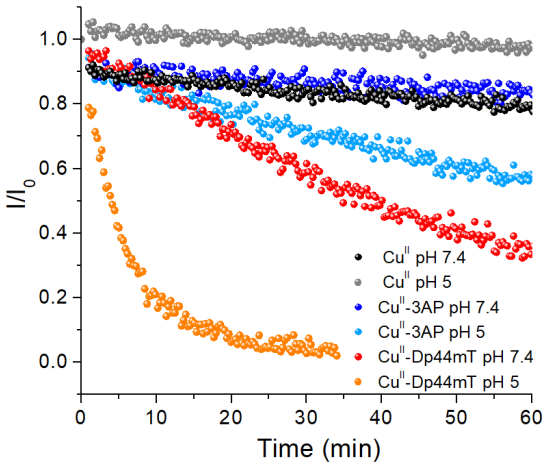

Figure 74. pH-dependent decay of TEMPOL EPR signal in the presence of Cu^{II} (black dots pH 7.4, grey dots pH 5), Cu^{II}-3AP (blue dots pH 7.4, light blue dots Ph 5) or Cu^{II}-Dp44mT (red dots pH 7.4, orange dots pH 5) and GSH. Conditions: [Cu^{II}] = 27 μM, [TSC] = 30 μM, [GSH] = 3 mM, [TEMPOL] = 20 μM, HEPES 100 mM pH 7.4 or MES 100 mM pH 5 (DMSO 3%).

Since thiol deprotonation is needed to form the RS-Cu^{II} intermediate (see Fig. 70, step i), thiol oxidation by Cu^{II} is supposed to get slower by lowering the pH, as actually observed for "free" Cu^{II}. Hence, the higher reactivity of Cu^{II}-TSC at lower pH appears very puzzling.

To get insight into such surprising behaviour, we first monitored the reaction via UV-vis absorption spectroscopy (see Fig. 75). Comparing the reactivity of Cu^{II}-3AP with GSH at pH 7.4 and 5, the Cu^{II}-3AP complex seems to be more stable against reduction and dissociation at lower pH, likely as a result of weaker reducing and Cu^{I}-binding power of GSH (see Fig. 75A). This might explain the higher pro-oxidant activity observed. On the contrary, in the case of Cu^{II}-Dp44mT, the higher thiol oxidation at lower pH is accompanied by a higher, albeit very weak and reversible, reduction (see Fig. 75B, inset). Indeed, in anaerobic conditions GSH reduced Cu^{II}-Dp44mT faster at pH 5 than at pH 7.4 (see Fig. 76), also suggesting that the reduction of Cu^{II} represents the rate-limiting step of the redox cycle.

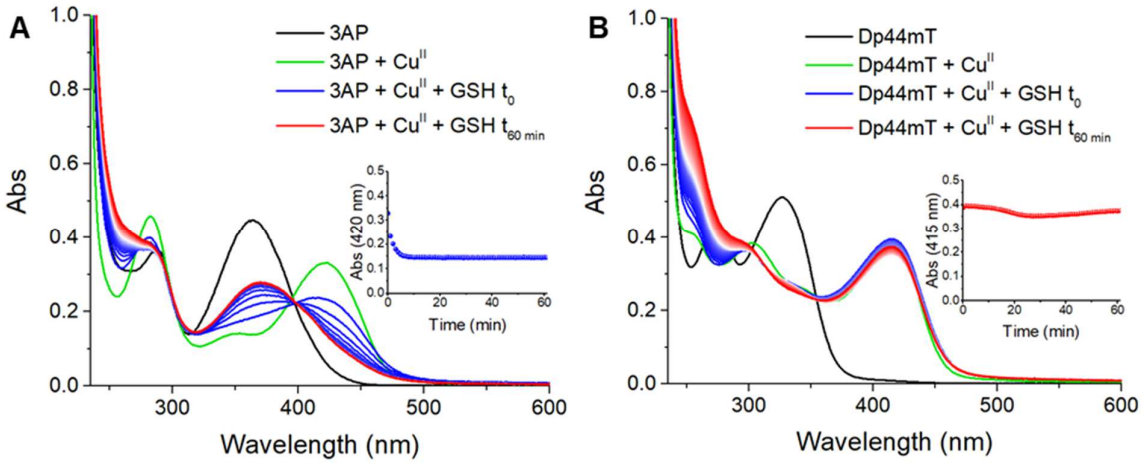

Figure 75. Reaction of Cu^{II}-3AP (A) and Cu^{II}-Dp44mT (B) with GSH at pH 5 monitored by UV-vis absorption spectroscopy. Conditions: [Cu^{II}] = 27 μM, [TSC] = 30 μM, [GSH] = 3 mM, HEPES 100 mM pH 7.4 (DMSO 2%).

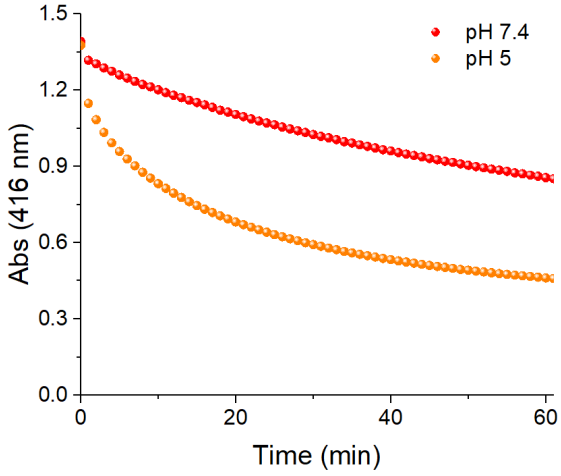

Figure 76. Anaerobic reduction of Cu^{II}-Dp44mT by GSH at pH 7.4 (red dots) or pH 5 (orange dots) monitored by UV-vis absorption spectroscopy. Conditions: [Cu^{II}] = 90 μM, [TSC] = 100 μM, [GSH] = 1 mM, HEPES 100 mM pH 7.4 or MES 100 mM pH 5 (DMSO ~5%).

In an effort to understand such pH-dependent reactivity, we analysed the UV-vis spectra of the Dp44mT and its Cu^{II}-complex at pH 5 and 7.4 (see Fig. 77). The comparison revealed that another Cu^{II} species seems to be also present at pH 5, as suggested by a shoulder at ~340 nm (see red arrow in Fig. 77A). This band could be attributed the Cu^{II}-complex with the N^2-protonated ligand (HTSC, see Fig. 78), even though the pK_a of such Cu-HDp44mT species has been reported to be as low as ~2.3.[460] To confirm such hypothesis and rule out interference from the buffers, a spectrophotometric pH titration of the Cu^{II}-Dp44mT in unbuffered water was conducted. Indeed, by lowering the pH from ~7 to 2, the appearance of a band centred at 342 nm was observed (see Fig. 77B), which support our previous speculation. Importantly, the HTSC ligand binds Cu^{II} with a (N_{py}, N, S) donor set in which the sulfur is found as neutral thione rather than negatively charged thiolate (see Fig. 78). Interestingly, as thiones are softer donors than thiolates,[480,481] the HTSC may stabilize Cu^{I} better than TSC. Besides, the thione also has likely lower affinity for Cu^{II} than a thiolate, hence a transient de-coordination of the thione group can be conceived, especially in the ternary Dp44mT-Cu^{II}-GS complex, leaving Cu^{II} bound in a trigonal fashion (i.e. by two N-donors

from the TSC and the thiolate of GSH) that favours the reduction. Both these factors could explain the easier reducibility of Dp44mT-bound Cu^{II} at lower pH. Indeed, our hypothesis is supported by a faster reduction of the N^2-methylated derivative of 3AP (reported in the literature), which exists only in the thione form.[482] Furthermore, preliminary data obtained via DFT (Density Functional Theory) calculations by the group of Prof. Emilia Sicilia (University of Calabria, Italy) confirmed a higher tendency of Cu^{II}-HTSC than Cu^{II}-TSC complexes toward reduction.

Therefore, we postulate that the higher amount of the N^2-protonated thione-form Cu^{II}-HTSC species at lower pH may be accountable for the higher thiol oxidase activity and related ROS production observed.

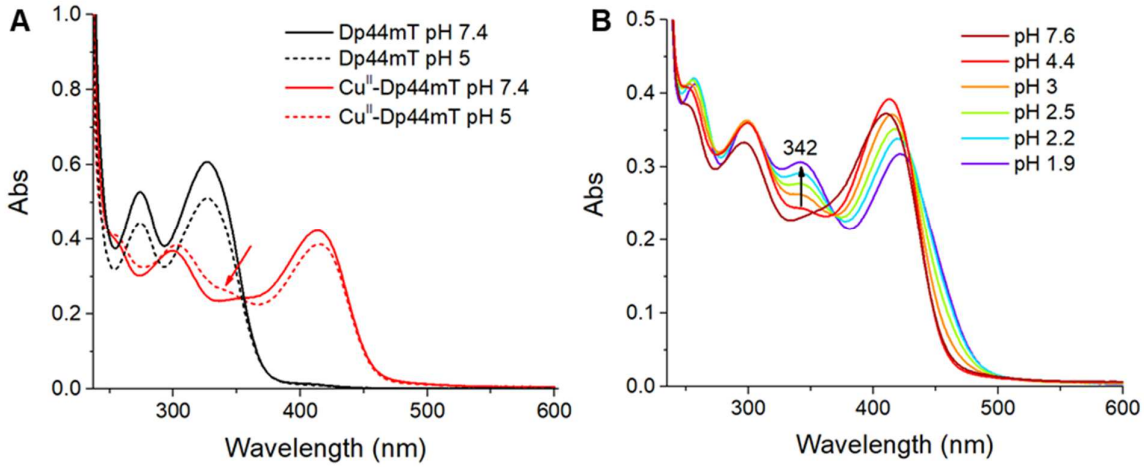

Figure 77. A) pH-dependent UV-vis absorption spectra of Dp44mT (black) and Cu^{II}-Dp44mT (red) at pH 7.4 (full line) or pH 5 (dashed line); B) Spectrophotometric pH titration of Cu^{II}-Dp44mT. Conditions: [Cu^{II}] = 27 μM, [Dp44mT] = 30 μM; HEPES 100 mM pH 7.4 or MES 100 mM pH 5 (A) or water (B).

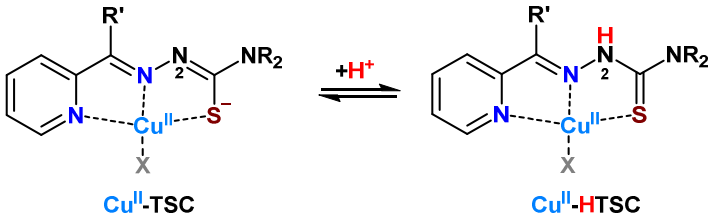

Figure 78. Formation of the Cu^{II}-HTSC complex by protonation of the Cu^{II}-TSC.

3.4.3 Experimental section

3.4.3.1 Materials

All solvents and reagents obtained from commercial suppliers were used without further purification. TSCs were purchased from Sigma Aldrich or provided by the group of Prof. C. Kowol (University of Vienna).

3.4.3.2 Preparation of stock solutions

TSC stock solutions were prepared in DMSO, and their concentration was verified via spectrophotometric Cu^{II} titrations. Cu^{II} stock solution was prepared dissolving $CuCl_2 \cdot 2H_2O$ in ultrapure water (ρ = 18.2 M$\Omega \cdot cm^{-1}$) and its concentration was verified by UV-vis spectroscopy (ε_{780} = 12 $M^{-1}cm^{-1}$). A stock solution of HEPES buffer (500 mM, pH 7.4) was prepared by dissolving free acid powder in ultrapure water and adjusting the pH with NaOH. A stock solution of MES buffer (500 mM, pH 5) was prepared by dissolving MES sodium salt in ultrapure water and adjusting the pH with HCl. GSH stock solutions were prepared in ultrapure water on a daily basis. TEMPOL stock solution was prepared in ultrapure water.

3.4.3.3 UV-vis spectroscopy

UV-vis spectra were recorded in 1 cm path quartz cuvettes using a Cary 60 spectrophotometer. The reaction of Cu^{II}-TSC complexes with GSH was performed by adding a small aliquot of a concentrated GSH solution to the pre-formed Cu^{II}-TSC complex in the buffer. For the anaerobic reduction and re-oxidation studies, solutions were thoroughly degassed under Ar before and after the insertion into a sealable cuvette equipped with a pierceable septum. GSH or TSCs were added through the septum with a micro-syringe. pH titrations were conducted adding small aliquots of concentrated HCl or NaOH solutions to the pre-formed Cu^{II} complex in water.

3.4.3.4 EPR spin scavenging

EPR spin scavenging experiments were performed at room temperature (T = 295 ± 1K) using an EMX-plus (Bruker Biospin GmbH, Germany) X-band EPR spectrometer equipped with a high sensitivity resonator (4119HS-W1, Bruker). The g factor was calibrated in the experimental conditions using the Bruker strong pitch (g = 2.0028). Samples were introduced into glass capillaries (Hirschmann, 25 µL) sealed at both the ends and rapidly transferred into the EPR cavity for measurement. The principal experimental parameters were microwave frequency of ~9.85 GHz, microwave power of ~4.5 mW, modulation amplitude 1 G, time constant of ~5 ms conversion time of ~12.5 ms. Every 17 s a single scan (sweeping time of ~10 s) was then acquired to obtain the kinetics of TEMPOL reduction over ~60 min. All spectra were best simulated and the resulting simulations were doubly integrated to relatively quantify the concentration of remaining TEMPOL. Data analysis and simulations based on experimental data were performed using Xenon (Bruker Biospin GmbH, Germany) and lab-made routines based on Easyspin Toolbox under Matlab (Mathworks) environment.[483]

3.5 Conclusions and perspectives

In conclusion, our investigations showed that TSCs can bind Cu^{II} in the presence of HSA. Interestingly, the nanomolar active Dp44mT and Me_2NNMe_2, but not 3AP, can also retrieve Zn^{II} from HSA. However, although Zn^{II} transfer is faster than Cu^{II}, transmetallation eventually occurs, and hence Zn^{II} does not seem to be a major concern for the formation of Cu^{II}-TSC complexes. Moreover, both metal-free TSCs and Cu^{II}/Zn^{II}-TSCs complexes bind to HSA. Interestingly, such interactions could enhance their half-life in the blood and also their uptake by cells. Overall, our findings support the potential role of Cu^{II}-binding in the mode of action of anticancer TSCs. Indeed, it is conceivable that in the bloodstream TSCs pick up Cu^{II} and/or Zn^{II} from HSA, forming ternary complexes with the protein, and enter as Cu^{II}/Zn^{II}-complexes into the cells. Noteworthy, the potential formation of Zn^{II}-TSC complexes does not necessarily hamper the Cu-mediated anticancer activity, as it has been suggested, for instance, that Zn^{II}-Dp44mT/DpC transmetallate with Cu^{II} into lysosomal vesicles.[470]

Furthermore, we demonstrated, by means of the radical scavenging activity of TEMPOL, that in the presence of Cu^{II} and GSH at cytosolic relevant concentrations, Dp44mT produces more ROS than 3AP, despite GSH has been reported to reduce Cu^{II}-3AP faster than Cu^{II}-Dp44mT. The reason for this is probably the higher stability of Cu^{II}-Dp44mT against the reductive dissociation by GSH. In other words, excess GSH reduces Cu^{II}-3AP faster and forms Cu^{I}-$(GS)_x$, which produces little ROS (see Fig. 79, step iii). In contrast, GSH reduces Cu^{II}-Dp44mT more slowly, but it is not able to retrieve Cu^{I}, hence Cu stays coordinated to Dp44mT and can produce continuously ROS via redox cycling with GSH (see Fig. 79, step iv). Interestingly, this could explain the Cu^{II} synergism and higher cytotoxicity of Dp44mT compared to 3AP.

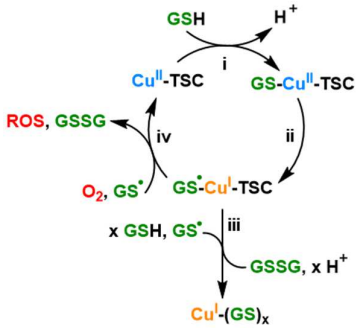

Figure 79. Different reactivity of Cu^{II}-3AP and Cu^{II}-Dp44mT complexes in the presence of GSH and O_2: GSH binds to both Cu^{II}-TSCs complexes (i) and reduces Cu^{II} to Cu^{I} with the formation of a thiyl radical (ii). Excess GSH takes out Cu from 3AP forming Cu^{I}-$(GS)_x$ that produces little ROS (iii), whereas it does not retrieve Cu from Dp44mT that can be re-oxidized producing ROS.

Finally, we also provided unprecedented evidence about a higher ROS production by Cu^{II}-TSC complexes, especially for Dp44mT, at lower pH. These findings need to be corroborated by independent techniques, for instance via the measurement of O_2 consumption and thiol oxidation. In addition, further mechanistic investigations will be conducted to understand thoroughly such unexpected behaviour. At the moment, we postulate that it arises from a higher population of the protonated form of the TSC ligand at lower pH, which promotes the Cu^{II} reduction through a switch of the sulfur donor from the thiolate to the thione form. Importantly, although such higher pro-oxidant activity at lysosomal pH supports the proposed mode of action of Dp44mT (see section 3.1.3), the stability of the Cu^{II}-Dp44mT complex, for instance against MTs, in lysosomal conditions remains to be assessed.

References

1 M. A. Zoroddu, J. Aaseth, G. Crisponi, S. Medici, M. Peana and V. M. Nurchi, *J. Inorg. Biochem.*, 2019, **195**, 120–129.
2 L. Belmonte and S. S. Mansy, *Elements*, 2016, **12**, 413–418.
3 H. A. Jahn and E. Teller, *Proc. R. Soc. London. Ser. A - Math. Phys. Sci.*, 1937, **161**, 220–235.
4 H. Irving and R. J. P. Williams, *Nature*, 1948, **162**, 746–747.
5 H. Irving and R. J. P. Williams, *J. Chem. Soc.*, 1953, 3192–3210.
6 J. T. Rubino and K. J. Franz, *J. Inorg. Biochem.*, 2012, **107**, 129–143.
7 R. G. Pearson, *J. Am. Chem. Soc.*, 1963, **85**, 3533–3539.
8 D. Njus and P. M. Kelley, *FEBS Lett.*, 1991, **284**, 147–151.
9 W. Kaim and J. Rall, *Angew. Chemie Int. Ed. English*, 1996, **35**, 43–60.
10 R. R. Crichton and J. L. Pierre, *BioMetals*, 2001, **14**, 99–112.
11 R. J. P. Williams, *J. Inorg. Biochem.*, 2002, **88**, 241–250.
12 R. J. P. Williams and J. J. R. Fraústo Da Silva, *J. Theor. Biol.*, 2003, **220**, 323–343.
13 R. A. Festa and D. J. Thiele, *Curr. Biol.*, 2011, **21**, R877–R883.
14 C. J. Chang, *Nat. Chem. Biol.*, 2015, **11**, 744–747.
15 J. Kardos, L. Héja, Á. Simon, I. Jablonkai, R. Kovács and K. Jemnitz, *Cell Commun. Signal.*, 2018, **16**, 71.
16 C. M. Ackerman and C. J. Chang, *J. Biol. Chem.*, 2018, **293**, 4628–4635.
17 A. Grubman and A. R. White, *Expert Rev. Mol. Med.*, 2014, **16**, E11.
18 F. I. Rodríguez, J. J. Esch, A. E. Hall, B. M. Binder, G. Eric Schaller and A. B. Bleecker, *Science*, 1999, **283**, 996–998.
19 E. Block, V. S. Batista, H. Matsunami, H. Zhuang and L. Ahmed, *Nat. Prod. Rep.*, 2017, **34**, 529–557.
20 F. Haag, L. Ahmed, K. Reiss, E. Block, V. S. Batista and D. Krautwurst, *Cell. Mol. Life Sci.*, 2020, **77**, 2157–2179.
21 M. L. Turski, D. C. Brady, H. J. Kim, B.-E. Kim, Y. Nose, C. M. Counter, D. R. Winge and D. J. Thiele, *Mol. Cell. Biol.*, 2012, **32**, 1284–1295.
22 D. C. Brady, M. S. Crowe, M. L. Turski, G. A. Hobbs, X. Yao, A. Chaikuad, S. Knapp, K. Xiao, S. L. Campbell, D. J. Thiele and C. M. Counter, *Nature*, 2014, **509**, 492–496.
23 F. He, C. Chang, B. Liu, Z. Li, H. Li, N. Cai and H. H. Wang, *Biomed Res. Int.*, 2019, **2019**, 4158415.
24 L. Finney, S. Vogt, T. Fukai and D. Glesne, *Clin. Exp. Pharmacol. Physiol.*, 2009, **36**, 88–94.
25 D. Denoyer, S. Masaldan, S. La Fontaine and M. A. Cater, *Metallomics*, 2015, **7**, 1459–1476.
26 S. C. Dodani, D. W. Domaille, C. I. Nam, E. W. Miller, L. A. Finney, S. Vogt and C. J. Chang, *Proc. Natl. Acad. Sci. U. S. A.*, 2011, **108**, 5980–5985.
27 J. Kardos, I. Kovács, F. Hajós, M. Kálmán and M. Simonyi, *Neurosci. Lett.*, 1989, **103**, 139–144.
28 N. D'Ambrosi and L. Rossi, *Neurochem. Int.*, 2015, **90**, 36–45.
29 M. L. Schlief and J. D. Gitlin, *Mol. Neurobiol.*, 2006, **33**, 81–90.
30 M. L. Schlief, A. M. Craig and J. D. Gitlin, *J. Neurosci.*, 2005, **25**, 239–246.
31 A. Travaglia, G. Arena, R. Fattorusso, C. Isernia, D. La Mendola, G. Malgieri, V. G. Nicoletti and E. Rizzarelli, *Chem. - A Eur. J.*, 2011, **17**, 3726–3738.
32 A. Travaglia, D. La Mendola, A. Magrì, V. G. Nicoletti, A. Pietropaolo and E. Rizzarelli, *Chem. - A Eur. J.*, 2012, **18**, 15618–15631.
33 G. Pandini, C. Satriano, A. Pietropaolo, F. Gianì, A. Travaglia, D. La Mendola, V. G. Nicoletti and E. Rizzarelli, *Front. Neurosci.*, 2016, **10**, 1–21.
34 D. La Mendola, G. Arena, A. Pietropaolo, C. Satriano and E. Rizzarelli, *Coord. Chem. Rev.*, 2021, **435**, 213790.
35 G. Tan, J. Yang, T. Li, J. Zhao, S. Sun, X. Li, C. Lin, J. Li, H. Zhou, J. Lyu and H. Ding, *Appl. Environ. Microbiol.*, 2017, **83**, e00867-17.
36 L. Macomber and J. A. Imlay, *Proc. Natl. Acad. Sci. U. S. A.*, 2009, **106**, 8344–8349.

37 C. Vallières, S. L. Holland and S. V. Avery, *Cell Chem. Biol.*, 2017, **24**, 1228-1237.e3.
38 D. Brancaccio, A. Gallo, M. Piccioli, E. Novellino, S. Ciofi-Baffoni and L. Banci, *J. Am. Chem. Soc.*, 2017, **139**, 719–730.
39 R. A. Festa and D. J. Thiele, *PLOS Pathog.*, 2012, **8**, e1002887.
40 S. L. Stafford, N. J. Bokil, M. E. S. Achard, R. Kapetanovic, M. A. Schembri, A. G. Mcewan and M. J. Sweet, *Biosci. Rep.*, 2013, **33**, 541–554.
41 K. Y. Djoko, C. L. Y. Ong, M. J. Walker and A. G. McEwan, *J. Biol. Chem.*, 2015, **290**, 1854–1861.
42 A. N. Besold, E. M. Culbertson and V. C. Culotta, *J. Biol. Inorg. Chem.*, 2016, **21**, 137–144.
43 P. V. E. Van Den Berghe and L. W. J. Klomp, *Nutr. Rev.*, 2009, **67**, 658–672.
44 R. A. Smallwood, H. A. Williams, V. M. Rosenoer and S. Sherlock, *Lancet*, 1968, **292**, 1310–1313.
45 G. P. Van Berge Henegouwen, T. N. Tangedahl, A. F. Hofmann, T. C. Northfield, N. F. LaRusso and J. T. McCall, *Gastroenterology*, 1977, **72**, 1228–1231.
46 G. J. Brewer, P. J. Gow, R. A. Smallwood, P. W. Angus, R. B. Sewell, A. L. Smith and A. J. Wall, *Gut*, 2002, **50**, 136.
47 M. C. Linder, *Metallomics*, 2016, **8**, 887–905.
48 F. Woimant, N. Djebrani-Oussedik and A. Poujois, *Ann. Transl. Med.*, 2019, **7**, S70–S70.
49 T. Kirsipuu, A. Zadoroznaja, J. Smirnova, M. Friedemann, T. Plitz, V. Tougu and P. Palumaa, *Sci. Rep.*, 2020, **10**, 1–11.
50 G. E. Jackson, P. M. May and D. R. Williams, *FEBS Lett.*, 1978, **90**, 173–177.
51 A. Cabrera, E. Alonzo, E. Sauble, Y. L. Chu, D. Nguyen, M. C. Linder, D. S. Sato and A. Z. Mason, *BioMetals*, 2008, **21**, 525–543.
52 K. C. Weiss and M. C. Linder, *Am. J. Physiol.*, 1985, **249**, E77–E88.
53 N. Liu, L. S. li Lo, S. H. Askary, L. T. Jones, T. Z. Kidane, T. T. M. Nguyen, J. Goforth, Y. H. Chu, E. Vivas, M. Tsai, T. Westbrook and M. C. Linder, *J. Nutr. Biochem.*, 2007, **18**, 597–608.
54 T. Kirsipuu, A. Zadorožnaja, J. Smirnova, M. Friedemann, T. Plitz, V. Tõugu and P. Palumaa, *Sci. Rep.*, 2020, **10**, 1–11.
55 P. M. May, P. W. Linder and D. R. Williams, *J. Chem. Soc. Dalt. Trans.*, 1977, 588–595.
56 L. W. Gray, F. Peng, S. A. Molloy, V. S. Pendyala, A. Muchenditsi, O. Muzik, J. Lee, J. H. Kaplan and S. Lutsenko, *PLoS One*, 2012, **7**, e38327.
57 S. Flynn, M. Dalphin, M. Tellez, H. Fieten, S. Weldy, A. Muchenditsi, S. Lutsenko and M. Linder, *FASEB J.*, 2015, **29**, 921.2.
58 M. Tellez, T. Alsky, M. Dalphin, S. Flynn, A. Munoz, D. Ibarra, H. Truong, M. C. Linder, S. Lutsenko and S. Weldy, *FASEB J.*, 2016, **30**, 1026.2-1026.2.
59 N. E. Hellman and J. D. Gitlin, *Annu. Rev. Nutr.*, 2002, **22**, 439–458.
60 S. Catalani, M. Paganelli, M. E. Gilberti, L. Rozzini, F. Lanfranchi, A. Padovani and P. Apostoli, *J. Trace Elem. Med. Biol.*, 2018, **45**, 176–180.
61 W. Bal, M. Sokołowska, E. Kurowska and P. Faller, *Biochim. Biophys. Acta - Gen. Subj.*, 2013, **1830**, 5444–5455.
62 K. Bossak-Ahmad, T. Frączyk, W. Bal and S. C. Drew, *ChemBioChem*, 2020, **21**, 331–334.
63 C. N. Beuning, B. Mestre-Voegtlé, P. Faller, C. Hureau and D. C. Crans, *Inorg. Chem.*, 2018, **57**, 4791–4794.
64 R. Kotuniak, M. J. F. Strampraad, K. Bossak-Ahmad, U. E. Wawrzyniak, I. Ufnalska, P. L. Hagedoorn and W. Bal, *Angew. Chemie - Int. Ed.*, 2020, **59**, 11234–11239.
65 E. Stefaniak, D. Płonka, S. C. Drew, K. Bossak-Ahmad, K. L. Haas, M. J. Pushie, P. Faller, N. E. Wezynfeld and W. Bal, *Metallomics*, 2018, **10**, 1723–1727.
66 L. Sottrup-Jensen, T. M. Stepanik and T. Kristensen, *J. Biol. Chem.*, 1984, **259**, 8313–8327.
67 M. Moriya, Y. Ho, A. Grana, L. Nguyen, A. Alvarez, R. Jamil, M. L. Ackland, A. Michalczyk, P. Hamer, D. Ramos, S. Kim, J. F. B. Mercer and M. C. Linder, 2008, **6866**, 708–721.
68 N. Lepage, N. Mcdonald, L. Dallaire and M. Lambert, *Clin. Chem.*, 1997, **43**, 2397–2402.
69 C. J. Sarell, C. D. Syme, S. E. J. Rigby and J. H. Viles, *Biochemistry*, 2009, **48**, 4388–4402.
70 L. W. Gray, F. Peng, S. A. Molloy, V. S. Pendyala, A. Muchenditsi, O. Muzik, J. Lee, J. H. Kaplan and S. Lutsenko, *PLoS One*, 2012, **7**, e38327.
71 L. Pickart, J. M. Vasquez-Soltero and A. Margolina, *Oxid. Med. Cell. Longev.*, 2012, **2012**, 324832.
72 P. Gonzalez, K. Bossak, E. Stefaniak, C. Hureau, L. Raibaut, W. Bal and P. Faller, *Chem. - A Eur. J.*, 2018, **24**, 8029–8041.

73 C. J. De Feo, S. G. Aller, G. S. Siluvai, N. J. Blackburn and V. M. Unger, *Proc. Natl. Acad. Sci. U. S. A.*, 2009, **106**, 4237–4242.
74 F. Ren, B. L. Logeman, X. Zhang, Y. Liu, D. J. Thiele and P. Yuan, *Nat. Commun.*, 2019, **10**, 1–9.
75 H. Öhrvik and D. J. Thiele, *Ann. N. Y. Acad. Sci.*, 2014, **1314**, 32–41.
76 C. Y. Tsai, J. K. Liebig, I. F. Tsigelny and S. B. Howell, *Metallomics*, 2015, **7**, 1477–1487.
77 H. Öhrvik, Y. Nose, L. K. Wood, B. E. Kim, S. C. Gleber, M. Ralle and D. J. Thiele, *Proc. Natl. Acad. Sci. U. S. A.*, 2013, **110**, E4279.
78 K. Bossak, S. C. Drew, E. Stefaniak, D. Płonka, A. Bonna and W. Bal, *J. Inorg. Biochem.*, 2018, **182**, 230–237.
79 K. L. Haas, A. B. Putterman, D. R. White, D. J. Thiele and K. J. Franz, *J. Am. Chem. Soc.*, 2011, **54**, 8544–8551.
80 N. E. Wezynfeld, B. Vileno and P. Faller, *Inorg. Chem.*, 2019, **58**, 7488–7498.
81 Y. Shenberger, A. Shimshi and S. Ruthstein, *J. Phys. Chem. B*, 2015, **119**, 4824–4830.
82 D. Ramos, D. Mar, M. Ishida, R. Vargas, M. Gaite, A. Montgomery and M. C. Linder, *PLoS One*, 2016, **11**, 1–23.
83 A. N. Besold, V. Shanbhag, M. J. Petris and V. C. Culotta, *J. Inorg. Biochem.*, 2021, **219**, 111424.
84 R. S. Ohgami, D. R. Campagna, A. McDonald and M. D. Fleming, *Blood*, 2006, **108**, 1388–1394.
85 V. B. Vassiliev, A. M. Kachurin, M. Beltramini, G. P. Rocco, B. Salvato and V. S. Gaitskboki, *J. Inorg. Biochem.*, 1997, **65**, 167–174.
86 G. Calabrese, B. Morgan and J. Riemer, *Antioxidants Redox Signal.*, 2017, **27**, 1162–1177.
87 M. T. Morgan, L. A. H. Nguyen, H. L. Hancock and C. J. Fahrni, *J. Biol. Chem.*, 2017, **292**, 21558–21567.
88 E. B. Maryon, S. A. Molloy and J. H. Kaplan, *Am. J. Physiol. - Cell Physiol.*, 2013, **304**, 768–779.
89 M. T. Morgan, D. Bourassa, S. Harankhedkar, A. M. McCallum, S. A. Zlatic, J. S. Calvo, G. Meloni, V. Faundez and C. J. Fahrni, *Proc. Natl. Acad. Sci.*, 2019, **116**, 12167–12172.
90 L. Banci, I. Bertini, F. Cantini, T. Kozyreva, C. Massagni, P. Palumaa, J. T. Rubino and K. Zovo, *Proc. Natl. Acad. Sci. U. S. A.*, 2012, **109**, 13555–13560.
91 P. J. Schmidt, C. Kunst and V. C. Culotta, *J. Biol. Chem.*, 2000, **275**, 33771–33776.
92 A. L. Lamb, A. K. Wernimont, R. A. Pufahl, T. V. O'Halloran and A. C. Rosenzweig, *Biochemistry*, 2000, **39**, 1589–1595.
93 A. L. Lamb, A. S. Torres, T. V. O'Halloran and A. C. Rosenzweig, *Nat. Struct. Biol.*, 2001, **8**, 751–755.
94 L. Banci, I. Bertini, F. Cantini and S. Ciofi-Baffoni, *Cell. Mol. Life Sci.*, 2010, **67**, 2563–2589.
95 Z. N. Baker, P. A. Cobine and S. C. Leary, *Metallomics*, 2017, **9**, 1501–1512.
96 H. Kawamata and G. Manfredi, *Antioxidants Redox Signal.*, 2010, **13**, 1375–1384.
97 P. A. Cobine, F. Pierrel, M. L. Bestwick and D. R. Winge, *J. Biol. Chem.*, 2006, **281**, 36552–36559.
98 A. Boulet, K. E. Vest, M. K. Maynard, M. G. Gammon, A. C. Russell, A. T. Mathews, S. E. Cole, X. Zhu, C. B. Phillips, J. Q. Kwong, S. C. Dodani, S. C. Leary and P. A. Cobine, *J. Biol. Chem.*, 2018, **293**, 1887–1896.
99 S. C. Dodani, S. C. Leary, P. A. Cobine, D. R. Winge and C. J. Chang, *J. Am. Chem. Soc.*, 2011, **133**, 8606–8616.
100 P. A. Cobine, S. A. Moore and S. C. Leary, *Biochim. Biophys. Acta - Mol. Cell Res.*, 2021, 1868, 118867.
101 I. Anastassopoulou, L. Banci, I. Bertini, F. Cantini, E. Katsari and A. Rosato, *Biochemistry*, 2004, **43**, 13046–13053.
102 L. Banci, I. Bertini, F. Cantini, N. Della-Malva, M. Migliardi and A. Rosato, *J. Biol. Chem.*, 2007, **282**, 23140–23146.
103 L. Banci, I. Bertini, F. Cantini, C. Massagni, M. Migliardi and A. Rosato, *J. Biol. Chem.*, 2009, **284**, 9354–9360.
104 S. Itoh, W. K. Ha, O. Nakagawa, K. Ozumi, S. M. Lessner, H. Aoki, K. Akram, R. D. McKinney, M. Ushio-Fukai and T. Fukai, *J. Biol. Chem.*, 2008, **283**, 9157–9167.
105 S. Itoh, K. Ozumi, H. W. Kim, O. Nakagawa, R. D. McKinney, R. J. Folz, I. N. Zelko, M. Ushio-Fukai and T. Fukai, *Free Radic. Biol. Med.*, 2009, **46**, 95–104.
106 T. Kamiya, K. Takeuchi, S. Fukudome, H. Hara and T. Adachi, *BioMetals*, 2018, **31**, 61–68.
107 P. A. J. Muller and L. W. J. Klomp, *Int. J. Biochem. Cell Biol.*, 2009, **41**, 1233–1236.

108 D. Kahra, T. Mondol, M. Niemiec and P. Wittung-Stafshede, *Protein Pept. Lett.*, 2015, **22**, 532–538.
109 H. Öhrvik and P. Wittung-Stafshede, *Int. J. Mol. Sci.*, 2015, **16**, 16728–16739.
110 K. Schmidt, M. Ralle, T. Schaffer, S. Jayakanthan, B. Bari, A. Muchenditsi and S. Lutsenko, *J. Biol. Chem.*, 2018, **293**, 20085–20098.
111 S. Lutsenko, C. Washington-Hughes, M. Ralle and K. Schmidt, *J. Biol. Inorg. Chem.*, 2019, **24**, 1179–1188.
112 J. Calvo, H. Jung and G. Meloni, *IUBMB Life*, 2017, **69**, 236–245.
113 L. Banci, I. Bertini, S. Ciofi-Baffoni, T. Kozyreva, K. Zovo and P. Palumaa, *Nature*, 2010, **465**, 645–648.
114 K. Balamurugan and W. Schaffner, *Biochim. Biophys. Acta - Mol. Cell Res.*, 2006, **1763**, 737–746.
115 V. Günther, U. Lindert and W. Schaffner, *Biochim. Biophys. Acta - Mol. Cell Res.*, 2012, **1823**, 1416–1425.
116 I. S. Song, H. H. W. Chen, I. Aiba, A. Hossain, Z. D. Liang, L. W. J. Klomp and M. T. Kuo, *Mol. Pharmacol.*, 2008, **74**, 705–713.
117 Z. D. Liang, W. Bin Tsai, M. Y. Lee, N. Savaraj and M. T. Kuo, *Mol. Pharmacol.*, 2012, **81**, 455–464.
118 S. Yuan, S. Chen, Z. Xi and Y. Liu, *Metallomics*, 2017, **9**, 1169–1175.
119 C. J. Hlynialuk, B. Ling, Z. N. Baker, P. A. Cobine, L. D. Yu, A. Boulet, T. Wai, A. Hossain, A. M. ElZawily, P. J. McFie, S. J. Stone, F. Diaz, C. T. Moraes, D. Viswanathan, M. J. Petris and S. C. Leary, *Cell Rep.*, 2015, **10**, 933–943.
120 S. C. Leary, P. A. Cobine, T. Nishimura, R. M. Verdijk, R. De Krijger, R. De Coo, M. A. Tarnopolsky, D. R. Winge and E. A. Shoubridge, *Mol. Biol. Cell*, 2013, **24**, 683–691.
121 M. C. Linder, *Int. J. Mol. Sci.*, 2020, **21**, 1–22.
122 J. R. Turnlund, C. L. Keen and R. G. Smith, *Am. J. Clin. Nutr.*, 1990, **51**, 658–664.
123 E. W. Rice and N. P. Goldstein, *Metabolism*, 1966, **15**, 1050–1053.
124 S. Melino, C. Santone, P. Di Nardo and B. Sarkar, *FEBS J.*, 2014, **281**, 657–672.
125 W. M. Tay, A. I. Hanafy, A. Angerhofer and L.-J. Ming, *Bioorg. Med. Chem. Lett.*, 2009, **19**, 6709–6712.
126 E. A. Houghton and K. M. Nicholas, *J. Biol. Inorg. Chem.*, 2009, **14**, 243–251.
127 M. Yamazaki, S. Ito, A. Usami, N. Tani, O. Hanyu, O. Nakagawa, H. Nakamura and A. Shibata, *Eur. J. Endocrinol.*, 1995, **132**, 681–687.
128 S. Ito, H. Fujita, T. Narita, T. Yaginuma, Y. Kawarada, M. Kawagoe and T. Sugiyama, *Nephron*, 2001, **88**, 307–312.
129 W. E. N. D. Evering, S. Haywood, I. Bremner, A. M. Wood and J. Trafford, *Chem. Biol. Interact.*, 1991, **78**, 297–305.
130 M. Vašák and G. Meloni, *Int. J. Mol. Sci.*, 2017, **18**, 1117.
131 E. Atrián-Blasco, A. Santoro, D. L. Pountney, G. Meloni, C. Hureau and P. Faller, *Chem. Soc. Rev.*, 2017, **46**, 7683–7693.
132 G. Meloni, P. Faller and M. Vašák, *J. Biol. Chem.*, 2007, **282**, 16068–16078.
133 C. R. Capo, M. Arciello, R. Squitti, E. Cassetta, P. M. Rossini, L. Calabrese and L. Rossi, *BioMetals*, 2008, **21**, 367–372.
134 V. Nischwitz, A. Berthele and B. Michalke, *Anal. Chim. Acta*, 2008, **627**, 258–269.
135 J. G. Dorea, *Nutrition*, 2000, **16**, 209–220.
136 L. V. Puchkova, P. S. Babich, Y. A. Zatulovskaia, E. Y. Ilyechova and F. Di Sole, *Nutrients*, 2018, **10**, 1591.
137 N. Platonova, N. Guolikhandanova, N. Tsymbalenko, E. Zhiguleva, T. Zhivulko, A. Vasin, I. Evsukova and L. Puchkova, *J. Trace Elem. Med. Biol.*, 2007, **21**, 184–193.
138 B. Lönnerdal, B. Hoffman and L. S. Hurley, *Am. J. Clin. Nutr.*, 1982, **36**, 1170–1176.
139 L. Wooten, R. A. Shulze, R. W. Lancey, M. Lietzow and M. C. Linder, *J. Nutr. Biochem.*, 1996, **7**, 632–639.
140 C. Hureau, H. Eury, R. Guillot, C. Bijani, S. Sayen, P. L. Solari, E. Guillon, P. Faller and P. Dorlet, *Chem. - A Eur. J.*, 2011, **17**, 10151–10160.
141 A. Santoro, G. Walke, B. Vileno, P. P. Kulkarni, L. Raibaut and P. Faller, *Chem. Commun.*, 2018, **54**, 11945–11948.

142 M. Sokolowska, A. Krezel, M. Dyba, Z. Szewczuk and W. Bal, *Eur. J. Biochem.*, 2002, **269**, 1323–1331.
143 T. Miyamoto, Y. Fukino, S. Kamino, M. Ueda and S. Enomoto, *Dalt. Trans.*, 2016, **45**, 9436–9445.
144 T. Frączyk, *Chem. Biodivers.*, 2021, **18**, e2100043.
145 D. L. Rabenstein, A. A. Isab, S. A. Daignault, A. P. Arnold and M. M. Shoukry, *J. Am. Chem. Soc.*, 1985, **107**, 6435–6439.
146 M. Bouraguba, E. Glattard, M. Naudé, R. Pelletier, C. Aisenbrey, B. Bechinger, L. Raibaut, V. Lebrun and P. Faller, *J. Inorg. Biochem.*, 2020, **213**, 111255.
147 C. N. Beuning, L. J. Zocchi, K. P. Malikidogo, C. Esmieu, P. Dorlet, D. C. Crans and C. Hureau, *Inorg. Chem.*, 2021, **60**, 7650–7659.
148 L. F. Wong, J. C. Cooper and D. W. Margerum, *J. Am. Chem. Soc.*, 1976, **98**, 7268–7274.
149 M. Scarpa, F. Vianello, L. Signor, L. Zennaro and A. Rigo, *Inorg. Chem.*, 1996, **35**, 5201–5206.
150 A. Ząbek-Adamska, R. Drozdz and J. W. Naskalski, *Acta Biochim. Pol.*, 2013, **60**, 565–571.
151 D. Kahra, M. Kovermann and P. Wittung-Stafshede, *Biophys. J.*, 2016, **110**, 95–102.
152 M. Ralle, S. Lutsenko and N. J. Blackburn, *J. Biol. Chem.*, 2003, **278**, 23163–23170.
153 A. Rodriguez-Granillo, A. Crespo, D. A. Estrin and P. Wittung-Stafshede, *J. Phys. Chem. B*, 2010, **114**, 3698–3706.
154 V. Tanchou, F. Gas, A. Urvoas, F. Cougouluègne, S. Ruat, O. Averseng and E. Quéméneur, *Biochem. Biophys. Res. Commun.*, 2004, **325**, 388–394.
155 L. Banci, I. Bertini, S. Ciofi-Baffoni, A. Janicka, M. Martinelli, H. Kozlowski and P. Palumaa, *J. Biol. Chem.*, 2008, **283**, 7912–7920.
156 L. Banci, I. Bertini, F. Cantini, S. Ciofi-Baffoni, L. Gonnelli and S. Mangani, *J. Biol. Chem.*, 2004, **279**, 34833–34839.
157 Y. C. Horng, S. C. Leary, P. A. Cobine, F. B. J. Young, G. N. George, E. A. Shoubridge and D. R. Winge, *J. Biol. Chem.*, 2005, **280**, 34113–34122.
158 M. Vašák and G. Meloni, *J. Biol. Inorg. Chem.*, 2011, **16**, 1067–1078.
159 A. Santoro, J. S. Calvo, M. D. Peris-Díaz, A. Krężel, G. Meloni and P. Faller, *Angew. Chemie - Int. Ed.*, 2020, **59**, 7830–7835.
160 B. L. Vallee and R. J. Williams, *Proc. Natl. Acad. Sci. U. S. A.*, 1968, **59**, 498–505.
161 J. Liu, S. Chakraborty, P. Hosseinzadeh, Y. Yu, S. Tian, I. Petrik, A. Bhagi and Y. Lu, *Chem. Rev.*, 2014, **114**, 4366–4369.
162 I. S. MacPherson and M. E. P. Murphy, *Cell. Mol. Life Sci.*, 2007, **64**, 2887–2899.
163 E. I. Solomon, U. M. Sundaram and T. E. Machonkin, *Chem. Rev.*, 1996, **96**, 2563–2605.
164 I. Bento, C. Peixoto, V. N. Zaitsev and P. F. Lindley, *Acta Crystallogr. Sect. D Biol. Crystallogr.*, 2007, **63**, 240–248.
165 T. E. Machonkin, H. H. Zhang, B. Hedman, K. O. Hodgson and E. I. Solomon, *Biochemistry*, 1998, **37**, 9570–9578.
166 M. Knop, T. Q. Dang, G. Jeschke and F. P. Seebeck, *ChemBioChem*, 2017, **18**, 161–165.
167 D. A. Miarzlou, F. Leisinger, D. Joss, D. Häussinger and F. P. Seebeck, *Chem. Sci.*, 2019, **10**, 7049–7058.
168 M. J. Appel, K. K. Meier, J. Lafrance-Vanasse, H. Lim, C. L. Tsai, B. Hedman, K. O. Hodgson, J. A. Tainer, E. I. Solomon and C. R. Bertozzi, *Proc. Natl. Acad. Sci. U. S. A.*, 2019, **116**, 5370–5375.
169 S. J. Kaur, S. R. McKeown and S. Rashid, *Gene*, 2016, **577**, 109–118.
170 W. S. Oetting, *Pigment Cell Res.*, 2000, **13**, 320–325.
171 G. Marchi, F. Busti, A. L. Zidanes, A. Castagna and D. Girelli, *Front. Neurosci.*, 2019, 13, 325.
172 A. Munnich and P. Rustin, *Am. J. Med. Genet. - Semin. Med. Genet.*, 2001, **106**, 46–52.
173 L. C. Papadopoulou, C. Sue M, M. M. Davidson, K. Tanji, I. Nishino, J. E. Sadlock, S. Krishna, W. Walker, J. Selby, D. M. Glerum, R. Van Coster, G. Lyon, E. Scalais, R. Lebel, P. Kaplan, S. Shanske, D. C. De Vivo, E. Bonilla, M. Hirano, S. DiMauro and E. A. Schon, *Nat. Genet.*, 1999, **23**, 333–337.
174 I. Valnot, S. Osmond, N. Gigarel, B. Mehaye, J. Amiel, V. Cormier-Daire, A. Munnich, J.-P. Bonnefont, P. Rustin and A. Rötig, *Am. J. Hum. Genet.*, 2000, **67**, 1104–1109.
175 I. Bertini and A. Rosato, *Cell. Mol. Life Sci.*, 2008, **65**, 89–91.
176 P. De Bie, P. Muller, C. Wijmenga and L. W. J. Klomp, *J. Med. Genet.*, 2007, **44**, 673–688.
177 S. G. Kaler, *Am. J. Clin. Nutr.*, 1998, **67**, 1029S-1034S.

178 F. P. e. Vairo, B. C. Chwal, S. Perini, M. A. P. Ferreira, A. C. de Freitas Lopes and J. A. M. Saute, *Mol. Genet. Metab.*, 2019, **126**, 6–13.
179 L. M. Guthrie, S. Soma, S. Yuan, A. Silva, M. Zulkifli, T. C. Snavely, H. F. Greene, E. Nunez, B. Lynch, C. de Ville, V. Shanbhag, F. R. Lopez, A. Acharya, M. J. Petris, B. E. Kim, V. M. Gohil and J. C. Sacchettini, *Science*, 2020, **368**, 620–625.
180 J. D. Gitlin, *Gastroenterology*, 2003, **125**, 1868–1877.
181 T. Litwin, G. Gromadzka, G. M. Szpak, K. Jabłonka-Salach, E. Bulska and A. Członkowska, *J. Neurol. Sci.*, 2013, **329**, 55–58.
182 M. Patil, K. A. Sheth, A. C. Krishnamurthy and H. Devarbhavi, *J. Clin. Exp. Hepatol.*, 2013, **3**, 321–336.
183 S. El Balkhi, J. M. Trocello, J. Poupon, P. Chappuis, F. Massicot, N. Girardot-Tinant and F. Woimant, *Clin. Chim. Acta*, 2011, **412**, 2254–2260.
184 W. Stremmel and R. Weiskirchen, *Ann. Transl. Med.*, 2021, **9**, 732–732.
185 G. Crisponi, V. M. Nurchi, D. Fanni, C. Gerosa, S. Nemolato and G. Faa, *Coord. Chem. Rev.*, 2010, 254, 876–889.
186 G. Gromadzka, B. Tarnacka, A. Flaga and A. Adamczyk, *Int. J. Mol. Sci.*, 2020, **21**, 1–35.
187 K. Blennow, M. J. de Leon and H. Zetterberg, *Lancet*, 2006, **368**, 387–403.
188 E. Stefaniak and W. Bal, *Inorg. Chem.*, 2019, **58**, 13561–13577.
189 M. Mital, W. Bal, T. Fraczyk and S. C. Drew, *Inorg. Chem.*, 2018, **57**, 6193–6197.
190 J. A. Hardy and G. A. Higgins, *Science*, 1992, **256**, 184–185.
191 G. M. Bishop and S. R. Robinson, *Drugs and Aging*, 2004, **21**, 621–630.
192 K. Wild, A. August, C. U. Pietrzik and S. Kins, *Front. Mol. Neurosci.*, 2017, **10**, 1–12.
193 L. M. Munter, H. Sieg, T. Bethge, F. Liebsch, F. S. Bierkandt, M. Schleeger, H. J. Bittner, J. Heberle, N. Jakubowski, P. W. Hildebrand and G. Multhaup, *J. Am. Chem. Soc.*, 2013, **135**, 19354–19361.
194 F. Baumkötter, N. Schmidt, C. Vargas, S. Schilling, R. Weber, K. Wagner, S. Fiedler, W. Klug, J. Radzimanowski, S. Nickolaus, S. Keller, S. Eggert, K. Wild and S. Kins, *J. Neurosci.*, 2014, **34**, 11159–11172.
195 K. M. Acevedo, Y. H. Hung, A. H. Dalziel, Q. X. Li, K. Laughton, K. Wikhe, A. Rembach, B. Roberts, C. L. Masters, A. I. Bush and J. Camakaris, *J. Biol. Chem.*, 2011, **286**, 8252–8262.
196 Y. Noda, M. Asada, M. Kubota, M. Maesako, K. Watanabe, M. Uemura, T. Kihara, S. Shimohama, R. Takahashi, A. Kinoshita and K. Uemura, *Neurosci. Lett.*, 2013, **547**, 10–15.
197 P. Faller, C. Hureau and O. Berthoumieu, *Inorg. Chem.*, 2013, **52**, 12193–12206.
198 L. M. Miller, Q. Wang, T. P. Telivala, R. J. Smith, A. Lanzirotti and J. Miklossy, *J. Struct. Biol.*, 2006, **155**, 30–37.
199 J. Dong, C. S. Atwood, V. E. Anderson, S. L. Siedlak, M. A. Smith, G. Perry and P. R. Carey, *Biochemistry*, 2003, **42**, 2768–2773.
200 M. Schrag, C. Mueller, U. Oyoyo, M. A. Smith and W. M. Kirsch, *Prog. Neurobiol.*, 2011, **94**, 296–306.
201 S. Bucossi, M. Ventriglia, V. Panetta, C. Salustri, P. Pasqualetti, S. Mariani, M. Siotto, P. M. Rossini and R. Squitti, *J. Alzheimer's Dis.*, 2011, **24**, 175–185.
202 M. A. Cater, K. T. McInnes, Q. X. Li, I. Volitakis, S. L. A. Fontaine, J. F. B. Mercer and A. I. Bush, *Biochem. J.*, 2008, **412**, 141–152.
203 R. Squitti, I. Simonelli, M. Ventriglia, M. Siotto, P. Pasqualetti, A. Rembach, J. Doecke and A. I. Bush, *J. Alzheimer's Dis.*, 2014, **38**, 809–822.
204 R. Squitti, R. Ghidoni, I. Simonelli, I. D. Ivanova, N. A. Colabufo, M. Zuin, L. Benussi, G. Binetti, E. Cassetta, M. Rongioletti and M. Siotto, *J. Trace Elem. Med. Biol.*, 2018, **45**, 181–188.
205 R. Squitti, M. Siotto, M. Arciello and L. Rossi, *Metallomics*, 2016, **8**, 863–873.
206 R. Squitti, *J. Trace Elem. Med. Biol.*, 2014, **28**, 482–485.
207 R. Squitti, R. Polimanti, M. Siotto, S. Bucossi, M. Ventriglia, S. Mariani, F. Vernieri, F. Scrascia, L. Trotta and P. M. Rossini, *NeuroMolecular Med.*, 2013, **15**, 515–522.
208 E. Atrián-Blasco, P. Gonzalez, A. Santoro, B. Alies, P. Faller and C. Hureau, *Coord. Chem. Rev.*, 2018, **371**, 38–55.
209 C. Cheignon, M. Tomas, D. Bonnefont-Rousselot, P. Faller, C. Hureau and F. Collin, *Redox Biol.*, 2018, **14**, 450–464.
210 M. Mital, N. E. Wezynfeld, T. Frączyk, M. Z. Wiloch, U. E. Wawrzyniak, A. Bonna, C. Tumpach,

K. J. Barnham, C. L. Haigh, W. Bal and S. C. Drew, *Angew. Chemie - Int. Ed.*, 2015, **54**, 10460–10464.
211 K. Bossak-Ahmad, M. Mital, D. Plonka, S. C. Drew and W. Bal, *Inorg. Chem.*, 2019, **58**, 932–943.
212 C. Esmieu, G. Ferrand, V. Borghesani and C. Hureau, *Chem. - A Eur. J.*, 2021, **27**, 1777–1786.
213 M. J. Pushie, E. Stefaniak, M. R. Sendzik, D. Sokaras, T. Kroll and K. L. Haas, *Inorg. Chem.*, 2019, **58**, 15138–15154.
214 V. A. Streltsov, R. S. K. Ekanayake, S. C. Drew, C. T. Chantler and S. P. Best, *Inorg. Chem.*, 2018, **57**, 11422–11435.
215 E. Stefaniak, D. Płonka, P. Szczerba, N. E. Wezynfeld and W. Bal, *Inorg. Chem.*, 2020, **59**, 4186–4190.
216 M. Bisaglia and L. Bubacco, *Biomolecules*, 2020, 10.
217 K. M. Davies, J. F. B. Mercer, N. Chen and K. L. Double, *Clin. Sci.*, 2016, **130**, 565–574.
218 X. Wang, D. Moualla, J. A. Wright and D. R. Brown, *J. Neurochem.*, 2010, **113**, 704–714.
219 Y. Okita, A. N. Rcom-H'cheo-Gauthier, M. Goulding, R. S. Chung, P. Faller and D. L. Pountney, *Front. Neurosci.*, 2017, **11**, 1–9.
220 A. Binolfi, L. Quintanar, C. W. Bertoncini, C. Griesinger and C. O. Fernández, *Coord. Chem. Rev.*, 2012, **256**, 2188–2201.
221 D. Valensin, S. Dell'Acqua, H. Kozlowski and L. Casella, *J. Inorg. Biochem.*, 2016, **163**, 292–300.
222 R. De Ricco, D. Valensin, S. Dell'Acqua, L. Casella, P. Dorlet, P. Faller and C. Hureau, *Inorg. Chem.*, 2015, **54**, 4744–4751.
223 E. Falcone, I. M. M. Ahmed, V. Oliveri, F. Bellia, B. Vileno, Y. El Khoury, P. Hellwig, P. Faller and G. Vecchio, *Chem. - A Eur. J.*, 2020, **26**, 1871–1879.
224 P. Davies, D. Moualla and D. R. Brown, *PLoS One*, 2011, **6**, e15814.
225 J. S. McDowall, I. Ntai, K. C. Honeychurch, J. P. Hart, P. Colin, B. L. Schneider and D. R. Brown, *Mol. Cell. Neurosci.*, 2017, **85**, 1–11.
226 J. S. McDowall, I. Ntai, J. Hake, P. R. Whitley, J. M. Mason, C. R. Pudney and D. R. Brown, *Biochemistry*, 2017, **56**, 2497–2505.
227 A. Gupte and R. J. Mumper, *Cancer Treat. Rev.*, 2009, **35**, 32–46.
228 P. Lelièvre, L. Sancey, J. L. Coll, A. Deniaud and B. Busser, *Cancers (Basel).*, 2020, 12, 1–25.
229 K. Gaur, A. M. Vázquez-Salgado, G. Duran-Camacho, I. Dominguez-Martinez, J. A. Benjamín-Rivera, L. Fernández-Vega, L. C. Sarabia, A. C. García, F. Pérez-Deliz, J. A. M. Román, M. Vega-Cartagena, S. A. Loza-Rosas, X. R. Acevedo and A. D. Tinoco, *Inorganics*, 2018, **6**, 126.
230 O. Krasnovskaya, A. Naumov, D. Guk, P. Gorelkin, A. Erofeev, E. Beloglazkina and A. Majouga, *Int. J. Mol. Sci.*, 2020, **21**, 3965.
231 V. Oliveri, *Coord. Chem. Rev.*, 2020, **422**, 213474.
232 A. M. Merlot, D. S. Kalinowski and D. R. Richardson, *Antioxidants Redox Signal.*, 2013, **18**, 973–1006.
233 A. M. Merlot, D. S. Kalinowski, Z. Kovacevic, P. J. Jansson, S. Sahni, M. L.-H. Huang, D. J. R. Lane, H. Lok and D. R. Richardson, *Curr. Med. Chem.*, 2019, **26**, 302–322.
234 C. Santini, M. Pellei, V. Gandin, M. Porchia, F. Tisato and C. Marzano, *Chem. Rev.*, 2014, **114**, 815–862.
235 R. Squitti, R. Ghidoni, I. Simonelli, I. D. Ivanova, N. A. Colabufo, M. Zuin, L. Benussi, G. Binetti, E. Cassetta, M. Rongioletti and M. Siotto, *J. Trace Elem. Med. Biol.*, 2018, **45**, 181–188.
236 E. Falcone, M. Okafor, N. Vitale, L. Raibaut, A. Sour and P. Faller, *Coord. Chem. Rev.*, 2021, **433**, 213727.
237 C. J. Fahrni, *Curr. Opin. Chem. Biol.*, 2013, **17**, 656–662.
238 E. Falcone, A. Sour, V. Lebrun, G. Ulrich, L. Raibaut and P. Faller, *Dalt. Trans.*, 2019, **48**, 14233–14237.
239 E. Falcone, P. Gonzalez, L. Lorusso, O. Sénèque, P. Faller and L. Raibaut, *Chem. Commun.*, 2020, **56**, 4797–4800.
240 E. Falcone, B. Vileno, M. Hoang, L. Raibaut and P. Faller, *J. Inorg. Biochem.*, 2021, **221**, 111478.
241 J. B. Dawson, D. J. Ellis and H. Newton-John, *Clin. Chim. Acta*, 1968, **21**, 33–42.
242 J. Szpunar, J. Bettmer, M. Robert, H. Chassaigne, K. Cammann, R. Lobinski and O. F. X. Donard, *Talanta*, 1997, **44**, 1389–1396.
243 P. Chappuis, J. Poupon and F. Rousselet, *Clin. Chim. Acta*, 1992, **206**, 155–165.

244 P. R. M. Correia, E. Oliveira and P. V. Oliveira, *Anal. Chim. Acta*, 2002, **458**, 321–329.
245 H. Spector, S. Glusman, P. Jatlow and D. Seligson, *Clin. Chim. Acta*, 1971, **31**, 5–11.
246 R. Ortega, G. Devès and A. Carmona, *J. R. Soc. Interface*, 2009, **6**, S649–S658.
247 C. M. Ackerman, P. K. Weber, T. Xiao, B. Thai, T. J. Kuo, E. Zhang, J. Pett-Ridge and C. J. Chang, *Metallomics*, 2018, **10**, 474–485.
248 J. M. Walshe, *Ann. Clin. Biochem.*, 2003, **40**, 115–121.
249 R. Squitti, M. Siotto, E. Cassetta, I. G. El Idrissi and N. A. Colabufo, *Clin. Chem. Lab. Med.*, 2017, **55**, 1360–1367.
250 M. C. Linder, *Biomedicines*, 2021, **9**, 233.
251 A. Favier and D. Ruffieux, *Biol. Trace Elem. Res.*, 1988, **18**, 145–160.
252 A. M. Noubah and M. A. Al-Awqati, *Clin. Chem.*, 1990, **36**, 860–864.
253 A. Chan, F. Wong and M. Arumanayagam, *Ann. Clin. Biochem.*, 1993, **30**, 545–549.
254 G. A. McMillin, J. J. Travis and J. W. Hunt, *Am. J. Clin. Pathol.*, 2009, **131**, 160–165.
255 S. El Balkhi, J. Poupon, J. M. Trocello, A. Leyendecker, F. Massicot, M. Galliot-Guilley and F. Woimant, *Anal. Bioanal. Chem.*, 2009, **394**, 1477–1484.
256 J. Labuda, M. Skatulokova, M. Nemeth and S. Gergely, *Chem. zvesti*, 1984, **38**, 597.
257 C. J. Gubler, M. E. Lahey, M. S. Chase, G. E. Cartwright and M. M. Wintrobe, *Blood*, 1952, **7**, 1075–1092.
258 W. T. Buckley, R. A. Vanderpool, D. V. Godfrey and P. E. Johnson, *J. Nutr. Biochem.*, 1996, **7**, 488–494.
259 T. I. Venelinov, I. M. Davies and J. H. Beattie, *Anal. Bioanal. Chem.*, 2004, **379**, 777–780.
260 W. A. E. McBryde, *Can. J. Chem.*, 1967, **45**, 2093–2100.
261 J. M. C. Gutteridge, *Biochem. J.*, 1984, **218**, 983–985.
262 A. Poujois, J. Poupon and F. Woimant, in *Clinical and Translational Perspectives on WILSON DISEASE*, 2019, pp. 249–255.
263 N. Solovyev, A. Ala, M. Schilsky, C. Mills, K. Willis and C. F. Harrington, *Anal. Chim. Acta*, 2020, **1098**, 27–36.
264 J. M. C. Gutteridge, D. A. Rowley, B. Halliwell, D. F. Cooper and D. M. Heeley, *Clin. Chim. Acta*, 1985, **145**, 267–273.
265 P. J. Evans, A. Bomford and B. Halliwell, *Free Radic. Res.*, 1989, **7**, 55–62.
266 H. Ogihara, T. Ogihara, M. Miki, H. Yasuda and M. Mino, *Pediatr. Res.*, 1995, **37**, 219–226.
267 S. A. James, I. Volitakis, P. A. Adlard, J. A. Duce, C. L. Masters, R. A. Cherny and A. I. Bush, *Free Radic. Biol. Med.*, 2012, **52**, 298–302.
268 H. S. Pall, D. R. Blake, J. M. Gutteridge, A. C. Williams, J. Lunec, M. Hall and A. Taylor, *Lancet*, 1987, **330**, 238–241.
269 J. M. C. Gutteridge, P. G. Winyard, D. R. Blake, J. Lunec, S. Brailsford and B. Halliwell, *Biochem. J.*, 1985, **230**, 517–523.
270 J. P. C. Coverdale, J. P. Barnett, A. H. Adamu, E. J. Griffiths, A. J. Stewart and C. A. Blindauer, *Metallomics*, 2019, **11**, 1805–1819.
271 S. Noël, S. Bustos Rodriguez, S. Sayen, E. Guillon, P. Faller and C. Hureau, *Metallomics*, 2014, **6**, 1220–1222.
272 A. Conte-Daban, A. Day, P. Faller and C. Hureau, *Dalt. Trans.*, 2016, **45**, 15671–15678.
273 M. Sokołowska and W. Bal, *J. Inorg. Biochem.*, 2005, **99**, 1653–1660.
274 A. Krężel, J. Wójcik, M. Maciejczyk and W. Bal, *Chem. Commun.*, 2003, **3**, 704–705.
275 A. Krężel and W. Maret, *Arch. Biochem. Biophys.*, 2016, **611**, 3–19.
276 H. Irving and D. H. Mellor, *J. Chem. Soc.*, 1962, 5222–5237.
277 C. Chen, R. Tian, Y. Zeng, C. Chu and G. Liu, *Bioconjug. Chem.*, 2020, **31**, 276–292.
278 C. Li, G. Chen, Y. Zhang, F. Wu and Q. Wang, *J. Am. Chem. Soc.*, 2020, **142**, 14789–14804.
279 N. Zhang, C. Lu, M. Chen, X. Xu, G. Shu, Y. Du and J. Ji, *J. Nanobiotechnology*, 2021, **19**, 132.
280 J. Shinn, S. Lee, H. K. Lee, J. Ahn, S. A. Lee, S. Lee and Y. Lee, *Arch. Pharm. Res.*, 2021, **44**, 165–181.
281 C. S. Lim and B. R. Cho, *BMB Rep.*, 2013, **46**, 188–194.
282 V. Juvekar, S. J. Park, J. Yoon and H. M. Kim, *Coord. Chem. Rev.*, 2021, **427**, 213574.
283 K. Y. Zhang, Q. Yu, H. Wei, S. Liu, Q. Zhao and W. Huang, *Chem. Rev.*, 2018, 118, 1770–1839.
284 R. Zhang and J. Yuan, *Acc. Chem. Res.*, 2020, **53**, 1316–1329.

285 W. Yang, X. Chen, H. Su, W. Fang and Y. Zhang, *Chem. Commun.*, 2015, **51**, 9616–9619.
286 G. Sivaraman, M. Iniya, T. Anand, N. G. Kotla, O. Sunnapu, S. Singaravadivel, A. Gulyani and D. Chellappa, *Coord. Chem. Rev.*, 2018, **357**, 50–104.
287 L. M. Hyman and K. J. Franz, *Coord. Chem. Rev.*, 2012, **256**, 2333–2356.
288 G. Trusso Sfrazzetto, C. Satriano, G. A. Tomaselli and E. Rizzarelli, *Coord. Chem. Rev.*, 2016, **311**, 125–167.
289 M. Saleem, M. Rafiq, M. Hanif, M. A. Shaheen and S. Y. Seo, *J. Fluoresc.*, 2018, **28**, 97–165.
290 L. Prodi, F. Bolletta, M. Montalti and N. Zaccheroni, *Coord. Chem. Rev.*, 2000, **205**, 59–83.
291 A. Ramdass, V. Sathish, E. Babu, M. Velayudham, P. Thanasekaran and S. Rajagopal, *Coord. Chem. Rev.*, 2017, **343**, 278–307.
292 A. Basu and G. Das, *Dalt. Trans.*, 2011, **40**, 2837–2843.
293 J. Jo, H. Y. Lee, W. Liu, A. Olasz, C. H. Chen and D. Lee, *J. Am. Chem. Soc.*, 2012, **134**, 16000–16007.
294 Q. Nan, P. Rong, Y. Jiang and R. Yang, *Spectrochim. Acta - Part A Mol. Biomol. Spectrosc.*, 2017, **174**, 307–315.
295 J. Jung, J. Jo and A. Dinescu, *Org. Process Res. Dev.*, 2017, **21**, 1689–1693.
296 L. F. Wei, C. Y. Chen, C. K. Lai, N. Thirumalaivasan and S. P. Wu, *Methods*, 2019, **168**, 18–23.
297 Z. Xu, Y. Liu, S. Zhou, Y. Fu and C. Li, *Int. J. Mol. Sci.*, 2016, **17**, 1–15.
298 D. P. Chauhan, T. Saha, M. Lahiri and P. Talukdar, *Tetrahedron Lett.*, 2014, **55**, 244–247.
299 Z. Du, D. Yu, X. Du, P. Scott, J. Ren and X. Qu, *Chem. Sci.*, 2019, **10**, 10343–10350.
300 C. Wang, L. Lu, W. Ye, O. Zheng, B. Qiu, Z. Lin, L. Guo and G. Chen, *Analyst*, 2014, **139**, 656–659.
301 W. Zheng, H. Li, W. Chen, J. Zhang, N. Wang, X. Guo and X. Jiang, *Small*, 2018, **14**, 1–8.
302 D. Li, W. Zhou, Y. Chai, R. Yuan and Y. Xiang, *Chem. Commun.*, 2015, **51**, 12637–12640.
303 D. C. Kennedy, C. S. McKay, M. C. B. Legault, D. C. Danielson, J. A. Blake, A. F. Pegoraro, A. Stolow, Z. Mester and J. P. Pezacki, *J. Am. Chem. Soc.*, 2011, **133**, 17993–18001.
304 S. P. Wu, T. H. Wang and S. R. Liu, *Tetrahedron*, 2010, **66**, 9655–9658.
305 S. P. Wu, Z. M. Huang, S. R. Liu and P. K. Chung, *J. Fluoresc.*, 2012, **22**, 253–259.
306 F. Nouri Moghadam, M. Amirnasr, S. Meghdadi, K. Eskandari, A. Buchholz and W. Plass, *Spectrochim. Acta - Part A Mol. Biomol. Spectrosc.*, 2019, **207**, 6–15.
307 S. Mukherjee and S. Betal, *J. Fluoresc.*, 2019, **29**, 27–40.
308 S. Bayindir and M. Toprak, *Spectrochim. Acta - Part A Mol. Biomol. Spectrosc.*, 2019, **213**, 6–11.
309 H. Fang, P. C. Huang and F. Y. Wu, *Spectrochim. Acta - Part A Mol. Biomol. Spectrosc.*, 2019, **214**, 233–238.
310 J. Nootem, R. Daengngern, C. Sattayanon, W. Wattanathana, S. Wannapaiboon, P. Rashatasakhon and K. Chansaenpak, *J. Photochem. Photobiol. A Chem.*, 2021, **415**, 113318.
311 H. F. Wang and S. P. Wu, *Sensors Actuators B Chem.*, 2013, **181**, 743–748.
312 Z. Chen, L. Wang, G. Zou, J. Tang, X. Cai, M. Teng and L. Chen, *Spectrochim. Acta - Part A Mol. Biomol. Spectrosc.*, 2013, **105**, 57–61.
313 S. Goswami, S. Chakraborty, S. Paul, S. Halder, S. Panja and S. K. Mukhopadhyay, *Org. Biomol. Chem.*, 2014, **12**, 3037–3044.
314 P. Venkatesan and S. P. Wu, *RSC Adv.*, 2015, **5**, 42591–42596.
315 A. K. Mahapatra, S. Mondal, S. K. Manna, K. Maiti, R. Maji, M. R. Uddin, S. Mandal, D. Sarkar, T. K. Mondal and D. K. Maiti, *Dalt. Trans.*, 2015, **44**, 6490–6501.
316 P. Torawane, K. Keshav, M. K. Kumawat, R. Srivastava, T. Anand, S. Sahoo, A. Borse and A. Kuwar, *Photochem. Photobiol. Sci.*, 2017, **16**, 1464–1470.
317 S. M. Saleh, R. Ali and I. A. I. Ali, *Spectrochim. Acta - Part A Mol. Biomol. Spectrosc.*, 2017, **183**, 225–231.
318 W. Nasomphan, P. Tangboriboonrat and S. Smanmoo, *J. Fluoresc.*, 2017, **27**, 2201–2212.
319 A. P. De Silva, T. S. Moody and G. D. Wright, *Analyst*, 2009, **134**, 2385–2393.
320 D. Escudero, *Acc. Chem. Res.*, 2016, **49**, 1816–1824.
321 S. Chowdhury, B. Rooj, A. Dutta and U. Mandal, *J. Fluoresc.*, 2018, **28**, 999–1021.
322 Y. You, Y. Han, Y. M. Lee, S. Y. Park, W. Nam and S. J. Lippard, *J. Am. Chem. Soc.*, 2011, **133**, 11488–11491.
323 Z. Liu, C. Zhang, X. Wang, W. He and Z. Guo, *Org. Lett.*, 2012, **14**, 4378–4381.

324 Y. Chen, C. Zhu, J. Cen, J. Li, W. He, Y. Jiao and Z. Guo, *Chem. Commun.*, 2013, **49**, 7632–7634.
325 X. Guan, W. Lin and W. Huang, *Org. Biomol. Chem.*, 2014, **12**, 3944–3949.
326 Z. Xu, Y. Xiao, X. Qian, J. Cui and D. Cui, *Org. Lett.*, 2005, **7**, 889–892.
327 N. Singh, N. Kaur, B. McCaughan and J. F. Callan, *Tetrahedron Lett.*, 2010, **51**, 3385–3387.
328 G. I. Grasso, S. Gentile, M. L. Giuffrida, C. Satriano, C. Sgarlata, M. Sgarzi, G. Tomaselli, G. Arena and L. Prodi, *RSC Adv.*, 2013, **3**, 24288–24297.
329 Z. Xu, X. Qian and J. Cui, *Org. Lett.*, 2005, **7**, 3029–3032.
330 J. Fan, P. Zhan, M. Hu, W. Sun, J. Tang, J. Wang, S. Sun, F. Song and X. Peng, *Org. Lett.*, 2013, **15**, 492–495.
331 N. C. Lim and C. Brückner, *Chem. Commun.*, 2004, **4**, 1094–1095.
332 L. Xue, H. H. Wang, X. J. Wang and H. Jiang, *Inorg. Chem.*, 2008, **47**, 4310–4318.
333 B. A. Wong, S. Friedle and S. J. Lippard, *J. Am. Chem. Soc.*, 2009, **131**, 7142–7152.
334 Y. You, S. Lee, T. Kim, K. Ohkubo, W. S. Chae, S. Fukuzumi, G. J. Jhon, W. Nam and S. J. Lippard, *J. Am. Chem. Soc.*, 2011, **133**, 18328–18342.
335 M. T. Morgan, D. Bourassa, S. Harankhedkar, A. M. McCallum, S. A. Zlatic, J. S. Calvo, G. Meloni, V. Faundez and C. J. Fahrni, *Proc. Natl. Acad. Sci.*, 2019, **116**, 12167–12172.
336 S. Areti, J. K. Khedkar, S. Bandaru, R. Teotia, J. Bellare and C. P. Rao, *Anal. Chim. Acta*, 2015, **873**, 80–87.
337 H. Vojoudi, B. Bastan, J. B. Ghasemi and A. Badiei, *Anal. Bioanal. Chem.*, 2019, **411**, 5593–5603.
338 X. Zhu, H. Jin, C. Gao, R. Gui and Z. Wang, *Talanta*, 2017, **162**, 65–71.
339 S. J. He, Y. W. Xie and Q. Y. Chen, *Spectrochim. Acta - Part A Mol. Biomol. Spectrosc.*, 2018, **195**, 210–214.
340 F. Chen, F. Xiao, W. Zhang, C. Lin and Y. Wu, *ACS Appl. Mater. Interfaces*, 2018, **10**, 26964–26971.
341 Y. Li, H. Zhou, S. Yin, H. Jiang, N. Niu, H. Huang, S. A. Shahzad and C. Yu, *Sensors Actuators, B Chem.*, 2016, **235**, 33–38.
342 H. S. Jung, P. S. Kwon, J. W. Lee, J. I. I. Kim, C. S. Hong, J. W. Kim, S. Yan, J. Y. Lee, J. H. Lee, T. Joo and J. S. Kim, *J. Am. Chem. Soc.*, 2009, **131**, 2008–2012.
343 P. Huang, F. Wu and L. Mao, *Anal. Chem.*, 2015, **87**, 6834–6841.
344 Y. Lin, C. Wang, L. Li, H. Wang, K. Liu, K. Wang and B. Li, *ACS Appl. Mater. Interfaces*, 2015, **7**, 27262–27270.
345 A. Hopt, S. Korte, H. Fink, U. Panne, R. Niessner, R. Jahn, H. Kretzschmar and J. Herms, *J. Neurosci. Methods*, 2003, **128**, 159–172.
346 Y. A. Choi, J. O. Keem, C. Y. Kim, H. R. Yoon, W. Do Heo, B. H. Chung and Y. Jung, *Chem. Sci.*, 2015, **6**, 1301–1307.
347 Y. Xie, L. Yan and J. Li, *Appl. Spectrosc.*, 2019, **73**, 794–800.
348 X. Yu, M. P. Strub, T. J. Barnard, N. Noinaj, G. Piszczek, S. K. Buchanan and J. W. Taraska, *PLoS One*, 2014, **9**, 1–11.
349 D. K. Johnson, M. J. Stevenson, Z. A. Almadidy, S. E. Jenkins, D. E. Wilcox and N. E. Grossoehme, *Dalt. Trans.*, 2015, **44**, 16494–16505.
350 M. Ciesielski, D. Pufky and M. Döring, *Tetrahedron*, 2005, **61**, 5942–5947.
351 J. Wu, Q. You, J. Lan, Q. Guo, X. Li, Y. Xue and J. You, *Org. Biomol. Chem.*, 2015, **13**, 5372–5375.
352 A. F. Li, H. He, Y. Bin Ruan, Z. C. Wen, J. S. Zhao, Q. J. Jiang and Y. B. Jiang, *Org. Biomol. Chem.*, 2009, **7**, 193–200.
353 Q. Nan, P. Rong, Y. Jiang and R. Yang, *Spectrochim. Acta - Part A Mol. Biomol. Spectrosc.*, 2017, **174**, 307–315.
354 A. Magrì, G. Tabbì, A. Giuffrida, G. Pappalardo, C. Satriano, I. Naletova, V. G. Nicoletti and F. Attanasio, *J. Inorg. Biochem.*, 2016, **164**, 59–69.
355 Y. Huang, N. Xia, M. Chen, P. Yang, L. Liu and J. Wang, *Metallomics*, 2020, **12**, 1802–1810.
356 A. Torrado, G. K. Walkup and B. Imperiali, *J. Am. Chem. Soc.*, 1998, **120**, 609–610.
357 C. Wende and N. Kulak, *Chem. Commun.*, 2015, **51**, 12395–12398.
358 A. Grüter, M. Hoffmann, R. Müller, T. Wohland and G. Jung, *Anal. Bioanal. Chem.*, 2019, **411**, 3229–3240.
359 Y. Hao, W. Chen, L. Wang, X. Zhu, Y. Zhang, P. Qu, L. Liu, B. Zhou, Y. N. Liu and M. Xu,

Talanta, 2015, **143**, 307–314.
360 Y. Zheng, K. M. Gattás-Asfura, V. Konka and R. M. Leblanc, *Chem. Commun.*, 2002, **2**, 2350–2351.
361 K. H. Jung and K. H. Lee, *Anal. Chem.*, 2015, **87**, 9308–9314.
362 J. C. G. Bünzli, *J. Coord. Chem.*, 2014, **67**, 3706–3733.
363 T. J. Sørensen and S. Faulkner, *Acc. Chem. Res.*, 2018, **51**, 2493–2501.
364 T. S. Grimes and K. L. Nash, *J. Solution Chem.*, 2014, **43**, 298–313.
365 J. M. Idée, M. Port, C. Robic, C. Medina, M. Sabatou and C. Corot, *J. Magn. Reson. Imaging*, 2009, **30**, 1249–1258.
366 J. P. Prybylski, R. C. Semelka and M. Jay, *Magn. Reson. Imaging*, 2017, **38**, 145–151.
367 L. Armelao, S. Quici, F. Barigelletti, G. Accorsi, G. Bottaro, M. Cavazzini and E. Tondello, *Coord. Chem. Rev.*, 2010, **254**, 487–505.
368 J. H. S. K. Monteiro, *Molecules*, 2020, **25**, 2089.
369 A. Beeby, I. M. Clarkson, R. S. Dickins, S. Faulkner, D. Parker, L. Royle, A. S. De Sousa, J. A. G. Williams and M. Woods, *J. Chem. Soc. Perkin Trans. 2*, 1999, **2**, 493–503.
370 S. I. Weissman, *J. Chem. Phys.*, 1942, **10**, 214–217.
371 M. Latva, H. Takalob, V. M. Mukkala, C. Matachescu, J. C. Rodríguez-Ubis and J. Kankare, *J. Lumin.*, 1997, **75**, 149–169.
372 J. H. S. K. Monteiro, A. De Bettencourt-Dias and F. A. Sigoli, *Inorg. Chem.*, 2017, **56**, 709–712.
373 Ó. Guzmán-Méndez, F. González, S. Bernès, M. Flores-Álamo, J. Ordóñez-Hernández, H. García-Ortega, J. Guerrero, W. Qian, N. Aliaga-Alcalde and L. Gasque, *Inorg. Chem.*, 2018, **57**, 908–911.
374 M. Li and P. R. Selvin, *J. Am. Chem. Soc.*, 1995, **117**, 8132–8138.
375 T. Lazarides, M. A. H. Alamiry, H. Adams, S. J. A. Pope, S. Faulkner, J. A. Weinstein and M. D. Ward, *Dalt. Trans.*, 2007, 1484–1491.
376 T. J. Sørensen, A. M. Kenwright and S. Faulkner, *Chem. Sci.*, 2015, **6**, 2054–2059.
377 A. M. Reynolds, B. R. Sculimbrene and B. Imperiali, *Bioconjug. Chem.*, 2008, **19**, 588–591.
378 A. M. Nonat, A. J. Harte, K. Sénéchal-David, J. P. Leonard and T. Gunnlaugsson, *J. Chem. Soc. Dalt. Trans.*, 2009, 4703–4711.
379 B. K. McMahon and T. Gunnlaugsson, *Tetrahedron Lett.*, 2010, **51**, 5406–5410.
380 Z. Liang, T. H. Tsoi, C. F. Chan, L. Dai, Y. Wu, G. Du, L. Zhu, C. S. Lee, W. T. Wong, G. L. Law and K. L. Wong, *Chem. Sci.*, 2016, **7**, 2151–2156.
381 Y. W. Yip, G. L. Law and W. T. Wong, *Dalt. Trans.*, 2016, **45**, 928–935.
382 Y. Wang, H. Wang, X. Zhao, Y. Jin, H. Xiong, J. Yuan and J. Wu, *New J. Chem.*, 2017, **41**, 5981–5987.
383 M. L. Aulsebrook, S. Biswas, F. M. Leaver, M. R. Grace, B. Graham, A. M. Barrios and K. L. Tuck, *Chem. Commun.*, 2017, **53**, 4911–4914.
384 M. Clerc, F. Heinemann, B. Spingler and G. Gasser, *Inorg. Chem.*, 2020, **59**, 669–677.
385 K. J. Franz, M. Nitz and B. Imperiali, *ChemBioChem*, 2003, **4**, 265–271.
386 M. Nitz, K. J. Franz, R. L. Maglathlin and B. Imperiali, *ChemBioChem*, 2003, **4**, 272–276.
387 Y. Jiang, B. Su, H. Chen, T. Zhang, H. Liu and Y. Yu, *Biochem. Biophys. Res. Commun.*, 2021, **561**, 40–44.
388 T. Hirayama, M. Taki, K. Akaoka and Y. Yamamoto, *Bioorganic Med. Chem. Lett.*, 2012, **22**, 7410–7413.
389 M. Isaac, L. Raibaut, C. Cepeda, A. Roux, D. Boturyn, S. V. Eliseeva, S. Petoud and O. Sénèque, *Chem. - A Eur. J.*, 2017, **23**, 10992–10996.
390 M. Isaac, A. Pallier, F. Szeremeta, P. A. Bayle, L. Barantin, C. S. Bonnet and O. Sénèque, *Chem. Commun.*, 2018, **54**, 7350–7353.
391 M. Isaac, S. A. Denisov, A. Roux, D. Imbert, G. Jonusauskas, N. D. McClenaghan and O. Sénèque, *Angew. Chemie - Int. Ed.*, 2015, **54**, 11453–11456.
392 F. G. Prendergast, J. Lu and P. J. Callahan, *J. Biol. Chem.*, 1983, **258**, 4075–4078.
393 T. Hirayama, M. Taki, A. Kodan, H. Kato and Y. Yamamoto, *Chem. Commun.*, 2009, 3196–3198.
394 A. Niedźwiecka, F. Cisnetti, C. Lebrun and P. Delangle, *Inorg. Chem.*, 2012, **51**, 5458–5464.
395 C. Harford and B. Sarkar, *Biochem. Biophys. Res. Commun.*, 1995, **209**, 877–882.
396 A. B. Uceda, L. Mariño, M. Adrover and B. Vilanova, *Inorganica Chim. Acta*, 2020, **499**, 119197.
397 H. Yorita, K. Otomo, H. Hiramatsu, A. Toyama, T. Miura and H. Takeuchi, *J. Am. Chem. Soc.*,

2008, **130**, 15266–15267.
398 P. Gonzalez, B. Vileno, K. Bossak, Y. El Khoury, P. Hellwig, W. Bal, C. Hureau and P. Faller, *Inorg. Chem.*, 2017, **56**, 14870–14879.
399 P. Gonzalez, K. Bossak-Ahmad, B. Vileno, N. E. Wezynfeld, Y. El Khoury, P. Hellwig, C. Hureau, W. Bal and P. Faller, *Chem. Commun.*, 2019, **55**, 8110–8113.
400 J. Nagaj, K. Stokowa-Sołtys, I. Zawisza, M. Jezowska-Bojczuk, A. Bonna and W. Bal, *J. Inorg. Biochem.*, 2013, **119**, 85–89.
401 C. Hureau, H. Eury, R. Guillot, C. Bijani, S. Sayen, P. L. Solari, E. Guillon, P. Faller and P. Dorlet, *Chem. - A Eur. J.*, 2011, **17**, 10151–10160.
402 A. Santoro, N. E. Wezynfeld, E. Stefaniak, A. Pomorski, D. Płonka, A. Krężel, W. Bal and P. Faller, *Chem. Commun.*, 2018, **54**, 12634–12637.
403 B. Chan, N. Dodsworth, J. Woodrow, A. Tucker and R. Harris, 1995, **528**, 524–528.
404 D. Y. Zhang, M. Azrad, W. Demark-Wahnefried, C. J. Frederickson, S. J. Lippard and R. J. Radford, *ACS Chem. Biol.*, 2015, **10**, 385–389.
405 T. R. Alderson, J. H. Lee, C. Charlier, J. Ying and A. Bax, *ChemBioChem*, 2018, **19**, 37–42.
406 T. P. Creamer and M. N. Campbell, *Adv. Protein Chem.*, 2002, **62**, 263–282.
407 A. A. Adzhubei, M. J. E. Sternberg and A. A. Makarov, *J. Mol. Biol.*, 2013, **425**, 2100–2132.
408 S. Dobitz, M. R. Aronoff and H. Wennemers, *Acc. Chem. Res.*, 2017, **50**, 2420–2428.
409 L. Stryer and R. P. Haugland, *Proc. Natl. Acad. Sci. U. S. A.*, 1967, **58**, 719–726.
410 B. Schuler, E. A. Lipman, P. J. Steinbach, M. Kumkell and W. A. Eaton, *Proc. Natl. Acad. Sci. U. S. A.*, 2005, **102**, 2754–2759.
411 E. J. Petersson, J. M. Goldberg and R. F. Wissner, *Phys. Chem. Chem. Phys.*, 2014, **16**, 6827–6837.
412 W. Bal, M. Jezowska-Bojczuk and K. S. Kasprzak, *Chem. Res. Toxicol.*, 1997, **10**, 906–914.
413 N. Sreerama and R. W. Woody, *Protein Sci.*, 2003, **12**, 384–388.
414 J. L. S. Lopes, A. J. Miles, L. Whitmore and B. A. Wallace, *Protein Sci.*, 2014, **23**, 1765–1772.
415 A. L. Rucker and T. P. Creamer, *Protein Sci.*, 2002, **11**, 980–985.
416 T. J. Sørensen, A. M. Kenwright and S. Faulkner, *Chem. Sci.*, 2015, **6**, 2054–2059.
417 C. Song, Z. Ye, G. Wang, J. Yuan and Y. Guan, *Chem. - A Eur. J.*, 2010, **16**, 6464–6472.
418 Z. Tang, B. Song, H. Ma, T. Luo, L. Guo and J. Yuan, *Anal. Chem.*, 2019, **91**, 2939–2946.
419 F. Qu, H. Wang and J. You, *Food Chem.*, 2020, **323**, 126815.
420 M. S. Tremblay, M. Halim and D. Sames, *J. Am. Chem. Soc.*, 2007, **129**, 7570–7577.
421 M. S. Tremblay and D. Sames, *Chem. Commun.*, 2006, 4116–4118.
422 L. S. Natrajan, A. J. L. Villaraza, A. M. Kenwright and S. Faulkner, *Chem. Commun.*, 2009, 6020–6022.
423 M. P. Placidi, L. S. Natrajan, D. Sykes, A. M. Kenwright and S. Faulkner, *Helv. Chim. Acta*, 2009, **92**, 2427–2438.
424 E. Kreidt, W. Leis and M. Seitz, *Nat. Commun.*, 2020, **11**, 1–7.
425 C. Cepeda, L. Raibaut, G. Fremy, S. V. Eliseeva, A. Romieu, J. Pécaut, D. Boturyn, S. Petoud and O. Sénèque, *Chem. - A Eur. J.*, 2020, **26**, 13476–13483.
426 P. E. Dawson, T. W. Muir, I. Clark-Lewis and S. B. H. Kent, *Science*, 1994, **266**, 776–779.
427 A. Romero-Casañas, V. Gordo, J. Castro and M. Ribó, in *Methods in Molecular Biology*, Humana Press Inc., 2020, vol. 2133, pp. 15–29.
428 N. Ollivier, J. Dheur, R. Mhidia, A. Blanpain and O. Melnyk, *Org. Lett.*, 2010, **12**, 5238–5241.
429 N. Ollivier, L. Raibaut, A. Blanpain, R. Desmet, J. Dheur, R. Mhidia, E. Boll, H. Drobecq, S. L. Pira and O. Melnyk, *J. Pept. Sci.*, 2014, **20**, 92–97.
430 G. Fremy, L. Raibaut, C. Cepeda, M. Sanson, M. Boujut and O. Sénèque, *J. Inorg. Biochem.*, 2020, **213**, 111257.
431 M. Lorusso, A. Pepe, N. Ibris and B. Bochicchio, *Soft Matter*, 2011, **7**, 6327–6336.
432 M. D. Shoulders and R. T. Raines, *Annu. Rev. Biochem.*, 2009, **78**, 929–958.
433 M. A. Kelly, B. W. Chellgren, A. L. Rucker, J. M. Troutman, M. G. Fried, A. F. Miller and T. P. Creamer, *Biochemistry*, 2001, **40**, 14376–14383.
434 M. S. Tremblay, M. Halim and D. Sames, *J. Am. Chem. Soc.*, 2007, **129**, 7570–7577.
435 L. Raibaut, W. Vasseur, G. D. Shimberg, C. Saint-Pierre, J. L. Ravanat, S. L. J. Michel and O. Sénèque, *Chem. Sci.*, 2017, **8**, 1658–1664.
436 A. K. Pandey, K. M. Thomas, C. R. Forbes and N. J. Zondlo, *Biochemistry*, 2014, **53**, 5307–5314.

437 J. Wu, J. R. Forbes, H. S. Chen and D. W. Cox, *Nat. Genet.*, 1994, **7**, 541–545.
438 Y. Togashi, Y. Li, J. -H Kang, N. Takeichi, Y. Fujioka, K. Nagashima and H. Kobayashi, *Hepatology*, 1992, **15**, 82–87.
439 D. Klein, J. Lichtmannegger, U. Heinzmann and K. H. Summer, *J. Hepatol.*, 2000, **32**, 193–201.
440 Q. Wan and S. J. Danishefsky, *Angew. Chemie - Int. Ed.*, 2007, **46**, 9248–9252.
441 J. Bouchenna, M. Sénéchal, H. Drobecq, J. Vicogne and O. Melnyk, *Bioconjug. Chem.*, 2019, **30**, 2967–2973.
442 Y. Doi, T. Hashimoto, H. Yamaguchi and A. Vertut-Doi, *Eur. J. Biochem.*, 1991, **199**, 277–283.
443 M. Regueiro-Figueroa, B. Bensenane, E. Ruscsák, D. Esteban-Gómez, L. J. Charbonnière, G. Tircsó, I. Tóth, A. De Blas, T. Rodríguez-Blas and C. Platas-Iglesias, *Inorg. Chem.*, 2011, **50**, 4125–4141.
444 P. Młynarz, W. Bal, T. Kowalik-Jankowska, M. Stasiak, M. T. Leplawy and H. Kozłowski, *J. Chem. Soc. - Dalt. Trans.*, 1999, 109–110.
445 X. Li, S. Chen, W. D. Zhang and H. G. Hu, *Chem. Rev.*, 2020, **120**, 10079–10144.
446 L. Raibaut, N. Ollivier and O. Melnyk, *Chem. Soc. Rev.*, 2012, **41**, 7001–7015.
447 P. Heffeter, V. F. S. Pape, É. A. Enyedy, B. K. Keppler, G. Szakacs and C. R. Kowol, *Antioxidants Redox Signal.*, 2019, **30**, 1062–1082.
448 S. Kallus, L. Uhlik, S. van Schoonhoven, K. Pelivan, W. Berger, É. A. Enyedy, T. Hofmann, P. Heffeter, C. R. Kowol and B. K. Keppler, *J. Inorg. Biochem.*, 2019, **190**, 85–97.
449 P. V. Bernhardt, P. C. Sharpe, M. Islam, D. B. Lovejoy, D. S. Kalinowski and D. R. Richardson, *J. Med. Chem.*, 2009, **52**, 407–415.
450 É. A. Enyedy, N. V. Nagy, É. Zsigó, C. R. Kowol, V. B. Arion, B. K. Keppler and T. Kiss, *Eur. J. Inorg. Chem.*, 2010, **2010**, 1717–1728.
451 O. Dömötör, N. V. May, K. Pelivan, T. Kiss, B. K. Keppler, C. R. Kowol and É. A. Enyedy, *Inorganica Chim. Acta*, 2018, **472**, 264–275.
452 Y. Yu, Y. S. Rahmanto, C. L. Hawkins and D. R. Richardson, *Mol. Pharmacol.*, 2011, **79**, 921–931.
453 P. J. Jansson, P. C. Sharpe, P. V. Bernhardt and D. R. Richardson, *J. Med. Chem.*, 2010, **53**, 5759–5769.
454 C. R. Kowol, P. Heffeter, W. Miklos, L. Gille, R. Trondl, L. Cappellacci, W. Berger and B. K. Keppler, *J. Biol. Inorg. Chem.*, 2012, **17**, 409–423.
455 D. B. Lovejoy, P. J. Jansson, U. T. Brunk, J. Wong, P. Ponka and D. R. Richardson, *Cancer Res.*, 2011, **71**, 5871–5880.
456 P. J. Jansson, T. Yamagishi, A. Arvind, N. Seebacher, E. Gutierrez, A. Stacy, S. Maleki, D. Sharp, S. Sahni and D. R. Richardson, *J. Biol. Chem.*, 2015, **290**, 9588–9603.
457 S. Hager, K. Korbula, B. Bielec, M. Grusch, C. Pirker, M. Schosserer, L. Liendl, M. Lang, J. Grillari, K. Nowikovsky, V. F. S. Pape, T. Mohr, G. Szakács, B. K. Keppler, W. Berger, C. R. Kowol and P. Heffeter, *Cell Death Dis.*, 2018, **9**, 1052.
458 C. R. Kowol, R. Trondl, P. Heffeter, V. B. Arion, M. A. Jakupec, A. Roller, M. Galanski, W. Berger and B. K. Keppler, *J. Med. Chem.*, 2009, **52**, 5032–5043.
459 C. R. Kowol, W. Miklos, S. Pfaff, S. Hager, S. Kallus, K. Pelivan, M. Kubanik, É. A. Enyedy, W. Berger, P. Heffeter and B. K. Keppler, *J. Med. Chem.*, 2016, **59**, 6739–6752.
460 S. Hager, V. F. S. Pape, V. Pósa, B. Montsch, L. Uhlik, G. Szakács, S. Tóth, N. Jabronka, B. K. Keppler, C. R. Kowol, É. A. Enyedy and P. Heffeter, *Antioxidants Redox Signal.*, 2020, **33**, 395–414.
461 A. Santoro, B. Vileno, Ò. Palacios, M. D. Peris-Díaz, G. Riegel, C. Gaiddon, A. Krężel and P. Faller, *Metallomics*, 2019, **11**, 994–1004.
462 K. Ishiguro, Z. P. Lin, P. G. Penketh, K. Shyam, R. Zhu, R. P. Baumann, Y. L. Zhu, A. C. Sartorelli, T. J. Rutherford and E. S. Ratner, *Biochem. Pharmacol.*, 2014, **91**, 312–322.
463 M. Bern, K. M. K. Sand, J. Nilsen, I. Sandlie and J. T. Andersen, *J. Control. Release*, 2015, **211**, 144–162.
464 A. M. Merlot, D. S. Kalinowski and D. R. Richardson, *Front. Physiol.*, 2014, **5**, 1–7.
465 F. Kratz, *J. Control. Release*, 2008, **132**, 171–183.
466 A. M. Merlot, S. Sahni, D. J. R. Lane, A. M. Fordham, N. Pantarat, D. E. Hibbs, V. Richardson, M. R. Doddareddy, J. A. Ong, M. L. H. Huang, D. R. Richardson and D. S. Kalinowski, *Oncotarget*, 2015, **6**, 10374–10398.

467 J. Qi, Y. Zhang, Y. Gou, Z. Zhang, Z. Zhou, X. Wu, F. Yang and H. Liang, *Mol. Pharm.*, 2016, **13**, 1501–1507.
468 J. Wang, Y. Gou, Z. Zhang, P. Yu, J. Qi, Q. Qin, H. Sun, X. Wu, H. Liang and F. Yang, *Mol. Pharm.*, 2018, **15**, 2180–2193.
469 Z. Zhang, P. Yu, Y. Gou, J. Zhang, S. Li, M. Cai, H. Sun, F. Yang and H. Liang, *J. Med. Chem.*, 2019, **62**, 10630–10644.
470 A. E. Stacy, D. Palanimuthu, P. V. Bernhardt, D. S. Kalinowski, P. J. Jansson and D. R. Richardson, *J. Med. Chem.*, 2016, **59**, 4965–4984.
471 S. Nigam, K. D. Asmus and R. L. Willson, *J. Chem. Soc. Faraday Trans. 1 Phys. Chem. Condens. Phases*, 1976, **72**, 2324–2340.
472 M. C. Krishna, D. A. Grahame, A. Samuni, J. B. Mitchell and A. Russo, *Proc. Natl. Acad. Sci. U. S. A.*, 1992, **89**, 5537–5541.
473 K. Takeshita, K. Saito, J. I. Ueda, K. Anzai and T. Ozawa, *Biochim. Biophys. Acta - Gen. Subj.*, 2002, **1573**, 156–164.
474 H. Speisky, M. Gómez, C. Carrasco-Pozo, E. Pastene, C. Lopez-Alarcón and C. Olea-Azar, *Bioorganic Med. Chem.*, 2008, **16**, 6568–6574.
475 R. C. Smith, V. D. Reed and W. E. Hill, *Phosphorus. Sulfur. Silicon Relat. Elem.*, 1994, **90**, 147–154.
476 A. V Kachur, C. J. Koch and J. E. Biaglow, 1998, **28**, 259–269.
477 D. Cavallini, C. De Marco, S. Duprè and G. Rotilio, *Arch. Biochem. Biophys.*, 1969, **130**, 354–361.
478 L. Pecci, G. Montefoschi, G. Musci and D. Cavallini, *Amino Acids*, 1997, **13**, 355–367.
479 A. R. Goldfarb, L. J. Saidel and E. Mosovich, *J. Biol. Chem.*, 1951, **193**, 397–404.
480 G. S. Kapsomenos and P. D. Akrivos, *Can. J. Chem.*, 1988, **66**, 2835–2838.
481 L. Jamir, A. R. Ali, H. Ghosh, F. A. S. Chipem and B. K. Patel, *Org. Biomol. Chem.*, 2010, **8**, 1674–1678.
482 É. A. Enyedy, N. V. May, V. F. S. Pape, P. Heffeter, G. Szakács, B. K. Keppler and C. R. Kowol, *Dalt. Trans.*, 2020, **49**, 16887–16902.
483 S. Stoll and A. Schweiger, *J. Magn. Reson.*, 2006, **178**, 42–55.

Enrico FALCONE

Étude de complexes de Cu^{II} à visée diagnostique et thérapeutique dans les maladies liées au cuivre

Résumé

La perturbation de l'homéostasie du Cu, en particulier l'augmentation du Cu échangeable dans le sang ou l'urine, est liée à la maladie de Wilson, d'Alzheimer ou des cancers. Cette thèse présente la conception de sondes luminescentes réversibles à Cu^{II} ayant une affinité, sélectivité et détectabilité adaptées pour mesurer le Cu^{II} échangeable dans des échantillons biologiques. Après avoir montré la difficulté de concevoir des sondes *turn-on* réversibles, nous avons développé des sondes *turn-off* et ratiométriques basées sur un motif peptidique liant le Cu^{II} (ATCUN) et des complexes luminescents de lanthanides, qui ont été capables de détecter le Cu^{II} dans des milieux biologiques.
En outre, nous avons étudié la capacité de médicaments anticancéreux tels que les thiosemicarbazones (TCSs) à extraire le Cu^{II} de l'albumine sérique et à produire des ROS en présence de glutathion et de dioxygène. Les résultats suggèrent que les TSCs sont capables de retirer le Cu^{II} par l'albumine, que la production de ROS par les complexes Cu^{II}-TSCs corrèle avec leur activité anticancéreuse et que le plus bas pH lysosomale pourrait être important pour leur activité.

Mots-clés : cuivre échangeable, sonde luminescente, ATCUN, lanthanide, médicaments anticancéreux, thiosemicarbazones, ROS

Résumé en anglais

Cu dyshomeostasis, notably increased levels of the exchangeable Cu in serum and/or urine, have been correlated with pathologies such as Wilson's and Alzheimer's diseases and cancer.
This thesis mostly focused on the design of reversible Cu^{II}-responsive luminescent probes having suited affinity and selectivity for Cu^{II}, as well as detectability, for the detection of exchangeable Cu^{II} in biological samples. After showing that the design of reversible turn-on probes is extremely challenging, we developed turn-off and ratiometric probes based on the Cu^{II}-binding Xxx-Zzz-His peptide motif and luminescent lanthanide complexes, which were able to detect Cu^{II} in biological media.
Moreover, we investigated the ability of the putative Cu-based anticancer drugs thiosemicarbazones (TSCs) to bind Cu^{II} in the presence of human serum albumin (HSA) and then to generate ROS in the presence of glutathione (GSH) and O_2 at different pHs. Our results suggest that (i) TCSs are able to pick up Cu^{II} from HSA, (ii) the ROS generation by Cu^{II}-TSCs in the presence of GSH and O_2 correlates with their anticancer activity and (iii) the lower lysosomal pH might play a key role in their activity.

Keywords : exchangeable copper, luminescent probe, ATCUN, lanthanide, anticancer drugs, thiosemicarbazones, ROS